frontiers | Research Topics

Oligodendrocytes: From their development to function and dysfunction

Edited by
Hiroaki Wake and Shingo Miyata

Published in
Frontiers in Cellular Neuroscience

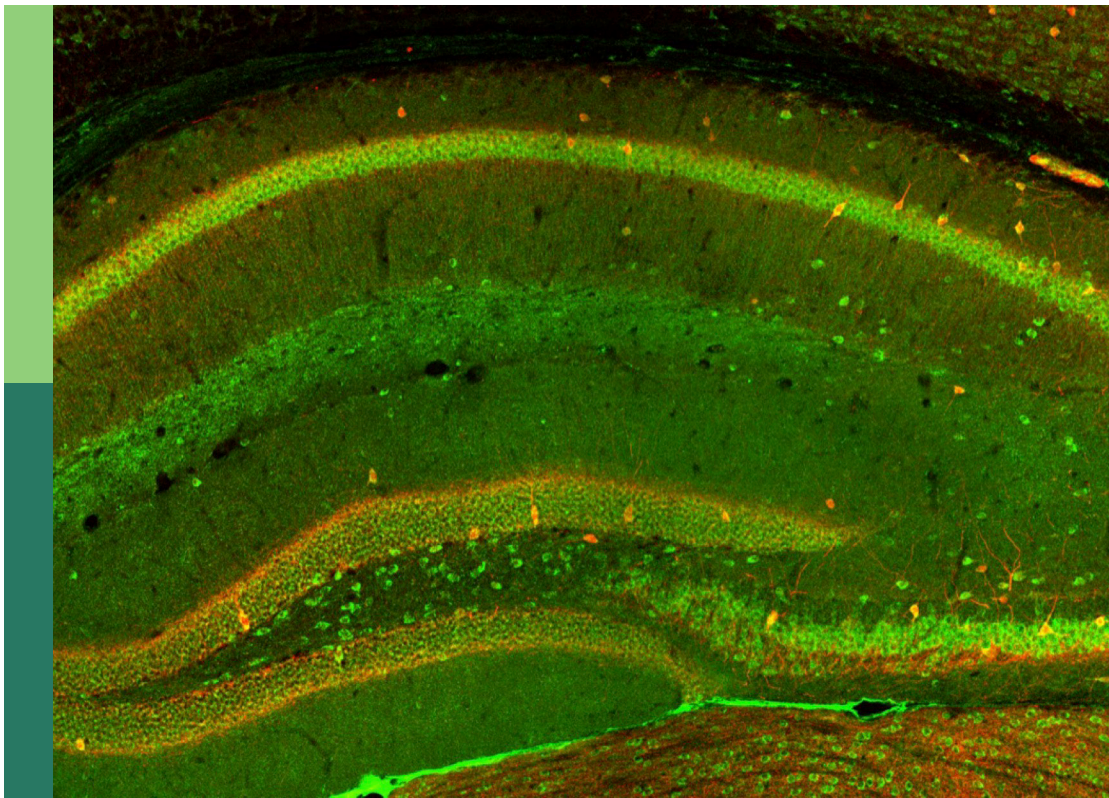

ISSN 1664-8714
ISBN 978-2-8325-4622-2
DOI 10.3389/978-2-8325-4622-2

About Frontiers

Frontiers is more than just an open access publisher of scholarly articles: it is a pioneering approach to the world of academia, radically improving the way scholarly research is managed. The grand vision of Frontiers is a world where all people have an equal opportunity to seek, share and generate knowledge. Frontiers provides immediate and permanent online open access to all its publications, but this alone is not enough to realize our grand goals.

Frontiers journal series

The Frontiers journal series is a multi-tier and interdisciplinary set of open-access, online journals, promising a paradigm shift from the current review, selection and dissemination processes in academic publishing. All Frontiers journals are driven by researchers for researchers; therefore, they constitute a service to the scholarly community. At the same time, the *Frontiers journal series* operates on a revolutionary invention, the tiered publishing system, initially addressing specific communities of scholars, and gradually climbing up to broader public understanding, thus serving the interests of the lay society, too.

Dedication to quality

Each Frontiers article is a landmark of the highest quality, thanks to genuinely collaborative interactions between authors and review editors, who include some of the world's best academicians. Research must be certified by peers before entering a stream of knowledge that may eventually reach the public - and shape society; therefore, Frontiers only applies the most rigorous and unbiased reviews. Frontiers revolutionizes research publishing by freely delivering the most outstanding research, evaluated with no bias from both the academic and social point of view. By applying the most advanced information technologies, Frontiers is catapulting scholarly publishing into a new generation.

What are Frontiers Research Topics?

Frontiers Research Topics are very popular trademarks of the *Frontiers journals series*: they are collections of at least ten articles, all centered on a particular subject. With their unique mix of varied contributions from Original Research to Review Articles, Frontiers Research Topics unify the most influential researchers, the latest key findings and historical advances in a hot research area.

Find out more on how to host your own Frontiers Research Topic or contribute to one as an author by contacting the Frontiers editorial office: frontiersin.org/about/contact

Oligodendrocytes: From their development to function and dysfunction

Topic editors
Hiroaki Wake — Nagoya University, Japan
Shingo Miyata — Kindai University, Japan

Citation
Wake, H., Miyata, S., eds. (2024). *Oligodendrocytes: From their development to function and dysfunction*. Lausanne: Frontiers Media SA.
doi: 10.3389/978-2-8325-4622-2

Table of contents

frontiers | Frontiers in Cellular Neuroscience

TYPE Editorial
PUBLISHED 07 March 2024
DOI 10.3389/fncel.2024.1376931

OPEN ACCESS

EDITED AND REVIEWED BY
Marie-Ève Tremblay,
University of Victoria, Canada

*CORRESPONDENCE
Shingo Miyata
✉ smiyata@med.kindai.ac.jp

RECEIVED 26 January 2024
ACCEPTED 16 February 2024
PUBLISHED 07 March 2024

CITATION
Miyata S and Wake H (2024) Editorial: Oligodendrocytes: from their development to function and dysfunction.
Front. Cell. Neurosci. 18:1376931.
doi: 10.3389/fncel.2024.1376931

Editorial: Oligodendrocytes: from their development to function and dysfunction

Shingo Miyata[1]* and Hiroaki Wake[2]

[1]Division of Molecular Brain Science, Research Institute of Traditional Asian Medicine, Kindai University, Osaka, Japan, [2]Department of Anatomy and Molecular Cell Biology, Nagoya University Graduate School of Medicine, Nagoya, Japan

KEYWORDS

oligodendrocytes, brain disease, neurodegeneration, oligodendrocyte progenitor cells, myelin, remyelination

Editorial on the Research Topic
Oligodendrocytes: from their development to function and dysfunction

Human central nervous system (CNS) myelination occurs before 20 years old and continues throughout our lives (Herbert and Monk, 2017). CNS myelination and remyelination by oligodendrocytes (OLs) is important for obtaining rapid conduction of action potentials and appropriate neuronal communications to support higher brain functions (Masson and Nait-Oumesmar, 2023). OLs and oligodendrocyte precursor cells (OPCs) exist in the corpus callosum, and OPCs have the ability to cell-divide and differentiate into OLs. Previous studies have examined various signal pathways of OL development, CNS myelination, and remyelination *in vivo* and *in vitro* analysis systems (Taylor and Monje, 2023). During CNS myelination and remyelination, OLs generate a multitude of processes and new myelin sheaths by wrapping suitable axons. However, the extent of involvement of various signal cascades and/or molecules in these developing OL lineage cells, CNS myelination, and remyelination remains to be fully elucidated. Thus, this Research Topic is looking to address key aspects of the function and dysfunction of OLs, promote the discussion around this Research Topic, and facilitate knowledge dissemination.

The co-editor, Wake's lab members Yoshida et al., report that the different properties of Ca^{2+} responses of OLs are induced activity-dependent glutamate and adenosine triphosphate (ATP) release from neurons or astrocytes. Further, these activity-dependent responses were lost in the Alzheimer's disease (AD) mice model, but a higher frequency of ATP release induced Ca^{2+} responses due to neurodegeneration. Hong et al. perform a systematic analysis of multiple brain regions and cerebrospinal fluid (CSF), and socially isolating dog groups during the juvenile stage led to a small number of differentially expressed genes in multiple brain regions except the prefrontal cortex (PFC). Maruyama et al. apply global lipidomic analyses to identify circulating lipids that mediate amyotrophic lateral sclerosis (ALS) pathogenesis. They identified a decrease in circulating free fatty acids, including oleic acid (OA) and linoleic acid (LA), and OA and LA inhibited excitotoxic oligodendrocyte cell death via the cell surface receptor FFAR1 (free fatty acid receptor1) in ALS model mice. Zhao et al. find that the OPC differentiation and OL morphology were significantly different between the brain and spinal cord, and inhibition of endoplasmic reticulum (ER) stress could effectively attenuate OPC death.

Han et al. discuss recent findings suggesting an unexpected role of oligodendroglia, the cells that received far less attention than neurons and other glial cells. They also reviewed the possibility that OL lineage cells might be one of the most vulnerable cell types responding to the changing microenvironment in the brain during neurodegenerative diseases. Delfino et al. report that only platelet-derived growth factor receptor alpha (PDGFR-α) positive oligodendrocyte lineage cells are ciliated and reveal heterogeneity in the frequency of cilium presence on OPCs, depending on primary culture conditions and cerebral regions of mice. Further, they show the plasticity of oligodendroglia primary cilium length in response to different drugs. Mei et al. indicate the important molecular and genetic evidence that inositol 1,4,5-trisphosphate receptor type 2 (Itpr2) is dramatically up-regulated in differentiating OLs and regulates OL differentiation and myelin development through an extracellular signal-regulated kinase (ERK)-dependent mechanism. Valihrach et al. review the current understanding of OL heterogeneity in health and disease based on single-cell and single-nucleus transcriptomic technologies. They provide our OL research community with a unified overview of key transcriptomic studies dealing with OL heterogeneity in the mammalian CNS and consensus marker genes of selected OL populations. Chacon-De-La-Rocha et al. report that there is a premature decrease in OPC density at 9 months in AD model mice and that at 14 months, OPC displayed a shrunken and fibrous morphology, indicative of morphological dystrophy. They also indicate that changes in OPCs are potential factors in the progression of AD pathology. This Research Topic highlights the important themes of unraveling the mechanisms behind oligodendrocytes' formation and function, which may lead to a better understanding of their dysfunction and role in CNS pathologies.

Author contributions

SM: Conceptualization, Writing—original draft. HW: Writing—review & editing.

Funding

The author(s) declare that no financial support was received for the research, authorship, and/or publication of this article.

Conflict of interest

The authors declare that the research was conducted in the absence of any commercial or financial relationships that could be construed as a potential conflict of interest.

The author(s) declared that they were an editorial board member of Frontiers, at the time of submission. This had no impact on the peer review process and the final decision.

Publisher's note

References

Herbert, A. L., and Monk, K. R. (2017). Advances in myelinating glial cell development. *Curr. Opin. Neurobiol.* 42, 53–60. doi: 10.1016/j.conb.2016.11.003

Masson, M. A., and Nait-Oumesmar, B. (2023). Emerging concepts in oligodendrocyte and myelin formation, inputs from the zebrafish model. *Glia* 71, 1147–1163. doi: 10.1002/glia.24336

Taylor, K. R., and Monje, M. (2023). Neuron-oligodendroglial interactions in health and malignant disease. *Nat. Rev. Neurosci.* 24, 733–746. doi: 10.1038/s41583-023-00744-3

frontiers in Cellular Neuroscience

ORIGINAL RESEARCH
published: 03 December 2020
doi: 10.3389/fncel.2020.575082

Accelerated Dystrophy and Decay of Oligodendrocyte Precursor Cells in the APP/PS1 Model of Alzheimer's-Like Pathology

Irene Chacon-De-La-Rocha[1†], Gemma Fryatt[2†], Andrea D. Rivera[1], Alexei Verkhratsky[3], Olivier Raineteau[4], Diego Gomez-Nicola[2] and Arthur M. Butt[1]**

[1]School of Pharmacy and Biomedical Sciences, Institute of Biomedical and Biomolecular Sciences, University of Portsmouth, Portsmouth, United Kingdom, [2]School of Biological Sciences, Southampton General Hospital, University of Southampton, Portsmouth, United Kingdom, [3]Faculty of Biology, Medicine, and Health, University of Manchester, Manchester, United Kingdom, [4]University of Lyon, Université Claude Bernard Lyon 1, Inserm, Stem Cell and Brain Research Institute U1208, Bron, France

OPEN ACCESS

Edited by:
Stefania Ceruti,
University of Milan, Italy

Reviewed by:
Hirohide Takebayashi,
Niigata University, Japan
Marta Fumagalli,
University of Milan, Italy
Chao Zhao,
University of Cambridge,
United Kingdom

***Correspondence:**
Arthur M. Butt
arthur.butt@port.ac.uk
Diego Gomez-Nicola
d.gomez-nicola@soton.ac.uk

[†]These authors have contributed equally to this work

Specialty section:
This article was submitted to Non-Neuronal Cells, a section of the journal Frontiers in Cellular Neuroscience

Received: 22 June 2020
Accepted: 22 October 2020
Published: 03 December 2020

Citation:
Chacon-De-La-Rocha I, Fryatt G, Rivera AD, Verkhratsky A, Raineteau O, Gomez-Nicola D and Butt AM (2020) Accelerated Dystrophy and Decay of Oligodendrocyte Precursor Cells in the APP/PS1 Model of Alzheimer's-Like Pathology. Front. Cell. Neurosci. 14:575082. doi: 10.3389/fncel.2020.575082

Myelin disruption is a feature of natural aging and Alzheimer's disease (AD). In the CNS, myelin is produced by oligodendrocytes, which are generated throughout life by oligodendrocyte progenitor cells (OPCs). Here, we examined age-related changes in OPCs in APP/PS1 mice, a model for AD-like pathology, compared with non-transgenic (Tg) age-matched controls. The analysis was performed in the CA1 area of the hippocampus following immunolabeling for NG2 with the nuclear dye Hoescht, to identify OPC and OPC sister cells, a measure of OPC replication. The results indicate a significant decrease in the number of OPCs at 9 months in APP/PS1 mice, compared to age-matched controls, without further decline at 14 months. Also, the number of OPC sister cells declined significantly at 14 months in APP/PS1 mice, which was not observed in age-matched controls. Notably, OPCs also displayed marked morphological changes at 14 months in APP/PS1 mice, characterized by an overall shrinkage of OPC process domains and increased process branching. The results indicate that OPC disruption is a pathological sign in the APP/PS1 mouse model of AD.

Keywords: hippocampus, myelin, OPC, oligodendrocyte progenitor cell, Alzheimer's disease

INTRODUCTION

Alzheimer's disease (AD) is the most common type of dementia and it is characterized by the formation of intracellular neurofibrillary tangles (NFTs) and extracellular amyloid-β (Aβ) plaques (Braak and Braak, 1991). White matter disruption is present at an early stage of AD pathology (Ihara et al., 2010; Bartzokis, 2011), and post-mortem analyses indicate that a loss of oligodendrocytes in AD could serve as a diagnostic tool for differentiating white matter pathologies in dementia (Sjöbeck and Englund, 2003; Brickman et al., 2015). Studies in human AD and mouse models indicate loss of oligodendrocytes and demyelination is most pronounced at the core of Aβ plaques (Mitew et al., 2010). Hence, myelin loss is a feature of human AD and mouse models (Desai et al., 2009), but the underlying causes are unresolved.

In the adult brain, oligodendrocyte progenitor cells (OPCs) are responsible for the life-long generation of oligodendrocytes, required to myelinate new connections formed in response to new life experiences, and to replace myelin lost in pathology (Young et al., 2013; McKenzie et al., 2014; Xiao et al., 2016; Hughes et al., 2018). OPCs are identified by their expression of the NG2 proteoglycan and are sometimes known as NG2-cells or NG2-glia (Butt et al., 2002). Before differentiating into mature myelinating oligodendrocytes, OPCs transition through an intermediate phase identified by expression of the G-protein coupled receptor GPR17 (Viganò et al., 2016). Notably, early changes in OPCs may be a pathological sign and underlie myelin loss in mouse models of AD-like pathology (Mitew et al., 2010; Rivera et al., 2016; Vanzulli et al., 2020). This possibility is supported by immunostaining of post-mortem AD brain showing changes in NG2 immunoreactivity in individuals with high Aβ plaque load (Nielsen et al., 2013).

The APP/PS1 transgenic mouse expresses familial AD-causing mutated forms of human APP (APPswe, Swedish familial AD-causing mutation) and presenilin1 (PS1dE9) and is used extensively as a model for AD-like pathology (Borchelt et al., 1997). The APP/PS1 mouse presents early Aβ plaque deposition in the hippocampus at 4–5 months of age and extensively throughout the forebrain by 8 months (Borchelt et al., 1997), which is linked to greatly impaired synaptic long-term potentiation (LTP) after 8 months of age in the CA1 area of the hippocampus in APP/PS1 (Gengler et al., 2010). Furthermore, several studies provide evidence that white matter and myelin disruption are early clinical signs of APP/PS1 mice (Shu et al., 2013; Wu et al., 2017; Chao et al., 2018; Dong et al., 2018), with evidence that myelin disruption in APP/PS1 mice aged 6 months is accompanied by decreased learning and spatial behavior performance (Chao et al., 2018; Dong et al., 2018). Also, there is evidence of increased NG2 cell numbers in the temporal lobe of 6 months old APP/PS1 mice (Dong et al., 2018), and clustering of hypertrophic NG2 cells around Aβ plaques in the cortex of 14-month-old APP/PS1 (Li et al., 2013). Here, we examined changes in OPCs in 9 and 14 months old APP/PS1 mice, compared to age-matched non-transgenic controls, and focused on the AD-relevant CA1 area of the hippocampus. Our results indicate a premature decline in OPC numbers at 9 months in APP/PS1, whilst at 14 months OPCs displayed cellular shrinkage and increased process branching in APP/PS1, characteristic of reactive changes in response to pathology (Ong and Levine, 1999; Butt et al., 2002). This study identifies pathological changes in OPCs in the APP/PS1 mouse model of AD.

MATERIALS AND METHODS

Ethics

The animal study was reviewed and approved by the University of Southampton Animal Welfare Ethical Review Body (AWERB). All procedures were carried out following the Animals (Scientific Procedures) Act 1986 of the UK.

Animals and Tissue

Transgenic APP/PS1 mice were used that contain human transgenes for both APP (KM670/671NL, Swedish) and PSEN1 (L166P). APPswe/PSEN1dE9 mice (APP/PS1) on a C57BL/6 background were originally obtained from The Jackson Laboratory and heterozygous males were bred at our local facilities with wild-type female C57BL/6J (Harlan). Offspring were ear punched and genotyped using PCR with primers specific for the APP-sequence (forward: GAATTCCGACATGA CTCAGG, reverse: GTTCTGCTGCATCTTGGACA). Mice not expressing the transgene were used as non-transgenic wild-type littermate controls. Mice were housed in groups of 4–10, under a 12-h light/12 h dark cycle at 21°C, with food and water *ad libitum*. No mice were excluded and experimental groups contained a spread of sexes. Mice weight was monitored throughout the experiment. APP/PS1 mice and age-matched non-transgenic controls aged 9 and 14 months old were perfusion-fixed intracardially under terminal anesthesia with 4% paraformaldehyde (PFA), then post-fixed for 2 h with 4% PFA. Sections were cut on a vibratome (Leica) at a thickness of 35 μm then stored in cryoprotectant at −70°C until use.

Immunohistochemistry

Sections were treated for a blocking stage of either 10–20% normal goat serum (NGS) or normal donkey serum (NDS) or 0.5% bovine serum albumin (BSA) for 1–2 h, depending on the primary antibodies to be used. Sections were washed three times in PBS and incubated overnight in primary antibody diluted in blocking solution containing 0.25% Triton-X: rabbit anti-NG2, 1:500 (Millipore); rabbit anti-Olig2, 1:500 (Millipore); rabbit anti-GPR17, 1:100 (Cayman Labs); rat anti-MBP, 1:300 (Millipore). Sections were washed three times in PBS and incubated overnight in primary antibody diluted in blocking solution containing 0.25% Triton-X: rabbit anti-NG2, 1:500 (Millipore); rabbit anti-Olig2, 1:500 (Millipore); rabbit anti-GPR17, 1:100 (Cayman Labs); rat anti-MBP, 1:300 (Millipore). Tissues were then washed three times in PBS and incubated with an appropriate fluorochrome secondary antibody (AlexaFluor® 488, AlexaFluor® 568, 1:400, Life Technologies), or biotinylated secondary antibody (Vector Labs) diluted in blocking solution for 1–2 h. Finally, sections were washed three times with PBS before being mounted on glass slides and covered with mounting medium and glass coverslips ready for imaging.

Imaging and Analysis

Immunofluorescence images were captured using a Zeiss Axiovert LSM 710 VIS40S confocal microscope and maintaining the acquisition parameters constant to allow comparison between samples within the same experiment. The acquisition of images for cell counts was done with ×20 objective. Images for OPC reconstruction were taken using ×100 objective and capturing *z*-stacks formed by 80–100 single plains with an interval of 0.3 μm. Cell counts were performed in the CA1 area in projected flattened images from *z*-stacks formed by 10 or 15 *z*-single plain images with 1 μm interval

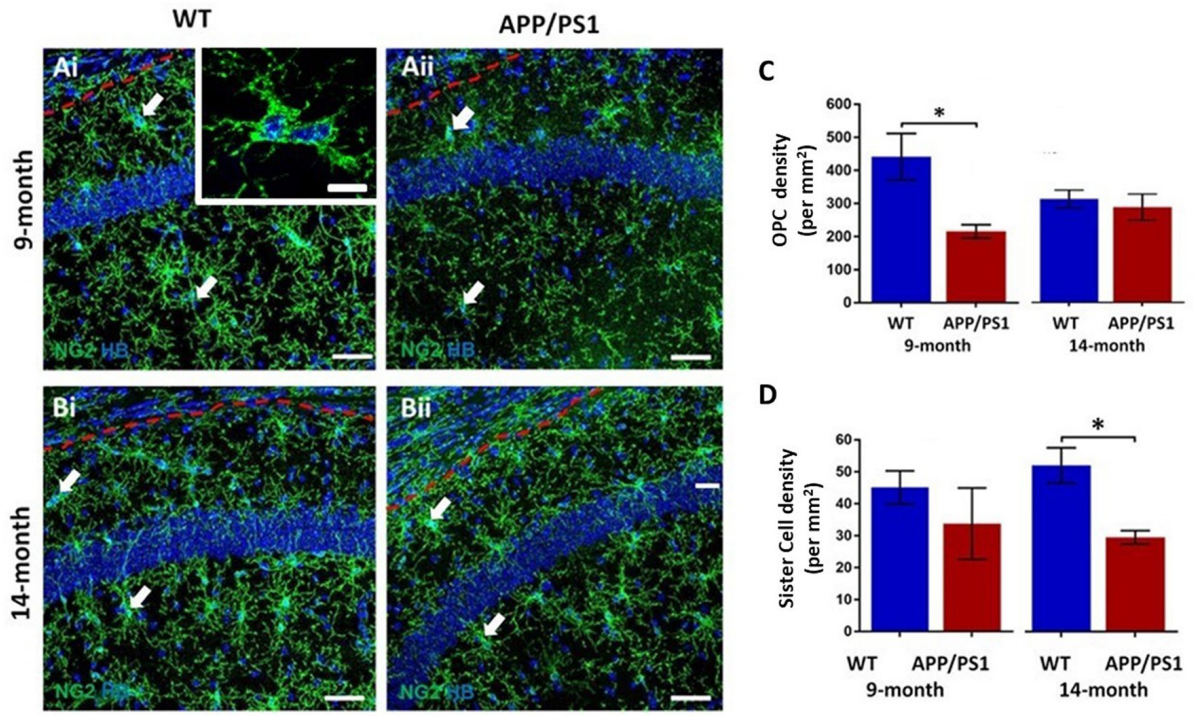

FIGURE 1 | Changes in oligodendrocyte progenitor cells (OPCs) in the CA1 area of the hippocampus of APP/PS1 mice. Hippocampi of 9 months old and 14 months old APP/PS1 mice were compared to age-matched controls. **(Ai,Aii,Bi,Bii)** Representative confocal images of immunofluorescence labeling for NG2 (green) to identify OPCs and counterstaining with Hoechst (blue) for nuclei, to identify OPC sister cells (some indicated by arrows), as illustrated at higher magnification (inset, **Ai**), from non-transgenic controls **(Ai,Bi)** and APP/PS1 mice **(Aii,Bii)**, aged 9 months **(Ai,Aii)** and 14 months **(Bi,Bii)**; scale bars = 50 μm in main panels and 10 μm in the inset. **(C,D)** Bar graphs of the numerical density of NG2+ OPCs **(C)** and OPC sister cells **(D)**. Data are expressed as Mean ± SEM; $*p \leq 0.05$, ANOVA followed by Tukey's *post hoc* test, $n = 3$ animals for each group.

between them, and cell density was calculated as the total number of cells per unit area expressed as cells per mm^2. The relative density of MBP immunolabeling was measured within a constant field of view (FOV) using ImageJ. For DAB immunostaining of Olig2+ oligodendrocytes, sections were examined on an Olympus dotSlide digital slide scanning system based on a BX51 microscope stand with an integrated scanning stage and Olympus CC12 color camera. The cell coverage of OPCs was measured using ImageJ by drawing a line around the cell processes and measuring the area enclosed within the line and expressing the data relative to the area of the CA1 in each section. For morphological analysis of single OPCs, cells were drawn using Neurolucida 360, and their morphology was analyzed using Neurolucida 360 explorer for measurements of the number of processes per cell, number of process terminals (end-points), number of nodes (branch points), and cell complexity; OPC cell complexity refers to the normalization and comparison of processes derived from the dendritic complexity index (Pillai et al., 2012), whereby Neurolucida 360 Explorer calculated cell *complexity* from the sum of (*terminal orders* + the *number of terminals*) multiplied by the (*total dendritic length*/*number of primary dendrites*), where the *terminal* is defined as a process ending and *terminal order* is the number of branches along a process, between the cell body and the terminal (calculated for each terminal). For Sholl analysis, the interval between Sholl shells was 5 μm. Data were expressed as Mean ± SEM and tested for significance by ANOVA followed by Tukey's *post hoc* test for cell numbers, myelin immunostaining, OPC cell domains, and neurolucida analyses of OPCs, and Sidak's multiple comparisons test for Sholl analysis, using GraphPad Prism 6.0.

RESULTS

Premature Decline of OPCs in the Hippocampus of APP/PS1 Mice

The hippocampus displays a high degree of adult oligodendrogenesis, which is important for learning and plasticity (Steadman et al., 2020). Here, we used NG2 immunolabeling to identify adult OPCs (Nishiyama et al., 2016) in the CA1 area of the hippocampus (**Figure 1**); NG2 is also expressed by pericytes, which are directly applied to blood vessels and readily distinguished from OPCs, which are distinguished by their complex process bearing morphology (Hamilton et al., 2010). OPCs are uniformly distributed throughout the hippocampus at both 9 and 14 months, in APP/PS1 mice and

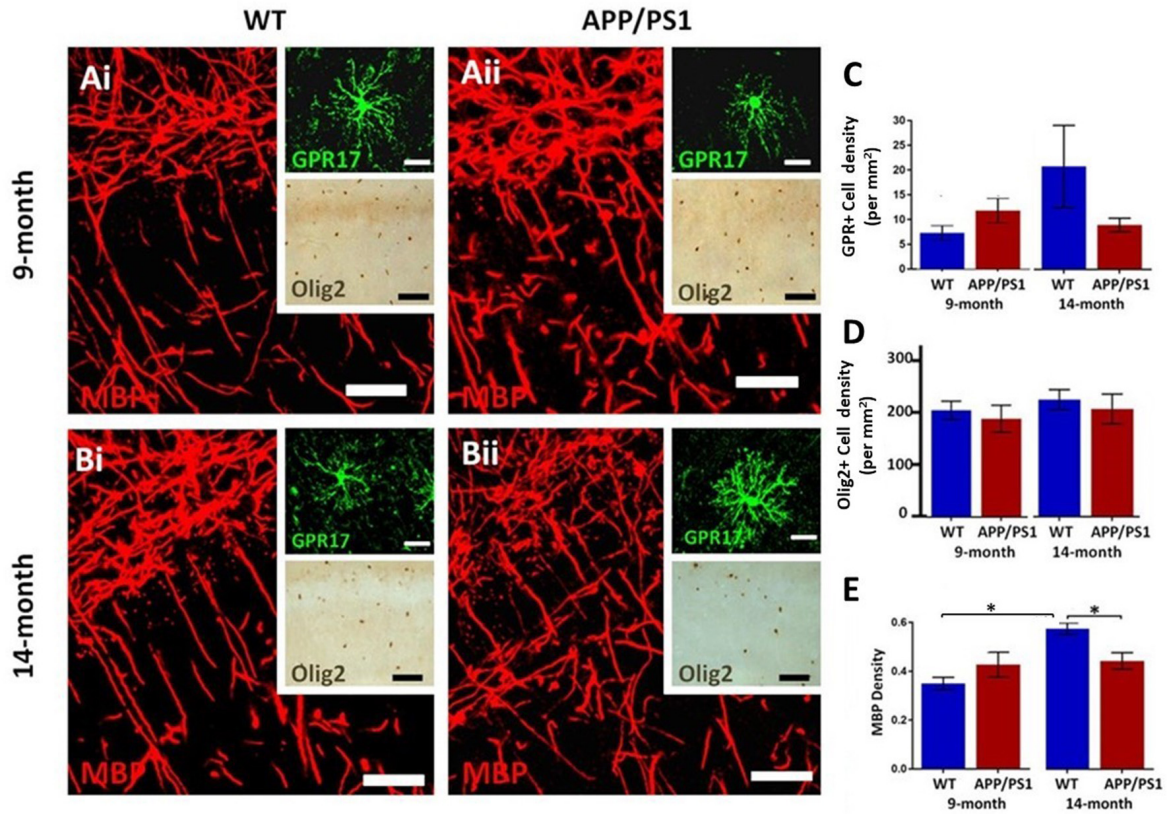

FIGURE 2 | Changes in oligodendrocytes and myelin in the CA1 area of the hippocampus of APP/PS1 mice. Hippocampi of 9 months old **(Ai,Bi)** and 14 months old **(Bi,Bii)** APP/PS1 mice **(Ai,Bi)** were compared to age-matched controls **(Aii,Bii)**. **(Ai,Aii,Bi,Bii)** Representative photomicrographs of immunolabeling for MBP (red in **Ai,Aii,Bi,Bii** main panels) to identify the extent of myelination, together with GPR17 for immature oligodendrocytes (green in upper insets in **Ai,Aii,Bi,Bii**) and Olig2 for the total number of oligodendrocyte lineage cells (brown in lower insets in **Ai,Aii,Bi,Bii**); scale bars = 50 μm, except upper insets = 20 μm. **(C–E)** Bar graphs of numerical density of GPR17+ cells **(C)** and Olig2+ cells **(D)**, together with MBP immunofluorescence density **(E)**; data are expressed as Mean ± SEM; $^*p \leq 0.05$ ANOVA followed by Tukey's *post hoc* test, $n = 3$ animals for each group.

age-matched controls (**Figures 1Ai,Aii,Bi,Bii**). NG2+ OPCs are often observed as duplets or triplets (some indicated by arrows in **Figures 1Ai,Aii,Bi,Bii**, and at higher magnification in the inset in **Figure 1Ai**). OPC duplets are recently divided sister-cells and their frequency is a measure of OPC cell division (Boda et al., 2015), confirming previous studies that adult OPCs continue to divide slowly in old age (Psachoulia et al., 2009; Young et al., 2013). Quantification confirmed a significant difference in the numerical density of NG2+ OPCs in APP/PS1 at 9 months compared to age-matched controls (**Figure 1C**; two-way ANOVA $p \leq 0.05$, followed by Tukey's *post hoc* test). The data indicated a 50% decrease in NG2+ OPCs at 9 months in APP/PS1 to a level observed at 14 months in natural aging (**Figure 1C**); there was no further decline in OPC numbers between 9 and 14 months APP/PS1 mice, which were the same as age-matched controls (**Figure 1C**). Also, there was a significant decrease in the numerical density of OPC sister cells at 14 months in APP/PS1 mice (**Figure 1D**; two-way ANOVA $p \leq 0.05$, followed by Tukey's *post hoc* test, $p \leq 0.05$). Overall, the results indicate a premature decline in OPC numbers at 9 months in APP/PS1 mice.

Decline in Myelination in the Hippocampus of APP/PS1 Mice

The hippocampus displays a high degree of myelination, which is essential for cognitive function (Abrahám et al., 2010), and myelination has been shown to be disrupted in APP/PS1 mice, which is relevant to AD pathology (Ota et al., 2019; Chao et al., 2018; Dong et al., 2018). Immunolabeling for MBP is prominent in the CA1 area at both 9 and 14 months in controls and in APP/PS1 (**Figures 2Ai,Aii,Bi,Bii**), as are GPR17+ cells, which are an intermediate stage between OPCs and myelinating oligodendrocytes (upper insets, **Figures 2Ai,Aii,Bi,Bii**), and Olig2+ cells, which is expressed by all oligodendroglial cells (lower insets, **Figures 2Ai,Aii,Bi,Bii**). Between 9 and 14 months of age, we observed no significant changes in the numerical density of GPR17+ and Olig2+ oligodendrocytes, in controls or APP/PS1 (**Figures 2C,D**), and so we did not analyze oligodendrocyte cell numbers further; it should be noted there was wide variability in GPR17+ cells at 14 months in controls, but overall there was no apparent difference in the number of GPR17+ cells in APP/PS1 between 9 and 14 months in the CA1 region of the hippocampus. Significant age-related changes

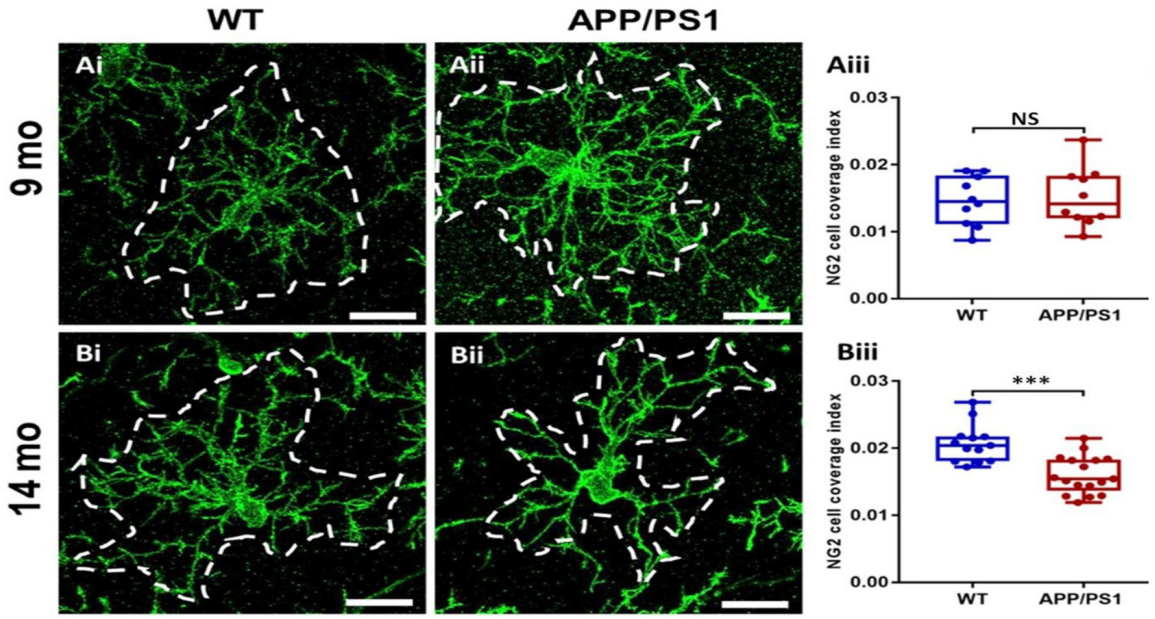

FIGURE 3 | OPC process domains in the CA1 area of the hippocampus of APP/PS1 mice. Hippocampi of 9 months old and 14 months old APP/PS1 mice were examined, compared to age-matched controls, using immunofluorescence labeling for NG2 (green) to identify OPCs. High magnification confocal projections of OPCs and their process domains (indicated by broken white lines) in the 9 months old hippocampus **(Ai,Aii)**, and the 14 months old hippocampus **(Bi,Bii)**, in controls **(Ai,Bi)** and APP/PS1 **(Aii,Bii)**. Scale bars = 20 μm. **(Aiii,Biii)** Box-Whisker plots of the total area of OPC process domains. Data are Mean ± SEM, $^{***}p \leq 0.001$, ANOVA, followed by Tukey's *post hoc* test; NS, not significant; $n = 10$ cells for WT-9 months and APP-9 months, $n = 13$ cells for WT-14 months and $n = 17$ cells for APP-14 months, from three animals in each group.

in MBP immunostaining were detected in the CA1 region and this was not observed in APP/PS1 mice (**Figure 2E**; ANOVA, $p \leq 0.01$, followed by Tukey's post hoc tests). Overall, the results indicate MBP immunostaining is retarded at later stages of pathology in APP/PS1 mice.

OPC Exhibit Cellular Shrinkage at 14 Months in APP/PS1 Mice

The results above indicate OPC are disrupted in APP/PS1 mice, which is often associated with changes in OPC morphology in AD and other pathologies (Butt et al., 2019a,b; Vanzulli et al., 2020). Therefore, we examined OPC morphology in-depth, using high magnification confocal images and measuring the process domains of individual cells and the total coverage of NG2 cells within the CA1 (**Figure 3**). Significant differences were detected in the size of OPC process domains in 14 months APP/PS1 (**Figure 3Biii**; ANOVA, $p \leq 0.001$, followed by Tukey's *post hoc* test, $p \leq 0.001$); no differences were observed in OPCs at 9 months in APP/PS1 compared to controls. The results indicate that at 14 months OPCs display a significant shrinkage in APP/PS1.

OPC Exhibit Increased Process Branching and Cellular Complexity at 14 Months in APP/PS1 Mice

The underlying morphological changes resulting in OPC shrinkage in APP/PS1 mice were examined in further detail using Neurolucida cell tracing. Confocal images of 80–100 *z*-sections, each of 0.3 μm thickness, were captured using an x100 oil objective and reconstructed and analyzed using Neurolucida 360 and Neurolucida 360 Explorer (**Figures 4Ai,Aii,Bi,Bii**; $n = 9$ cells from three animals in each group). Consistent with the results above, OPC morphology was significantly altered at 14 months in APP/PS1 compared to age-matched controls, with the average number of processes per cell being unaltered (**Figure 4C**), whereas processes displayed increased branching, with a significantly greater number of process terminals or endpoints (**Figure 4D**; ANOVA $p \leq 0.01$, followed by Tukey's *post hoc* test, $p \leq 0.05$) and several branch points or nodes (**Figure 4E**; ANOVA $p \leq 0.01$, followed by Tukey's *post hoc* test, $p \leq 0.01$), with a consequent 3-fold increase in the Neurolucida measurement of cell complexity in 14 month APP/PS1 compared to age-match controls (**Figure 4F**; ANOVA $p \leq 0.01$, followed by Tukey's *post hoc* test, $p \leq 0.01$). In contrast, no changes in the morphological parameters of OPCs were detected between 9 and 14 months in wild-type mice (**Figures 4C–F**) or in 9 month APP/PS1 OPC compared to age-matched controls (**Figures 4C–F**). The age-related changes in OPC complexity in APP/PS1 mice were examined further using Sholl analysis (**Figure 5A**; $n = 9$ cells for each group, ANOVA followed by Sidak's multiple comparisons test). Sholl analysis confirmed significant differences in OPC morphology in APP/PS1 mice between 9 and 14 months, with significant increases in the number of endpoints (**Figure 5B**), the number of nodes

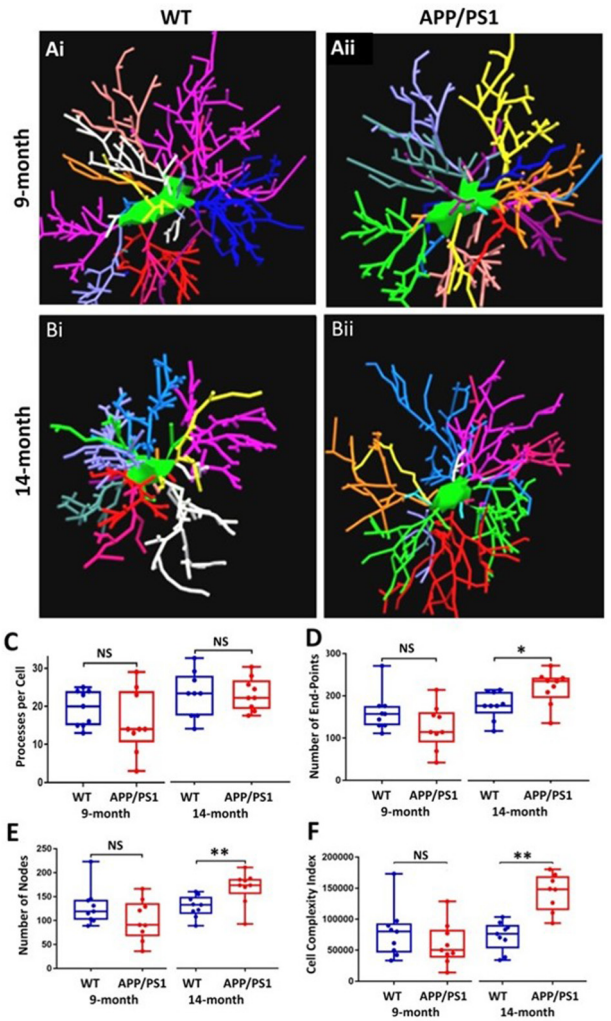

FIGURE 4 | OPC morphological changes in the CA1 of the APP/PS1 mouse model compared to an age-matched controls. Data were generated by Neurolucida 360 analysis of NG2 immunostained cells **(Ai,Aii,Bi,Bii)**. Box-whisker plots of **(C)** processes per cell, **(D)** number of end-points, **(E)** number of nodes, **(F)** cell complexity index. Data expressed as Mean ± SEM. ANOVA, followed by Tukey's *post hoc* test, $*p \leq 0.05$, $**p \leq 0.01$; NS, not significant; $n = 9$ cells from three animals in each group.

(**Figure 5C**), and inprocess lengths (**Figure 5D**). Also, analysis of processes length in the different branch orders identified that OPCs displayed increased process length in the distal branches (**Figure 5E**). In contrast to these changes in APP/PS1, no significant differences were found in OPC morphology in natural aging (**Figure 5**, insets); at 14 months, OPCs displayed a decrease in process lengths in the proximal branches, whereas this parameter was increased in APP/PS1 at 14 months (**Figure 5E**, inset). It is important to note that the small number of cells analyzed by Neurolucida and Sholl may have introduced the possibility of bias. Nonetheless, the measurements of OPC process domains, together with Neurolucida and Sholl analyses, all indicate that OPC shrinkage is a key feature in APP/PS1 at 14 months and is associated with increased process branching, giving OPCs a more fibrous appearance that is similar to "reactive" NG2 cells reported in human AD and AD models (Li et al., 2013; Nielsen et al., 2013; Vanzulli et al., 2020), as well as injury models (Ong and Levine, 1999; Butt et al., 2005; Jin et al., 2018), and this was not observed in age-matched controls.

DISCUSSION

Age-related loss of myelin is a pathological feature of human AD (Bartzokis, 2011; Brickman et al., 2015) and in animal models of AD (Desai et al., 2009; Mitew et al., 2010; Dong et al., 2018; Vanzulli et al., 2020). We observed a decrease in MBP immunostaining at 14 months in the hippocampus of APP/PS1 mice, consistent with evidence that myelination is disrupted in this model of AD (Shu et al., 2013; Wu et al., 2017; Chao et al., 2018; Dong et al., 2018). The key findings of the present study are that there is a premature decrease in OPC density at 9 months in APP/PS1 mice and that at 14 months OPC displayed a shrunken and fibrous morphology, indicative of morphological dystrophy. These findings indicate that changes in OPCs are potential factors in the progression of AD pathology.

Our data support previous studies that there is a decline in the number of OPCs in natural aging (Young et al., 2013). Notably, this age-related loss of OPCs occurred at 9 months of age in APP/PS1, indicating a premature loss of OPCs in this model of AD. The reduction in OPCs numbers at any point is a measure of changes in cell proliferation and/or death at earlier points, hence the reduction in OPC numbers at 9 months in APP/PS1 mice reflects an acceleration of the age-related loss of OPCs, which in natural aging occurs at later ages. The decrease in OPCs at 9 months in APP/PS1 indicates their capacity for self-renewal, defined as maintaining OPC numbers relatively constant over time, was reduced at a point before this age, which is consistent with the evidence of advanced OPC senescence in 7.5-month-old APP/PS1 mice (Zhang et al., 2019). We observed a reduction in OPC sister cells at 14 months in APP/PS1, which is a measure of recently divided OPCs (Boda et al., 2015), suggesting that OPC self-renewal may be compromised at later ages in APP/PS1, although further studies are required to confirm this, for example using multiple injections of BrdU. The changes in OPCs were associated with a reduction in MBP immunostaining at 14 months in APP/PS1 mice compared to controls. MBP immunostaining, taken as a measure of the overall extent of myelination, was increased between 9 and 14 months in wild-type controls, but not in APP/PS1 mice, consistent with multiple lines of evidence that myelination is disrupted in AD-like pathology (Desai et al., 2009; Mitew et al., 2010; Shu et al., 2013; Wu et al., 2017; Chao et al., 2018; Dong et al., 2018; Vanzulli et al., 2020). We did not detect evident changes in GPR17+ and Olig2+ oligodendrocytes, and no conclusions can be drawn on the overall numbers of oligodendrocytes at this time. The decrease in MBP immunostaining at 14 months in APP/PS1 mice may reflect changes in the number and lengths of myelin sheaths, which has been reported in aging (Hill et al., 2018; Hughes et al., 2018). Myelin remodeling is important for nervous system plasticity and repair (Chorghay et al., 2018; Williamson and Lyons, 2018; Foster et al., 2019; Ortiz et al.,

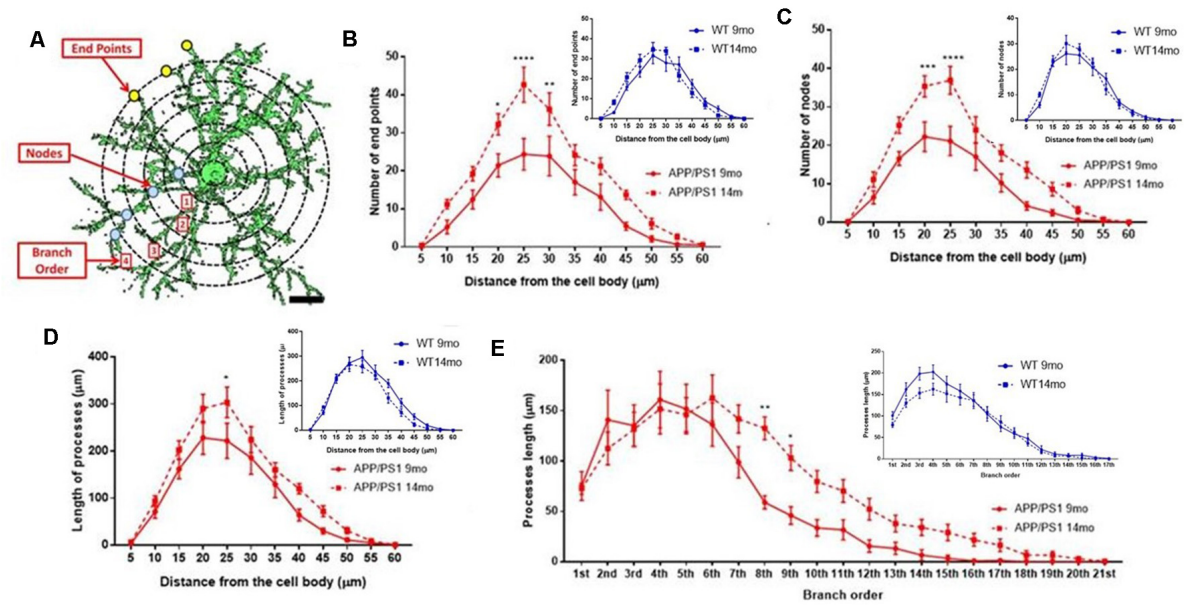

FIGURE 5 | Sholl analysis of age-related changes in OPC morphology in APP/PS1 and age-matched controls. **(A)** 3D morphology of NG2 immunolabeled OPC in the CA1 area of the hippocampus (generated using isosurface rendering with Volocity software, PerkinElmer), illustrating Sholl shells (concentric circles, 5 μm apart, with the cell body in the middle), and the morphological parameters measured; the points of process branching are termed nodes (blue dots), the points where the processes intersect the Sholl shells are termed intersections (yellow dots), the number of process terminals or endpoints, and the process branch order, with 1st order closest to the cell body (adapted from Sholl, 1953, and Rietveld et al., 2015). **(B–E)** Graphs comparing OPC morphological parameters in AAP/PS1 mice aged 9 months (-●-) and 14 months (-■-), together with age-matched controls (insets); two-way ANOVA followed by Sidak's multiple comparisons test. *$p \leq 0.05$, **$p \leq 0.01$, ***$p \leq 0.001$, ****$p \leq 0.0001$, $n = 9$ cells from three animals in each group.

2019), and the decline in myelination in APP/PS1 may be related to neuronal loss and learning dysfunction in these mice (Chao et al., 2018). The results provide evidence of OPC and myelin disruption in the hippocampus of APP/PS1 mice, suggesting key features of human AD are replicated in this mouse model.

Notably, the early loss of OPCs at 9 months in APP/PS1 hippocampus is followed at 14 months by a more fibrous appearance of NG2+ OPCs due to cell shrinkage and increased branching, similar to the fibrous morphology of "reactive" NG2-glia (Ong and Levine, 1999; Butt et al., 2002). Fibrous or reactive NG2-glia have been reported to be associated with amyloid-β plaques in human AD and mouse models (Li et al., 2013; Nielsen et al., 2013; Zhang et al., 2019; Vanzulli et al., 2020), and further studies are required to determine whether OPC morphological changes depend on their relation to amyloid-β plaques, as has been reported for astrocytes (Rodríguez et al., 2016). Since OPCs are the source of new myelinating oligodendrocytes in the adult brain (Dimou et al., 2008; Rivers et al., 2008; Zhu et al., 2008; Kang et al., 2010), it is possible their dystrophy in AD-like pathology may be a causative factor in myelin loss, but this will require comprehensive analyses to verify, using techniques such as fate-mapping and live-cell imaging. Furthermore, the underlying causes of OPC shrinkage in APP/PS1 are unresolved, but OPC are known to contact synapses in the hippocampus (Bergles et al., 2000), and reduced synaptic activity is an important feature in APP/PS1 mice (Gengler et al., 2010), which could result in retraction of OPC processes (Chacon-De-La-Rocha et al., 2020). Also, neuronal activity regulates myelination and myelin repair (Wake et al., 2011; Gibson et al., 2014; Ortiz et al., 2019), and the observed disruption of OPCs suggests this may be an important factor in myelin loss in AD-like pathology.

CONCLUSION

Our findings demonstrate that OPCs undergo complex age-related changes in the hippocampus of the APP/PS1 mouse model of AD-like pathology. We conclude that OPC disruption is a pathological sign in AD and is a potential factor in accelerated myelin loss and cognitive decline.

DATA AVAILABILITY STATEMENT

The datasets presented in this article are not readily available because no datasets were generated in this study. All data generated or analyzed during this study are included in this published article. Requests to access the datasets should be directed to arthur.butt@port.ac.uk.

ETHICS STATEMENT

The animal study was reviewed and approved by the University of Southampton Animal Welfare Ethical Review Body (AWERB).

All procedures were carried out in accordance with the Animals (Scientific Procedures) Act 1986 of the UK.

AUTHOR CONTRIBUTIONS

IC-D-L-R: formal analysis, investigation, methodology and writing—original draft. GF: formal analysis, investigation, methodology and validation. AR: investigation. AV: conceptualization, writing—review and editing. OR: resources, writing—review and editing. DG-N: conceptualization, data curation, formal analysis, funding acquisition, project administration, resources, supervision, validation, visualization, writing—review and editing. AB: conceptualization, data curation, formal analysis, funding acquisition, project administration, resources, supervision, validation, visualization, writing—original draft, writing—review and editing. All authors contributed to the article and approved the submitted version.

FUNDING

This research was supported by grants from the Biotechnology and Biological Sciences Research Council (BBSRC; AB, AR, Grant Number BB/M029379/1), Medical Research Council (MRC; AB, Grant Number MR/P025811/1), Alzheimer's Research UK (DG-N, AB, Grant Number ARUK-PPG2014B-2), University of Portsmouth Ph.D. Program (AB, IC-D-L-R), and a grant from the "Programme Avenir Lyon Saint-Etienne" (OR).

REFERENCES

Abrahám, H., Vincze, A., Jewgenow, I., Veszprémi, B., Kravják, A., Gömöri, E., et al. (2010). Myelination in the human hippocampal formation from midgestation to adulthood. *Int. J. Dev. Neurosci.* 28, 401–410. doi: 10.1016/j.ijdevneu.2010.03.004

Bartzokis, G. (2011). Alzheimer's disease as homeostatic responses to age-related myelin breakdown. *Neurobiol. Aging* 32, 1341–1371. doi: 10.1016/j.neurobiolaging.2009.08.007

Bergles, D. E., Roberts, J. D., Somogyi, P., and Jahr, C. E. (2000). Glutamatergic synapses on oligodendrocyte precursor cells in the hippocampus. *Nature* 405, 187–191. doi: 10.1038/35012083

Boda, E., Di Maria, S., Rosa, P., Taylor, V., Abbracchio, M. P., and Buffo, A. (2015). Early phenotypic asymmetry of sister oligodendrocyte progenitor cells after mitosis and its modulation by aging and extrinsic factors. *Glia* 63, 271–286. doi: 10.1002/glia.22750

Borchelt, D. R., Ratovitski, T., van Lare, J., Lee, M. K., Gonzales, V., Jenkins, N. A., et al. (1997). Accelerated amyloid deposition in the brains of transgenic mice coexpressing mutant presenilin 1 and amyloid precursor proteins. *Neuron* 19, 939–945. doi: 10.1016/s0896-6273(00)80974-5

Braak, H., and Braak, E. (1991). Neuropathological stageing of Alzheimer-related changes. *Acta Neuropathol.* 82, 239–259. doi: 10.1007/BF00308809

Brickman, A. M., Zahodne, L. B., Guzman, V. A., Narkhede, A., Meier, I. B., Griffith, E. Y., et al. (2015). Reconsidering harbingers of dementia: progression of parietal lobe white matter hyperintensities predicts Alzheimer's disease incidence. *Neurobiol. Aging* 36, 27–32. doi: 10.1016/j.neurobiolaging.2014.07.019

Butt, A. M., De La Rocha, I. C., and Rivera, A. (2019a). Oligodendroglial cells in Alzheimer's disease. *Adv. Exp. Med. Biol.* 1175, 325–333. doi: 10.1007/978-981-13-9913-8_12

Butt, A. M., Papanikolaou, M., and Rivera, A. (2019b). Physiology of oligodendroglia. *Adv. Exp. Med. Biol.* 1175, 117–128. doi: 10.1007/978-981-13-9913-8_5

Butt, A. M., Hamilton, N., Hubbard, P., Pugh, M., and Ibrahim, M. (2005). Synantocytes: the fifth element. *J. Anat.* 207, 695–706. doi: 10.1111/j.1469-7580.2005.00458.x

Butt, A. M., Kiff, J., Hubbard, P., and Berry, M. (2002). Synantocytes: new functions for novel NG2 expressing glia. *J. Neurocytol.* 31, 551–565. doi: 10.1023/a:1025751900356

Chacon-De-La-Rocha, I., Fryatt, G. L., Rivera, A. D., Restani, L., Caleo, M., Raineteau, O., et al. (2020). Synaptic silencing affects the density and complexity of oligodendrocyte precursor cells in the adult mouse hippocampus. *BioRxiv* [Preprint]. doi: 10.1101/2020.09.23.309682

Chao, F.-L., Zhang, L., Zhang, Y., Zhou, C.-N., Jiang, L., Xiao, Q., et al. (2018). Running exercise protects against myelin breakdown in the absence of neurogenesis in the hippocampus of AD mice. *Brain Res.* 1684, 50–59. doi: 10.1016/j.brainres.2018.01.007

Chorghay, Z., Káradóttir, R. T., and Ruthazer, E. S. (2018). White matter plasticity keeps the brain in tune: axons conduct while glia wrap. *Front. Cell. Neurosci.* 12:428. doi: 10.3389/fncel.2018.00428

Desai, M. K., Sudol, K. L., Janelsins, M. C., Mastrangelo, M. A., Frazer, M. E., and Bowers, W. J. (2009). Triple-transgenic Alzheimer's disease mice exhibit region-specific abnormalities in brain myelination patterns prior to appearance of amyloid and tau pathology. *Glia* 57, 54–65. doi: 10.1002/glia.20734

Dimou, L., Simon, C., Kirchhoff, F., Takebayashi, H., and Götz, M. (2008). Progeny of Olig2-expressing progenitors in the gray and white matter of the adult mouse cerebral cortex. *J. Neurosci.* 28, 10434–10442. doi: 10.1523/JNEUROSCI.2831-08.2008

Dong, Y.-X., Zhang, H.-Y., Li, H.-Y., Liu, P.-H., Sui, Y., and Sun, X.-H. (2018). Association between Alzheimer's disease pathogenesis and early demyelination and oligodendrocyte dysfunction. *Neural Regen. Res.* 13, 908–914. doi: 10.4103/1673-5374.232486

Foster, A. Y., Bujalka, H., and Emery, B. (2019). Axoglial interactions in myelin plasticity: evaluating the relationship between neuronal activity and oligodendrocyte dynamics. *Glia* 67, 2038–2049. doi: 10.1002/glia.23629

Gengler, S., Hamilton, A., and Hölscher, C. (2010). Synaptic plasticity in the hippocampus of a APP/PS1 mouse model of Alzheimer's disease is impaired in old but not young mice. *PLoS One* 5:e9764. doi: 10.1371/journal.pone.0009764

Gibson, E. M., Purger, D., Mount, C. W., Goldstein, A. K., Lin, G. L., Wood, L. S., et al. (2014). Neuronal activity promotes oligodendrogenesis and adaptive myelination in the mammalian brain. *Science* 344:1252304. doi: 10.1126/science.1252304

Hamilton, N., Vayro, S., Wigley, R., and Butt, A. M. (2010). Axons and astrocytes release ATP and glutamate to evoke calcium signals in NG2-glia. *Glia* 58, 66–79. doi: 10.1002/glia.20902

Hill, R. A., Li, A. M., and Grutzendler, J. (2018). Lifelong cortical myelin plasticity and age-related degeneration in the live mammalian brain. *Nat. Neurosci.* 21, 683–695. doi: 10.1038/s41593-018-0120-6

Hughes, E. G., Orthmann-Murphy, J. L., Langseth, A. J., and Bergles, D. E. (2018). Myelin remodeling through experience-dependent oligodendrogenesis in the adult somatosensory cortex. *Nat. Neurosci.* 21, 696–706. doi: 10.1038/s41593-018-0121-5

Ihara, M., Polvikoski, T. M., Hall, R., Slade, J. Y., Perry, R. H., Oakley, A. E., et al. (2010). Quantification of myelin loss in frontal lobe white matter in vascular dementia, Alzheimer's disease and dementia with Lewy bodies. *Acta Neuropathol.* 119, 579–589. doi: 10.1007/s00401-009-0635-8

Jin, X., Riew, T.-R., Kim, H. L., Choi, J.-H., and Lee, M.-Y. (2018). Morphological characterization of NG2 glia and their association with neuroglial cells in the 3-nitropropionic acid-lesioned striatum of rat. *Sci. Rep.* 8, 5942–5942. doi: 10.1038/s41598-018-24385-0

Kang, S. H., Fukaya, M., Yang, J. K., Rothstein, J. D., and Bergles, D. E. (2010). NG2+ CNS glial progenitors remain committed to the oligodendrocyte lineage in postnatal life and following neurodegeneration. *Neuron* 68, 668–681. doi: 10.1016/j.neuron.2010.09.009

Li, W., Tang, Y., Fan, Z., Meng, Y., Yang, G., Luo, J., et al. (2013). Autophagy is involved in oligodendroglial precursor-mediated clearance of amyloid peptide. *Mol. Neurodegener.* 8:27. doi: 10.1186/1750-1326-8-27

McKenzie, I. A., Ohayon, D., Li, H., De Faria, J. P., Emery, B., Tohyama, K., et al. (2014). Motor skill learning requires active central myelination. *Science* 346, 318–322. doi: 10.1126/science.1254960

Mitew, S., Kirkcaldie, M. T., Halliday, G. M., Shepherd, C. E., Vickers, J. C., and Dickson, T. C. (2010). Focal demyelination in Alzheimer's disease and transgenic mouse models. *Acta Neuropathol.* 119, 567–677. doi: 10.1007/s00401-010-0657-2

Nielsen, H. M., Ek, D., Avdic, U., Orbjörn, C., Hansson, O., Veerhuis, R., et al. (2013). NG2 cells, a new trail for Alzheimer's disease mechanisms? *Acta Neuropathol. Commun.* 1:7. doi: 10.1186/2051-5960-1-7

Nishiyama, A., Boshans, L., Goncalves, C. M., Wegrzyn, J., and Patel, K. D. (2016). Lineage, fate, and fate potential of NG2-glia. *Brain Res.* 1638, 116–128. doi: 10.1016/j.brainres.2015.08.013

Ong, W. Y., and Levine, J. M. (1999). A light and electron microscopic study of NG2 chondroitin sulfate proteoglycan-positive oligodendrocyte precursor cells in the normal and kainate-lesioned rat hippocampus. *Neuroscience* 92, 83–95. doi: 10.1016/s0306-4522(98)00751-9

Ortiz, F. C., Habermacher, C., Graciarena, M., Houry, P. Y., Nishiyama, A., Oumesmar, B. N., et al. (2019). Neuronal activity *in vivo* enhances functional myelin repair. *JCI Insight* 5:e123434. doi: 10.1172/jci.insight.123434

Ota, M., Sato, N., Kimura, Y., Shigemoto, Y., Kunugi, H., and Matsuda, H. (2019). Changes of myelin organization in patients with Alzheimer's disease shown by q-space myelin map imaging. *Dement. Geriatr. Cogn. Disord. Extra* 9, 24–33. doi: 10.1159/000493937

Pillai, A. G., De Jong, D., Kanatsou, S., Krugers, H., Knapman, A., Heinzmann, J.-M., et al. (2012). Dendritic morphology of hippocampal and amygdalar neurons in adolescent mice is resilient to genetic differences in stress reactivity. *PLoS One* 7:e38971. doi: 10.1371/journal.pone.0038971

Psachoulia, K., Jamen, F., Young, K. M., and Richardson, W. D. (2009). Cell cycle dynamics of NG2 cells in the postnatal and ageing brain. *Neuron Glia Biol.* 5, 57–67. doi: 10.1017/S1740925X09990354

Rietveld, L., Stuss, D. P., McPhee, D., and Delaney, K. R. (2015). Genotype-specific effects of *Mecp2* loss-of-function on morphology of Layer V pyramidal neurons in heterozygous female Rett syndrome model mice. *Front. Cell. Neurosci.* 9:145. doi: 10.3389/fncel.2015.00145

Rivera, A., Vanzuli, I., Arellano, J. J., and Butt, A. (2016). Decreased regenerative capacity of oligodendrocyte progenitor cells (NG2-Glia) in the ageing brain: a vicious cycle of synaptic dysfunction, myelin loss and neuronal disruption? *Curr. Alzheimer Res.* 13, 413–438. doi: 10.2174/1567205013666151116125518

Rivers, L. E., Young, K. M., Rizzi, M., Jamen, F., Psachoulia, K., Wade, A., et al. (2008). PDGFRA/NG2 glia generate myelinating oligodendrocytes and piriform projection neurons in adult mice. *Nat. Neurosci.* 11, 1392–1401. doi: 10.1038/nn.2220

Rodríguez, J. J., Butt, A. M., Gardenal, E., Parpura, V., and Verkhratsky, A. (2016). Complex and differential glial responses in Alzheimer's disease and ageing. *Curr. Alzheimer Res.* 13, 343–358. doi: 10.2174/1567205013666160229112911

Sholl, D. A. (1953). Dendritic organization in the neurons of the visual and motor cortices of the cat. *J. Anat.* 87, 387–406.

Shu, X., Qin, Y. Y., Zhang, S., Jiang, J. J., Zhang, Y., Zhao, L. Y., et al. (2013). Voxel-based diffusion tensor imaging of an APP/PS1 mouse model of Alzheimer's disease. *Mol. Neurobiol.* 48, 78–83. doi: 10.1007/s12035-013-8418-6

Sjöbeck, M., and Englund, E. (2003). Glial levels determine severity of white matter disease in Alzheimer's disease: a neuropathological study of glial changes. *Neuropathol. Appl. Neurobiol.* 29, 159–169. doi: 10.1046/j.1365-2990.2003.00456.x

Steadman, P. E., Xia, F., Ahmed, M., Mocle, A. J., Penning, A. R. A., Geraghty, A. C., et al. (2020). Disruption of oligodendrogenesis impairs memory consolidation in adult mice. *Neuron* 105, 150.e6–164.e6.doi: 10.1016/j.neuron.2019.10.013

Vanzulli, I., Papanikolaou, M., De La Rocha, I. C., Pieropan, F., Rivera, A. D., Gomez-Nicola, D., et al. (2020). Disruption of oligodendrocyte progenitor cells is an early sign of pathology in the triple transgenic mouse model of Alzheimer's disease. *Neurobiol. Aging* 94, 130–139. doi: 10.1016/j.neurobiolaging.2020.05.016

Viganò, F., Schneider, S., Cimino, M., Bonfanti, E., Gelosa, P., Sironi, L., et al. (2016). GPR17 expressing NG2-Glia: oligodendrocyte progenitors serving as a reserve pool after injury. *Glia* 64, 287–299. doi: 10.1002/glia.22929

Wake, H., Lee, P. R., and Fields, R. D. (2011). Control of local protein synthesis and initial events in myelination by action potentials. *Science* 333, 1647–1651. doi: 10.1126/science.1206998

Williamson, J. M., and Lyons, D. A. (2018). Myelin dynamics throughout life: an ever-changing landscape? *Front. Cell. Neurosci.* 12:424. doi: 10.3389/fncel.2018.00424

Wu, Y., Ma, Y., Liu, Z., Geng, Q., Chen, Z., and Zhang, Y. (2017). Alterations of myelin morphology and oligodendrocyte development in early stage of Alzheimer's disease mouse model. *Neurosci. Lett.* 642, 102–106. doi: 10.1016/j.neulet.2017.02.007

Xiao, L., Ohayon, D., Mckenzie, I. A., Sinclair-Wilson, A., Wright, J. L., Fudge, A. D., et al. (2016). Rapid production of new oligodendrocytes is required in the earliest stages of motor-skill learning. *Nat. Neurosci.* 19, 1210–1217. doi: 10.1038/nn.4351

Young, K. M., Psachoulia, K., Tripathi, R. B., Dunn, S.-J., Cossell, L., Attwell, D., et al. (2013). Oligodendrocyte dynamics in the healthy adult CNS: evidence for myelin remodeling. *Neuron* 77, 873–885. doi: 10.1016/j.neuron.2013.01.006

Zhang, P., Kishimoto, Y., Grammatikakis, I., Gottimukkala, K., Cutler, R. G., Zhang, S., et al. (2019). Senolytic therapy alleviates Aβ-associated oligodendrocyte progenitor cell senescence and cognitive deficits in an Alzheimer's disease model. *Nat. Neurosci.* 22, 719–728. doi: 10.1038/s41593-019-0372-9

Zhu, X., Hill, R. A., and Nishiyama, A. (2008). NG2 cells generate oligodendrocytes and gray matter astrocytes in the spinal cord. *Neuron Glia Biol.* 4, 19–26. doi: 10.1017/S1740925X09000015

Conflict of Interest: AB and AR declare they are share-holders and co-founders of the company GliaGenesis Limited.

The remaining authors declare that the research was conducted in the absence of any commercial or financial relationships that could be construed as a potential conflict of interest.

frontiers in Cellular Neuroscience

ORIGINAL RESEARCH
published: 22 September 2021
doi: 10.3389/fncel.2021.751439

Evidence That *ITPR2*-Mediated Intracellular Calcium Release in Oligodendrocytes Regulates the Development of Carbonic Anhydrase II + Type I/II Oligodendrocytes and the Sizes of Myelin Fibers

Ruyi Mei[1,2], Linyu Huang[2], Mengyuan Wu[2], Chunxia Jiang[1,2], Aifen Yang[2], Huaping Tao[2], Kang Zheng[2], Junlin Yang[2], Wanhua Shen[2], Xianjun Chen[3], Xiaofeng Zhao[2] and Mengsheng Qiu[1,2]**

[1] College of Life Sciences, Zhejiang University, Hangzhou, China, [2] Zhejiang Key Laboratory of Organ Development and Regeneration, College of Life and Environmental Sciences, Institute of Developmental and Regenerative Biology, Hangzhou Normal University, Hangzhou, China, [3] Department of Physiology, Research Center of Neuroscience, Chongqing Medical University, Chongqing, China

OPEN ACCESS

Edited by:
Hiroaki Wake,
Nagoya University, Japan

Reviewed by:
Kenji Tanaka,
Keio University, Japan
Shingo Miyata,
Kindai University, Japan

***Correspondence:**
Xiaofeng Zhao
xiaofengzhao@yahoo.com
Mengsheng Qiu
m0qiu001@yahoo.com

Specialty section:
This article was submitted to Non-Neuronal Cells, a section of the journal Frontiers in Cellular Neuroscience

Received: 01 August 2021
Accepted: 03 September 2021
Published: 22 September 2021

Citation:
Mei R, Huang L, Wu M, Jiang C, Yang A, Tao H, Zheng K, Yang J, Shen W, Chen X, Zhao X and Qiu M (2021) Evidence That ITPR2-Mediated Intracellular Calcium Release in Oligodendrocytes Regulates the Development of Carbonic Anhydrase II + Type I/II Oligodendrocytes and the Sizes of Myelin Fibers. Front. Cell. Neurosci. 15:751439. doi: 10.3389/fncel.2021.751439

Myelination of neuronal axons in the central nervous system (CNS) by oligodendrocytes (OLs) enables rapid saltatory conductance and axonal integrity, which are crucial for normal brain functioning. Previous studies suggested that different subtypes of oligodendrocytes in the CNS form different types of myelin determined by the diameter of axons in the unit. However, the molecular mechanisms underlying the developmental association of different types of oligodendrocytes with different fiber sizes remain elusive. In the present study, we present the evidence that the intracellular Ca^{2+} release channel associated receptor (*Itpr2)* contributes to this developmental process. During early development, *Itpr2* is selectively up-regulated in oligodendrocytes coinciding with the initiation of myelination. Functional analyses in both conventional and conditional *Itpr2* mutant mice revealed that *Itpr2* deficiency causes a developmental delay of OL differentiation, resulting in an increased percentage of $CAII^{+}$ type I/II OLs which prefer to myelinate small-diameter axons in the CNS. The increased percentage of small caliber myelinated axons leads to an abnormal compound action potentials (CAP) in the optic nerves. Together, these findings revealed a previously unrecognized role for *Itpr2*-mediated calcium signaling in regulating the development of different types of oligodendrocytes.

Keywords: axon diameter, conduction velocity, oligodendrocyte, myelination, *ITPR2*

INTRODUCTION

In the central nervous system (CNS), myelin is elaborated by oligodendrocytes (OLs) and plays a crucial role in axonal conductance and integrity (Fields, 2008; Martins-de-Souza, 2010; Nave, 2010; Miron et al., 2011; Edgar and Sibille, 2012). Abnormal myelin development has been implicated in several neuropsychiatric diseases including schizophrenia and major depression (Fields, 2008; Martins-de-Souza, 2010; Edgar and Sibille, 2012), and defective motor skill

learning (McKenzie et al., 2014). Previous studies demonstrated that not all axons in the CNS are myelinated, and in general, only larger axons of certain diameters (>0.2 μm) are ensheathed by oligodendrocyte processes. In 1928, del Río Hortega classified the oligodendrocytes into four types (type I–type IV) according to their morphological features (HP, 1928). Among these four types, type I/II oligodendrocytes predominantly myelinate small diameter axons (0.2–0.4 μm), whereas type III/IV oligodendrocytes that myelinate larger caliber axons (Butt et al., 1995). More recent studies showed that isoenzyme carbonic anhydrase II (CAII) is a specific marker for type I/II oligodendrocytes, while type III/IV oligodendrocytes are CAII-negative (Butt et al., 1998; Butt and Berry, 2000). Intriguingly, oligodendrocytes appear to be very plastic and can change their phenotype, as oligodendrocytes that normally myelinate small diameter axons are able to myelinate large diameter axons when transplanted into demyelinated tracts (Fanarraga et al., 1998), and expression of CAII increases when the volume of supported myelin decreases (O'Leary and Blakemore, 1997; Berry et al., 1998). Although recent single-cell sequencing analyses have provided additional molecular evidence for the existence of different types of oligodendroglia (Zeisel et al., 2015; Marques et al., 2016), the molecular mechanisms underlying the development of oligodendrocyte subpopulations and their association with different fiber sizes have remained elusive.

Early studies have suggested that intracellular calcium signaling plays an important role in the survival and differentiation of oligodendrocyte progenitor cells (OPCs), and the maintenance of the myelin sheath as well (Soliven, 2001; Paez et al., 2012). The calcium homeostasis imbalance can result in demyelinating disease (Tsutsui and Stys, 2013). Although oligodendrocytes can release Ca^{2+} from internal stores through both inositol 1,4,5-trisphosphate receptors (ITPRs) and ryanodine receptors (RyRs), only ITPRs could evoke the Ca^{2+} waves in newly differentiated OLs and initiate the myelin formation process (Haak et al., 2001). ITPRs are intracellular Ca^{2+} release channels that are mainly localized in the endoplasmic reticulum (ER). There are three isoforms of ITPRs (ITPR1-3) that are differentially expressed in the CNS tissues, with ITPR2 being solely transcribed in glial cells (Sharp et al., 1999). However, the expression and functional involvement of *Itpr2* in oligodendrocyte development and myelinogenesis has not been defined.

In this study, we report that *Itpr2* is selectively upregulated in oligodendrocytes during differentiation and myelin formation stages. Functional studies with both conventional and conditional mutants revealed that *Itpr2* deficiency causes a developmental delay of oligodendrocyte differentiation in the CNS, resulting in an increased percentage of $CAII^+$ type I/II OLs and small-diameter myelinated axons with abnormal CAP.

MATERIALS AND METHODS

Animals

All animal experiments were performed in accordance with the institutional guidelines drafted by the Laboratory Animal Center, Hangzhou Normal University, and were approved by the Animal Ethics Committee of Hangzhou Normal University, China. The *Itpr2-KO, Itpr2*^{flox}, *Myrf*^{flox}, *Nkx2.2*^{flox}, *Olig1*-Cre, *Cnp*-Cre, and *Sox10-GFP* mouse lines were described previously (Lu et al., 2002; Lappe-Siefke et al., 2003; Li et al., 2005; Emery et al., 2009; Tripathi et al., 2011; Mastracci et al., 2013). For the removal of *Itpr2* in oligodendrocyte lineage, *Itpr2*^{flox} mice were interbred with *Cnp*-Cre transgenic mice to confirm that the myelination phenotypes observed in *Itpr2* conventional knockouts are attributable to oligodendrocyte-specific defects. Animals of either sex were used for analyses.

Electron Microscopy

Wild type and mutant mice perfused with a phosphate buffer solution containing 2.5% glutaraldehyde and 4% paraformaldehyde (PFA, pH 7.2). The optic nerve and corpus callosum tissues were isolated and post-fixed in 1% osmium tetroxide for 1 h. Tissues were then washed in 0.1 M cacodylate buffer, dehydrated in graded ethanol and embedded in epoxy resins. Ultrathin sections (0.5 μm) were stained with toluidine blue and observed under a transmission electronic microscope.

Electrophysiology

All experiments were performed at room temperature (22–25°C). During preparation, artificial cerebrospinal fluid (aCSF) containing (in mM): NaCl 126, KCl 3.0, $CaCl_2$ 2.0, $MgCl_2$ 2.0, NaH_2PO_4 1.2, $NaHCO_3$ 26, and glucose 10, was continuously equilibrated with a humidified gas mixture of 95% O_2/5% CO_2. The optic nerves were dissected out at the optic chiasm behind the orbit. The nerve tissues were equilibrated in the beaker with aCSF for 30 min before each experiment. Recording micropipettes were pulled from borosilicate glass capillaries and the glass nozzles were polished until they could adhere to the optic nerves tightly. One micropipette was attached to the rostral end of the nerve for stimulation, the end of which was held by a custom-made stimulating suction electrode, which was made of a polished glass wrapped with silver wires and controlled by an isolator. The second micropipette was attached to the caudal end of the nerve for recording, and all recordings were orthodromic. The maximum compound action potentials (CAP) were evoked with electrical pulses at 0.05 ms in duration elicited at 0.2 Hz. While this process was completed, the stimulus pulse intensity was reduced to evoke 70% maximum reaction and recorded for 20 min. Signals were filtered at 2 kHz with a MultiClamp 700B amplifier (Molecular Devices, Palo Alto, CA). Data were sampled at 10 kHz and analyzed using ClampFit 10 (Molecular Devices). The curve fitting routine for describing the CAP in terms of Gaussian functions has previously been described (Allen et al., 2006), and data were fit using Microsoft Excel. The stimulus artifact was included in the fitting procedure as it impinges upon the 1st CAP peak. The best fit of a CAP by multiple Gaussian functions provides parameters that can be used to reconstruct the CAP.

In situ RNA Hybridization

Tissues were fixed with 4% PFA in PBS (pH 7.4) at 4°C overnight. Tissues were then cryo-protected in 30% sucrose, embedded in optimal cutting temperature compound (OCT) medium, and sectioned on a cryostat at 16–18 μm. The procedures for *in situ* hybridization (ISH) have been described previously (Zhu et al., 2013). The digoxin-labeled RNA probes used for ISH corresponded to nucleotides 1210–2178 of mouse *Plp1* mRNA (NM_011123.4), nucleotides 7028–7970 of mouse *Itpr1* mRNA (NM_010585.5), nucleotides 134–698 of mouse *Itpr2* mRNA (NM_019923.4), and nucleotides 6818–7761 of mouse *Itpr3* mRNA (NM_080553.3).

Immunofluorescence Staining

Animals were fixed by transcardial perfusion with cold 4% PFA after the animals were deeply anesthetized. Brains, spinal cords and optic nerves were isolated and post fixed overnight, cryoprotected in 30% sucrose, embedded in OCT compound and stored at −80°C for cryo-sectioning. After incubation in blocking buffer (10% goat serum and 0.2% Triton X-100 in PBS), tissue sections (16 μm thickness) were first incubated with primary antibodies at 4°C overnight and then with second antibodies at room temperature for 2 h, followed with 1 mg/mL DAPI for 5–10 min. Slides were mounted with mowiol mounting medium. The primary antibodies were used as follows: anti-OLIG2 (1:1,000, Millipore, Cat# AB9610, RRID: AB_570666), anti-CC1 (1:500, Abcam, Cat# ab16794, RRID: AB_443473), anti-ITPR2 (1:10, Millipore, Cat# AB3000, RRID: AB_91282), anti-NeuN (1:500, R and D Systems, Cat# MAB377, RRID: AB_2298767), anti-CAII (1:50, ABclonal, Cat# A1440, RRID: AB_2761269), anti-SOX10 (1:400, Oasis Biofarm), anti-ALDH1L1 (1:200, Oasis Biofarm). The secondary antibodies used were Alexa Fluor 488/594-conjugated antibodies (Invitrogen, Carlsbad, CA, United States).

Western Blotting

Brainstem tissues were lysed in lysis buffer (Sigma, R0278) with protease inhibitor cocktail (Sigma, P8340). Proteins from control and mutant mice (30 μg each) were loaded for SDS-PAGE electrophoresis and subsequently detected with anti-ERK1/2 (1:5,000, Abcam, Cat# ab184699, RRID: AB_2802136), anti-Phospho-ERK1/2 (1:5,000, Abcam, Cat# ab76299, RRID: AB_1523577), anti-CNPase (1:2,000, Abcam, Cat# ab6319, RRID: AB_2082593), anti-β-Actin (1:10,000, ABclonal, Cat# AC026, RRID: AB_2768234) antibodies according to the protocol (Ray et al., 2000).

Organotypic Slice Cultures

OL lineage-specific reporter mice *Sox10-GFP* at postnatal day 10 were sacrificed by cervical dislocation and then decapitated. Coronal slices (230 μm thick) from the mouse cerebral cortex were first sectioned in aCSF (pH 7.4), transferred onto 30 mm diameter semiporous membrane inserts (Millicell-CM PICM03050) and then cultured in six-well tissue culture dishes containing 3 mL of culture medium per well. The brain slice culture medium consisted of 50% Eagle's minimal essential medium, 25% heat-inactivated horse serum, 25% Hank's balanced salt solution, 1% L-glutamine, and 1% penicillin/streptomycin. Slices were maintained at 37°C in an incubator in atmosphere of humidified air and 5% CO_2. After 1 day in culture, intracellular calcium chelator BAPTA-AM (20 μm) (Solarbio, S1102) was added to the culture medium to assess its impact on oligodendrocyte differentiation. For localization studies, the slices were fixed with 4% PFA for 24 h at 4°C after 5 days in culture and then detected the expression of CAII.

Statistical Analysis

Data statistical analyses were performed using the GraphPad Prism software (version 8.0.2). For the quantitative analysis of the distribution of axonal size in the corpus callosum and optic nerve tissues, data were measured with a two-way analysis of variance (ANOVA) followed by a *post hoc* holm-sidak test. For the other data, one-way ANOVA followed by Sidak's test was used for comparison among three groups, and unpaired *t*-test was used for comparison among two groups. All the error bars represent mean ± standard error of the mean (SEM) unless specified otherwise. And p-value < 0.05 was considered as statistically significant. For each analysis, the results from independent animals were treated as biological replicates ($n \geq 3$).

RESULTS

Itpr2 Is Selectively Up-Regulated in Newly Differential Oligodendrocytes

A recent study suggested that *Itpr2* is strongly expressed in postnatal oligodendrocytes (Zeisel et al., 2015; Marques et al., 2016). To determine the specificity and developmental stages of *Itpr2* expression during oligodendrocyte development, we first performed RNA *in situ* hybridization (ISH) in the CNS tissues from different developmental stages. In the brain region, *Itpr2* expression started to emerge in the corpus callosum (CC) at around postnatal day (P7) stage, increased progressively thereafter (**Figures 1A,B**). By P15, its expression was detected throughout the entire CC tissue (**Figure 1C**). However, at P30, its expression was significantly down-regulated (**Figure 1D**). Similarly, in the spinal cord region, *Itpr2* was detected in the white matter glial cells starting at about embryonic day 18.5 (E18.5), and the number of $Itpr2^{+}$ cells gradually increased with time and reached the maximum at P3-P7 stages (**Supplementary Figures 1A–D**). At later postnatal stages, *Itpr2* expression was gradually diminished in the white matter of spinal cord (**Supplementary Figures 1E,F**). The spatiotemporal pattern of *Itpr2* expression suggests its selective up-regulation in differentiating OLs (**Figures 1A–D** and **Supplementary Figures 1A–F**).

To further confirm that *Itpr2* is indeed expressed in differentiating OLs, we next examined the expression of *Itpr2* in the spinal cords of $Cnp^{cre/+}$; $Nkx2.2^{fl/fl}$ and $Olig^{cre/+}$; $Myrf^{fl/fl}$ mice. In the *Olig1*-Cre mouse line, the Cre activity is expressed in OPCs and mature OLs (Lu et al., 2002), whereas in the *Cnp*-Cre mouse line, the Cre is primarily expressed in early differentiating OLs (Yu et al., 1994; Baumann and Pham-Dinh, 2001). The $Cnp^{cre/+}$; $Nkx2.2^{fl/fl}$ conditional mutant mice

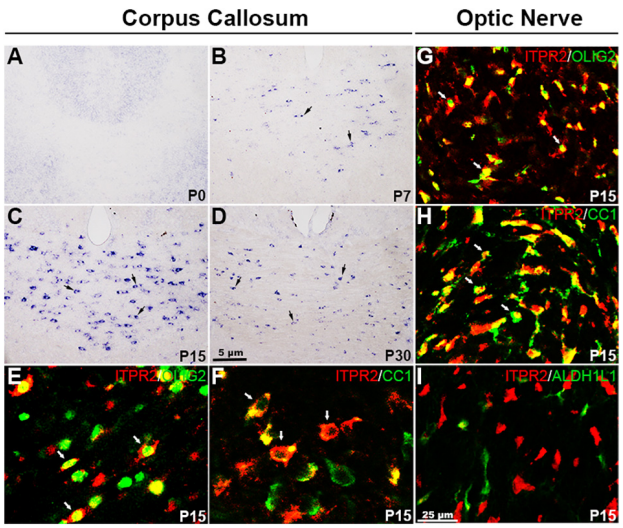

FIGURE 1 | *Itpr2* is selectively up-regulated in differentiating OLs in the CNS. **(A–D)** Expression of *Itpr2* in the forebrain tissues as detected by RNA *in situ* hybridization (ISH). Black arrows highlight *Itpr2*$^{+}$ cells. The number of *Itpr2* positive cells in the corpus callosum increased progressively from P7 to P15 and then decreased gradually thereafter. Scale bar represents 5 μm. **(E,F)** Double immunofluorescence of anti-ITPR2 combined with anti-OLIG2 or anti-CC1 in P15 corpus callosum. Double positive cells are represented by white arrows. CC, corpus callosum; CTX, Cortex. **(G–I)** Representative images of ITPR2^{+} cells that co-express OLIG2, CC1 but not ALDH1L1 in P15 optic nerve. Scale bar represents 25 μm.

delayed OPC differentiation in the spinal cord (Q. Zhu et al., 2014), while *Olig*$^{cre/+}$; *Myrf*$^{fl/fl}$ mice arrested oligodendrocyte differentiation and myelin gene expression (Emery et al., 2009; McKenzie et al., 2014; Xiao et al., 2016). As expected, the number of *Itpr2*$^{+}$ cells was dramatically reduced in both *Nkx2.2* and *Myrf* conditional knock-out mice compared to the control groups (**Supplementary Figure 2**).

The selective expression of ITPR2 in differentiating OLs was further validated by double immunostaining with two well-established oligodendrocyte markers, CC1 and OLIG2, in P15 brain. Indeed, the majority of ITPR2-positive cells were co-stained with the newly formed OL marker CC1 (Cai et al., 2010; Young et al., 2013) or the general oligodendrocyte lineage marker OLIG2 in the corpus callosum (**Figures 1E,F**) and the optic nerves (**Figures 1G,H**). In addition, ITPR2^{+} cells did not co-express the astrocyte lineage marker ALDH1L1 in the optic nerves at early postnatal stage (**Figure 1I**). Similarly, ITPR2^{+} cells in P4-P7 spinal tissues (white matter) also co-expressed OLIG2 and CC1 but not with neuronal marker NeuN (**Supplementary Figures 1G–J**). Together, these data manifest that *Itpr2* is highly and selectively expressed in differentiating OLs in early postnatal CNS tissues, suggestive of its important role in OL maturation and myelination.

Delayed Oligodendrocyte Differentiation in *Itpr2* Mutant Brain

To assess the *in vivo* role of *Itpr2* in regulating OLs differentiation and myelin development, we next examined the expression of mature OL marker *Plp1* in postnatal brain tissues by ISH. It was found that the number of *Plp1*$^{+}$ myelinating OLs in *Itpr2*$^{-/-}$ corpus callosum was significantly lower than that of controls between P7 and P15 stages (**Figures 2A–B′,D**) when OLs undergo active differentiation and myelination in this region (Franco-Pons et al., 2006; Korrell et al., 2019). Intriguingly, the number of *Plp1*$^{+}$ OLs was not altered in P21 control

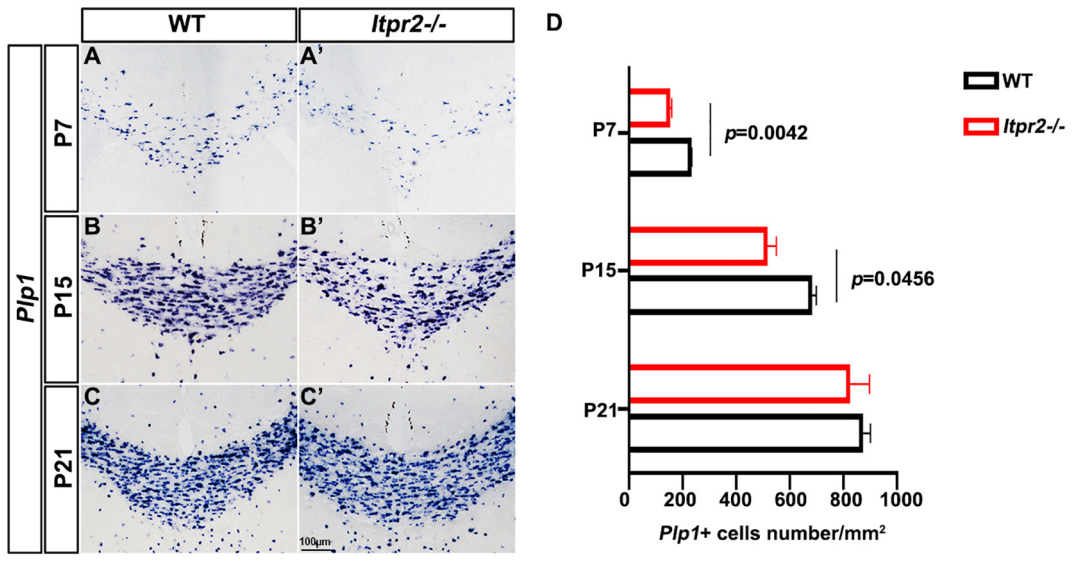

FIGURE 2 | Ablation of *Itpr2* gene delays the differentiation of oligodendrocytes. **(A–C′)** *Plp1* mRNA expression in coronal forebrain sections of wild-type **(A–C)** and *Itpr2-KO* **(A′–C′)** mice at indicated stages. **(D)** Quantification of *Plp1*$^{+}$ cells per section ($n = 3$) in the corpus callosum of *Itpr2KO* mice. Error bars indicate Means ± SEM. Scale bar represents 100 μm.

and mutant tissues (**Figures 2C,C′,D**). These results indicate a transient developmental delay of OL differentiation when *Itpr2* gene is inactivated.

Increased Percentage of Small Diameter Myelinated Axons in *Itpr2* Mutants

To examine the effects of ITPR2 ablation on axonal myelination, we performed transmission electron microscopy (TEM) analysis on cross-sections of the corpus callosum (CC) and the optic nerve (ON) of postnatal day 60 (P60) wild-type and $Itpr2^{-/-}$ mice (**Figures 3A–B′**). Strikingly, ultrastructural analyses showed that there were significantly more myelinated axons in CC of $Itpr2^{-/-}$ mice compared with the controls. And optic nerve tissues showed a similar number of myelinated axons between wild-type and $Itpr2^{-/-}$ mice (**Supplementary Figure 5**). To evaluate whether axons of a certain caliber were more severely affected in the absence of ITPR2, we quantified the relative frequency of myelinated axons with respect to their corresponding diameters. Quantitative analyses showed that a larger proportion of myelinated axons had small diameters (0.2–0.7 μm) in the CC region of mutants, and the percentage of myelinated axons with large diameters was markedly reduced (larger than 1.5 μm) (**Figure 3C**; Two-way ANOVA *P*-values summary: interaction: $F = 4.720$, $p = 0.0036$; axon diameter: $F = 36.29$, $p = 0.0010$; genotype: $F = 0.7167$, $p = 0.4359$. For small diameters, WT: $59.95 \pm 0.4234\%$, $Itpr2^{-/-}$: $76.34 \pm 4.492\%$; for large diameters, WT: $7.68 \pm 0.9467\%$, $Itpr2^{-/-}$: $0.13 \pm 0.07336\%$). Similarly, the proportion of small-diameter myelinated axons in the *Itpr2* mutant optic nerve also increased significantly, while the large-diameter myelinated axons decreased (**Figure 3D**; Two-way ANOVA *P*-values summary: interaction: $F = 11.61$, $p < 0.0001$; axon diameter: $F = 111.1$, $p < 0.0001$; genotype: $F = 0.5946$, $p = 0.4837$. For small diameters, WT: $28.71 \pm 0.3378\%$, $Itpr2^{-/-}$: $43.35 \pm 0.9538\%$; for large diameters, WT: $14.48 \pm 1.055\%$, $Itpr2^{-/-}$: $6.33 \pm 1.253\%$). Thus, *Itpr2* mutation significantly reduced the diameters of myelinated axons. As a whole group, g-ratios were unaltered in the corpus callosum and optic nerves between the two groups of animals, but the g-ratios in different diameter range displayed different trends. As the scatter plots of g-ratio against axon caliber showed the small-diameter myelinated axons exhibited smaller g-ratios indicative of thicker myelin sheath in the mutant CC and optic nerves, while the large-diameter myelinated axons showed the opposite result (**Figures 3E,F**). Together, these data manifest that *Itpr2* deficiency altered the size population of myelinated axons in the CNS, increasing the percentage of smaller axons for myelination.

Reduced Conduction Velocity in the *Itpr2* Deficient Central Nervous System

Previous studies showed CAP recorded from rodent optic nerve is polyphasic in profile, with total area under the CAP as an index of nerve function. It is suggested that the CAP is related to the composition of the axons (Evans et al., 2010). To further confirm our results, we recorded the CAP of optic nerves from wild-type, $Itpr2^{-/-}$ and *Itpr2cKO* mice (**Figure 4A**). With the increase of stimulation intensity, the total CAP area increased continuously and finally reached a stable plateau for control, *Itpr2cKO* and *KO* groups (**Figure 4B**). However, the total CAP area was significantly decreased in *Itpr2cKO* and *KO* mice compared to wild-type mice (**Figure 4D**; One-way ANOVA, $F = 18485$, $p < 0.0001$). The typical evoked CAP response was polyphasic in profile (**Figure 4C**), which is in line with the previous findings (Govind and Lang, 1976; Evans et al., 2010; Horowitz et al., 2015). Prior studies showed that CAP could exhibit multiple peaks, with the largest diameter axons contributing to the 1st CAP peak and the smaller axons contributing to the 2nd and 3rd CAP peaks (Evans et al., 2010). Thus, the shift in the relative proportion of small vs. large axons would suggest that the peaks of the axons shift in size. Compared to the control groups, the first peak became smaller in both *Itpr2cKO* and *KO* groups (**Figure 4E**; One-way ANOVA, $F = 18485$, $p < 0.0001$), in agreement with our electron microscopy results (**Figure 3**). We also found that the values for the latency for the 1st peak increased in the *Itpr2cKO* and *KO* mice compared to wild-type mice (**Figure 4F**; One-way ANOVA, $F = 29.99$, $p < 0.0001$). Collectively, these data indicated that a higher proportion of smaller myelinated fibers in *Itpr2* mutant mice adversely affected their CAP in the CNS.

Increased Percentage of Type I/II Oligodendrocytes Was Increased in *Itpr2* Mutants

We next explored the possible mechanism underlying the increased percentage of small caliber axons that are myelinated in the mutants. Early studies identified four types of oligodendrocytes, among which $CAII^+$ type I/II OLs tend to myelinate small caliber axons (Butt et al., 1998; Butt and Berry, 2000). Thus, we next investigated the possibility that the delayed OL differentiation in the mutants may cause an increased proportion of type I/II OLs, leading to a higher percentage of smaller myelinated axons. Immunostaining of the wild-type brain tissues revealed that at P4, $CAII^+/CC1^+$ double positive cells were rarely seen in the corpus callosum (**Figure 5A**). At P7, a small number of $CAII^+$ positive cells began to emerge in the corpus callosum (**Figure 5B**). By P15, the density of $CAII^+/CC1^+$ type I/II cells was significantly increased in the corpus callosum (**Figures 5C,D**), suggesting that the type I/II group were later-born OLs. Consistently, the percentage of $CAII^+SOX10^+$ OLs in $SOX10^+$ population (white arrows) in *Itpr2* mutant mice was significantly elevated in the white matter at all postnatal stages examined (**Figures 5E–H**). A similar increase in the ratio of $CAII^+SOX10^+$ OLs was also found in the *Itpr2* conditional mutant (*cKO*) brain tissues (**Figures 5I–L**). Together, these data strongly suggest that the delayed OL differentiation in *Itpr2* deficiency results in an increased ratio of type I/II oligodendrocytes.

Given that ITPR2 is the main receptor for intracellular release of calcium, it is plausible that Ca^{2+} signaling may be involved in the differentiation of OL subtypes. To address this possibility, membrane permeable Ca^{2+} chelator BAPTA-AM was applied to brain slice culture of *Sox10-GFP* mice to block intracellular calcium release. After 5 days of treatment, brain slices were subjected to CAII immunostaining (**Figure 5M**). Consistent with

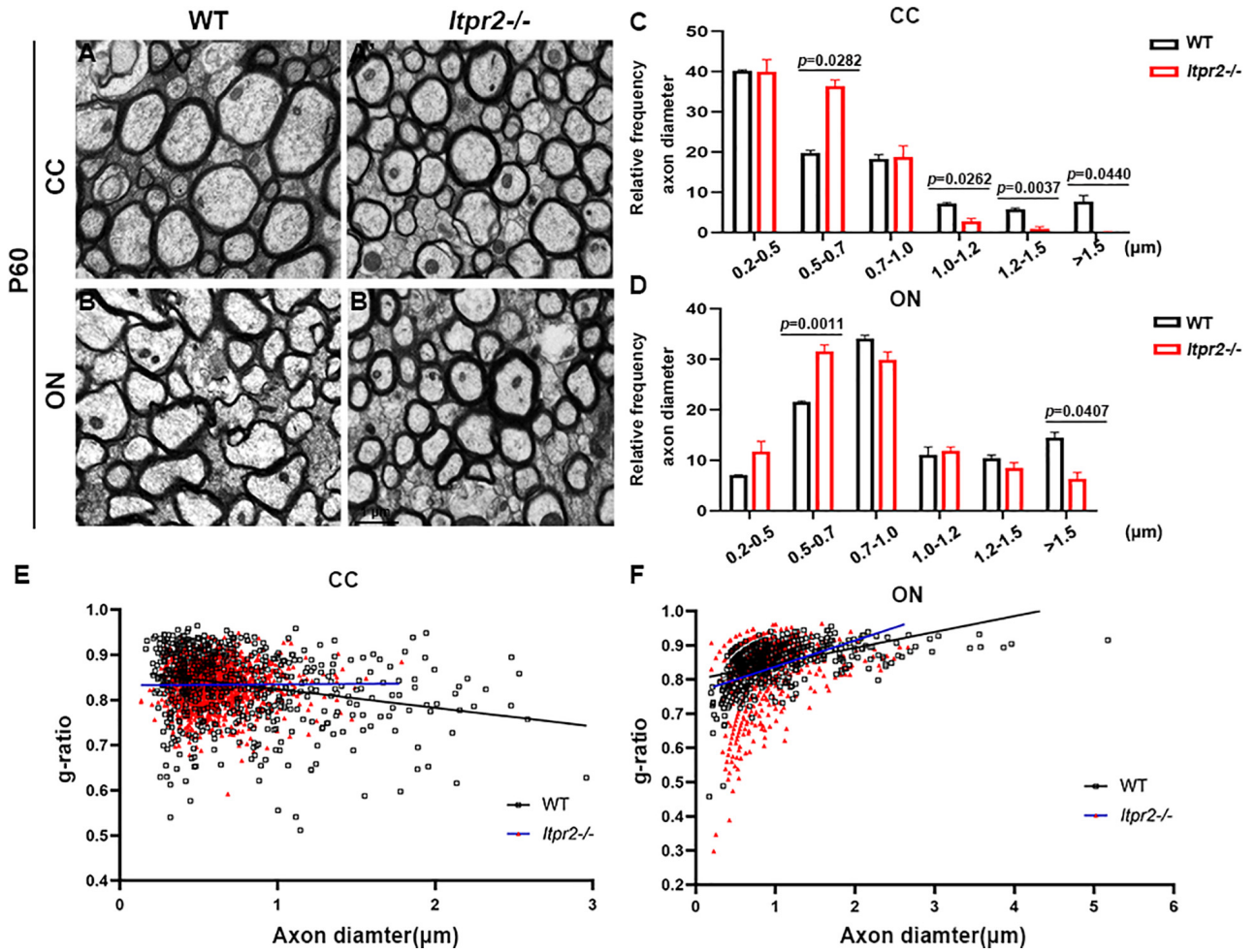

FIGURE 3 | Knockout *Itpr2* increases the percentage of small-diameter myelinated axons in corpus callosum and optic nerve. **(A–B′)** Electron microscopy images of the corpus callosum (CC) **(A,A′)** and optic nerve (ON) **(B,B′)** from P60 wild-type and *Itpr2*$^{-/-}$ mice. Scale bar represents 1 μm. **(C)** Quantification of percentage of myelinated axons in the corpus callosum by size. An increased number of myelinated small-diameter axons (<0.7 μm) and a decreased number of myelinated large-diameter axons (>1.5 μm) were observed in *Itpr2* mutants. Two-way ANOVA *P*-values summary: interaction: $F = 4.720$, $p = 0.0036$; axon diameter: $F = 36.29$, $p = 0.0010$; genotype: $F = 0.7167$, $p = 0.4359$. **(D)** The distribution of axonal size in optic nerve is similar to that in the corpus callosum. Two-way ANOVA *P*-values summary: interaction: $F = 11.61$, $p < 0.0001$; axon diameter: $F = 111.1$, $p < 0.0001$; genotype: $F = 0.5946$, $p = 0.4837$. **(E)** The relationship between diameters and g-ratios of axons from the corpus callosum of wild-type and *Itpr2KO* mice at P60. Averaged g-ratios were 0.836 ± 0.007 (wild-type, 654 axons from 3 animals, black squares) and 0.833 ± 0.008 (*Itpr2*$^{-/-}$, 1,447 axons from 4 animals, red triangles), $p = 0.72$. **(F)** The relationship between diameters and g-ratios of axons from the optic nerve of wild-type and *Itpr2KO* mice at P60. Averaged g-ratios were 0.858 ± 0.001 (wild-type, 635 axons from 3 animals, black squares) and 0.825 ± 0.070 (*Itpr2*$^{-/-}$, 696 axons from 3 animals, red triangles), $p = 0.55$. Error bars indicate Means ± SEM.

the *in vivo* findings, the density of CAII^{+} type I/II OLs was significantly increased after treatment with 20 μm BAPTA-AM (**Figures 5N,N′,O**). Thus, disruption of ITPR2 gene and blocking intracellular calcium release had the same effect of significantly increasing the proportion of type I/II oligodendrocytes both *in vivo* and *in vitro*.

The ERK1/2 pathway has been shown to be critical for OL differentiation both *in vitro* and *in vivo* (Guardiola-Diaz et al., 2012; Chen et al., 2015; Rodgers et al., 2015; Mei et al., 2021). Previous studies have shown that the release of calcium from intracellular stores can stimulate the ERK activity which can directly influence OL differentiation (Kim et al., 2020). Consequently, we conjectured whether preventing the release of intracellular calcium influx by deletion of ITPR2 can down-regulate the ERK phosphorylation level. To test this possibility, we examined the expression of CNPase, ERK and p-ERK via Western blotting (**Figures 6A,D**), and found a decrease of CNPase expression and p-ERK level in the brainstem of *Itpr2cKO* and *KO* mice at P7 and P15, while the total level of ERK protein was not significantly altered (**Figures 6B,C,E,F**). Thus, the expression of CNPase and ERK phosphorylation level was indeed down-regulated in the conventional and conditional mutant brainstem at early developmental stages. Taken together, our studies suggest that ITPR2 deletion may affect the differentiation of oligodendrocytes and the ratio of type I/II oligodendrocytes by abating Ca^{2+}-dependent ERK activation.

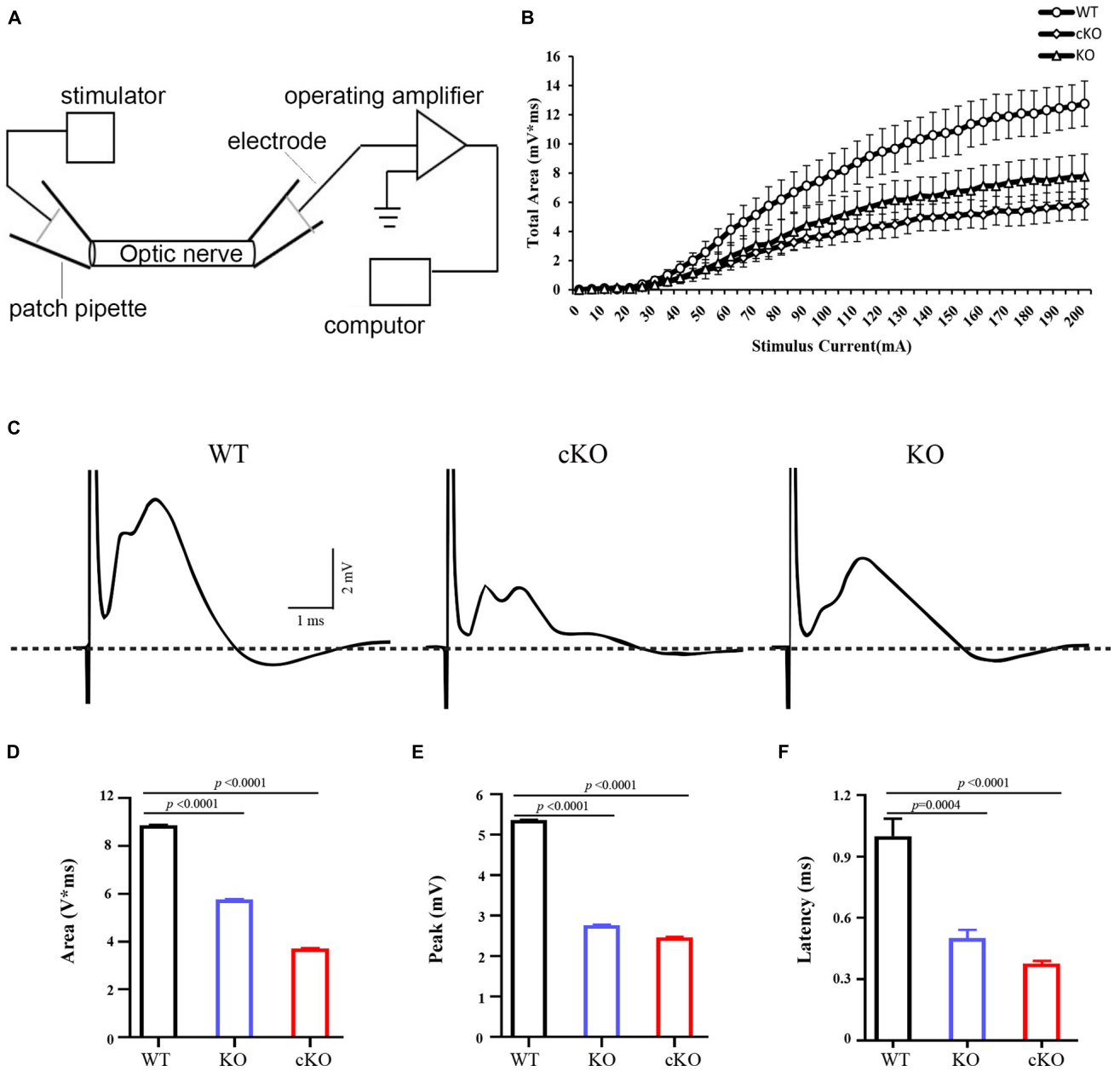

FIGURE 4 | Electrophysiological measurements of CAP from optic nerves. **(A)** The diagram of electrophysiological measurements of CAP from optic nerve. **(B)** Normalized total CAP area of optic nerves showing a S-type growth in response to increasing stimulus current ($n = 5, 7, 4$). **(C)** Representative 70% maximum CAP of optic nerves from wild-type (WT), conditional knockout (*cKO*) and conventional mutants (*KO*) mice. The large stimulus artifact has been truncated and is followed by a polyphasic waveform peaks. And compared to the control groups, the first peak became smaller and the third peak became larger in the *Itpr2 cKO* and *KO* groups. **(D)** Analysis of the values for the CAP area (WT: 8.878 ± 0.01151 mV*ms, *KO*: 5.759 ± 0.03151 mV*ms, *cKO*: 3.713 ± 0.01563 mV*ms, one-way ANOVA, $F = 14817$, $p < 0.0001$, $n = 6, 6, 6.$) in the optic nerves. **(E)** Analysis of the values for CAP peak (WT: 5.364 ± 0.01007 mV, *KO*: 2.763 ± 0.01365 mV, *cKO*: 2.464 ± 0.01118 mV, one-way ANOVA, $F = 18485$, $p < 0.0001$, $n = 6, 6, 6$) in the optic nerves. **(F)** Analysis of the values for CAP latency (WT: 1.000 ± 0.08515 ms, *KO*: 0.5000 ± 0.04082 ms, *cKO*: 0.3750 ± 0.01443 ms, one-way ANOVA, $F = 29.99$, $p < 0.0001$, $n = 5, 4, 4.$) in the optic nerves. Error bars indicate Means ± SEM.

DISCUSSION

Oligodendrocytes arise from specific regions of neural epithelium and then migrate to the entire CNS before they differentiate and form myelin sheaths wrapping around neuronal axons. These progressive processes are accurately controlled by a large number of intracellular factors and extracellular signals. Calcium signaling emerges as an important regulator for oligodendrocyte development and axonal myelination (Soliven, 2001). There are three IP_3R subtypes (ITPR1-3) in mammals

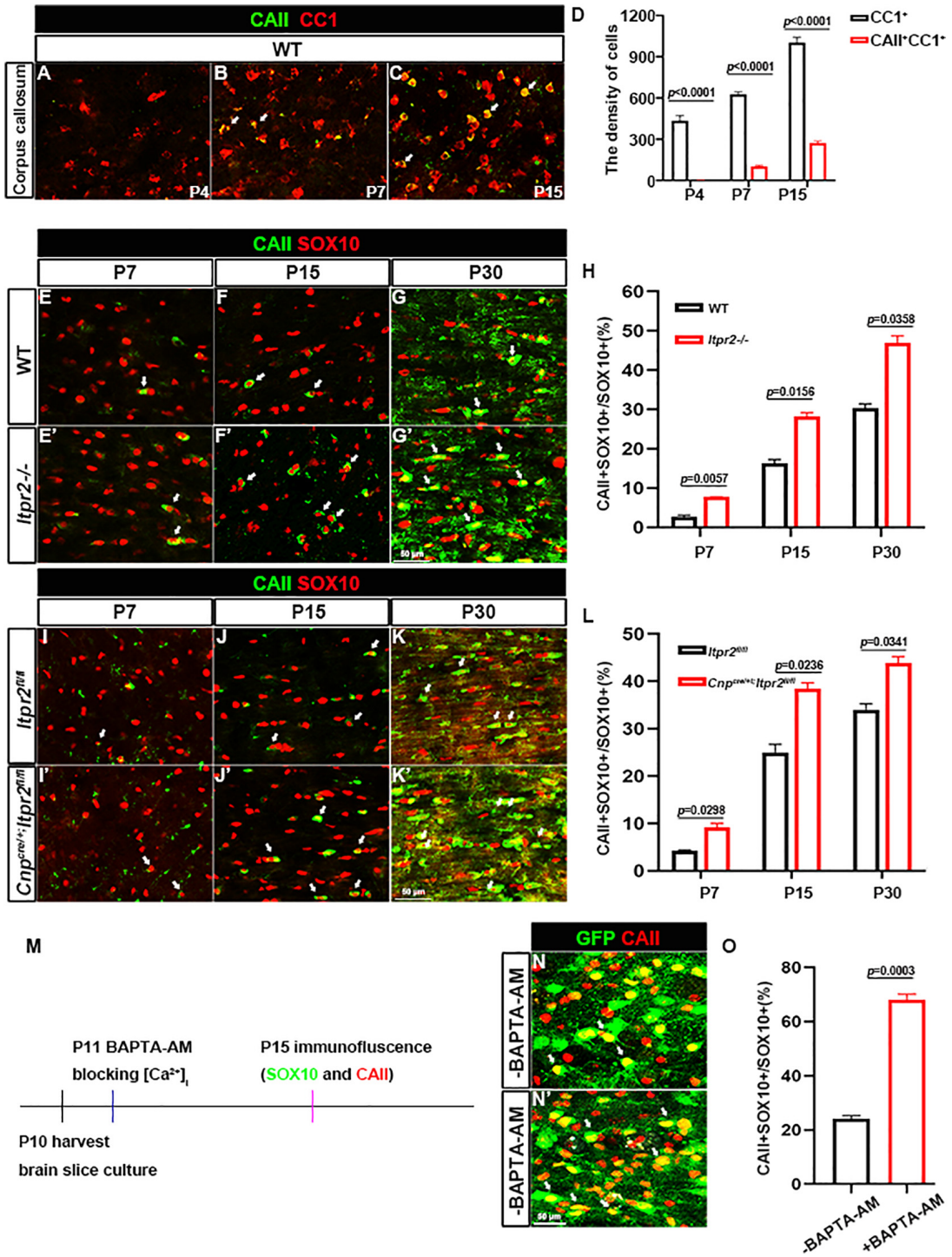

FIGURE 5 | Disruption of ITPR2 increases the proportion of type I/II oligodendrocytes. **(A–C)** Double immunostaining of CAII and CC1 in early postnatal brain tissues. **(D)** Quantification of the density of CC1 positive cells and CAII/CC1 double positive cells in the corpus callosum of wild-type mice. **(E–G′)** Immunofluorescent images of CAII and SOX10 staining in corpus callosum tissues from various stages of WT and *Itpr2-/-*mice. Double positive cells are represented by white arrows. **(H)** Quantitative analysis of the ratio of CAII^{+} cells in SOX10^{+} oligodendrocytes at indicated stages. **(I–K′)** CAII and SOX10 double-immunostaining in corpus callosum tissues from various stages of control and *Cnp*$^{cre/+}$; *Itpr2*$^{fl/fl}$ mice. Double positive cells are represented by white arrows. Scale bar represents 50 μm. **(L)** Quantitative analysis of the percentage of CAII^{+} cells in SOX10^{+} oligodendrocytes at indicated stages. **(M)** Schematic of workflow of organotypic slice cultures. **(N,N′)** Immunostaining of CAII in the corpus callosum of cultured *Sox10-GFP* slices. Compared with the control groups, the ratio of CAII^{+}SOX10^{+} oligodendrocytes remarkably increased in the corpus callosum of cultured slices treated with 20 μM BAPTA-AM. Scale bar represents 50 μm. **(O)** Quantification of the percentage of CAII/SOX10-GFP double positive cells in SOX10-GFP^{+} population in brain slice culture from **(N,N′)**. Error bar indicates Means ± SEM. $n \geq 3$.

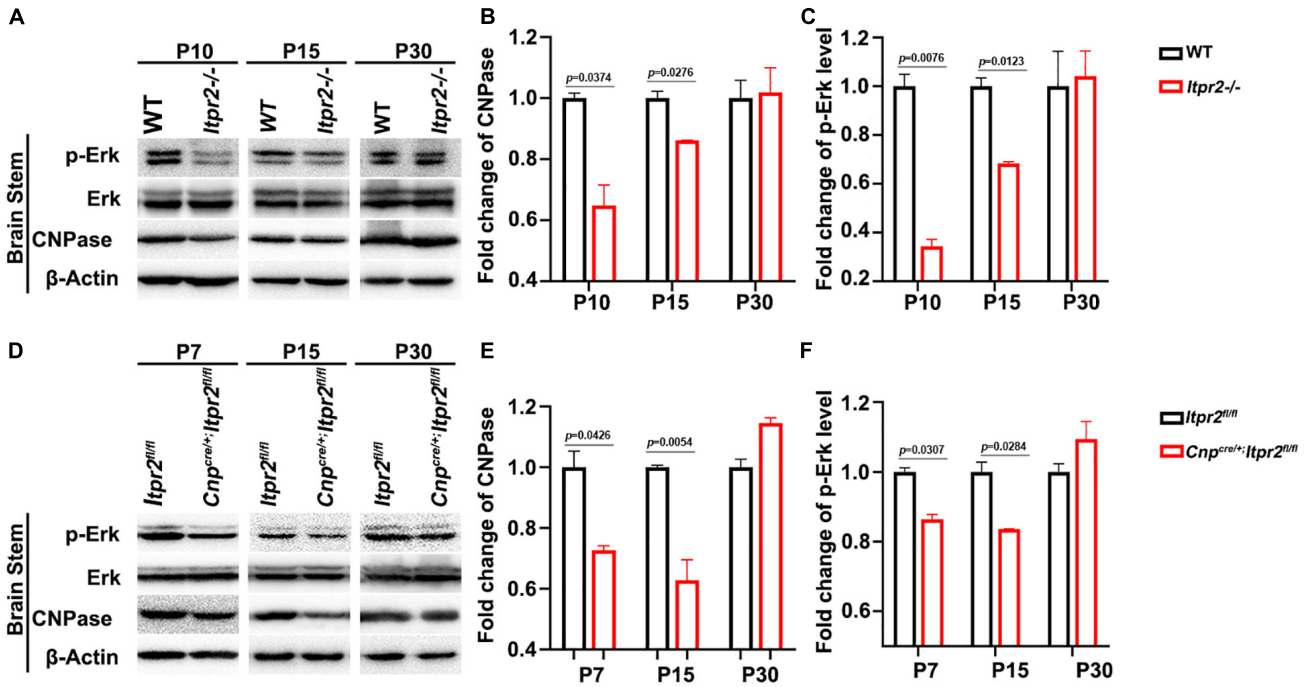

FIGURE 6 | *Itpr2* deletion inhibits the Ca^{2+}-dependent ERK activation. **(A)** The expression and phosphorylation of ERK, CNPase and ERK in brainstem tissues from wild-type and $Itpr2^{-/-}$ mice at P10, P15 and P30 in grouping image. β-actin was used as the internal control. **(B)** Quantification of CNPase protein level in the brainstem of $Itpr2^{-/-}$ mice which were normalized to the wild-type group. **(C)** Quantification of ERK1/2 phosphorylation level in the brainstem of $Itpr2^{-/-}$ mice which were normalized to the wild-type group. **(D)** The expression and phosphorylation of ERK, CNPase, and ERK in brainstem tissues from control and $Cnp^{cre/+}$; $Itpr2^{fl/fl}$ mice at P7, P15, and P30 in grouping image. β-actin was used as the internal control. **(E)** Quantification of CNPase protein level in the brainstem of $Cnp^{cre/+}$; $Itpr2^{fl/fl}$ mice which were normalized to the control group. **(F)** Quantification of ERK phosphorylation level in the brainstem of $Cnp^{cre/+}$; $Itpr2^{fl/fl}$ mice which were normalized to the control group. Error bar indicates Means ± SEM. $n = 3$.

(Furuichi et al., 1994). We found that only ITPR2 is highly expressed in differentiating OLs, consistent with the recent studies with RNA-seq analyses showing that *Itpr2* is expressed in cells of oligodendrocyte lineage (Zeisel et al., 2015; Marques et al., 2016). Expression of the other two isoforms is not detected in the white matter in both control and $Itpr2^{-/-}$ spinal tissues (**Supplementary Figure 3**), indicating a lack of compensatory up-regulation of *Itpr1/3* in the absence of *Itpr2*. Based on these findings, we believe that ITPR2 is the predominant channel responsible for intracellular release of calcium in OLs.

Our expression analyses established that *Itpr2* is highly up-regulated in differentiating OLs at early postnatal stages (**Figure 1** and **Supplementary Figure 1**) when oligodendrocytes undergo active differentiation and myelination (Franco-Pons et al., 2006; Korrell et al., 2019). In fact, its expression is not detected in immature OPCs in embryonic tissues and is downregulated after axonal myelination in adult tissues (**Figure 1** and **Supplementary Figure 1**). The strong expression of *Itpr2* in differentiating OLs suggests its important role in regulating OL differentiation and myelin formation. In support of this idea, *Itpr2* deficiency induced a transient developmental delay of OL differentiation and myelin gene expression (**Figure 2**). The delayed OL differentiation in the mutants is apparently associated with the abnormal myelin sheath development and axonal function, as suggested by the marked increase in the percentage of small diameter myelinated axons in the corpus callosum and optic nerve, and the abnormal CAP in *Itpr2* knockout (**Figures 3**, **4**). Since our expression analyses clearly demonstrate that *Itpr2* is not expressed in neurons or astrocytes at the early postnatal stages when oligodendrocyte differentiating, we would argue that the phenotypic alterations observed in both conventional and conditional mutants are cell-autonomous and attributed to defects in oligodendrocyte development. Consistent with this idea, deleting *Itpr2* in conditional mutants does not appear to affect the expression of astrocyte markers in the corpus callosum or neuronal markers in the cortex (**Supplementary Figure 4**).

It was previously demonstrated that type I/II oligodendrocytes predominantly myelinate small diameter axons, and these myelin sheaths display fewer lamellae and shorter internodal lengths (Butt and Berry, 2000). In keeping with this early finding, we detected an increased population of type I/II OLs in *Itpr2* mutant brain tissues (**Figure 5**). Meanwhile, the ratio of small diameter myelinated axons to larger ones is increased in the mutant tissues, which negatively impacts the saltatory conduction of electrical signals. It has been previously demonstrated that the generation of the precise number of OLs is necessary to myelinate entirely a given population of axons (Barres et al., 1992; Burne et al., 1996; Barres and Raff, 1999), and that small fiber diameter (0.2–0.4 μm) is sufficient to initiate wrapping by oligodendrocytes (Lee et al., 2012). It is conceivable that an excess number of type I/II

OLs shifts myelination to smaller diameter axons, and the ratio of small/large diameter myelinated axons was altered together with the conduction velocity of electrical signals. A similar observation was made in $Gab1^{f/f}$; $Olig1^{cre/+}$ mice, in which ablation *Gab1* in the OLs resulted in delayed OL differentiation and an increased proportion of small-diameter axons being myelinated (Zhou et al., 2020). At this stage, it is not known why type I/II OLs are associated with small caliber axons. One possibility is that these late-born OLs fail to provide certain trophic or nourishing factors for further growth of myelinated axons. Alternatively, ITPR2 deficiency may affect the formation of Ca^{2+} wave which in turn affects the neuronal activity that has been suggested to regulate the sizes of axon (Sinclair et al., 2017). In addition, earlier reports have showed that ERK signaling pathway is necessary for oligodendrocyte differentiation (Sun et al., 2013; Gaesser and Fyffe-Maricich, 2016). Interestingly, the release of calcium from intracellular stores can stimulate the ERK activity (Kim et al., 2020). Our data have shown that *Itpr2* expression is correlated with the elevation of ERK phosphorylation (**Figure 6**), raising the possibility that ITPR2 might regulate oligodendrocyte differentiation via the intracellular calcium-dependent activation of the ERK pathway.

In summary, our studies provide the important molecular and genetic evidence that *Itpr2* is dramatically up-regulated in differentiating OLs and regulates OL differentiation and myelin development. To our knowledge, this is the first report that ITPR2-mediated calcium signaling can directly affect the differentiation of OL subtypes possibly through an ERK-dependent mechanism, and therefore influence the development of myelinated axons.

DATA AVAILABILITY STATEMENT

The raw data supporting the conclusions of this article will be made available by the authors, without undue reservation.

ETHICS STATEMENT

The animal study was reviewed and approved by the Animal Ethics Committee of Hangzhou Normal University, China.

AUTHOR CONTRIBUTIONS

MQ and XZ conceived the main ideas and supervised the project. RM and LH performed most of the experimental operations. MW and CJ carried out the main parts of the numerical calculations. RM, AY, and HT carried out the rest of them. KZ, JY, WS, and XC conceived the experiments and supervised this research. All authors discussed and interpreted the results, and reviewed the manuscript.

FUNDING

This work was supported by the National Natural Sciences Foundation of China (32070965, 32000684, and 31771621).

SUPPLEMENTARY MATERIAL

The Supplementary Material for this article can be found online at: https://www.frontiersin.org/articles/10.3389/fncel.2021.751439/full#supplementary-material

Supplementary Figure 1 | Expression pattern of ITPR2 in the spinal cord. **(A–F)** *Itpr2* ISH in mouse spinal cord from E18.5 to P30. Scale bar represents 25 μm. Black arrows highlight *Itpr2*$^{+}$ cells. **(G–J)** ITPR2 double immunofluorescence with anti-OLIG2, anti-CC1 or anti- NeuN in P4, and P7 spinal cord sections. ITPR2 positive cells are mostly co-labeled with OLIG2 and CC1 (white arrows), but not with anti-NeuN. Scale bar represents 50 μm.

Supplementary Figure 2 | Expression of *Itpr2* in *Nkx2.2-cKO* **(A,B)** and *Myrf-cKO*. **(C,D)** Mutant spinal cords is dramatically reduced at P3 stages. Scale bar represents 100 μm.

Supplementary Figure 3 | Disruption of *Itpr2* has no effect on *Itpr1* and *Itpr3* expression in the white matter. Spinal cord tissues from P3 **(A–D)** and P7 **(E–H)** wild-type and *Itpr2*$^{-/-}$ mice were examined for expression of *Itpr1* and *Itpr3* by ISH. Scale bar represents 100 μm.

Supplementary Figure 4 | ITPR2 deletion produces no difference to the astrocytes in the corpus callosum and neurons in the cortex. Brain tissues from P15 wild-type and *Itpr2* knockout mice were immunostaining with astrocyte marker GFAP **(A,B)** and neuron marker NeuN **(C,D)**. Scale bar represents 50 μm.

Supplementary Figure 5 | Analyses of the number of myelinated axons in the corpus callosum **(A)** and optic nerves **(B)** from wild-type and *Itpr2-/–* mice. Error bar indicates Means ± SEM. $n \geq 3$.

REFERENCES

Allen, L., Anderson, S., Wender, R., Meakin, P., Ransom, B. R., Ray, D. E., et al. (2006). Fructose supports energy metabolism of some, but not all, axons in adult mouse optic nerve. *J. Neurophysiol.* 95, 1917–1925. doi: 10.1152/jn.00637.2005

Barres, B. A., and Raff, M. C. (1999). Axonal control of oligodendrocyte development. *J Cell Biol.* 147, 1123–1128.

Barres, B. A., Hart, I. K., Coles, H. S., Burne, J. F., Voyvodic, J. T., Richardson, W. D., et al. (1992). Cell death and control of cell survival in the oligodendrocyte lineage. *Cell* 70, 31–46.

Baumann, N., and Pham-Dinh, D. (2001). Biology of oligodendrocyte and myelin in the mammalian central nervous system. *Physiol. Rev.* 81, 871–927. doi: 10.1152/physrev.2001.81.2.871

Berry, M., Hunter, A. S., Duncan, A., Lordan, J., Kirvell, S., Tsang, W. L., et al. (1998). Axon-glial relations during regeneration of axons in the adult rat anterior medullary velum. *J. Neurocytol.* 27, 915–937. doi: 10.1023/a:1006953107636

Burne, J. F., Staple, J. K., and Raff, M. C. (1996). Glial cells are increased proportionally in transgenic optic nerves with increased numbers of axons. *J. Neurosci.* 16, 2064–2073.

Butt, A. M., and Berry, M. (2000). Oligodendrocytes and the control of myelination in vivo: new insights from the rat anterior medullary velum. *J. Neurosci Res.* 59, 477–488. doi: 10.1002/(sici)1097-4547(20000215)59:4<477::Aid-jnr2<3.0.Co;2-j

Butt, A. M., Ibrahim, M., Gregson, N., and Berry, M. (1998). Differential expression of the L- and S-isoforms of myelin associated glycoprotein (MAG) in oligodendrocyte unit phenotypes in the adult rat anterior medullary velum. *J. Neurocytol.* 27, 271–280. doi: 10.1023/a:1006996713413

Butt, A. M., Ibrahim, M., Ruge, F. M., and Berry, M. (1995). Biochemical subtypes of oligodendrocyte in the anterior medullary velum of the rat as revealed by the monoclonal antibody Rip. *Glia* 14, 185–197. doi: 10.1002/glia.440140304

Cai, J., Zhu, Q., Zheng, K., Li, H., Qi, Y., Cao, Q., et al. (2010). Co-localization of Nkx6.2 and Nkx2.2 homeodomain proteins in differentiated myelinating oligodendrocytes. *Glia* 58, 458–468. doi: 10.1002/glia.20937

Chen, Y., Mei, R., Teng, P., Yang, A., Hu, X., Zhang, Z., et al. (2015). TAPP1 inhibits the differentiation of oligodendrocyte precursor cells via suppressing the Mek/Erk pathway. *Neurosci. Bull.* 31, 517–526. doi: 10.1007/s12264-015-1537-5

Edgar, N., and Sibille, E. (2012). A putative functional role for oligodendrocytes in mood regulation. *Transl. Psychiatry* 2:e109. doi: 10.1038/tp.2012.34

Emery, B., Agalliu, D., Cahoy, J. D., Watkins, T. A., Dugas, J. C., Mulinyawe, S. B., et al. (2009). Myelin gene regulatory factor is a critical transcriptional regulator required for CNS myelination. *Cell* 138, 172–185. doi: 10.1016/j.cell.2009.04.031

Evans, R. D., Weston, D. A., McLaughlin, M., and Brown, A. M. (2010). A non-linear regression analysis method for quantitative resolution of the stimulus-evoked compound action potential from rodent optic nerve. *J. Neurosci. Methods* 188, 174–178. doi: 10.1016/j.jneumeth.2010.02.004

Fanarraga, M. L., Griffiths, I. R., Zhao, M., and Duncan, I. D. (1998). Oligodendrocytes are not inherently programmed to myelinate a specific size of axon. *J. Comp. Neurol.* 399, 94–100.

Fields, R. D. (2008). White matter in learning, cognition and psychiatric disorders. *Trends Neurosci.* 31, 361–370. doi: 10.1016/j.tins.2008.04.001

Franco-Pons, N., Virgos, C., Vogel, W. F., Urena, J. M., Soriano, E., del Rio, J. A., et al. (2006). Expression of discoidin domain receptor 1 during mouse brain development follows the progress of myelination. *Neuroscience* 140, 463–475. doi: 10.1016/j.neuroscience.2006.02.033

Furuichi, T., Kohda, K., Miyawaki, A., and Mikoshiba, K. (1994). Intracellular channels. *Curr. Opin. Neurobiol.* 4, 294–303.

Gaesser, J. M., and Fyffe-Maricich, S. L. (2016). Intracellular signaling pathway regulation of myelination and remyelination in the CNS. *Exp. Neurol.* 283, 501–511. doi: 10.1016/j.expneurol.2016.03.008

Govind, C. K., and Lang, F. (1976). Growth of lobster giant axons: correlation between conduction velocity and axon diameter. *J. Comp. Neurol.* 170, 421–433. doi: 10.1002/cne.901700403

Guardiola-Diaz, H. M., Ishii, A., and Bansal, R. (2012). Erk1/2 MAPK and mTOR signaling sequentially regulates progression through distinct stages of oligodendrocyte differentiation. *Glia* 60, 476–486. doi: 10.1002/glia.22281

Haak, L. L., Song, L. S., Molinski, T. F., Pessah, I. N., Cheng, H., and Russell, J. T. (2001). Sparks and puffs in oligodendrocyte progenitors: cross talk between ryanodine receptors and inositol trisphosphate receptors. *J. Neurosci.* 21, 3860–3870.

Horowitz, A., Barazany, D., Tavor, I., Bernstein, M., Yovel, G., and Assaf, Y. (2015). In vivo correlation between axon diameter and conduction velocity in the human brain. *Brain Struct. Funct.* 220, 1777–1788. doi: 10.1007/s00429-014-0871-0

HP, D. R. (1928). Tercera aportación al conocimiento morfológico e interpretación funcional de la oligodendroglía. *Memor. Real Soc. Esp. Hist. Nat.* 14, 5–122.

Kim, J., Adams, A. A., Gokina, P., Zambrano, B., Jayakumaran, J., Dobrowolski, R., et al. (2020). Mechanical stretch induces myelin protein loss in oligodendrocytes by activating Erk1/2 in a calcium-dependent manner. *Glia* 68, 2070–2085. doi: 10.1002/glia.23827

Korrell, K. V., Disser, J., Parley, K., Vadisiute, A., Requena-Komuro, M. C., Fodder, H., et al. (2019). Differential effect on myelination through abolition of activity-dependent synaptic vesicle release or reduction of overall electrical activity of selected cortical projections in the mouse. *J. Anat.* 235, 452–467. doi: 10.1111/joa.12974

Lappe-Siefke, C., Goebbels, S., Gravel, M., Nicksch, E., Lee, J., Braun, P. E., et al. (2003). Disruption of Cnp1 uncouples oligodendroglial functions in axonal support and myelination. *Nat. Genet.* 33, 366–374. doi: 10.1038/ng1095

Lee, S., Leach, M. K., Redmond, S. A., Chong, S. Y., Mellon, S. H., Tuck, S. J., et al. (2012). A culture system to study oligodendrocyte myelination processes using engineered nanofibers. *Nat. Methods* 9, 917–922. doi: 10.1038/nmeth.2105

Li, X., Zima, A. V., Sheikh, F., Blatter, L. A., and Chen, J. (2005). Endothelin-1-induced arrhythmogenic Ca2+ signaling is abolished in atrial myocytes of inositol-1,4,5-trisphosphate(IP3)-receptor type 2-deficient mice. *Circ. Res.* 96, 1274–1281. doi: 10.1161/01.RES.0000172556.05576.4c

Lu, Q. R., Sun, T., Zhu, Z., Ma, N., Garcia, M., Stiles, C. D., et al. (2002). Common developmental requirement for Olig function indicates a motor neuron/oligodendrocyte connection. *Cell* 109, 75–86. doi: 10.1016/s0092-8674(02)00678-5

Marques, S., Zeisel, A., Codeluppi, S., van Bruggen, D., Mendanha Falcao, A., Xiao, L., et al. (2016). Oligodendrocyte heterogeneity in the mouse juvenile and adult central nervous system. *Science* 352, 1326–1329. doi: 10.1126/science.aaf6463

Martins-de-Souza, D. (2010). Proteome and transcriptome analysis suggests oligodendrocyte dysfunction in schizophrenia. *J. Psychiatr. Res.* 44, 149–156. doi: 10.1016/j.jpsychires.2009.07.007

Mastracci, T. L., Lin, C. S., and Sussel, L. (2013). Generation of mice encoding a conditional allele of Nkx2.2. *Transgenic Res.* 22, 965–972. doi: 10.1007/s11248-013-9700-0

McKenzie, I. A., Ohayon, D., Li, H., de Faria, J. P., Emery, B., Tohyama, K., et al. (2014). Motor skill learning requires active central myelination. *Science* 346, 318–322. doi: 10.1126/science.1254960

Mei, R., Fu, J., Jiang, C., Yang, J., Zheng, K., Yang, A., et al. (2021). TAPP1 represses the differentiation of oligodendrocyte and its deficiency accelerates myelin regeneration after demyelinating injuries. *Neurosci. Bull.* 37, 385–388. doi: 10.1007/s12264-020-00609-0

Miron, V. E., Kuhlmann, T., and Antel, J. P. (2011). Cells of the oligodendroglial lineage, myelination, and remyelination. *Biochim. Biophys. Acta.* 1812, 184–193. doi: 10.1016/j.bbadis.2010.09.010

Nave, K. A. (2010). Myelination and support of axonal integrity by glia. *Nature* 468, 244–252. doi: 10.1038/nature09614

O'Leary, M. T., and Blakemore, W. F. (1997). Use of a rat Y chromosome probe to determine the long-term survival of glial cells transplanted into areas of CNS demyelination. *J. Neurocytol.* 26, 191–206. doi: 10.1023/a:1018536130578

Paez, P. M., Cheli, V. T., Ghiani, C. A., Spreuer, V., Handley, V. W., and Campagnoni, A. T. (2012). Golli myelin basic proteins stimulate oligodendrocyte progenitor cell proliferation and differentiation in remyelinating adult mouse brain. *Glia* 60, 1078–1093. doi: 10.1002/glia.22336

Ray, S. K., Schaecher, K. E., Shields, D. C., Hogan, E. L., and Banik, N. L. (2000). Combined TUNEL and double immunofluorescent labeling for detection of apoptotic mononuclear phagocytes in autoimmune demyelinating disease. *Brain Res. Brain Res. Protoc.* 5, 305–311. doi: 10.1016/s1385-299x(00)00027-1

Rodgers, J. M., Robinson, A. P., Rosler, E. S., Lariosa-Willingham, K., Persons, R. E., Dugas, J. C., et al. (2015). IL-17A activates ERK1/2 and enhances differentiation of oligodendrocyte progenitor cells. *Glia* 63, 768–779. doi: 10.1002/glia.22783

Sharp, A. H., Nucifora, F. C. Jr., Blondel, O., Sheppard, C. A., Zhang, C., Snyder, S. H., et al. (1999). Differential cellular expression of isoforms of inositol 1,4,5-triphosphate receptors in neurons and glia in brain. *J. Comp. Neurol.* 406, 207–220.

Sinclair, J. L., Fischl, M. J., Alexandrova, O., Hebeta, M., Grothe, B., and Leibold, C. (2017). Sound-evoked activity influences myelination of brainstem axons in the trapezoid body. *J. Neurosci.* 37, 8239–8255. doi: 10.1523/jneurosci.3728-16.2017

Soliven, B. (2001). Calcium signalling in cells of oligodendroglial lineage. *Microsc. Res. Tech.* 52, 672–679. doi: 10.1002/jemt.1051

Sun, J., Fang, Y., Chen, T., Guo, J., Yan, J., Song, S., et al. (2013). WIN55, 212-2 promotes differentiation of oligodendrocyte precursor cells and improve remyelination through regulation of the phosphorylation level of the ERK 1/2 via cannabinoid receptor 1 after stroke-induced demyelination. *Brain Res.* 1491, 225–235. doi: 10.1016/j.brainres.2012.11.006

Tripathi, R. B., Clarke, L. E., Burzomato, V., Kessaris, N., Anderson, P. N., Attwell, D., et al. (2011). Dorsally and ventrally derived oligodendrocytes have similar electrical properties but myelinate preferred tracts. *J. Neurosci.* 31, 6809–6819. doi: 10.1523/jneurosci.6474-10.2011

Tsutsui, S., and Stys, P. K. (2013). Metabolic injury to axons and myelin. *Exp. Neurol.* 246, 26–34. doi: 10.1016/j.expneurol.2012.04.016

Xiao, L., Ohayon, D., McKenzie, I. A., Sinclair-Wilson, A., Wright, J. L., Fudge, A. D., et al. (2016). Rapid production of new oligodendrocytes is required in the earliest stages of motor-skill learning. *Nat. Neurosci.* 19, 1210–1217. doi: 10.1038/nn.4351

Young, K. M., Psachoulia, K., Tripathi, R. B., Dunn, S. J., Cossell, L., Attwell, D., et al. (2013). Oligodendrocyte dynamics in the healthy adult CNS: evidence for myelin remodeling. *Neuron* 77, 873–885. doi: 10.1016/j.neuron.2013.01.006

Yu, W. P., Collarini, E. J., Pringle, N. P., and Richardson, W. D. (1994). Embryonic expression of myelin genes: evidence for a focal source of oligodendrocyte

precursors in the ventricular zone of the neural tube. *Neuron* 12, 1353–1362. doi: 10.1016/0896-6273(94)90450-2

Zeisel, A., Munoz-Manchado, A. B., Codeluppi, S., Lonnerberg, P., La Manno, G., Jureus, A., et al. (2015). Brain structure. Cell types in the mouse cortex and hippocampus revealed by single-cell RNA-seq. *Science* 347, 1138–1142. doi: 10.1126/science.aaa1934

Zhou, L., Shao, C. Y., Xie, Y. J., Wang, N., Xu, S. M., Luo, B. Y., et al. (2020). Gab1 mediates PDGF signaling and is essential to oligodendrocyte differentiation and CNS myelination. *Elife* 9:e52056. doi: 10.7554/eLife.52056

Zhu, Q., Zhao, X., Zheng, K., Li, H., Huang, H., Zhang, Z., et al. (2014). Genetic evidence that Nkx2.2 and Pdgfra are major determinants of the timing of oligodendrocyte differentiation in the developing CNS. *Development* 141, 548–555. doi: 10.1242/dev.095323

Zhu, Y., Li, H., Li, K., Zhao, X., An, T., Hu, X., et al. (2013). Necl-4/SynCAM-4 is expressed in myelinating oligodendrocytes but not required for axonal myelination. *PLoS One* 8:e64264. doi: 10.1371/journal.pone.0064264

Conflict of Interest: The authors declare that the research was conducted in the absence of any commercial or financial relationships that could be construed as a potential conflict of interest.

Publisher's Note: All claims expressed in this article are solely those of the authors and do not necessarily represent those of their affiliated organizations, or those of the publisher, the editors and the reviewers. Any product that may be evaluated in this article, or claim that may be made by its manufacturer, is not guaranteed or endorsed by the publisher.

frontiers | Frontiers in Cellular Neuroscience

TYPE Mini Review
PUBLISHED 13 October 2022
DOI 10.3389/fncel.2022.1025012

OPEN ACCESS

EDITED BY
Hiroaki Wake,
Nagoya University, Japan

REVIEWED BY
Patrick D. Parker,
Johns Hopkins University,
United States

*CORRESPONDENCE
Lukas Valihrach
lukas.valihrach@ibt.cas.cz
Miroslava Anderova
miroslava.anderova@iem.cas.cz

SPECIALTY SECTION
This article was submitted to Non-Neuronal Cells, a section of the journal Frontiers in Cellular Neuroscience

RECEIVED 22 August 2022
ACCEPTED 22 September 2022
PUBLISHED 13 October 2022

CITATION
Valihrach L, Matusova Z, Zucha D, Klassen R, Benesova S, Abaffy P, Kubista M and Anderova M (2022) Recent advances in deciphering oligodendrocyte heterogeneity with single-cell transcriptomics. *Front. Cell. Neurosci.* 16:1025012. doi: 10.3389/fncel.2022.1025012

Recent advances in deciphering oligodendrocyte heterogeneity with single-cell transcriptomics

Lukas Valihrach[1,2]*, Zuzana Matusova[1,3], Daniel Zucha[1,4], Ruslan Klassen[1,5], Sarka Benesova[1,4], Pavel Abaffy[1], Mikael Kubista[1,6] and Miroslava Anderova[2]*

[1]Laboratory of Gene Expression, Institute of Biotechnology of the Czech Academy of Sciences, Vestec, Czechia, [2]Department of Cellular Neurophysiology, Institute of Experimental Medicine of the Czech Academy of Sciences, Prague, Czechia, [3]Faculty of Science, Charles University, Prague, Czechia, [4]Department of Informatics and Chemistry, Faculty of Chemical Technology, University of Chemistry and Technology, Prague, Czechia, [5]Department of Biochemistry and Microbiology, Faculty of Food and Biochemical Technology, University of Chemistry and Technology, Prague, Czechia, [6]TATAA Biocenter AB, Gothenburg, Sweden

Oligodendrocytes (OL) have been for decades considered a passive, homogenous population of cells that provide support to neurons, and show a limited response to pathological stimuli. This view has been dramatically changed by the introduction of powerful transcriptomic methods that have uncovered a broad spectrum of OL populations that co-exist within the healthy central nervous system (CNS) and also across a variety of diseases. Specifically, single-cell and single-nucleus RNA-sequencing (scRNA-seq, snRNA-seq) have been used to reveal OL variations in maturation, myelination and immune status. The newly discovered immunomodulatory role suggests that OL may serve as targets for future therapies. In this review, we summarize the current understanding of OL heterogeneity in mammalian CNS as revealed by scRNA-seq and snRNA-seq. We provide a list of key studies that identify consensus marker genes defining the currently known OL populations. This resource can be used to standardize analysis of OL related datasets and improve their interpretation, ultimately leading to a better understanding of OL functions in health and disease.

KEYWORDS

oligodendrocyte, heterogeneity, scRNA-seq, snRNA-seq, populations, marker genes

Introduction

OLs represent a type of glial cells found in the CNS of invertebrates and vertebrates. Their primary role is to envelop the axons of the neurons in myelin, which provides insulation and maintains the electrical impulse conduction. Since their first description in 1921, they have been considered a heterogeneous population, displaying variable

morphology and spatial distribution (Del Rio-Hortega, 1921). However, decades of subsequent research have led to the general understanding that OLs are instead a homogenous population of cells, without any major functional heterogeneity. It was not until recently that advances in single-cell analysis revealed a new spectrum and sources of OL heterogeneity, including their variations related to differentiation state, developmental origin, anatomical site, age and sex (for an extensive review, see Seeker and Williams, 2022).

A completely new area of OL characterization started with the advent of single-cell transcriptomic techniques allowing analysis of thousands of cells, each characterized by the activity of thousands of genes. The first landmark studies characterizing OL transcriptional heterogeneity were performed on single cells in healthy animals (Zeisel et al., 2015, 2018; Marques et al., 2016). The introduction of protocols for the analysis of single nuclei isolated from archived samples facilitated the expansion and application of the technique to investigations from human tissues. Currently, we are experiencing a boom in transcriptional studies characterizing OLs in a variety of pathological conditions and disease states, rapidly extending our understanding of OL heterogeneity. However, with the increasing number of scRNA-seq and snRNA-seq studies, and the enormous complexity of the information embedded within each dataset, there is a new challenge for OL researchers that is the comparison and the interpretation of newly acquired data with existing studies. Although this step is not mandatory and often missed in reports, it provides an important insight into the general function of OLs, potentially transferring knowledge derived from one particular model to a broader spectrum of pathological states.

The process of data interpretation using other studies as reference is typically done by comparing selected marker genes to a defined OL population or by integrative analysis. The relation of OL populations is then assessed by the overlap of these marker genes or by enrichment type of analysis. The downside is that the calculation of marker genes is heavily influenced by the data processing and the particular downstream analysis, which biases the comparison of populations. Integrative analysis is therefore a more robust way to interpret new data (Stuart and Satija, 2019). Integration allows merging of data for the unified processing of multiple datasets, even if they are derived using different protocols or experimental models. Although more robust, this method is biased by the choice and settings of the integration tool. Finally, the choice of reference studies is of uttermost importance. This is far from trivial as features of OL heterogeneity of interest, may be hidden in studies characterizing completely unrelated biological questions.

To guide OL researchers in the wealth of current knowledge, we prepared a compact review summarizing the current understanding of OL heterogeneity in health and disease based on single-cell and single-nucleus transcriptomic technologies. Our motivation is to provide the community a unified overview of key transcriptomic studies dealing with OL heterogeneity in the mammalian CNS (**Table 1**) and consensus marker genes of selected OL populations (**Table 2**). We hope that the interpretation of new datasets with respect to those already available will lead to a standardization of OL nomenclature and our better understanding of their transcriptional heterogeneity.

Oligodendrocyte heterogeneity in health

Since the advent of scRNA-seq analysis, there have been efforts to classify the CNS cell types. Early datasets comprised only of tens of cell types represented by hundreds to thousands of cells. The low proportion of OLs did not allow for their in-depth characterization or the OLs were not the primary focus of the studies. The first milestone deciphering OL heterogeneity was made in murine CNS, in studies published by researchers from the Division of Molecular Neurobiology at Karolinska Institute (Zeisel et al., 2015, 2018; Marques et al., 2016).

The study of Zeisel et al. (2015) focused on somatosensory cortex and hippocampal CA1 region of juvenile mice, and analyzed over 3,000 cells, including more than 800 OLs. Clustering revealed six OL populations representing various stages of maturation: post-mitotic, immature, pre-myelinating, myelinating, intermediate, and terminally differentiated post-myelination OLs. Marques et al. (2016) provided further details by analyzing over 5,000 cells of OL lineage in 10 regions of murine juvenile and adult CNS. In total, they observed 12 clusters of OL lineage, representing a continuum from oligodendrocyte precursor cells (OPC) to mature OLs (OPC, COP, NFOL1-2, MFOL1-2, and MOL1-6; **Table 2**). Whereas the initial stages of OL maturation (to MFOL1-2) were found sequential and uniform across CNS regions, mature OLs showed regional specificity, being present in unique proportions in each brain region. Moreover, cells sampled from adult mice comprised mostly of OPCs and two populations of mature OLs (MOL5-6), while juvenile cells were represented by the full spectrum of the OL populations. Lastly, the study of Zeisel et al. (2018) expanded the scope of the previous datasets by analyzing 19 CNS regions, counting over half a million of cells, with a large fraction comprising of OLs. Their analysis identified 10 clusters of OL lineage (OPC, COP1-2, NFOL1-2, MFOL1-2, MOL1-3; **Table 2**), but even with the increased sample size, it did not reveal any additional OL subtypes beyond those already described by Marques et al. (2016). Notably, despite the large similarity of the two datasets, there was not a perfect cluster match, probably due to different scRNA-seq technology and data processing protocols used. These differences might be possible to remove with integrative analysis, standardizing the nomenclature, and defining a set of consensus marker genes for future studies. For now, the marker genes and the reference for interpretation of new datasets might be selected based on

TABLE 1 Selection of key transcriptomic studies for understanding OL heterogeneity in health and disease*.

Study	Species (mouse/human)	Condition	Methods	# of OL cluster (incl. OPCs)	Significance	Accession number (custom database if available)
Zeisel et al. (2015)	Mouse	Ctrl	scRNA-seq	6	First large-scale scRNA-seq study of all cell types in mouse CTX and HC	GSE60361 (link)
Marques et al. (2016)	Mouse	Ctrl	scRNA-seq	12	First large-scale OL focused scRNA-seq study in mouse CNS	GSE75330 (link)
Zeisel et al. (2018)	Mouse	Ctrl	scRNA-seq	10	First large-scale scRNA-seq of all cell types in mouse CNS	SRP135960 (link)
Falcao et al. (2018)	Mouse	Ctrl, EAE	scRNA-seq	14	First scRNA-seq defining disease related OL clusters	GSE113973 (link)
Jakel et al. (2019)	Human	Ctrl, MS	snRNA-seq	9	First OL focused snRNA-seq of MS patients and healthy controls	GSE118257 (link)
Mathys et al. (2019)	Human	Ctrl, AD	snRNA-seq	5	First large-scale snRNA-seq of AD patients and healthy controls	syn18485175
Floriddia et al. (2020)	Mouse	Ctrl, SCI	ISH/ISS, scRNA-seq	11	Spatial distribution of mature OLs in WM and GM of murine brain and SC	GSE128525 (link)
Zhou et al. (2020)	Both	Ctrl, AD	snRNA-seq	2–5	Description of *Serpina3n*$^{+}$ *C4b*$^{+}$ reactive OLs in AD mice	GSE140511, syn21125841
Chen et al. (2020)	Both	Ctrl, AD	ISS, ST	–	Spatial characterization of plaque-induced transcriptomic response in AD	GSE152506, syn22153884 (link)
Lee et al. (2021)	Mouse	Ctrl, AD	scRNA-seq	7–8	Description of two disease-associated OL clusters across three AD models	GSE160512, GSE181786, GSE153895
Yao et al. (2021)	Mouse	Ctrl	sc + snRNA-seq, snATAC-seq, snmC-seq2	9	BICCN—transcriptomic and epigenomic cell atlas of mouse CTX	nemo:dat-ch1nqb7 (link)
Bakken et al. (2021)	Both	Ctrl	snRNA-seq, snmC-seq2, SNARE-seq2	4–9	BICCN—comparison of motor CTX in human, marmoset and mouse	nemo:dat-ek5dbmu (link)
Russ et al. (2021)	Mouse	Ctrl	sc + snRNA-seq	5	Harmonized atlas of mouse SC cell types (six integrated datasets)	GSE158380 (link)
Morabito et al. (2021)	Human	Ctrl, AD	snRNA-seq, snATAC-seq	14–15	Chromatin accessibility and transcriptomic characterization of AD	syn22079621 (link)
Bartosovic et al. (2021)	Mouse	Ctrl	scCUT&Tag	5	scCUT&Tag profiling of histone modification and TFs in murine OLs	GSE163532 (link)
Hilscher et al. (2022)	Mouse	Ctrl	ISS	12	Spatial distribution of OL populations from Marques et al. (2016)	Data not available
Sadick et al. (2022)	Human	Ctrl, AD	snRNA-seq	7	OL integration in multiple human AD datasets	GSE167494 (link)
Kenigsbuch et al. (2022)	Mouse	Ctrl, EAE, aging	scRNA-seq	14	Definition of DOLs in murine models of AD, MS and aging	GSE202297
Kaya et al. (2022)	Mouse	Aging	scRNA-seq	4–7	Identification of interferon-responsive OLs during WM aging	Data not yet released
Yadav et al. (2022)	Human	Ctrl	snRNA-seq, ST	8	Cellular taxonomy of adult human SC	GSE190442 (link)
Meijer et al. (2022)	Both	Ctrl, EAE	snATAC-seq, multiome	12	In-depth epigenomic analysis of immune genes in OLs	GSE166179 (link)
Pandey et al. (2022)	Both	AD, MS	sc + snRNA-seq, smFISH	4–17	Characterization of three OL activation states across disease models	GSE180041, GSE182846 (link)

*For a curated database of all available single-cell transcriptomics studies with key experimental information (see Svensson et al., 2020).
Ctrl, healthy conditions; EAE, experimental autoimmune encephalomyelitis; MS, multiple sclerosis; AD, Alzheimer's disease; SCI, spinal cord injury; ISH, *in situ* hybridization; ISS, *in situ* sequencing; snATAC-seq, single-nucleus assay for transposase-accessible chromatin using sequencing; snmC-seq2, single nucleus methylcytosine sequencing; SNARE–seq2, single-nucleus chromatin accessibility and messenger RNA expression sequencing; snRNA/ATAC multiome, Chromium Single Cell Multiome ATAC + Gene Expression; ST, Spatial transcriptomics (Visium, 10x Genomics); smFISH, multiplexed single-molecule fluorescence *in situ* hybridization; CTX, cortex; HC, hippocampus; WM/GM, white/gray matter; SC, spinal cord; TFs, transcription factors; DOLs, disease-associated oligodendrocytes.

TABLE 2 Marker genes of selected OL populations as reported by authors.

Study	OL clusters	Gene signature	Source
Marques et al. (2016)	OPC	*Ptprz1, Pdgfra, Serpine2, Cspg5, Vcan, Cspg4*	**Supplementary Table 1**—Top 6 marker genes of each branch of the dendrogram in **Figure 1C** (out of 50). For subclusters of the same differentiation stage, top 3 genes defining the stage and top3 genes defining the subcluster were selected. Of note, the list of genes is strictly related to the dendrogram in **Figure 1C**.
	COP	*Cd9, Neu, 43110035E14Rik, Bmp4, Gpr17, Vcan*	
	NFOL1	*9630013A20Rik, Arpc1b, Tmem2, Chn2, Mpzl1, Frmd4a*	
	NFOL2	*9630013A20Rik, Arpc1b, Tmem2, Mobp, Ddr1, Tspan2*	
	MFOL1	*Ctps, Tmem141, Opalin, 9630013A20Rik*	
	MFOL2	*Ctps, Tmem141, Opalin, Mal, Ptgds, Evi2a-evi2b*	
	MOL1	*Apod, Sepp1, S100b, Fosb, Dusp1, Dnajb1*	
	MOL2	*Apod, Sepp1, S100b, Anxa5, Klk6, Mgst3*	
	MOL3	*Apod, Sepp1, S100b, Car2, Cntn2, Gad2*	
	MOL4	*Apod, Sepp1, S100b, Serpinb1a, Neat1, Sepp1*	
	MOL5	*Apod, Sepp1, S100b, Cyp51, Dhcr24, Pdlim2*	
	MOL6	*Apod, Sepp1, S100b, Il33, Apoe, Ptgds*	
Zeisel et al. (2018)	OPC	*Pdgfra, C1ql1, Sapcd2, Emid1, Lhfpl3*	**Supplementary Table 4**—Combination of markers genes uniquely identifying populations based on "trinarization" scoring procedure developed by authors.
	COP1	*Neu4, Brca1, Bmp4, Pak4, Lims2*	
	COP2	*Tnr, Rinl, Gpr17, Enpp6, Pdcd4*	
	NFOL1	*Cnksr3, H2-Ab1, Rras2, Il23a, Tmem163*	
	NFOL2	*Tmem2, Gm26834, Rras2, Itpr2, Sema4d*	
	MFOL1	*Ccp110, Snx33, Hhip, Tmem88b, Arap2*	
	MFOL2	*2210011C24Rik, Wfdc18, Tmem141, Birc2, Fam214a*	
	MOL1	*Opalin, Ninj2, Efhd1, Mal, Ppp1r14a*	
	MOL2	*Hapln2, Dock5, Anln, Ugt8a, Gjb1*	
	MOL3	*Klk6, Nkx2-9, Cdkn1c, Rab37, 2700046A07Rik*	
Falcao et al. (2018)	EAE_m1	*Serpina3m, Klk8, Serpina3c, Serping1, Irf7, Cd74, Ifih1*	**Supplementary Figure 4B**—Representative genes for EAE-associated modules (sortable list in **Supplementary Table 1**)
	EAE_m3	*Lyz2, C4b, Serpina3n, Klk6, Igtp, Irgm2, Ccdc13*	
	EAE_m13	*Plin4, Hif3a, Fam107a, Phyhd1, Cdkn1a, Sult1a1*	
Jakel et al. (2019)	ImOLs	*ARHGAP24, MEF2C, C10orf11, APOE, CD74, DOCK8, PLXDC2, ELL2, APBB1IP, HLA.DRA, C3, PTPRC*	**Supplementary Figure 8C**—Selection of key markers (sortable list in **Supplementary Table 4**)
Zhou et al. (2020)	Reactive OLs	*C4b, Serpina3n, H2-d1*	**Figure 2A**—Three highlighted marker genes (sortable list in **Supplementary Table 1**)
Lee et al. (2021)	MOL-DA1	*C4b, Serpina3n*	**Figure 2D**—Selected marker genes (full list in **Supplementary Table 8**)
	MOL-DA2	*C4b, Serpina3n, Cdkn1a, Ddit3, Gadd45a*	
Yao et al. (2021)	OPC Pdgfra	*Col14a1, Cnr1, Gad2, Spock3, Sema3c, Zfp385b*	**Supplementary Table 6**—Top 6 marker genes for each consensus OL population (full list available)
	Oligo Enpp6_1	*Col14a1, Kcnip1, Cxcl14, Spock3, Sema3c, Chrna7*	
	Oligo Enpp6_2	*Col14a1, Gad2, Cxcl14, Cnr1, Rab3c, A830018L16Rik*	
	Oligo Enpp6_3	*Col14a1, Grik1, Cxcl14, Spock3, Sema3c, Necab1*	
	Oligo Enpp6_4	*Kcnip1, Gad1, Col14a1, Gad2, Grik1, Pax6*	
	Oligo Opalin_1	*Adarb2, Grip1, Col14a1, Kcnip1, Gad1, Dab1*	
	Oligo Opalin_2	*A830018L16Rik, Kcnip1, Col14a1, Grik1, Slc2a13, Gad1*	
	Oligo Opalin_3	*Grip1, Col14a1, Kcnip1, A830018L16Rik, Grik1, Gad1*	
	Oligo Opalin_4	*Col14a1, Kcnip1, Gad1, Maf, Shisa9, Neto1*	
Sadick et al. (2022)	Int0	*SVEP1, LINC01608, PLXDC2, DYSF*	**Figure 3E**—Selection of top markers of four integrated OL datasets (sortable list in **Supplementary Table 5**)
	Int1	*CTNNA2, CNDP1, ST3GAL6, QDPR, CRYAB*	
	Int2	*FP236383.3, MT-ND4, MT-ND3, MT-CO2, MT-ATP6*	
	Int3	*ACTN2, SLC5A11, RASGRF1, LINC00609, ANKRD18A*	
	Int4	*SGCZ, MDGA2, CNTN1, KCNIP4, FRY*	
	Int5	*RBFOX1, AFF3, ACSBG1, COL18A1*	
	Int6	*NRP2, LUCAT1, NAV2, CAMK2D, NEAT1*	
Kenigsbuch et al. (2022)	DOLs	*Serpina3n, C4b, H2-d1, H2-k1, B2m, Il33, Klk6, CD9, CD63*	**Figure 2F**—Highlighted marker genes
Pandey et al. (2022)	MOL-DA1	*Serpina3n, C4b, Anxa2, Plvap, Thbs3, Steap3, Emp3, Parvb, S100a10, Tnfrsf1a, Col6a1, Sema4f*	**Figure 2B**—Selected marker genes (sortable list in **Supplementary Table 2**)
	MOL-DA2	*Cdkn1a, Bax, Ddit3, Fos, Atf4, Egr1, Ccnd1, Tnfrsf12a, Btg1, Egr2, Klf4, Fgf7, Rrad, Gdf15*	
	MOL-INF	*H2-d1, Stat1, Bst2, Igtp, Psmb8, Irgm1, Ifit1, Irf7, Psme1, Oasl2, H2-q4, Tap1, Ifit2*	
Kaya et al. (2022)	AROs IROs	*C4b, Serpina3n, Socs3, Vim, Gadd45a, Bbc3* *Ifi27l2a, H2-k1, Usp18, B2m, Stat1*	**Figure 1G**—Highlighted marker genes

OPC, oligodendrocyte precursor cells; COP, committed OL; NFOL, newly formed OL; MFOL, myelin forming OL; MOL, mature OL; EAE, experimental autoimmune encephalomyelitis; ImOLs, immune OLs; MOL-DA, mature OL disease-associated; Int, integrated cluster of OLs, DOLs, disease-associated OLs; MOL-INF, mature OL interferon-associated; AROs, aging-related OLs; IROs, interferon-responsive OLs.

specific preferences. While the annotation used by Marques et al. (2016) has been applied in several subsequent studies (Falcao et al., 2018; Jakel et al., 2019; Floriddia et al., 2020; Bartosovic et al., 2021; Hilscher et al., 2022; Meijer et al., 2022; Pandey et al., 2022) and has become a standard in the field, an advantage of the Zeisel et al. (2018) annotation are the region-specific references rich in OLs, whose transcriptome was measured with the widely used 10x Genomics technology.

The classification of OLs in human CNS lagged behind the progress in mouse because of practical constrains in obtaining fresh samples for isolation of single cells. This has since changed with the introduction of protocols for the analysis of single nuclei, making it possible to process archived samples from the human brain biobanks. Using snRNA-seq, the first studies comprised of only a small number of OLs, limiting the annotation to a few clusters vaguely reflecting OL maturation (Habib et al., 2017; Lake et al., 2018). The first comprehensive characterization was a study describing altered OL heterogeneity in the white matter (WM) of five healthy donors and four individuals with progressive multiple sclerosis (MS) (Jakel et al., 2019). The authors identified seven clusters of mature OLs (Oligo1-6 and ImOLs), and clusters of OPC and committed oligodendrocyte precursors (COP). Integrative analysis with two previous datasets (Habib et al., 2017; Lake et al., 2018), re-annotated the Oligo6 cluster to an intermediate state, connecting the OPC and COP clusters with the mature OLs. Immune OLs (ImOLs) resembled the OPC and COP, but also expressed immune response related genes (**Table 2**). Comparison of the human clusters with those previously obtained for the mouse OLs by Falcao et al. (2018), revealed similarities between the two species. In short, several other publications characterizing OL heterogeneity in CNS diseases have appeared (see next chapter). These reported varying numbers of clusters, most likely affected by the particular experimental design and data-processing pipeline used. It is likely that the complexity of human CNS will require dedicated efforts to determine and annotate the full spectrum of human OL heterogeneity. The first step in this direction was recently taken by Sadick et al. (2022), who integrated their data with three other studies (Grubman et al., 2019; Mathys et al., 2019; Zhou et al., 2020) identifying seven OL populations (**Table 2**), that appeared consistently across the datasets. However, an in-depth functional characterization was not performed. Of note, a similar integrative approach was used to create a harmonized atlas of mouse spinal cord cell types, but with limited details of OLs (Russ et al., 2021). Lastly, a comprehensive cellular taxonomy of the adult human spinal cord was recently released by Yadav et al. (2022), including an integrative analysis of mouse and human data.

Leaving the strictly OL-oriented research, the BRAIN Initiative Cell Census Consortium (BICCC) provides a great source of information that reveals additional layers of OL heterogeneity. Recently, BICCN released results of its first implementation phase presenting a multimodal cell census and an atlas of the mammalian primary motor cortex (BICCN, 2021). This massive resource provides a detailed transcriptomic and epigenomic cell atlas of the mouse primary motor cortex (Yao et al., 2021), including its spatial organization (Zhang et al., 2021) and comparison across human, marmoset (a new world monkey) and mouse (Bakken et al., 2021). The integrative analysis of seven scRNA-seq and snRNA-seq datasets led to the identification of 116 cell types, counting 59 classes of inhibitory and 31 classes of excitatory neurons, highlighting their large transcriptional diversity. Non-neuronal cells were categorized into 26 clusters, of which eight classes defined the populations of OLs (**Table 2**). As the BICCN is mostly a neuron-oriented effort, OL heterogeneity receives less attention and many of the interesting findings are waiting to be revealed by the community. The ultimate goal of BICCN is to perform the complete characterization of mouse and human CNS, and therefore another wealth of knowledge is expected in the upcoming years.

The recent developments in spatial transcriptomic technologies have made it possible to correlate OL transcriptional variation to their anatomical location. Floriddia et al. (2020) inspected spatial distribution of three populations of mature OLs in white and gray matter (GM) of murine brain and spinal cord. Specifically, they focused on populations of MOL1, MOL2, and MOL5/6 as defined by Marques et al. (2016), which showed the most distinctive expression profiles. Using a limited number of marker genes, the authors demonstrated different spatial preference and response to spinal cord injury. Further details were provided by Hilscher et al. (2022), who utilized probabilistic cell typing by *in situ* sequencing (pciSeq; Qian et al., 2020), and measured the expression of 124 marker genes of all 12 OL populations as described by Marques et al. (2016). The study focused on murine GM and WM in brain and spinal cord at postnatal, juvenile and young adult age, and revealed age and region related alterations in the composition of OL populations. Together, these two pioneering efforts provided the first hints for the understanding of the functional roles of the OL populations with respect to their anatomical locations.

Oligodendrocyte heterogeneity in disease

Falcao et al. (2018) represents a landmark study in understanding OL heterogeneity in disease, describing several disease specific OL populations in the spinal cord of mice induced by experimental autoimmune encephalomyelitis (EAE), which is an experimental model of multiple sclerosis (MS). In total, the authors identified 14 clusters, including three populations specific for the controls and five specific for EAE. Notably, even when separated into controls and EAE clusters, all the OLs resembled the clusters from Marques et al. (2016).

The analysis of major data trends revealed modules associated with EAE (**Table 2**), composed of genes related to interferon response, antigen processing and presentation *via* the major histocompatibility complex class I and II (MHC-I and -II) and immune protection, represented by the *Serpina3* gene family. Altogether, the data showed active immunomodulatory function of OLs in EAE, contesting the long-term dogma of their passive role with limited responsiveness to pathogenic stimuli. Extending the study, Jakel et al. (2019) performed an analysis of OLs in human samples with various levels of MS pathology. They identified a cluster of immune *CD74*$^+$ OLs (ImOLs), resembling the data from the mouse EAE model. Notably, the recent study by Meijer et al. (2022) showed epigenomic priming of immune genes, further confirming OL immunomodulatory role. Moreover, the positioning of MS susceptibility single-nucleotide polymorphisms (SNPs) within the accessible regulatory regions of genes involved in immune regulation, suggested an altered function of OLs in disease progression.

The initial findings on OL heterogeneity in EAE/MS were soon accompanied by reports from intensive Alzheimer's disease (AD) research. Focusing on the murine AD model, Zhou et al. (2020) reported *Serpina3n*$^+$ *C4b*$^+$ reactive OL population (**Table 2**), specifically enriched in plaque-bearing regions. The gene signature markedly overlapped with EAE-enriched populations of OLs identified earlier by Falcao et al. (2018), suggesting a shared response of OLs in two distinct neurodegenerative models. The identical population of reactive OLs (annotated MOL-DA1) was subsequently confirmed by Lee et al. (2021), who assayed OL heterogeneity in AD models of amyloidosis and tauopathy (**Table 2**). Moreover, combined tau-amyloid pathology showed more extensive OL response, giving rise to population of OLs with strong Tp53 signaling (MOL-DA2), potentially leading to cell-cycle arrest and apoptosis, however, without any prominent loss of OLs. *In situ* hybridization (ISH) across brain regions confirmed the existence of cell clusters in affected areas and absence in control old animals except aged WM, suggesting age related neurodegenerative changes in this compartment. Notably, both astrocytes and OLs contributed substantially to the overall *C4b* and *Serpina3n* signal. Finally, a recent study of Kenigsbuch et al. (2022) largely confirmed the findings of the aforementioned reports by defining a population of disease-associated oligodendrocytes (DOLs, **Table 2**), whose gene signature was found in multiple CNS pathologies, including models of MS, AD and aging. Majority of the 26 markers defining DOLs were related to immune response, and regulated by the transcription factor families Stat/Irf, YY1/NF-κB and Sox9, in accordance with the findings of Meijer et al. (2022), who demonstrated a role of Stat1 in the immune OL population. Using human protein homologs of mouse Serpina3n as a key DOLs marker, authors detected SERPINA3 in human AD samples, demonstrating the relevance of the mouse data for human pathology. This, however, contrasts the report of Zhou et al. (2020), who did not detect reactive OLs in human AD samples using snRNA-seq, or Chen et al. (2020), who screened plaque regions for *C4A/C4B* and *SERPINA3* transcripts by *in situ* sequencing (ISS).

Turning attention to human AD samples, OL heterogeneity has been interrogated in several studies investigating multiple brain regions (Del-Aguila et al., 2019; Grubman et al., 2019; Mathys et al., 2019; Lau et al., 2020; Zhou et al., 2020; Gerrits et al., 2021; Leng et al., 2021; Morabito et al., 2021; Sadick et al., 2022). Majority of studies concluded dysregulated OL functions in AD, including changes in differentiation, myelination and metabolic adaptation to neuronal degeneration. OLs have been accented as important players in disease progression, showing sexual dimorphism (Mathys et al., 2019), dysregulation of AD susceptible genes (Grubman et al., 2019), and expression of potential targets for novel AD therapeutics (Morabito et al., 2021). Interestingly, distinctive immune related response observed in murine models of MS and AD were not captured in any of the human studies, except for the very rare *CD74*$^+$ OLs (counting for 0.001% of all OLs) identified by Morabito et al. (2021) and a minor cluster of antigen presenting OLs identified by Sadick et al. (2022). Moreover, these cells were not characterized by the expression of neither *C4B* nor *SERPINA3*, which constitute the key markers of reactive OLs, alias DOLs.

The lack of immune OL signature in AD samples was recently scrutinized by Pandey et al. (2022). Using multi-dataset integration, the authors defined three distinct activation states of OLs across the mouse models of AD and MS (MOL-DA1, MOL-DA2, and MOL-IFN), which were characterized by expression of inflammatory-, survival- and interferon-associated genes (**Table 2**). Follow-up integrative analysis of human OL datasets revealed similar gene signatures in MS patients, but not in AD, indicating a distinct transcriptional response of OLs in human AD pathology. The latest contribution to the understanding of OL heterogeneity in neurodegeneration was provided by Kaya et al. (2022), who studied WM aging in mouse. The authors identified clusters of aging-related *Serpina3n*$^+$ *C4b*$^+$ OLs (AROs) and interferon-responsive *Stat1*$^+$ *B2m*$^+$ OLs (IROs) characterized by the expression of type I interferon response genes and MHC-I genes (**Table 2**). The two populations resembled the inflammatory- and interferon- clusters described by Pandey et al. (2022), but the population presumably involved in the OL survival (MOL-DA2) was missing. Altogether, the data indicates shared, but also distinct response of OLs in different pathologies that requests further investigation.

To date, single-cell and single-nucleus transcriptomics have been applied to most neurodegenerative and neuropsychiatric disorders, e.g., amyotrophic lateral sclerosis (Pineda et al., 2021), Parkinson's disease (Smajic et al., 2022), schizophrenia (Ruzicka et al., 2020), major depressive disorders (Nagy et al., 2020),

and autism (Velmeshev et al., 2019). Unfortunately, the analysis of OLs has often not been of primary interest and therefore not explored in detail. Other CNS disorders with a recently discovered role of OLs in its disease etiology, e.g., epilepsy (Knowles et al., 2022), are still awaiting in-depth single-cell transcriptomic characterization. Attention is also required for the OLs in the acute CNS injuries, where their role is largely unexplored.

Conclusion

We provide a comprehensive overview of key studies defining the current spectrum of OL heterogeneity in health and disease. We document a first standardized OL nomenclature in murine healthy CNS and strong indication of distinct reactive immune OL gene signature present in multiple models of CNS pathologies. OL heterogeneity in human is less defined and there are distinct transcriptional OL phenotypes present in MS and AD patients. Future studies are needed to establish a robust nomenclature of human OLs and characterize the full spectrum of OL activation states in other CNS disorders.

Author contributions

LV, ZM, and DZ drafted the manuscript. RK, SB, PA, MK, and MA participated in subsequent review and editing process. All authors have read and agreed to the published version of the manuscript.

Funding

This study was supported by project LX22NPO5107 (MEYS): Financed by EU—Next Generation EU and institutional support RVO 86652036.

Acknowledgments

We thank Ravindra Naraine for his assistance with language editing.

Conflict of interest

Author MK was employed by TATAA Biocenter AB.

The remaining authors declare that the research was conducted in the absence of any commercial or financial relationships that could be construed as a potential conflict of interest.

Publisher's note

All claims expressed in this article are solely those of the authors and do not necessarily represent those of their affiliated organizations, or those of the publisher, the editors and the reviewers. Any product that may be evaluated in this article, or claim that may be made by its manufacturer, is not guaranteed or endorsed by the publisher.

References

Bakken, T. E., Jorstad, N. L., Hu, Q., Lake, B. B., Tian, W., Kalmbach, B. E., et al. (2021). Comparative cellular analysis of motor cortex in human, marmoset and mouse. *Nature* 598, 111–119. doi: 10.1038/s41586-021-03465-8

Bartosovic, M., Kabbe, M., and Castelo-Branco, G. (2021). Single-cell CUT&Tag profiles histone modifications and transcription factors in complex tissues. *Nat. Biotechnol.* 39, 825–835. doi: 10.1038/s41587-021-00869-9

BICCN (2021). A multimodal cell census and atlas of the mammalian primary motor cortex. *Nature* 598, 86–102. doi: 10.1038/s41586-021-03950-0

Chen, W. T., Lu, A., Craessaerts, K., Pavie, B., Sala Frigerio, C., Corthout, N., et al. (2020). Spatial transcriptomics and in situ sequencing to study alzheimer's disease. *Cell* 182:e919. doi: 10.1016/j.cell.2020.06.038

Del Rio-Hortega, P. (1921). Estudios sobre la neurogia. La glia de escasas rediaciones (oligodendroglia). *Bol. Real Soc. Esp. Hist. Nat.* 21, 63–92.

Del-Aguila, J. L., Li, Z., Dube, U., Mihindukulasuriya, K. A., Budde, J. P., Fernandez, M. V., et al. (2019). A single-nuclei RNA sequencing study of Mendelian and sporadic AD in the human brain. *Alzheimers Res. Ther.* 11:71. doi: 10.1186/s13195-019-0524-x

Falcao, A. M., van Bruggen, D., Marques, S., Meijer, M., Jakel, S., Agirre, E., et al. (2018). Disease-specific oligodendrocyte lineage cells arise in multiple sclerosis. *Nat. Med.* 24, 1837–1844. doi: 10.1038/s41591-018-0236-y

Floriddia, E. M., Lourenco, T., Zhang, S., van Bruggen, D., Hilscher, M. M., Kukanja, P., et al. (2020). Distinct oligodendrocyte populations have spatial preference and different responses to spinal cord injury. *Nat. Commun.* 11:5860. doi: 10.1038/s41467-020-19453-x

Gerrits, E., Brouwer, N., Kooistra, S. M., Woodbury, M. E., Vermeiren, Y., Lambourne, M., et al. (2021). Distinct amyloid-beta and tau-associated microglia profiles in Alzheimer's disease. *Acta Neuropathol.* 141, 681–696. doi: 10.1007/s00401-021-02263-w

Grubman, A., Chew, G., Ouyang, J. F., Sun, G., Choo, X. Y., McLean, C., et al. (2019). A single-cell atlas of entorhinal cortex from individuals with Alzheimer's disease reveals cell-type-specific gene expression regulation. *Nat. Neurosci.* 22, 2087–2097. doi: 10.1038/s41593-019-0539-4

Habib, N., Avraham-Davidi, I., Basu, A., Burks, T., Shekhar, K., Hofree, M., et al. (2017). Massively parallel single-nucleus RNA-seq with DroNc-seq. *Nat. Methods* 14, 955–958. doi: 10.1038/nmeth.4407

Hilscher, M. M., Langseth, C. M., Kukanja, P., Yokota, C., Nilsson, M., and Castelo-Branco, G. (2022). Spatial and temporal heterogeneity in the lineage progression of fine oligodendrocyte subtypes. *BMC Biol.* 20:122. doi: 10.1186/s12915-022-01325-z

Jakel, S., Agirre, E., Mendanha Falcao, A., van Bruggen, D., Lee, K. W., Knuesel, I., et al. (2019). Altered human oligodendrocyte heterogeneity in multiple sclerosis. *Nature* 566, 543–547. doi: 10.1038/s41586-019-0903-2

Kaya, T., Mattugini, N., Liu, L., Ji, H., Besson-Girard, S., Kaiji, S., et al. (2022). T cells induce interferon-responsive oligodendrocytes during white matter aging. *bioRxiv* [Preprint]. doi: 10.1101/2022.03.26.485917

Kenigsbuch, M., Bost, P., Halevi, S., Chang, Y., Chen, S., Ma, Q., et al. (2022). A shared disease-associated oligodendrocyte signature among multiple CNS pathologies. *Nature Neurosci.* 25, 876–886. doi: 10.1038/s41593-022-01104-7

Knowles, J. K., Xu, H., Soane, C., Batra, A., Saucedo, T., Frost, E., et al. (2022). Maladaptive myelination promotes generalized epilepsy progression. *Nat. Neurosci.* 25, 596–606. doi: 10.1038/s41593-022-01052-2

Lake, B. B., Chen, S., Sos, B. C., Fan, J., Kaeser, G. E., Yung, Y. C., et al. (2018). Integrative single-cell analysis of transcriptional and epigenetic states in the human adult brain. *Nat. Biotechnol.* 36, 70–80. doi: 10.1038/nbt.4038

Lau, S. F., Cao, H., Fu, A. K. Y., and Ip, N. Y. (2020). Single-nucleus transcriptome analysis reveals dysregulation of angiogenic endothelial cells and neuroprotective glia in Alzheimer's disease. *Proc. Natl. Acad. Sci. U.S.A.* 117, 25800–25809. doi: 10.1073/pnas.2008762117

Lee, S. H., Rezzonico, M. G., Friedman, B. A., Huntley, M. H., Meilandt, W. J., Pandey, S., et al. (2021). TREM2-independent oligodendrocyte, astrocyte, and T cell responses to tau and amyloid pathology in mouse models of Alzheimer disease. *Cell Rep.* 37:110158. doi: 10.1016/j.celrep.2021.110158

Leng, K., Li, E., Eser, R., Piergies, A., Sit, R., Tan, M., et al. (2021). Molecular characterization of selectively vulnerable neurons in Alzheimer's disease. *Nat. Neurosci.* 24, 276–287. doi: 10.1038/s41593-020-00764-7

Marques, S., Zeisel, A., Codeluppi, S., van Bruggen, D., Mendanha Falcao, A., Xiao, L., et al. (2016). Oligodendrocyte heterogeneity in the mouse juvenile and adult central nervous system. *Science* 352, 1326–1329. doi: 10.1126/science.aaf6463

Mathys, H., Davila-Velderrain, J., Peng, Z., Gao, F., Mohammadi, S., Young, J. Z., et al. (2019). Single-cell transcriptomic analysis of Alzheimer's disease. *Nature* 570, 332–337. doi: 10.1038/s41586-019-1195-2

Meijer, M., Agirre, E., Kabbe, M., van Tuijn, C. A., Heskol, A., Zheng, C., et al. (2022). Epigenomic priming of immune genes implicates oligodendroglia in multiple sclerosis susceptibility. *Neuron* 110:e1113.

Morabito, S., Miyoshi, E., Michael, N., Shahin, S., Martini, A. C., Head, E., et al. (2021). Single-nucleus chromatin accessibility and transcriptomic characterization of Alzheimer's disease. *Nat. Genet.* 53, 1143–1155.

Nagy, C., Maitra, M., Tanti, A., Suderman, M., Theroux, J. F., Davoli, M. A., et al. (2020). Single-nucleus transcriptomics of the prefrontal cortex in major depressive disorder implicates oligodendrocyte precursor cells and excitatory neurons. *Nat. Neurosci.* 23, 771–781. doi: 10.1038/s41593-020-0621-y

Pandey, S., Shen, K., Lee, S. H., Shen, Y. A., Wang, Y., Otero-Garcia, M., et al. (2022). Disease-associated oligodendrocyte responses across neurodegenerative diseases. *Cell Rep.* 40:111189. doi: 10.1016/j.celrep.2022.111189

Pineda, S. S., Lee, H., Fitzwalter, B. E., Mohammadi, S., Pregent, L. J., Gardashli, M. E., et al. (2021). Single-cell profiling of the human primary motor cortex in ALS and FTLD. *bioRxiv* [Preprint]. doi: 10.1101/2021.07.07.451374

Qian, X., Harris, K. D., Hauling, T., Nicoloutsopoulos, D., Munoz-Manchado, A. B., Skene, N., et al. (2020). Probabilistic cell typing enables fine mapping of closely related cell types in situ. *Nat. Methods* 17, 101–106. doi: 10.1038/s41592-019-0631-4

Russ, D. E., Cross, R. B. P., Li, L., Koch, S. C., Matson, K. J. E., Yadav, A., et al. (2021). A harmonized atlas of mouse spinal cord cell types and their spatial organization. *Nat. Commun.* 12:5722. doi: 10.1038/s41467-021-25125-1

Ruzicka, W. B., Mohammadi, S., Davila-Velderrain, J., Subburaju, S., Tso, D. R., Hourihan, M., et al. (2020). Single-cell dissection of schizophrenia reveals neurodevelopmental-synaptic axis and transcriptional resilience. *medRxiv* [Preprint]. doi: 10.1101/2020.11.06.20225342

Sadick, J. S., O'Dea, M. R., Hasel, P., Dykstra, T., Faustin, A., and Liddelow, S. A. (2022). Astrocytes and oligodendrocytes undergo subtype-specific transcriptional changes in Alzheimer's disease. *Neuron* 110, 1788–1805.e1710. doi: 10.1016/j.neuron.2022.03.008

Seeker, L. A., and Williams, A. (2022). Oligodendroglia heterogeneity in the human central nervous system. *Acta Neuropathol.* 143, 143–157. doi: 10.1007/s00401-021-02390-4

Smajic, S., Prada-Medina, C. A., Landoulsi, Z., Ghelfi, J., Delcambre, S., Dietrich, C., et al. (2022). Single-cell sequencing of human midbrain reveals glial activation and a Parkinson-specific neuronal state. *Brain* 145, 964–978. doi: 10.1093/brain/awab446

Stuart, T., and Satija, R. (2019). Integrative single-cell analysis. *Nat. Rev. Genet.* 20, 257–272. doi: 10.1038/s41576-019-0093-7

Svensson, V., da Veiga Beltrame, E., and Pachter, L. (2020). A curated database reveals trends in single-cell transcriptomics. *Database* 2020:baaa073. doi: 10.1093/database/baaa073

Velmeshev, D., Schirmer, L., Jung, D., Haeussler, M., Perez, Y., Mayer, S., et al. (2019). Single-cell genomics identifies cell type-specific molecular changes in autism. *Science* 364, 685–689. doi: 10.1126/science.aav8130

Yadav, A., Matson, K. J. E., Li, L., Hua, I., Petrescu, J., Kang, K., et al. (2022). A Cellular Taxonomy of the Adult Human Spinal Cord. *bioRxiv* [Preprint]. doi: 10.1101/2022.03.25.485808

Yao, Z., Liu, H., Xie, F., Fischer, S., Adkins, R. S., Aldridge, A. I., et al. (2021). A transcriptomic and epigenomic cell atlas of the mouse primary motor cortex. *Nature* 598, 103–110. doi: 10.1038/s41586-021-03500-8

Zeisel, A., Hochgerner, H., Lonnerberg, P., Johnsson, A., Memic, F., van der Zwan, J., et al. (2018). Molecular Architecture of the Mouse Nervous System. *Cell* 174:e1022. doi: 10.1016/j.cell.2018.06.021

Zeisel, A., Munoz-Manchado, A. B., Codeluppi, S., Lonnerberg, P., La Manno, G., Jureus, A., et al. (2015). Cell types in the mouse cortex and hippocampus revealed by single-cell RNA-seq. *Science* 347, 1138–1142. doi: 10.1126/science.aaa1934

Zhang, M., Eichhorn, S. W., Zingg, B., Yao, Z., Cotter, K., Zeng, H., et al. (2021). Spatially resolved cell atlas of the mouse primary motor cortex by MERFISH. *Nature* 598, 137–143. doi: 10.1038/s41586-021-03705-x

Zhou, Y., Song, W. M., Andhey, P. S., Swain, A., Levy, T., Miller, K. R., et al. (2020). Human and mouse single-nucleus transcriptomics reveal TREM2-dependent and TREM2-independent cellular responses in Alzheimer's disease. *Nat. Med.* 26, 131–142. doi: 10.1038/s41591-019-0695-9

frontiers | Frontiers in Cellular Neuroscience

TYPE Original Research
PUBLISHED 24 November 2022
DOI 10.3389/fncel.2022.1049468

OPEN ACCESS

EDITED BY
Hiroaki Wake,
Nagoya University, Japan

REVIEWED BY
Holly Colognato,
Stony Brook University, United States
Enrica Boda,
University of Turin, Italy

*CORRESPONDENCE
Giada Delfino
giada.delfino@inserm.fr

SPECIALTY SECTION
This article was submitted to Non-Neuronal Cells, a section of the journal Frontiers in Cellular Neuroscience

RECEIVED 20 September 2022
ACCEPTED 03 November 2022
PUBLISHED 24 November 2022

CITATION
Delfino G, Bénardais K, Graff J, Samama B, Antal MC, Ghandour MS and Boehm N (2022) Oligodendroglial primary cilium heterogeneity during development and demyelination/remyelination. *Front. Cell. Neurosci.* 16:1049468. doi: 10.3389/fncel.2022.1049468

Oligodendroglial primary cilium heterogeneity during development and demyelination/remyelination

Giada Delfino[1,2,3]*, Karelle Bénardais[1,2,3,4], Julien Graff[2,3], Brigitte Samama[1,2,3,4], Maria Cristina Antal[1,2,3,4], M. Said Ghandour[1,3] and Nelly Boehm[1,2,3,4]

[1]ICube Laboratory UMR 7357, Team IMIS, Strasbourg, France, [2]Institut d'Histologie, Service Central de Microscopie Electronique, Faculté de Médecine, Université de Strasbourg, Strasbourg, France, [3]Fédération de Médecine Translationnelle de Strasbourg (FMTS), Strasbourg, France, [4]Hôpitaux Universitaires de Strasbourg, Strasbourg, France

The primary cilium (PC) has emerged as an indispensable cellular antenna essential for signal transduction of important cell signaling pathways. The rapid acquisition of knowledge about PC biology has raised attention to PC as a therapeutic target in some neurological and psychiatric diseases. However, the role of PC in oligodendrocytes and its participation in myelination/remyelination remain poorly understood. Oligodendrocyte precursor cells (OPCs) give rise to oligodendrocytes during central nervous system (CNS) development. In adult, a small percentage of OPCs remains as undifferentiated cells located sparsely in the different regions of the CNS. These cells can regenerate oligodendrocytes and participate to certain extent in remyelination. This study aims characterize PC in oligodendrocyte lineage cells during post-natal development and in a mouse model of demyelination/remyelination. We show heterogeneity in the frequency of cilium presence on OPCs, depending on culture conditions *in vitro* and cerebral regions *in vivo* during development and demyelination/remyelination. *In vitro*, Lithium chloride (LiCl), Forskolin and Chloral Hydrate differentially affect cilium, depending on culture environment and PC length correlates with the cell differentiation state. Beside the role of PC as a keeper of cell proliferation, our results suggest its involvement in myelination/remyelination.

KEYWORDS

OPCs, primary cilium, development, myelination, demyelinating diseases

Introduction

In the last two decades, a century-forgotten organelle, the primary cilium (PC), has emerged as an indispensable cellular antenna, involved in several cell functions. PC forms when a cell has completed mitosis and enters G0/G1 phase (Hsu et al., 2017; Wang and Dynlacht, 2018). PC is essential for transduction of numerous important cells signaling pathways, particularly Sonic hedgehog (Shh) (Corbit et al., 2005). In the central nervous system (CNS), PC has been largely studied in neurons (Baudoin et al., 2012; Bae et al., 2019; Toro-Tapia and Das, 2020), which possess a PC from neuroepithelial to post-mitotic stage. During brain development, PC affects neuronal precursors migration and differentiation, and the ablation of PC impairs interneurons migration from ganglionic eminence to the dorsal cortex (Higginbotham et al., 2012). In adult, PC seems to play a role in neuronal energy metabolism (Han et al., 2014; Song et al., 2018) and learning and memory cognitive functions (Berbari et al., 2014).

For long time, ciliary disfunctions have been correlated exclusively with the pathogenesis of ciliopathies. In a previous study, we showed the presence of one of the Bardet-Biedl syndrome proteins, in oligodendrocytes lineage in human and mouse CNS (Bénardais et al., 2021). Recent studies now point at PC implication in other pathologies such as neurological and psychiatric diseases (Hu et al., 2017; Muñoz-Estrada et al., 2018; Bae et al., 2019; Mustafa et al., 2019). A correlation between cilium length and cellular functions has been observed in some cell types. For examples, elongated PC in hippocampal neurons, through overexpression of serotonin 5-HT6 receptor at PC membrane, has been correlated with cognition impairment in APP/PS1 mouse (Hu et al., 2017). Also, in striatal neurons of a mouse model of Huntington's disease, shorter PC were correlated with age progression and mHTT (mutant Huntingtin) accumulation (Mustafa et al., 2019).

PC length adapts to environmental cues or drug treatments. Lithium Chloride (LiCl), a well-known treatment for bipolar disease is a potent PC elongation drug. LiCl elongates PC in different cell types, such as neurons (Miyoshi et al., 2009), synoviocytes, astrocytes (Ou et al., 2009), fibroblasts (Nakakura et al., 2015), chondrocytes (Thompson et al., 2016), or osteoblasts (Oliazadeh et al., 2017). In human, PC in olfactory neurons precursors cells obtained from schizophrenia and bipolar disorders patients were elongated in Lithium treated patients (Muñoz-Estrada et al., 2018). Several intracellular pathways have been implicated in cilium length control, among them cAMP pathway; for example, cAMP and forskolin elongate PC in renal (Sherpa et al., 2019) or endothelial cells (Besschetnova et al., 2010; Abdul-Majeed et al., 2012), although cAMP elevation induced cilia resorption in an embryonic renal cell line (Porpora et al., 2018). Ablation of PC by Chloral Hydrate has also been used to study correlation between PC and cell function (Deren et al., 2016; Martín-Guerrero et al., 2020; Shi et al., 2020; Wei et al., 2022).

The acquisition of knowledge about PC biology in some cell types during the past years has raised the possibility that PC might be a therapeutic target in some diseases (Arrighi et al., 2017; Spasic and Jacobs, 2017; Wang et al., 2021). However, the role of PC in oligodendroglial cells remains poorly understood and particularly in relation to myelination/remyelination. In myelin degenerating diseases, such as multiple sclerosis, enhancing regeneration of CNS myelin is an important therapeutic goal (Franklin and Ffrench-Constant, 2017). Indeed, chronic loss of myelin will lead to axonal and neuronal degeneration. Preventing neurodegeneration may be achieved by directly targeting the neurons or by accelerating remyelination. Remyelination following oligodendrocytes loss relies on oligodendrocyte precursor cells (OPCs) either deriving from quiescent resident OPCs (Franklin and Ffrench-Constant, 2008; Zawadzka et al., 2010) or from subventricular neural progenitor cells (Nait-Oumesmar et al., 2007; Xing et al., 2014; Kang et al., 2019) which migrate and differentiate in the damaged area. Heterogeneity in OPCs cells has appeared in lasts years (Bribián et al., 2020; Beiter et al., 2022; Hilscher et al., 2022); a spectrum of OPCs phenotypes depending on age (Spitzer et al., 2019), transcriptional factors (Beiter et al., 2022), environmental cues (Bribián et al., 2020), and regional localization (Hilscher et al., 2022) has been described. Recent studies report the presence of a PC in OPCs that disappears concomitantly with cells differentiation (Falcon-Urrutia et al., 2015; Cullen et al., 2020). The present work aims at studying the status of oligodendrocyte PC during oligodendrocytes development and in a mouse model of demyelination/remyelination in relation with their microenvironment and anatomical localization.

Materials and methods

Animals

The *plp*-eGFP transgenic mice expressing the enhanced green fluorescent protein (eGFP) driven by the myelin proteolipid protein gene (*plp*) promoter in C57BL/6 genetic background were generously provided by Dr. W. Macklin (Cleveland Clinic Foundation, Ohio, USA) and housed in the central animal facility of the Faculty of Medicine in Strasbourg. Animals were maintained under fixed 12 h light/dark cycle with free access to water and food. All procedures were conducted in accord with the guidelines for animal care and the experimental protocol was approved by the local ethics committee (CREMEAS, reference n° #17089-2018101116367904 v2).

Mouse purified oligodendrocyte precursor cells cultures

Mixed primary glial cell cultures were prepared according to O'Meara et al. (2011) with slight modifications. Briefly, post-natal day 0 (P0) *plp*-eGFP pups were killed by decapitation and cerebral hemispheres were isolated, diced and digested in 0.3% Papain, 0.3% L-cysteine and 0.06% DNase I at 37°C for 20 min. Enzymatic reaction was stopped by DMEM (1X) Glutamax medium (Gibco, France) supplemented with 10% fetal bovine serum (FBS) (Gibco, France) and 0.5% penicillin/streptomycin. Cells were dissociated, filtered through a 40μm nylon cell strainer, and centrifuged at 1,200 rpm. The pellet was resuspended in supplemented DMEM (1X) Glutamax and cells were plated into 100 mm Petri dishes previously coated with poly-L-lysine and placed at 37°C in humified 5% CO_2 incubator for 12 days. OPCs grown on the bed layer of astrocytes were mechanically dissociated, the medium was collected, replated in uncoated Petri dish, and incubated at 37°C in humified 5% CO_2 for 30 min. After incubation, the medium was collected, centrifuged at 1,200 rpm and the pellet was resuspended in proliferation or differentiation medium. Proliferation and differentiation media components are listed in **Supplementary Table 1**. Cells were plated on poly-L-lysine coated coverslips at 5×10^4 per well into 24-well plates and grown in the same incubation conditions as above during 24, 48 and 72 h (1, 2, 3 DIV).

Oligodendroglial cell line 158N culture

The immortalized murine oligodendroglia cell line 158N (Feutz et al., 1995) was cultured on poly-L-lysine coated coverslips in DMEM (1X) Glutamax medium supplemented with 10% FBS and 0.5% penicillin/streptomycin in an incubator at 37°C in humified 5% CO_2 until 70% confluence was reached.

Cell culture treatments

Purified OPCs cultures and cell line 158N were treated for 20 h with 10 mM of LiCl (Sigma, France) or 50 μM forskolin (Sigma, France) dissolved, respectively, in proliferation or differentiation medium or in serum free DMEM (1X) Glutamax. To study primary cilium ablation, purified OPCs were treated for 20 h with or without 2 mM Chloral Hydrate dissolved in proliferation or differentiation medium and fixed at 2 DIV.

Cuprizone induced demyelination mouse model

Plp-eGFP mice, 8 weeks old, were used to study oligodendrocytes PC during demyelination.

At the time of weaning, experimental mice were placed randomly four per cage and fed with a normal chow. At 8 weeks old, control and treated mice were assigned randomly to their experimental group and weighed. The mean weight of mice was 20 g.

Cuprizone 0.2% (bis-cyclohexanone-oxaldihydrazone; Sigma, France) was mixed with milled chows and added to feeders each day (5–8 g per mouse). Animals were treated with or without 0.2% of cuprizone for 3 or 6 weeks; a last group of animals was treated or not for 6 weeks with cuprizone and euthanized 6 weeks after treatment withdrawal.

Immunocytochemistry

Freshly prepared 4% formaldehyde in 0.1 M phosphate buffer pH 7.4 was used as the fixative. Cells were fixed for 24 h. P2 mice were anesthetized by ice, all the others were anaesthetized by ketamine (8 mg/kg)/Xylazine (5–16 mg/kg) and fixed by transcardial perfusion. Brains were post-fixed for three days in the same fixative and then coronal 50 or 20 μm sections were prepared on a vibratome and processed as free-floating sections.

Antibodies were diluted in blocking solution (2% normal horse serum in PBS containing 0.2% of Triton X-100). For single staining, cells or sections were exposed to primary antibodies diluted in blocking solution overnight at room temperature, then washed in PBS/0.2% of Triton X-100 and incubated for 2 h in appropriate secondary antibodies. Biotinylated antibody reaction was revealed using peroxidase-labeled streptavidin complex (Vectastain Elite kit, Vector Laboratories, Abcys, France) followed by VIP, SG (Vector Laboratories, Abcys, France) or HistoGreen (Novus Biologicals, France) as peroxidase substrates.

When double immunofluorescence was performed using antibodies from two different species (mouse/rabbit), cells were exposed to the mix of primary antibodies overnight and then incubated for 2 h in appropriate secondary antibodies.

For double staining using a fluorochrome and a chromogen or when the two primary antibodies derived from the same species, immunocytochemistry was completed first using a chromogen followed by a second immunostaining using a fluorochrome or a chromogen—tagged secondary antibody.

Mounting medium with Dapi (Vectashield, Vector Laboratories, Abcys, France) was used for fluorescence-labeled sections or cultures. Chromogen-revealed sections were mounted with Eukitt. The list of antibodies used in this study is accessible in **Supplementary Tables 2**, **3**.

Electron microscopy

158N cells were detached by a non-enzymatic cell dissociation solution (Ref. S-014-M, Sigma) and the pellet was

fixed in 2.5% glutaraldehyde in cacodylate buffer, post-fixed in osmium tetroxyde and embedded in epon.

Ultrathin sections were stained with uranyl acetate and lead citrate and observed in a Phillips M208 electron microscope.

Primary cilium length measurement

For the measurement of PC length, images were captured with a BX60 microscope equipped with DP70 digital camera (Olympus). For each cilium, three z-stacks were captured with 100X objective to analyze the full axoneme. Length was measured using ImageJ software (Image J, US National Institutes of Health, Bethesda, MD, USA).

Study of oligodendrocyte precursor cells cilium during development and demyelination/remyelination

For developmental study, four groups of three male *plp*-eGFP mice were used at P2, P10, P15, P30. For demyelination experiments, six animals for each condition were analyzed.

All analyses were performed in three coronal sections located between Bregma 0.98 mm and Bregma −0.46 mm (Franklin and Paxinos atlas) from each animal. Cortex was segmented in two regions, a superficial region, corresponding to layers I, II and III, and a deep region, corresponding to layers IV, VI. Only the middle region of the corpus callosum was studied.

Images were captured with 20X objective on a light microscope (Coolpix 995, Nikon, France) for cells counting or with a 100X objective on fluorescent microscope (BX60, Olympus, France) to visualize PC.

OPCs, oligodendroglial cells and myelin were characterized respectively by PDGFR-a, OLIG2 and MBP immunostaining. Proliferating OPCs and ciliated OPCs were detected by double staining Ki67/PDGFR-a and ARL13b/PDGFR-a, respectively. Astrocytic and microglial reactions were determined, respectively, by GFAP$^+$ and Iba1$^+$ immunoreactivity. Bilateral areas for each section were photographed and analyzed using ImageJ software (Image J, US National Institutes of Health, Bethesda, MD, USA; see text footnote 1).

Statistical analysis

Analyses were performed with GraphPad Prism 7 Software (GraphPad Software, USA). Oligodendroglial cells distribution (qualitative variables) in **Figures 1E,F** was analyzed using Chi-Square test.

For other experiences, Student's *t*-test or ANOVA (One- or Two-way) followed by Bonferroni *post-hoc* test were employed. Data are presented as mean ± standard error of the mean (SEM). The list of the applied statistical tests is included in **Supplementary Table 4**.

Results

The proportion of ciliated oligodendrocyte precursor cells depends on culture medium

We first studied the occurrence of a PC on oligodendroglial purified cells grown in two different culture environments, respectively, called proliferation and differentiation medium, based on their composition. Cells were classified in four differentiation stages according to their morphological complexity, markers expression (PDGFR-a, CC1 and MBP) and eGFP fluorescence intensity as shown in **Figures 1A–D**.

Analysis of cells distribution showed predominant OPCs and pre-oligodendrocytes at the three times of culture in proliferation medium (**Figure 1E**), while in differentiation medium (**Figure 1F**), immature and mature oligodendrocytes appeared gradually, in a time-dependent manner.

PCs were stained by acetylated tubulin (**Figure 1G**) and ARL13b (**Figure 1H**). Since all acetylated tubulin PCs were also ARL13b$^+$ (**Figure 1H**), we used ARL13b as cilium marker for quantification. Only OPCs and pre-oligodendrocytes had a PC and the percentage of ciliated PDGFR-a$^+$ cells increased with time in proliferation medium (**Figure 1I**) but not in differentiation medium (**Figure 1J**).

Culture medium impacts cilium response to Lithium and forskolin

To study the plasticity of PC in oligodendroglial cells, we treated oligodendroglial cell line 158N and murine purified OPCs cultures with LiCl and forskolin, two chemicals able to elongate PC in some cell types.

In cell line 158N, cilia were clearly identified by acetylated tubulin and were longer than those of primary oligodendroglial cells. **Figures 2A–F** illustrates the effect of treatment on cilium length observed by immunofluorescence and electron microscopy. In these cells, LiCl and forskolin importantly increased PC length (**Figure 2G**).

In contrast, PC response in primary oligodendroglial cells cultures depended on culture conditions. Both, LiCl and forskolin elongated PC in proliferation medium (**Figure 2H**) but only Lithium acted in differentiation medium (**Figure 2I**).

The distribution of cells at 2 DIV was not modified by Lithium and forskolin treatment in proliferation medium (**Figure 2J**) while in differentiation medium, forskolin had no effect and Lithium maintained cells in a less differentiated state as compared to controls (**Figure 2K**).

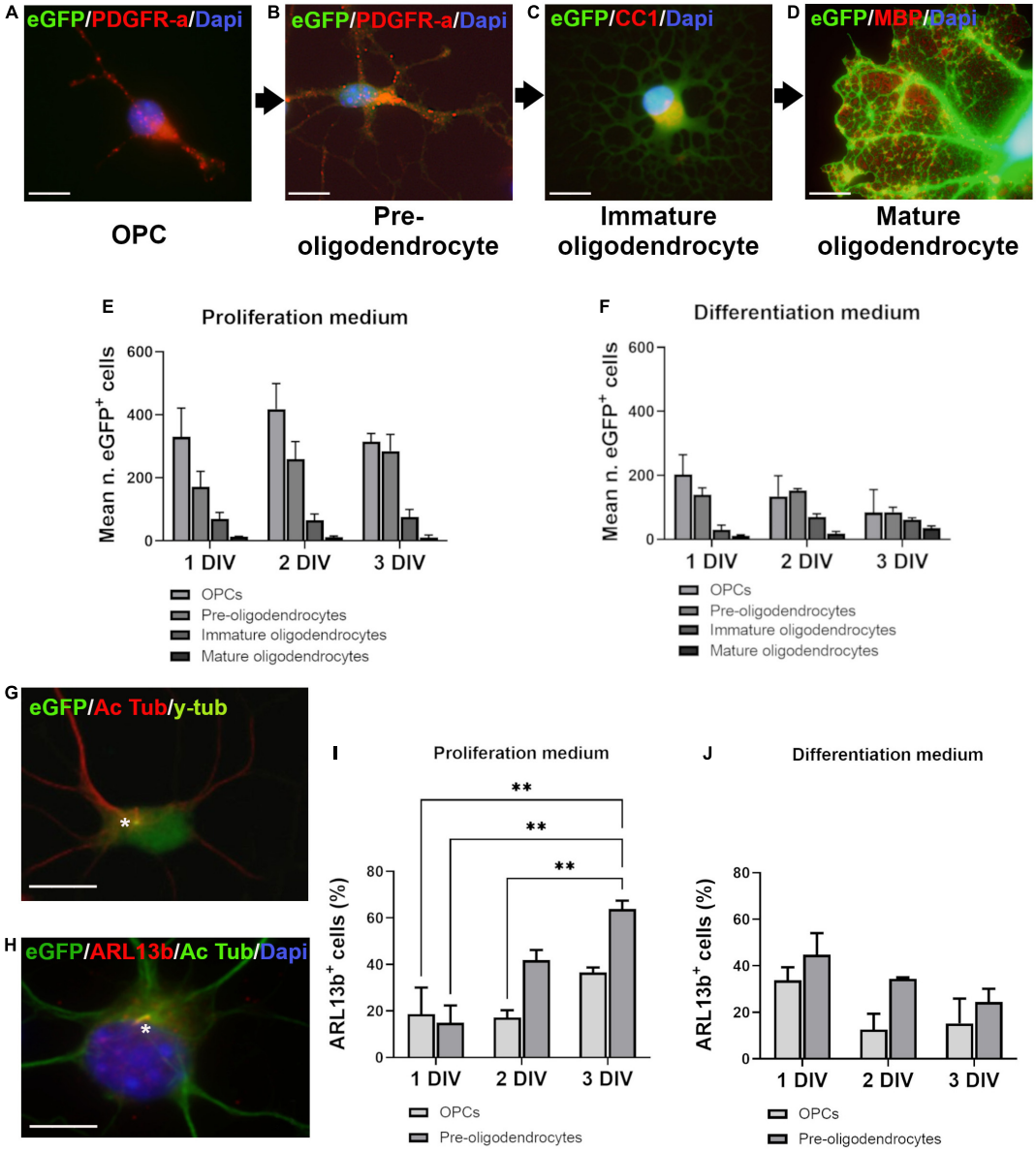

FIGURE 1
Ciliated cells in proliferation and differentiation media. **(A–D)** Oligodendroglial cells in culture were classified in four stages according to branching development, eGFP intensity and markers expression. PDGFR-a$^+$ cells were divided in two stages: very weakly fluorescent bipolar cells (OPCs) **(A)** and more intensely fluorescent multipolar cells with short processes (pre-oligodendrocytes) **(B)**. Immature oligodendrocytes were CC1$^+$/MBP$^-$, intensely fluorescent highly branching cells **(C)**. The late stage cells were brightly fluorescent mature oligodendrocytes characterized by large flat membrane sheets, MBP$^+$ **(D)**. **(E,F)** Distribution of eGFP$^+$ cells in proliferation and differentiation media at three times of culture (days *in vitro*: DIV). Statistical significance was determined by Chi-Square Test (χ^2). Proliferation medium: *df* 83.26, $p < 0.001$***; Differentiation medium: *df* 242.9, $p < 0.001$***. Graphs in **(E,F)** represent de mean number of eGFP$^+$ cells analyzed in three coverslips from three independent experiences for each time. **(G,H)** Representative images of OPCs after double staining for acetylated tubulin (Ac Tub)/y-tubulin **(G)** and Ac Tub/ARL13b **(H)**. Stars indicate cilia. **(I,J)** Quantification of ARL13b$^+$/PDGFR-a$^+$ cells respectively in proliferation **(I)** and differentiation medium **(J)**. Statistical significance was determined by two-way ANOVA and Bonferroni *post-hoc* test was employed for multiple comparisons. Data are presented as mean ± error of the mean (SEM) and asterisks indicate: **$p < 0.01$. Scale bar is 10 μm in **(A–C)**, 5 μm in **(D)**, 10 μm in **(G,H)**.

Further we treated purified oligodendrocytes cultures with Chloral Hydrate (CH), a chemical able to ablate PC in some cell types. CH reduced the proportion of ciliated cells only in differentiation medium (Figures 2L,M). In proliferation medium, as expected for an anti-mitotic drug, the total number of cells was reduced by CH treatment and the cells were maintained in an immature stage (Figure 2N) while in differentiation medium,

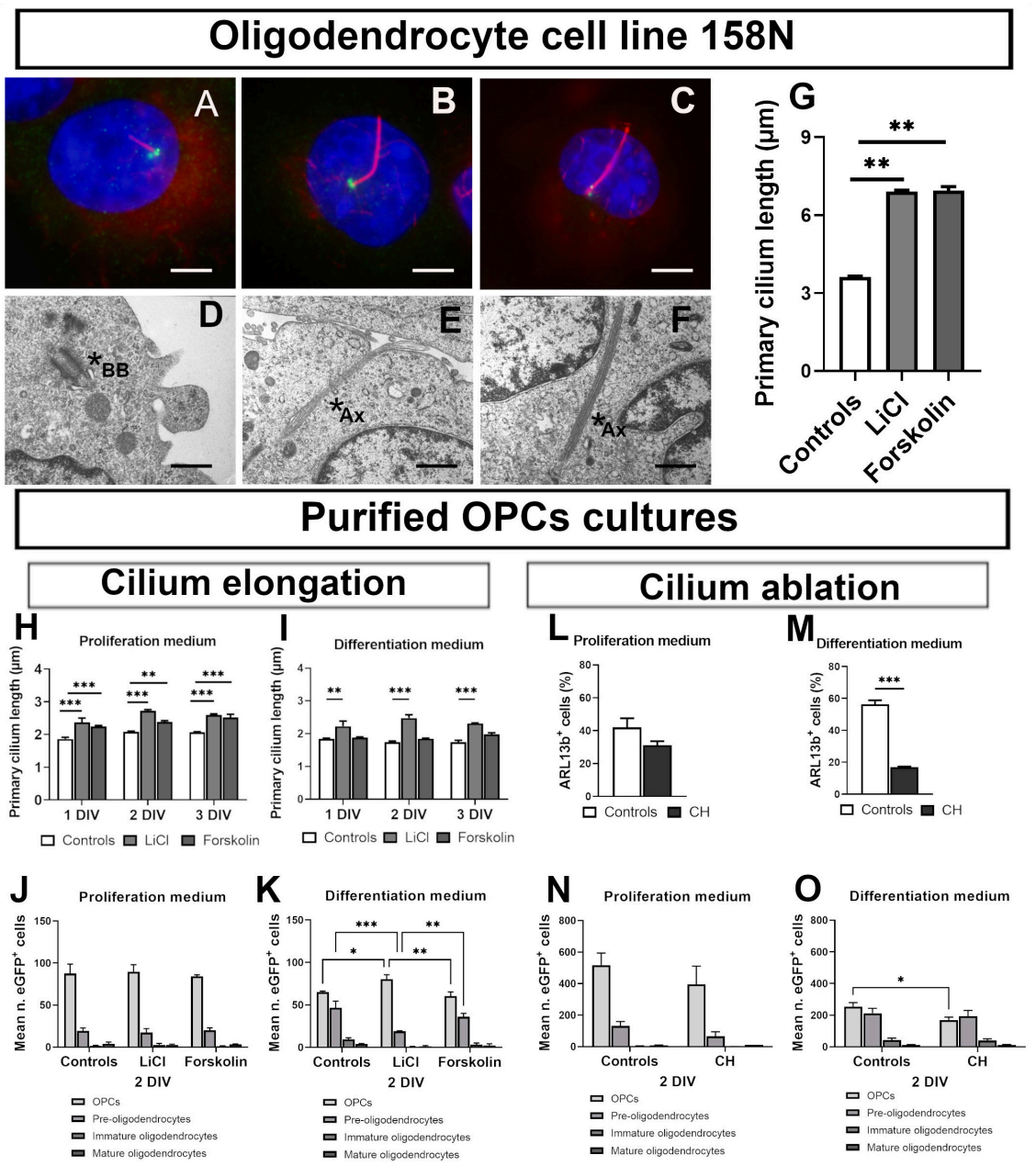

FIGURE 2
Primary cilium plasticity in oligodendroglial cell line 158N and purified OPCs cultures. **(A–F)** Cilium in 158 cell line. **(A–C)** Representative photomicrographs of cilia in controls **(A)**, LiCl **(B)** and forskolin **(C)** treated 158N cells. Primary cilium was stained by acetylated tubulin (Ac Tub) and basal body by y-tubulin. Scale bar: 5 μm. **(D–F)** Representative ultrastructural PC morphology. Mother centriole beginning to extend a short axoneme associated to its membrane vesicle in the cytoplasm **(D)** and long axonemes in LiCl treated cells **(E,F)**; scale bar: 300 nm. Stars shown basal body (BB) in **(D)** and ciliary axoneme (Ax) in **(E,F)**. **(G)** Both Lithium and forskolin lengthened cilia in 158N cells (One-way ANOVA followed by Bonferroni *post-hoc* test; $^{**}p < 0.01$; $n = 3$). **(H–O)** Cilium in primary oligodendroglial cell cultures. **(H–K)** Effect of lithium chloride and forskolin. In proliferation medium, both lithium and forskolin lengthened cilia **(H)**. In differentiation medium only lithium was able to elongate primary cilium **(I)** at the tree times studied (one-way ANOVA followed by Bonferroni *post-hoc* test; $^{**}p < 0.01$, $^{***}p < 0.001$. $n = 3$). **(J,K)** The distribution of eGFP^{+} cells at 2 DIV of culture was not modified in proliferation medium. **(J)** In differentiation medium, lithium maintains cells in an immature state while forskolin had no effect. **(K)** Statistical significance was determined by two-way ANOVA and Bonferroni *post-hoc* test was employed for multiple comparisons. Data are presented as mean ± error of the mean (SEM) and asterisks indicate: $^{*}p < 0.05$, $^{**}p < 0.01$, $^{***}p < 0.001$. **(L–O)** Effect of chloral hydrate (CH). CH did not ablate PDGFR-a^{+} cells PC in proliferation medium **(L)** but only in differentiation medium **(M)** (student's *t*-test; $^{***}p < 0.001$). **(N,O)** Effect of CH on eGFP^{+} cells distribution in proliferation and differentiation media at 2 DIV of culture. CH did not modify cells distribution in proliferation medium **(N)**; in differentiation medium **(O)**, CH treatment reduced the number of cells in the less differentiated stages. Statistical significance was determined by Two-way ANOVA and Bonferroni *post-hoc* test was employed for multiple comparisons. Data are presented as mean ± error of the mean (SEM) and asterisks indicate: $^{*}p < 0.05$.

CH reduces the number of cells less differentiated (Figure 2O).

Oligodendrocyte precursor cells primary cilium heterogeneity in corpus callosum and cerebral cortex during development

To attest the relevance of data obtained *in vitro*, showing that OPCs differently develop a PC depending on their environment, we studied PC in oligodendroglial cells in white (corpus callosum) and gray (cerebral cortex) matters during post-natal myelination from P2 to P30.

OPCs and proliferating OPCs during development were identified by PDGFR-a/OLIG2 (Figure 3A) and Ki67/PDGFR-a (Figures 3B,C) double staining. *In vivo* as was the case in cultures, only PDGFR-a$^+$ cells had an ARL13b$^+$ cilium (Figures 3D–F).

As expected, the proportion of PDGFR-a$^+$ cells decreased in corpus callosum and deep cortex (Figures 3G,H) from P2 to P30 in parallel with the progressive myelination. In contrast, in superficial cortex, this proportion increased continuously from P2 to P30 (Figure 3I). The rate of proliferation of PDGFR-a$^+$ cells was highest in corpus callosum and decreased during post-natal myelination in both corpus callosum and cortex (Figures 3J–L).

The proportion of ciliated PDGFR-a$^+$ cells and their development differed between corpus callosum and cortex. This proportion was lowest in corpus callosum and highest in superficial cortex (Figures 3M–O). In corpus callosum, the proportion sharply decreased from P2 to P10 followed by a progressive increase until P30 (Figure 3M), as was also observed in superficial cortex (Figure 3O). In deep cortex, the proportion of ciliated PDGFR-a$^+$ cells did not vary during post-natal development (Figure 3N).

Characterization of ciliated oligodendrocyte precursor cells during demyelination/remyelination in cuprizone mouse model

Myelin loss started at 3 weeks and became severe at 6 weeks of cuprizone treatment (Figures 4A–D) as confirmed by important loss of OLIG2$^+$ cells in corpus callosum and deep cortex (Figures 4E–G). After 3 weeks of cuprizone treatment, MBP immunostaining remained strong due to the presence of MBP$^+$ debris from myelin and oligodendrocytes in corpus callosum and cortex (Supplementary Figure 1). Six weeks after the end of cuprizone treatment, the number of oligodendroglial cells was recovered in superficial cortex (Figure 4G), partially recovered in corpus callosum (Figure 4E) while remaining very low in deep cortex (Figure 4F).

As expected in the cuprizone model, we found strong astrocytic and microglial reactions in corpus callosum and deep cortex; 6 weeks after the end of treatment, these reactions were attenuated. No astrocytic and microglial reactions were observed in superficial cortex (Supplementary Figure 2).

The number of PDGFR-a$^+$ cells was increased in corpus callosum at early (3 weeks) and late (6 weeks) demyelination stages (Figure 4H), while in deep cortex, a small increase in the number of PDGFR-a$^+$ cells was observed only at 6 weeks of cuprizone treatment (Figure 4I). In superficial cortex the number of PDGFR-a$^+$ cells did not differ from that of controls at any time of treatment (Figure 4J). In the three regions, 6 weeks after the end of cuprizone treatment, there were no differences in the number of PDGFR-a$^+$ cells in treated and control mice (Figure 4H–J).

Interestingly, the changes in ciliated cells (ARL13B$^+$/PDGFR-a$^+$) population did not match that of PDGFR-a$^+$ cells. We only observed a sharp increase of ciliated cells in corpus callosum at 3 weeks of demyelination (Figure 4K). At later stages in corpus callosum and in deep and superficial cortex during the different stages, the proportion of ciliated cells did not differ in treated mice as compared to controls (Figure 4K–M).

Discussion

The main aim of this investigation was to study PC in oligodendrocyte lineage cells during post-natal development and in a mouse model of demyelination/remyelination. Our results confirm that only PDGFR-a$^+$ cells are ciliated and reveal heterogeneity in the frequency of cilium presence on OPCs, depending on culture conditions *in vitro* and cerebral regions *in vivo*. We showed the plasticity of oligodendroglial PC length in response to different drugs. Since dramatic morphological changes of oligodendroglia are correlated with the progression of differentiation and sensitivity to environmental cues (Barateiro and Fernandes, 2014), we analyzed oligodendroglial PC in different culture conditions and in cerebral regions with different myelination levels The dynamic of OPCs proliferation and differentiation *in vitro* intimately correlates with the components of culture media (Lü et al., 2008). The mitogen factors, PDGF and Shh (Merchán et al., 2007) maintain cells in a proliferating state, while when thyroid hormones are added, proliferation and differentiation simultaneously occur, recapitulating *in vivo* development (Durand and Raff, 2000; Tang et al., 2000; Franco et al., 2008). The proportion of ciliated cells in culture increased in proliferation medium, where proliferation index was high, while in differentiation medium, the proportion did not vary. This observation reinforce the role of oligodendroglial cilium in

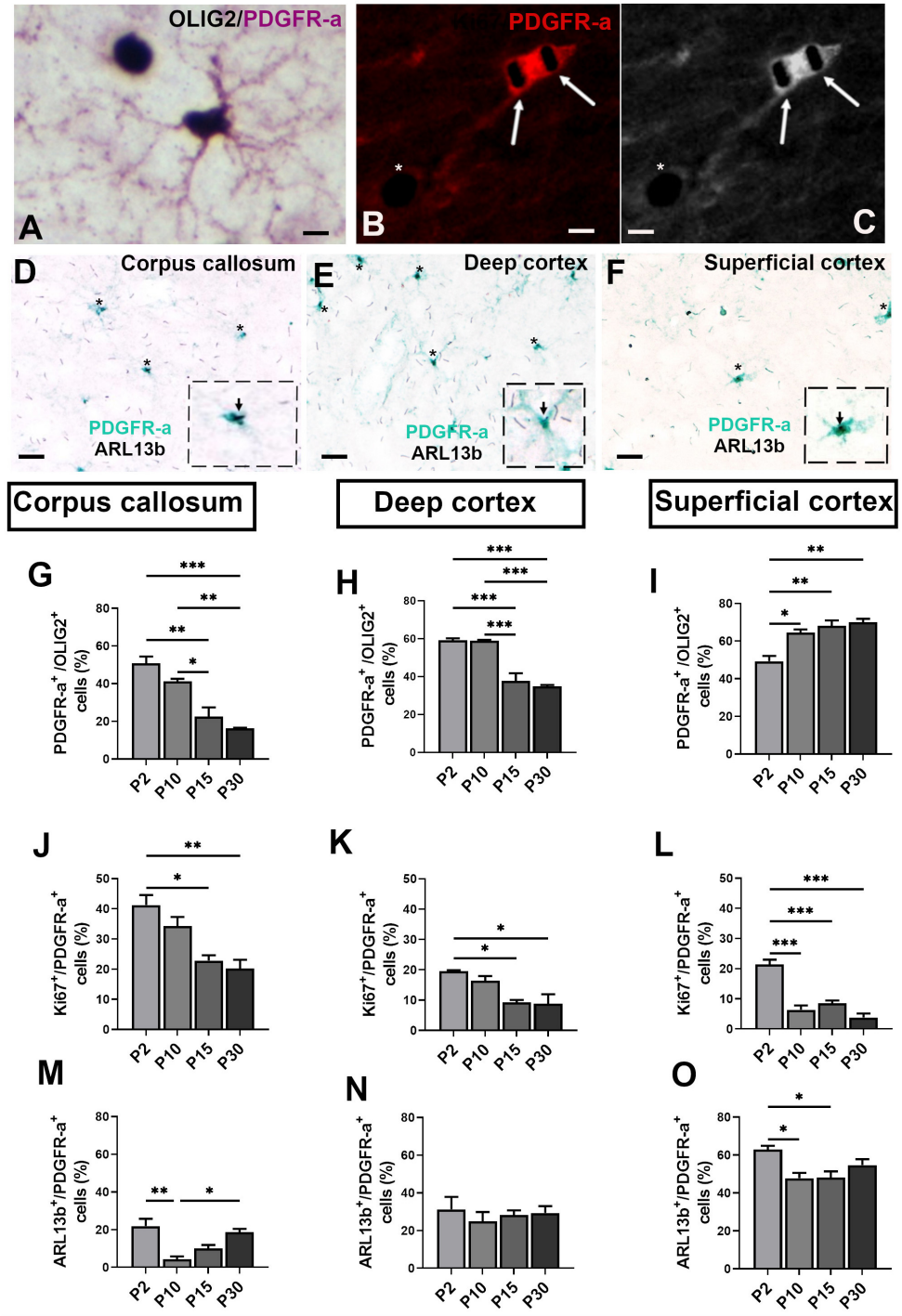

FIGURE 3
Ciliated oligodendroglial cells distribution in corpus callosum and cortex during mouse post-natal development. **(A,B)** Representative images of double staining PDGFR-a/OLIG2 **(A)** and Ki67/PDGFR-a **(B,C)**, respectively. Arrows in **(B)** indicate $Ki67^+$ nuclei staining in black (SG HRP Substrate) in a $PDGFR\text{-}a^+$ cell (red fluorochrome) and asterisk shown a $Ki67^+$ nucleus in a $PDGFR\text{-}a^-$ cell. **(C)** Black and white image of **(B)**. **(D–F)** Representative image of ciliated $PDGFR\text{-}a^+$ cells in mouse corpus callosum, deep and superficial cortex at post-natal day 15. Asterisks indicate primary cilia stained with ARL13b in black (SG HRP Substrate) in $PDGFR\text{-}a^+$ cells stained by a green HRP Substrate (HistoGreen). In the dotted squares, high magnification of a $PDGFR^+/ARL13b^+$ cells. **(G–O)** Quantification of $PDGFR\text{-}a^+$ **(G–I)**, $Ki67^+$ **(J–L)** and $ARL13b^+$ cells **(M–O)** in corpus callosum, deep and superficial cortex. Groups were compared using one-way ANOVA followed by Bonferroni *post-hoc* test. Data are presented as mean ± error of the mean (SEM) and asterisks indicate: $*p < 0.05$, $**p < 0.01$, $***p < 0.001$; the values for n are available in **Supplementary Table 4**. Scale bar is 10 μm in **(A–C)** and 20 μm in **(D–F)**. The inspected cells for the evaluation of ciliated $PDGFR\text{-}a^+$ percentage was 40–50 cells repeated in three different slices for each animal and each anatomical region studied at the different ages.

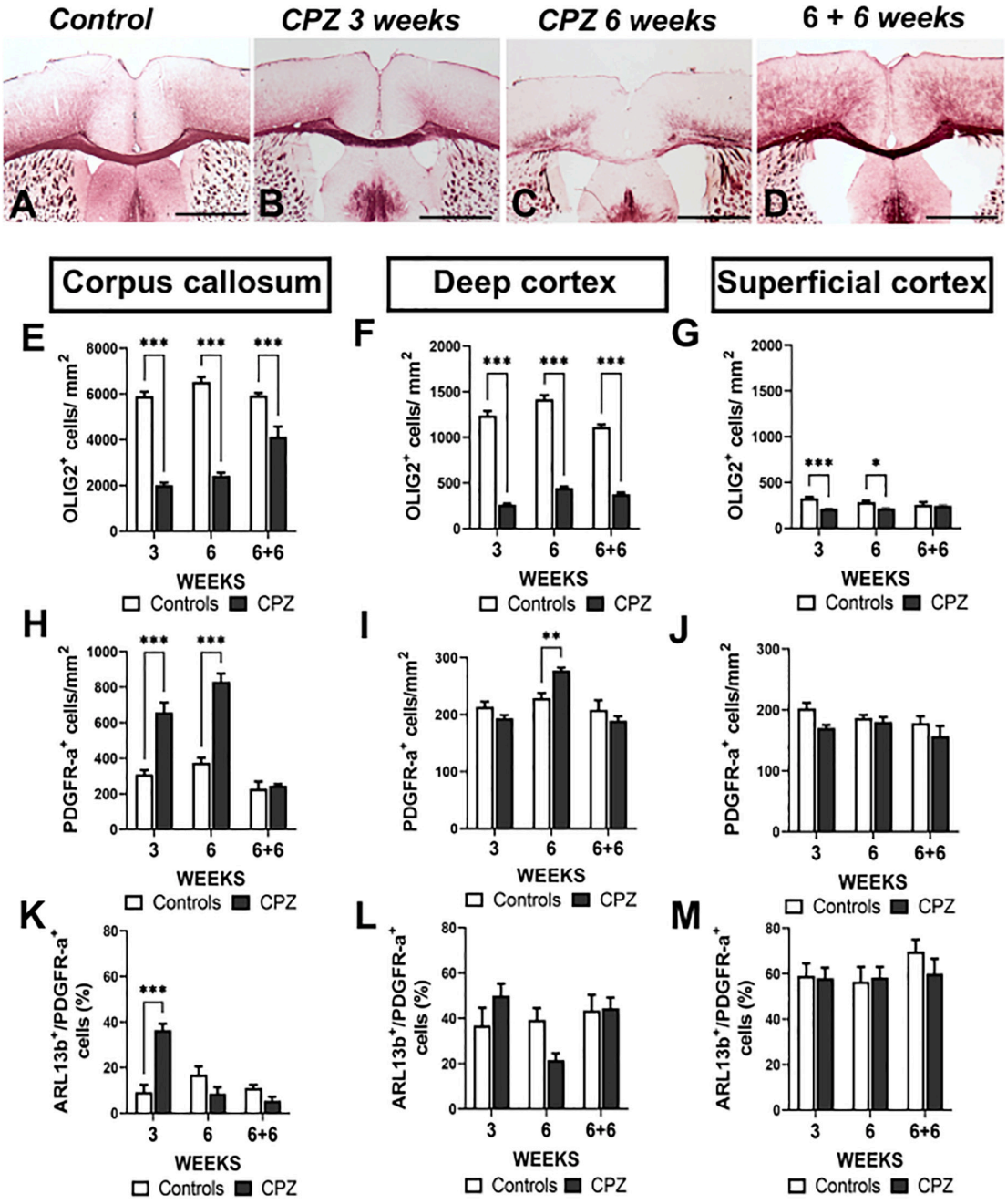

FIGURE 4
Ciliated oligodendroglial cells distribution in corpus callosum and cortex during demyelination in cuprizone mouse model. **(A–D)** Representative images of MBP immunostaining in controls **(A)**, after 3 **(B)** and 6 weeks **(C)** of cuprizone (CPZ) administration and 6 weeks after treatment withdrawal **(D)**. **(E–M)** Quantification of OLIG2$^+$ **(E–G)**, PDGFR-a$^+$ **(H–J)** and ARL13b$^+$ cells **(K–M)** in corpus callosum, superficial cortex and deep cortex during cuprizone induced demyelination. Groups were compered using Two-way ANOVA followed by Bonferroni *post-hoc* test. Data are presented as mean ± error of the mean (SEM) and asterisks indicate: *$p < 0.05$, **$p < 0.01$, ***$p < 0.001$. The values for n are available in **Supplementary Table 4**. Scale bar is 500 μm in **(A–D)**. The inspected cells for the evaluation of ciliated PDGFR-a$^+$ percentage was 30–50 cells repeated in three different slices for each animal and each anatomical region studied.

proliferation, as suggested by Cullen et al. (2020). However, this result also suggests that PC could be implicated in transition from proliferative to differentiating stages. Under proliferative environment, many ciliated cells are generated awaiting for differentiation signals This hypothesis may explain why in the absence of proliferation factors in differentiation medium, the proportion of ciliated cells is higher than in proliferation medium after 1 day of culture but does not change over time.

One point concerning OPCs *in vitro* needs to be raised: in our cultures, cells from the whole cerebral cortex are cultured, the subventricular zone (SVZ) as well as parenchymal OPCs. We observed *in vivo* heterogeneity in the presence of a PC in OPCs depending on cerebral regions, longitudinal single cells studies may help refining our understanding on oligodendroglial PC.

Our results suggest the PC as a new marker of OPCs heterogeneity regarding the difference between cerebral cortex and corpus callosum in ciliated OPCs. We found different number of OPCs available for myelination and different frequencies in the presence of PC in different regions with different myelin levels. This is in keeping in mind with recent studies pointing to a molecular and functional heterogeneity of OPCs, attributed to their developmental origin (Foerster et al., 2019; Spitzer et al., 2019), their localization in white and gray matter (Foerster et al., 2019; Spitzer et al., 2019; Winkler and Franco, 2019) and their transduction signaling for proliferation and differentiation (Spitzer et al., 2019; Winkler and Franco, 2019).

In corpus callosum, the most myelinated region, we observed the lowest frequency of ciliated OPCs. This frequency is much lower than that reported by Cullen et al. (2020); indeed we only considered elongated PC and not punctate PC because the latter may be remnants of PC (Paridaen et al., 2013) with either capacity to reassemble a fully developed PC or to disappear with centrosome loss. During post-natal development, the number of ciliated OPCs sharply decreased in corpus callosum from P2 to P10 stage, concomitantly with the onset of myelination. The same situation occurred after cuprizone treatment: following a sharp rise in ciliated OPCs at 3 weeks treatment, the frequency was decreased in correlation with the onset of myelination (Gudi et al., 2009). This raises the question of OPCs origin: during the first post-natal week, OPCs present in the corpus callosum are deriving most from the dorsal SVZ, migrating within corpus callosum and deep cortex (Kessaris et al., 2006), although ventrally derived OPCs are still present. Later, corpus callosum OPCs derive mainly from parenchymal OPCs proliferation. During acute phase of demyelination, OPCs originate from both SVZ and corpus callosum parenchyma (Brousse et al., 2015). Then, two hypothesis may be proposed for the sharp rise of ciliated OPCs at 3 weeks of CPZ treatment: pre-existing parenchymal OPCs with remnants of PC in the cytoplasm could reassemble a PC and proliferate; however, our observation of the highest concentration of ciliated OPCs above the SVZ rather favors a SVZ origin. Proliferating OPCs migrating in the corpus callosum could there encounter a favorable environment for differentiation. Previous studies showed that white matter is more favorable for OPCs differentiation than gray matter and during demyelination in CC (Viganò et al., 2013), cells expressing the morphogen Shh have been identified (Ferent et al., 2013). Moreover, astrocytes are involved in OPCs proliferation by secretion of growth factors (Houben et al., 2020; Rawji et al., 2020).

In deep cortex, where adult myelination is important as compared to superficial cortex, we did not observe modifications in the proportion of ciliated OPCs during post-natal development and demyelination/remyelination. Most studies focus on corpus callosum and very little is known about OL and myelination/remyelination in cortex. However, recent studies suggest that developmental OPCs differentiation and myelination occur earlier in cortex as compared to corpus callosum (Hilscher et al., 2022). We observed that the increase in OPCs due to demyelination was delayed in deep cortex as compared to corpus callosum. Other authors also mentioned a delay in demyelination between cortex and corpus callosum (Gudi et al., 2009). At our knowledge, it is not fully known to which extent both origins of new OPCs contribute to deep cortex remyelination, and which are the migrating capacities of SVZ-derived OPCs during cuprizone-induced demyelination. Further studies will be needed to determine if the ciliated OPCs we observed in corpus callosum during early demyelination participate to cortex remyelination or if there are two separate pools, region-specific, of remyelinating OPCs. Our results also suggest a limitation in ciliated OPCs for differentiation in deep cortex compared to corpus callosum. Indeed, in corpus callosum the sharp increase in ciliated OPCs followed by a sharp decrease suggests that the cells underwent differentiation before a steady state in proliferation/differentiation of parenchymal OPCs. However, less pronounced microgliosis and astrogliosis could also reduced OPCs recruitment and differentiation (Kotter et al., 2001; Buschmann et al., 2012; Sen et al., 2022).

In superficial cortex, where myelination and OPCs proliferation are weak, the remyelination is efficient as previously observed by Orthmann-Murphy et al. (2020), we found the highest level of ciliated OPCs. This region has also the lowest astrogliosis and microgliosis following cuprizone treatment. It has been suggested that the inability to fully recover myelin in deep cortex results from inhibition of myelination, in part due to inflammation (Baxi et al., 2017; Kirby et al., 2019). However, the difference in remyelination between superficial and deep cortex could also result from the availability in new OPCs, resident OPCs being sufficient in the low myelinated superficial cortex. During homeostasis, resident OPCs are perhaps in a non-proliferating non-differentiating favorable environment, explaining the high frequency of ciliated OPCs; these ciliated OPCs could be immediately receptive to differentiating cues due to the presence of PC.

Cells can regulate several of their functions by PC morphological and functional modifications. PC length can be modulated by drugs such as Lithium salts in mesenchymal cells or neurons *in vitro* and *in vivo* (Miyoshi et al., 2009, 2011; Thompson et al., 2016; Oliazadeh et al., 2017; Spasic and Jacobs, 2017) or by cAMP (Besschetnova et al., 2010; Abdul-Majeed et al., 2012). This prompted us to test the possibility

to modify oligodendroglial PC. Forskolin only elongated PC in proliferation medium. cAMP signaling is complex in cells with a PC; recent studies revealed that ciliary and cytoplasmic cAMP constitute two pools which can be differently produced and can differently act on cell biology and cilium length (Pazour and Witman, 2003; Anvarian et al., 2019; Nachury and Mick, 2019; Hansen et al., 2020, 2022; Truong et al., 2021; Wachten and Mick, 2021). Moreover, cAMP induces oligodendroglial differentiation (Raible and McMorris, 1993; Ghandour et al., 2002) but this effect was not observed here, probably because of the short time exposure to forskolin. Oppositely, PC length increased in OPCs in response to Lithium independently from culture environment without modifying the number of ciliated OPCs (Ou et al., 2009). Lithium maintained oligodendroglial cells in an immature state in both proliferation and differentiation media. However, in a previous study, Meffre et al. (2015) observed a morphological differentiation of oligodendrocytes attested by a 6-fold increase in MBP mRNA under Lithium treatment in primary mixed glial cells cultures. The difference in results may be explained by culture conditions: Meffre et al. (2015) used primary culture where oligodendrocytes lie on astrocytes bed-layer. It has been recently observed that astrocytes are also direct targets of Lithium (Rivera and Butt, 2019) and they support OPCs differentiation by secreting soluble growth factors or by establishing physical contacts (Nutma et al., 2021). In contrast, as our cultures are oligodendrocytes enriched at 90%, Lithium action may rather be direct on oligodendroglial cells.

To reinforce a possible correlation between PC elongation and OPCs lithium-induced differentiation impairment, we ablated PC using Chloral Hydrate (Chakrabarti et al., 1998; Praetorius and Spring, 2003; Overgaard et al., 2009). Chloral hydrate was not able to decrease the number of ciliated cells in proliferation medium and the cells were maintained in undifferentiated stage. However, in presence of differentiation factors, the absence of cilium had a slight effect in favor of differentiation This effect is not due to proliferation impairment since proliferation was not affected by Chloral Hydrate in differentiation medium. Cullen et al. (2020) showed a reduction of OPCs proliferation using a Cre lox approach to prevent cilia assembly. However, the effects on OPCs differentiation were not reported. Recently, several authors compared the effects of inhibiting PC by either small interfering RNAs for the PC protein IFT88, as used by Cullen et al. (2020) or PC specific inhibitor (chloral hydrate) and observed similar effects on bone and cartilage cells physiology (Martín-Guerrero et al., 2020; Shi et al., 2020). The plasticity of PC in oligodendroglial cells is a complex mechanism. Although our results need to be reinforced to highlight the relationships between cilium length modifications and OPCs differentiation, they suggest a potential effect of Lithium in OPCs proliferation/differentiation through PC modulation.

Recently, several studies showed PC dysfunctions in the pathogenesis of neurodegenerative (Karunakaran et al., 2020) and psychiatric diseases (Muñoz-Estrada et al., 2018) and pointed PC as a new marker of disease and as a potential target for new drugs development. Since, Lithium has beneficial impact on peripheral remyelination (Makoukji et al., 2012; da Silva et al., 2014; Fang et al., 2016; Kuffler, 2021), in a preliminary study (data not shown), we treated mice with Lithium during the 6 weeks period after withdrawal of cuprizone; in deep cortex where remyelination is delayed as compared to corpus callosum, myelin deficit was even more pronounced as compared to Lithium-untreated mice. This can be explained by our *in vitro* results where Lithium maintained oligodendroglial cells in an undifferentiated state.

However, Lithium treatment seemed to induce a shift to higher values of both myelinated axons and fibers diameters. These preliminary observations suggest differential roles of Lithium, dependent on oligodendroglial stage of differentiation.

In conclusion, our results suggest the PC as a new marker of heterogeneity of oligodendroglial lineage cells and present new data, in CNS developmental myelination and remyelination. Although we are aware of some limitations in our study which remains on a descriptive level, it opens a field of research where molecular approaches could answer why PC occurs only in a subset of OPCs, how PC in these OPCs maintain them apart from other OPCs and what are the real functions of PC during development and in demyelination/remyelination.

Data availability statement

The raw data supporting the conclusions of this article will be made available by the authors, without undue reservation.

Ethics statement

This animal study was reviewed and approved by the Comité d'Éthique en Matière d'Expérimentation Animale de Strasbourg (CREMEAS).

Author contributions

GD performed the experiments, analyzed the data, and participated to the experimental design under the supervision of NB. KB and BS contributed to the experiments, data analysis, and experimental design. MG and MA contributed to the experimental design and edited the manuscript. JG performed the material preparation and experiments. NB conceived the idea. GD and NB wrote and edited the manuscript together. All authors approved the final manuscript.

Conflict of interest

The authors declare that the research was conducted in the absence of any commercial or financial relationships that could be construed as a potential conflict of interest.

Publisher's note

All claims expressed in this article are solely those of the authors and do not necessarily represent those of their affiliated organizations, or those of the publisher, the editors and the reviewers. Any product that may be evaluated in this article, or claim that may be made by its manufacturer, is not guaranteed or endorsed by the publisher.

Supplementary material

The Supplementary Material for this article can be found online at: https://www.frontiersin.org/articles/10.3389/fncel.2022.1049468/full#supplementary-material

References

Abdul-Majeed, S., Moloney, B. C., and Nauli, S. M. (2012). Mechanisms regulating cilia growth and cilia function in endothelial cells. *Cell. Mol. Life Sci.* 69, 165–173. doi: 10.1007/s00018-011-0744-0

Anvarian, Z., Mykytyn, K., Mukhopadhyay, S., Pedersen, L. B., and Christensen, S. T. (2019). Cellular signalling by primary cilia in development, organ function and disease. *Nat. Rev. Nephrol.* 15, 199–219. doi: 10.1038/s41581-019-0116-9

Arrighi, N., Lypovetska, K., Moratal, C., Giorgetti-Peraldi, S., Dechesne, C. A., Dani, C., et al. (2017). The primary cilium is necessary for the differentiation and the maintenance of human adipose progenitors into myofibroblasts. *Sci. Rep.* 7:15248. doi: 10.1038/s41598-017-15649-2

Bae, J.-E., Kang, G. M., Min, S. H., Jo, D. S., Jung, Y.-K., Kim, K., et al. (2019). Primary cilia mediate mitochondrial stress responses to promote dopamine neuron survival in a Parkinson's disease model. *Cell Death Dis.* 10:952. doi: 10.1038/s41419-019-2184-y

Barateiro, A., and Fernandes, A. (2014). Temporal oligodendrocyte lineage progression: In vitro models of proliferation, differentiation and myelination. *Biochim. Biophys. Acta* 1843, 1917–1929. doi: 10.1016/j.bbamcr.2014.04.018

Baudoin, J.-P., Viou, L., Launay, P.-S., Luccardini, C., Espeso Gil, S., Kiyasova, V., et al. (2012). Tangentially migrating neurons assemble a primary cilium that promotes their reorientation to the cortical plate. *Neuron* 76, 1108–1122. doi: 10.1016/j.neuron.2012.10.027

Baxi, E. G., DeBruin, J., Jin, J., Strasburger, H. J., Smith, M. D., Orthmann-Murphy, J. L., et al. (2017). Lineage tracing reveals dynamic changes in oligodendrocyte precursor cells following cuprizone-induced demyelination. *Glia* 65, 2087–2098. doi: 10.1002/glia.23229

Beiter, R. M., Rivet-Noor, C., Merchak, A. R., Bai, R., Johanson, D. M., Slogar, E., et al. (2022). Evidence for oligodendrocyte progenitor cell heterogeneity in the adult mouse brain. *Sci. Rep.* 12:12921. doi: 10.1038/s41598-022-17081-7

Bénardais, K., Delfino, G., Samama, B., Devys, D., Antal, M. C., Ghandour, M. S., et al. (2021). BBS4 protein has basal body/ciliary localization in sensory organs but extra-ciliary localization in oligodendrocytes during human development. *Cell Tissue Res.* 385:3748. doi: 10.1007/s00441-021-03440-9

Berbari, N. F., Malarkey, E. B., Yazdi, S. M. Z. R., McNair, A. D., Kippe, J. M., Croyle, M. J., et al. (2014). Hippocampal and cortical primary cilia are required for aversive memory in mice. *PLoS One* 9:e106576. doi: 10.1371/journal.pone.0106576

Besschetnova, T. Y., Kolpakova-Hart, E., Guan, Y., Zhou, J., Olsen, B. R., and Shah, J. V. (2010). Identification of signaling pathways regulating primary cilium length and flow-mediated adaptation. *Curr. Biol.* 20, 182–187. doi: 10.1016/j.cub.2009.11.072

Bribián, A., Medina-Rodríguez, E. M., Josa-Prado, F., García-Álvarez, I., Machín-Díaz, I., Esteban, P. F., et al. (2020). Functional heterogeneity of mouse and human brain OPCs: Relevance for preclinical studies in multiple Sclerosis. *J. Clin. Med.* 9:1681. doi: 10.3390/jcm9061681

Brousse, B., Magalon, K., Durbec, P., and Cayre, M. (2015). Region and dynamic specificities of adult neural stem cells and oligodendrocyte precursors in myelin regeneration in the mouse brain. *Biol. Open* 4, 980–992. doi: 10.1242/bio.012773

Buschmann, J. P., Berger, K., Awad, H., Clarner, T., Beyer, C., and Kipp, M. (2012). Inflammatory response and chemokine expression in the white matter corpus callosum and gray matter cortex region during cuprizone-induced demyelination. *J. Mol. Neurosci.* 48, 66–76. doi: 10.1007/s12031-012-9773-x

Chakrabarti, A., Schatten, H., Mitchell, K. D., Crosser, M., and Taylor, M. (1998). Chloral hydrate alters the organization of the ciliary basal apparatus and cell organelles in sea urchin embryos. *Cell Tissue Res.* 293, 453–462. doi: 10.1007/s004410051137

Corbit, K. C., Aanstad, P., Singla, V., Norman, A. R., Stainier, D. Y. R., and Reiter, J. F. (2005). Vertebrate smoothened functions at the primary cilium. *Nature* 437, 1018–1021. doi: 10.1038/nature04117

Cullen, C. L., O'Rourke, M., Beasley, S. J., Auderset, L., Zhen, Y., Pepper, R. E., et al. (2020). *Kif3a* deletion prevents primary cilia assembly on oligodendrocyte progenitor cells, reduces oligodendrogenesis and impairs fine motor function. *Glia* 69, 1184–1203. doi: 10.1002/glia.23957

da Silva, T. F., Eira, J., Lopes, A. T., Malheiro, A. R., Sousa, V., Luoma, A., et al. (2014). Peripheral nervous system plasmalogens regulate Schwann cell differentiation and myelination. *J. Clin. Invest.* 124, 2560–2570. doi: 10.1172/JCI72063

Deren, M., Yang, X., Guan, Y., and Chen, Q. (2016). Biological and chemical removal of primary cilia affects mechanical activation of chondrogenesis markers in chondroprogenitors and hypertrophic chondrocytes. *Int. J. Mol. Sci.* 17:188. doi: 10.3390/ijms17020188

Durand, B., and Raff, M. (2000). A cell-intrinsic timer that operates during oligodendrocyte development. *Bioessays* 22, 64–71. doi: 10.1002/(SICI)1521-1878(200001)22:1<64::AID-BIES11<3.0.CO;2-Q

Falcon-Urrutia, P., Carrasco, C. M., Lois, P., Palma, V., and Roth, A. D. (2015). Shh signaling through primary cilium modulates rat oligodendrocyte differentiation. *PLoS One* 10:e0133567. doi: 10.1371/journal.pone.0133567

Fang, X.-Y., Zhang, W.-M., Zhang, C.-F., Wong, W.-M., Li, W., Wu, W., et al. (2016). Lithium accelerates functional motor recovery by improving remyelination of regenerating axons following ventral root avulsion and reimplantation. *Neuroscience* 329, 213–225. doi: 10.1016/j.neuroscience.2016.05.010

Ferent, J., Zimmer, C., Durbec, P., Ruat, M., and Traiffort, E. (2013). Sonic hedgehog signaling is a positive oligodendrocyte regulator during demyelination. *J. Neurosci.* 33, 1759–1772. doi: 10.1523/JNEUROSCI.3334-12.2013

Feutz A.-C., Bellomi I., Allinquant B., Schladenhaufen Y., and Ghandour M. S. (1995). Isolation and caracterization of defective jimpy oligodendrocytes in culture. *J. Neurocytol.* 24, 865–877. doi: 10.1007/BF01179985

Foerster, S., Hill, M. F. E., and Franklin, R. J. M. (2019). Diversity in the oligodendrocyte lineage: Plasticity or heterogeneity? *Glia* 67, 1797–1805. doi: 10.1002/glia.23607

Franco, P. G., Silvestroff, L., Soto, E. F., and Pasquini, J. M. (2008). Thyroid hormones promote differentiation of oligodendrocyte progenitor cells and improve remyelination after cuprizone-induced demyelination. *Exp. Neurol.* 212, 458–467. doi: 10.1016/j.expneurol.2008.04.039

Franklin, R. J. M., and Ffrench-Constant, C. (2008). Remyelination in the CNS: From biology to therapy. *Nat. Rev. Neurosci.* 9, 839–855. doi: 10.1038/nrn2480

Franklin, R. J. M., and Ffrench-Constant, C. (2017). Regenerating CNS myelin – from mechanisms to experimental medicines. *Nat. Rev. Neurosci.* 18, 753–769. doi: 10.1038/nrn.2017.136

Ghandour, M. S., Feutz, A.-C., Jalabi, W., Taleb, O., Bessert, D., Cypher, M., et al. (2002). Trafficking of PLP/DM20 and cAMP signaling in

immortalized jimpy oligodendrocytes. *Glia* 40, 300–311. doi: 10.1002/glia.10122

Gudi, V., Moharregh-Khiabani, D., Skripuletz, T., Koutsoudaki, P. N., Kotsiari, A., Skuljec, J., et al. (2009). Regional differences between grey and white matter in cuprizone induced demyelination. *Brain Res.* 1283, 127–138. doi: 10.1016/j.brainres.2009.06.005

Han, Y. M., Kang, G. M., Byun, K., Ko, H. W., Kim, J., Shin, M.-S., et al. (2014). Leptin-promoted cilia assembly is critical for normal energy balance. *J. Clin. Invest.* 124, 2193–2197. doi: 10.1172/JCI69395

Hansen, J. N., Kaiser, F., Klausen, C., Stüven, B., Chong, R., Bönigk, W., et al. (2020). Nanobody-directed targeting of optogenetic tools to study signaling in the primary cilium. *Elife* 9:e57907. doi: 10.7554/eLife.57907

Hansen, J. N., Kaiser, F., Leyendecker, P., Stüven, B., Krause, J.-H., Derakhshandeh, F., et al. (2022). A cAMP signalosome in primary cilia drives gene expression and kidney cyst formation. *EMBO Rep.* 23:e54315. doi: 10.15252/embr.202154315

Higginbotham, H., Eom, T.-Y., Mariani, L. E., Bachleda, A., Hirt, J., Gukassyan, V., et al. (2012). Arl13b in primary cilia regulates the migration and placement of interneurons in the developing cerebral cortex. *Dev. Cell* 23, 925–938. doi: 10.1016/j.devcel.2012.09.019

Hilscher, M. M., Langseth, C. M., Kukanja, P., Yokota, C., Nilsson, M., and Castelo-Branco, G. (2022). Spatial and temporal heterogeneity in the lineage progression of fine oligodendrocyte subtypes. *BMC Biol.* 20:122. doi: 10.1186/s12915-022-01325-z

Houben, E., Janssens, K., Hermans, D., Vandooren, J., Van den Haute, C., Schepers, M., et al. (2020). Oncostatin M-induced astrocytic tissue inhibitor of metalloproteinases-1 drives remyelination. *Proc. Natl. Acad. Sci. U.S.A.* 117, 5028–5038. doi: 10.1073/pnas.1912910117

Hsu, K.-S., Chuang, J.-Z., and Sung, C.-H. (2017). The biology of ciliary dynamics. *Cold Spring Harb. Perspect. Biol.* 9:a027904. doi: 10.1101/cshperspect.a027904

Hu, L., Wang, B., and Zhang, Y. (2017). Serotonin 5-HT6 receptors affect cognition in a mouse model of Alzheimer's disease by regulating cilia function. *Alzheimers Res. Ther.* 9:76. doi: 10.1186/s13195-017-0304-4

Kang, W., Nguyen, K. C. Q., and Hébert, J. M. (2019). Transient redirection of SVZ stem cells to oligodendrogenesis by FGFR3 activation promotes remyelination. *Stem Cell Rep.* 12, 1223–1231. doi: 10.1016/j.stemcr.2019.05.006

Karunakaran, K. B., Chaparala, S., Lo, C. W., and Ganapathiraju, M. K. (2020). Cilia interactome with predicted protein–protein interactions reveals connections to Alzheimer's disease, aging and other neuropsychiatric processes. *Sci. Rep.* 10:15629. doi: 10.1038/s41598-020-72024-4

Kessaris, N., Fogarty, M., Iannarelli, P., Grist, M., Wegner, M., and Richardson, W. D. (2006). Competing waves of oligodendrocytes in the forebrain and postnatal elimination of an embryonic lineage. *Nat. Neurosci.* 9, 173–179. doi: 10.1038/nn1620

Kirby, L., Jin, J., Cardona, J. G., Smith, M. D., Martin, K. A., Wang, J., et al. (2019). Oligodendrocyte precursor cells present antigen and are cytotoxic targets in inflammatory demyelination. *Nat. Commun.* 10:3887. doi: 10.1038/s41467-019-11638-3

Kotter, M. R., Setzu, A., Sim, F. J., Van Rooijen, N., and Franklin, R. J. (2001). Macrophage depletion impairs oligodendrocyte remyelination following lysolecithin-induced demyelination. *Glia* 35, 204–212. doi: 10.1002/glia.1085

Kuffler, D. P. (2021). Can lithium enhance the extent of axon regeneration and neurological recovery following peripheral nerve trauma? *Neural Regen. Res.* 17, 948–952. doi: 10.4103/1673-5374.324830

Lü, H.-Z., Wang, Y.-X., Li, Y., Fu, S.-L., Hang, Q., and Lu, P.-H. (2008). Proliferation and differentiation of oligodendrocyte progenitor cells induced from rat embryonic neural precursor cells followed by flow cytometry. *Cytometry A* 73, 754–760. doi: 10.1002/cyto.a.20577

Makoukji, J., Belle, M., Meffre, D., Stassart, R., Grenier, J., Shackleford, G., et al. (2012). Lithium enhances remyelination of peripheral nerves. *Proc. Natl. Acad. Sci. U.S.A.* 109, 3973–3978. doi: 10.1073/pnas.1121367109

Martín-Guerrero, E., Tirado-Cabrera, I., Buendía, I., Alonso, V., Gortázar, A. R., and Ardura, J. A. (2020). Primary cilia mediate parathyroid hormone receptor type 1 osteogenic actions in osteocytes and osteoblasts via Gli activation. *J. Cell. Physiol.* 235, 7356–7369. doi: 10.1002/jcp.29636

Meffre, D., Massaad, C., and Grenier, J. (2015). Lithium chloride stimulates PLP and MBP expression in oligodendrocytes via Wnt/β-catenin and Akt/CREB pathways. *Neuroscience* 284, 962–971. doi: 10.1016/j.neuroscience.2014.10.064

Merchán, P., Bribián, A., Sánchez-Camacho, C., Lezameta, M., Bovolenta, P., and de Castro, F. (2007). Sonic hedgehog promotes the migration and proliferation of optic nerve oligodendrocyte precursors. *Mol. Cell. Neurosci.* 36, 355–368. doi: 10.1016/j.mcn.2007.07.012

Miyoshi, K., Kasahara, K., Miyazaki, I., and Asanuma, M. (2009). Lithium treatment elongates primary cilia in the mouse brain and in cultured cells. *Biochem. Biophys. Res. Commun.* 388, 757–762. doi: 10.1016/j.bbrc.2009.08.099

Miyoshi, K., Kasahara, K., Miyazaki, I., and Asanuma, M. (2011). Factors that influence primary cilium length. *Acta Med. Okayama* 65, 279–285. doi: 10.18926/AMO/47009

Muñoz-Estrada, J., Lora-Castellanos, A., Meza, I., Alarcón Elizalde, S., and Benítez-King, G. (2018). Primary cilia formation is diminished in schizophrenia and bipolar disorder: A possible marker for these psychiatric diseases. *Schizophr. Res.* 195, 412–420. doi: 10.1016/j.schres.2017.08.055

Mustafa, R., Kreiner, G., Kamińska, K., Wood, A.-E. J., Kirsch, J., Tucker, K. L., et al. (2019). Targeted depletion of primary cilia in dopaminoceptive neurons in a preclinical mouse model of Huntington's disease. *Front. Cell. Neurosci.* 13:565. doi: 10.3389/fncel.2019.00565

Nachury, M. V., and Mick, D. U. (2019). Establishing and regulating the composition of cilia for signal transduction. *Nat. Rev. Mol. Cell Biol.* 20, 389–405. doi: 10.1038/s41580-019-0116-4

Nait-Oumesmar, B., Picard-Riera, N., Kerninon, C., Decker, L., Seilhean, D., Höglinger, G. U., et al. (2007). Activation of the subventricular zone in multiple sclerosis: Evidence for early glial progenitors. *Proc. Natl. Acad. Sci. U.S.A.* 104, 4694–4699. doi: 10.1073/pnas.0606835104

Nakakura, T., Asano-Hoshino, A., Suzuki, T., Arisawa, K., Tanaka, H., Sekino, Y., et al. (2015). The elongation of primary cilia via the acetylation of α-tubulin by the treatment with lithium chloride in human fibroblast KD cells. *Med. Mol. Morphol.* 48, 44–53. doi: 10.1007/s00795-014-0076-x

Nutma, E., Gebro, E., Marzin, M. C., van der Valk, P., Matthews, P. M., Owen, D. R., et al. (2021). Activated microglia do not increase 18 kDa translocator protein (TSPO) expression in the multiple sclerosis brain. *Glia* 69, 2447–2458. doi: 10.1002/glia.24052

Oliazadeh, N., Gorman, K. F., Eveleigh, R., Bourque, G., and Moreau, A. (2017). Identification of elongated primary cilia with impaired mechanotransduction in idiopathic scoliosis patients. *Sci. Rep.* 7:44260. doi: 10.1038/srep44260

O'Meara, R. W., Ryan, S. D., Colognato, H., and Kothary, R. (2011). Derivation of enriched oligodendrocyte cultures and oligodendrocyte/neuron myelinating co-cultures from post-natal murine tissues. *J. Vis. Exp.* 54:3324. doi: 10.3791/3324

Orthmann-Murphy, J., Call, C. L., Molina-Castro, G. C., Hsieh, Y. C., Rasband, M. N., Calabresi, P. A., et al. (2020). Remyelination alters the pattern of myelin in the cerebral cortex. *Elife* 9:e56621. doi: 10.7554/eLife.56621

Ou, Y., Ruan, Y., Cheng, M., Moser, J. J., Rattner, J. B., and van der Hoorn, F. A. (2009). Adenylate cyclase regulates elongation of mammalian primary cilia. *Exp. Cell Res.* 315, 2802–2817. doi: 10.1016/j.yexcr.2009.06.028

Overgaard, C. E., Sanzone, K. M., Spiczka, K. S., Sheff, D. R., Sandra, A., and Yeaman, C. (2009). Deciliation is associated with dramatic remodeling of epithelial cell junctions and surface domains. *Mol. Biol. Cell* 20, 102–113. doi: 10.1091/mbc.E08-07-0741

Paridaen, J. T. M. L., Wilsch-Bräuninger, M., and Huttner, W. B. (2013). Asymmetric inheritance of centrosome-associated primary cilium membrane directs ciliogenesis after cell division. *Cell* 155, 333–344. doi: 10.1016/j.cell.2013.08.060

Pazour, G. J., and Witman, G. B. (2003). The vertebrate primary cilium is a sensory organelle. *Curr. Opin. Cell Biol.* 15, 105–110. doi: 10.1016/S0955-0674(02)00012-1

Porpora, M., Sauchella, S., Rinaldi, L., Delle Donne, R., Sepe, M., Torres-Quesada, O., et al. (2018). Counterregulation of cAMP-directed kinase activities controls ciliogenesis. *Nat. Commun.* 9:1224. doi: 10.1038/s41467-018-03643-9

Praetorius, H. A., and Spring, K. R. (2003). Removal of the MDCK cell primary cilium abolishes flow sensing. *J. Membr. Biol.* 191, 69–76. doi: 10.1007/s00232-002-1042-4

Raible, D. W., and McMorris, F. A. (1993). Oligodendrocyte differentiation and progenitor cell proliferation are independently regulated by cyclic AMP. *J. Neurosci. Res.* 34, 287–294. doi: 10.1002/jnr.490340305

Rawji, K. S., Gonzalez Martinez, G. A., Sharma, A., and Franklin, R. J. M. (2020). The role of astrocytes in remyelination. *Trends Neurosci.* 43, 596–607. doi: 10.1016/j.tins.2020.05.006

Rivera, A. D., and Butt, A. M. (2019). Astrocytes are direct cellular targets of lithium treatment: Novel roles for lysyl oxidase and peroxisome-proliferator activated receptor-γ as astroglial targets of lithium. *Transl. Psychiatry* 9:211. doi: 10.1038/s41398-019-0542-2

Sen, M. K., Mahns, D. A., Coorssen, J. R., and Shortland, P. J. (2022). The roles of microglia and astrocytes in phagocytosis and myelination: Insights from the cuprizone model of multiple sclerosis. *Glia* 70, 1215–1250. doi: 10.1002/glia.24148

Sherpa, R. T., Mohieldin, A. M., Pala, R., Wachten, D., Ostrom, R. S., and Nauli, S. M. (2019). Sensory primary cilium is a responsive cAMP microdomain in renal epithelia. *Sci. Rep.* 9:6523. doi: 10.1038/s41598-019-43002-2

Shi, W., Zhang, Y., Chen, K., He, J., Feng, X., Wei, W., et al. (2020). Primary cilia act as microgravity sensors by depolymerizing microtubules to inhibit osteoblastic differentiation and mineralization. *Bone* 136:115346. doi: 10.1016/j.bone.2020.115346

Song, D. K., Choi, J. H., and Kim, M.-S. (2018). Primary cilia as a signaling platform for control of energy metabolism. *Diabetes Metab. J.* 42, 117–127. doi: 10.4093/dmj.2018.42.2.117

Spasic, M., and Jacobs, C. R. (2017). Lengthening primary cilia enhances cellular mechanosensitivity. *Eur. Cell. Mater.* 33, 158–168. doi: 10.22203/eCM.v033a12

Spitzer, S. O., Sitnikov, S., Kamen, Y., Evans, K. A., Kronenberg-Versteeg, D., Dietmann, S., et al. (2019). Oligodendrocyte progenitor cells become regionally diverse and heterogeneous with age. *Neuron* 101, 459–471.e5. doi: 10.1016/j.neuron.2018.12.020

Tang, D. G., Tokumoto, Y. M., and Raff, M. C. (2000). Long-term culture of purified postnatal oligodendrocyte precursor cells. *J. Cell Biol.* 148, 971–984.

Thompson, C. L., Wiles, A., Poole, C. A., and Knight, M. M. (2016). Lithium chloride modulates chondrocyte primary cilia and inhibits hedgehog signaling. *FASEB J.* 30, 716–726. doi: 10.1096/fj.15-274944

Toro-Tapia, G., and Das, R. M. (2020). Primary cilium remodeling mediates a cell signaling switch in differentiating neurons. *Sci. Adv.* 6:eabb0601. doi: 10.1126/sciadv.abb0601

Truong, M. E., Bilekova, S., Choksi, S. P., Li, W., Bugaj, L. J., Xu, K., et al. (2021). Vertebrate cells differentially interpret ciliary and extraciliary cAMP. *Cell* 184, 2911–2926.e18. doi: 10.1016/j.cell.2021.04.002

Viganò, F., Möbius, W., Götz, M., and Dimou, L. (2013). Transplantation reveals regional differences in oligodendrocyte differentiation in the adult brain. *Nat. Neurosci.* 16, 1370–1372. doi: 10.1038/nn.3503

Wachten, D., and Mick, D. U. (2021). Signal transduction in primary cilia – analyzing and manipulating GPCR and second messenger signaling. *Pharmacol. Ther.* 224:107836. doi: 10.1016/j.pharmthera.2021.107836

Wang, L., and Dynlacht, B. D. (2018). The regulation of cilium assembly and disassembly in development and disease. *Development* 145:dev151407. doi: 10.1242/dev.151407

Wang, Z.-M., Gao, X.-F., Zhang, J.-J., and Chen, S.-L. (2021). Primary cilia and atherosclerosis. *Front. Physiol.* 12:640774. doi: 10.3389/fphys.2021.640774

Wei, L., Ma, W., Cai, H., Peng, S. P., Tian, H. B., Wang, J. F., et al. (2022). Inhibition of ciliogenesis enhances the cellular sensitivity to temozolomide and ionizing radiation in human glioblastoma cells. *Biomed. Environ. Sci.* 35, 419–436. doi: 10.3967/bes2022.058

Winkler, C. C., and Franco, S. J. (2019). Loss of shh signaling in the neocortex reveals heterogeneous cell recovery responses from distinct oligodendrocyte populations. *Dev. Biol.* 452, 55–65. doi: 10.1016/j.ydbio.2019.04.016

Xing, Y. L., Röth, P. T., Stratton, J. A. S., Chuang, B. H. A., Danne, J., Ellis, S. L., et al. (2014). Adult neural precursor cells from the subventricular zone contribute significantly to oligodendrocyte regeneration and remyelination. *J. Neurosci.* 34, 14128–14146. doi: 10.1523/JNEUROSCI.3491-13.2014

Zawadzka, M., Rivers, L. E., Fancy, S. P. J., Zhao, C., Tripathi, R., Jamen, F., et al. (2010). CNS-resident glial progenitor/stem cells produce schwann cells as well as oligodendrocytes during repair of CNS demyelination. *Cell Stem Cell* 6, 578–590. doi: 10.1016/j.stem.2010.04.002

frontiers | Frontiers in Cellular Neuroscience

TYPE Review
PUBLISHED 20 December 2022
DOI 10.3389/fncel.2022.1083159

OPEN ACCESS

EDITED BY
Hiroaki Wake,
Nagoya University, Japan

REVIEWED BY
Bilal Ersen Kerman,
Istanbul Medipol University, Turkey
Lukas Valihrach,
Institute of Biotechnology (ASCR),
Czechia

*CORRESPONDENCE
Eun-Mi Hur
✉ ehur1@snu.ac.kr

†These authors have contributed equally to this work and share first authorship

SPECIALTY SECTION
This article was submitted to Non-Neuronal Cells, a section of the journal Frontiers in Cellular Neuroscience

RECEIVED 28 October 2022
ACCEPTED 05 December 2022
PUBLISHED 20 December 2022

CITATION
Han S, Gim Y, Jang E-H and Hur E-M (2022) Functions and dysfunctions of oligodendrocytes in neurodegenerative diseases. *Front. Cell. Neurosci.* 16:1083159. doi: 10.3389/fncel.2022.1083159

Functions and dysfunctions of oligodendrocytes in neurodegenerative diseases

Seungwan Han[1,2†], Yunho Gim[1,2†], Eun-Hae Jang[1,3] and Eun-Mi Hur[1,2,3,4*]

[1]Laboratory of Neuroscience, College of Veterinary Medicine and Research Institute for Veterinary Science, Seoul National University, Seoul, South Korea, [2]BK21 Four Future Veterinary Medicine Leading Education and Research Center, College of Veterinary Medicine, Seoul National University, Seoul, South Korea, [3]Comparative Medicine Disease Research Center, Seoul National University, Seoul, South Korea, [4]Interdisciplinary Program in Neuroscience, College of Natural Sciences, Seoul National University, Seoul, South Korea

Neurodegenerative diseases (NDDs) are characterized by the progressive loss of selectively vulnerable populations of neurons, which is responsible for the clinical symptoms. Although degeneration of neurons is a prominent feature that undoubtedly contributes to and defines NDD pathology, it is now clear that neuronal cell death is by no means mediated solely by cell-autonomous mechanisms. Oligodendrocytes (OLs), the myelinating cells of the central nervous system (CNS), enable rapid transmission of electrical signals and provide metabolic and trophic support to neurons. Recent evidence suggests that OLs and their progenitor population play a role in the onset and progression of NDDs. In this review, we discuss emerging evidence suggesting a role of OL lineage cells in the pathogenesis of age-related NDDs. We start with multiple system atrophy, an NDD with a well-known oligodendroglial pathology, and then discuss Alzheimer's disease (AD) and Parkinson's disease (PD), NDDs which have been thought of as neuronal origins. Understanding the functions and dysfunctions of OLs might lead to the advent of disease-modifying strategies against NDDs.

KEYWORDS

oligodendrocyte, neurodegenerative disease, multiple system atrophy, Alzheimer's disease, Parkinson's disease

Abbreviations: AD, Alzheimer's disease; APP, amyloid precursor protein; Aβ, amyloid beta; BBB, blood-brain barrier; CNS, central nervous system; GCI, glial cytoplasmic inclusion; LB, Lewy body; MBP, myelin basic protein; MCT, monocarboxylate transporter; MS, multiple sclerosis; MSA, multiple system atrophy; NCI, neuronal cytoplasmic inclusion; NDD, neurodegenerative disease; OL, oligodendrocyte; OPC, oligodendrocyte progenitor cell; PD, Parkinson's disease; PS1, presenilin-1; SN, substantia nigra; TPPP, tubulin polymerization promoting protein; α-Syn, α-synuclein.

1 Introduction

Due to the lack of electrical activity, it was previously assumed that glial cells functioned as nerve-glue and performed housekeeping functions (Virchow et al., 1860). However, it is now clear that glia are key components of the nervous system, and their roles go far beyond housekeeping. Glia perform vital tasks including regulatory roles in neural circuit formation, synaptic transmission, ion homeostasis, metabolic support, and waste disposal (Allen and Lyons, 2018; Kato and Wake, 2021). Neurodegenerative diseases (NDDs) are characterized by the progressive loss of selectively vulnerable populations of neurons, and clinical symptoms manifested in each NDD depend on neurons that are primarily affected. Accordingly, NDD research focused on cell-autonomous neuronal mechanisms that lead to neuronal dysfunction and death. However, as in many other physiological and pathological processes, increasing evidence suggests that glia play much more active roles in NDDs than originally envisioned and may causally contribute to the onset and progression of NDDs.

Oligodendrocytes (OLs) are highly specialized cells that wrap axons with multiple myelin sheaths, which enable fast and efficient transduction of electrical signals. In the human brain, OLs comprise the most frequent glial cell population comprising 45–75% of glial cells, followed by astrocytes (19–40%) (von Bartheld et al., 2016). OL progenitor cells (OPCs) are present in the white and the gray matter, and they represent the largest population of dividing cells in the adult central nervous system (CNS) (Geha et al., 2010). OPCs retain the potential to proliferate, differentiate, and generate myelin-forming OLs throughout life (Rivers et al., 2008; Gibson et al., 2014). In the adult brain, new OLs are continually produced, and although the efficiency may not be high, newly formed OLs can become stably integrated into mature neural circuits and contribute to the generation of new myelin sheaths (Yeung et al., 2014; Hughes et al., 2018; Franklin et al., 2021). In addition to the formation and repair of myelin, oligodendroglia play a role in immunomodulation (Kirby and Castelo-Branco, 2021) and assure the long-term integrity of axons by providing metabolic and trophic support (Nave, 2010; Narine and Colognato, 2022), all of which are particularly relevant in the context of NDDs.

Multiple sclerosis (MS) is a neurodegenerative, demyelinating, and chronic inflammatory disease of the CNS, typically affecting young adults (Thompson et al., 2018; Tintore et al., 2019; McGinley et al., 2021). The pathological hallmark of MS is focal demyelinating lesions in the white and the gray matter of the brain and the spinal cord, and MS represents a disease in which OLs and myelin are prime targets of pathology (Filippi et al., 2018). Chronic demyelination is thought to trigger a pathogenic cascade of events that cause neurodegeneration: the loss of trophic and metabolic support from OLs, redistribution of ion channels along denuded axons, mitochondrial dysfunction, and enhanced oxidative stress have been proposed as potential mechanistic links leading to axon degeneration and neuronal cell death following myelin loss (Reich et al., 2018; Correale et al., 2019). In recent years, myelin loss and OL dysfunction have been implicated in many other NDDs, not only in the diseases where OL pathology is prominent, such as multiple system atrophy (MSA), but also in NDDs that have been thought of as primarily neuronal origins, such as Alzheimer's disease (AD) and Parkinson's disease (PD), two of the most prevalent NDDs. Thus, the relationship among oligodendroglia dysfunction, myelin loss, and neurodegeneration hinted from MS studies might be more general and applied to many other NDDs.

Here we discuss the role of oligodendroglia, which include OPCs and OLs, in NDDs, especially those associated with aging. Increasing evidence suggests that oligodendroglia respond sensitively to NDD pathology, and play an active role in the initiation and progression of NDDs. Deciphering the molecular mechanisms that regulate oligodendroglia function is likely to provide novel insights into developing regenerative therapies that may attenuate, halt, or even reverse the progression of NDDs.

2 OL and myelin dysfunction in NDDs

2.1 Multiple system atrophy

MSA is a devastating, adult-onset NDD in which multiple neuronal pathways degenerate, causing a multifaceted clinical presentation, including parkinsonism, cerebellar impairment, and autonomic dysfunctions in various combinations (Fanciulli and Wenning, 2015; Poewe et al., 2022). The pathological hallmark of MSA is the presence of glial cytoplasmic inclusions (GCIs), predominantly in OLs (Papp et al., 1989). GCIs are composed of α-synuclein (α-Syn) aggregates, classifying MSA as a synucleinopathy together with PD and dementia with Lewy bodies (LBs) (Malfertheiner et al., 2021). MSA histopathology also includes neuronal and astroglial inclusions, selective neuronal loss and axon degeneration, and myelin pallor accompanying gliosis (Jellinger, 2018). Controversy exists over whether myelin loss is the initial event that leads to neuronal cell death, or whether it is a secondary event as a result of neuronal degeneration, but evidence from postmortem studies and preclinical models supports the view that MSA is a primary oligodendrogliopathy (Fanciulli and Wenning, 2015; Ettle et al., 2016b). Consistent with this notion, restoring oligodendroglial function and enhancing the formation of new myelin have been suggested as a promising approach that may slow or halt disease progression (Ettle et al., 2016a).

Postmortem studies of MSA brains have shown significant correlations between GCI density and the severity of striatonigral degeneration and olivopontocerebellar atrophy

(Inoue et al., 1997; Ozawa et al., 2004), as well as the correlation between GCI pathology and disease duration (Ozawa et al., 2004). In MSA, neuronal pathology in the form of α-Syn-immunoreactive inclusions has also been reported and might be widespread (Cykowski et al., 2015). However, the topography of neuronal inclusions is poorly defined and their distribution and frequency show little correlation with neuronal cell death or the clinical symptoms of MSA.

Capturing the earliest changes, especially those that occur prior to the manifestation of MSA pathology might provide critical insights into the primary trigger of the disease. Although much can be learned from autopsy studies, postmortem data are not longitudinal in nature. To understand how the disease progresses and to investigate the cause-effect relationship between GCI and neurodegeneration, several rodent models of MSA designed to express human α-Syn in OLs have been generated. They develop GCI-like inclusions within OLs and exhibit neurodegeneration, myelin abnormalities, and/or motor deficits (Kahle et al., 2002; Shults et al., 2005; Yazawa et al., 2005). Although these transgenic lines force OLs to overexpress α-Syn, studies from these models suggest that the formation of GCI is sufficient to drive neurological dysfunction.

2.1.1 Progression of α-Syn pathology

α-Syn is produced primarily in neurons, and oligodendroglia do not normally express the protein (Solano et al., 2000; Miller et al., 2005). Although controversial, a few studies reported the presence of *SNCA* mRNA in OLs (Asi et al., 2014; Djelloul et al., 2015), suggesting the possibility that endogenous α-Syn in OLs might provide a source for GCIs. The mechanisms responsible for the accumulation of α-Syn in GCIs within OLs are unclear, but two hypotheses have been proposed. One possibility is that OLs pathologically increase the expression of α-Syn in MSA brains. However, postmortem studies of MSA brains failed to elucidate the increase of *SNCA* in OLs (Ozawa et al., 2001; Honglian et al., 2008; Asi et al., 2014). Another possibility is that OLs take up α-Syn secreted from neurons. Several studies have shown that OLs can internalize diverse forms of α-Syn and that neuronal α-Syn can be transferred to OLs (Kisos et al., 2012; Konno et al., 2012; Reyes et al., 2014). It is still enigmatic how α-Syn pathology propagates and selectively accumulates among oligodendroglia in MSA brains, but in the context of MSA, OLs might become more vulnerable to the invasion of α-Syn, and the mechanisms responsible for clearing pathogenic α-Syn might operate less effectively compared to neurons.

Tubulin polymerization promoting protein (TPPP)/p25α, an OL-specific phosphoprotein, is a component of GCI (Kovács et al., 2004) and has been suggested to contribute to the formation of OL-specific α-Syn strain (Ferreira et al., 2021). TPPP/p25α is known to play a role in organizing cellular microtubule network and promoting OL differentiation (Lehotzky et al., 2010; Fu et al., 2019). In normal brains, TPPP/p25α colocalizes with myelin basic protein (MBP), but in MSA brains, TPPP/p25α is found in the cell body (Song et al., 2007). Translocation of TPPP/p25α precedes GCI formation (Song et al., 2007), and this relocalization is thought to promote α-Syn aggregation by stabilizing unstructured α-Syn (Lindersson et al., 2005; Szunyogh et al., 2015). TPPP/p25α has also been suggested to counteract α-Syn degradation by inhibiting the maturation of autophagosome and its fusion with the lysosome (Ejlerskov et al., 2013; Lehotzky et al., 2021). TPPP/p25α bears a KFERQ-like motif and could be recognized and cleared via chaperone-mediated autophagy (Mavroeidi et al., 2022). These studies suggest that enhancing the autophagy-lysosome pathway might prevent GCI formation by facilitating the clearance of α-Syn and TPPP/p25α in OLs.

Accumulation of α-Syn in OLs has been shown to cause demyelination, iron overload, and exacerbate autophagy impairment (Poewe et al., 2022). Interestingly, in contrast to the severe neuronal loss, previous studies have reported that MSA brains show only a modest reduction in the number of OLs (Salvesen et al., 2015; Nykjær et al., 2017), suggesting that cellular dysfunction of OLs, and not necessarily cell death, induced by GCIs may be sufficient to cause neurodegeneration. These results were in disagreement with earlier studies documenting apoptotic cell death of OLs in MSA brains (Probst-Cousin et al., 1998; Kragh et al., 2009, 2013). Further studies are needed to thoroughly examine if the accumulation of α-Syn causes oligodendroglial death in MSA brains and if the death of GCI-positive OLs precedes and mediates neurodegeneration. Accumulation of α-Syn has also been detected in PDGFRα$^+$ OPCs and BCAS1$^+$ immature oligodendroglia in the brains of MSA patients and MSA transgenic mice overexpressing human wild-type α-Syn under the control of MBP promoter (May et al., 2014; Kaji et al., 2020). In MSA brains, the number of OPCs was increased (Ahmed et al., 2013; May et al., 2014), reminiscent of the increase in OPC number in a variety of other CNS damages (Keirstead et al., 1998; Schönrock et al., 1998; Hampton et al., 2004; Magnus et al., 2008). Enhanced proliferation of OPCs might occur in an attempt to compensate for the myelin loss (Franklin et al., 2021). However, under the burden of α-Syn, immature oligodendroglia cannot differentiate into mature OLs (Ettle et al., 2016a) and undergo cell death (May et al., 2014; Kaji et al., 2020), and thus fail to replace the defective OLs. Defective oligodendroglia will not be able to provide sufficient trophic and metabolic support to neurons (Jha and Morrison, 2020), and pathogenic α-Syn may induce neurodegeneration by directly disrupting essential cellular functions in neurons (Wong and Krainc, 2017) and indirectly via the aberrant activation of micro- and astrogliosis (Harms et al., 2021; **Figure 1**).

Both intraneuronal LBs, the pathological hallmark of PD, and GCIs are composed of α-Syn aggregates. However, MSA and PD show prominent differences not only in the clinical manifestations and the rate of disease progression, but also in the brain regions and cell types vulnerable to the deposition of

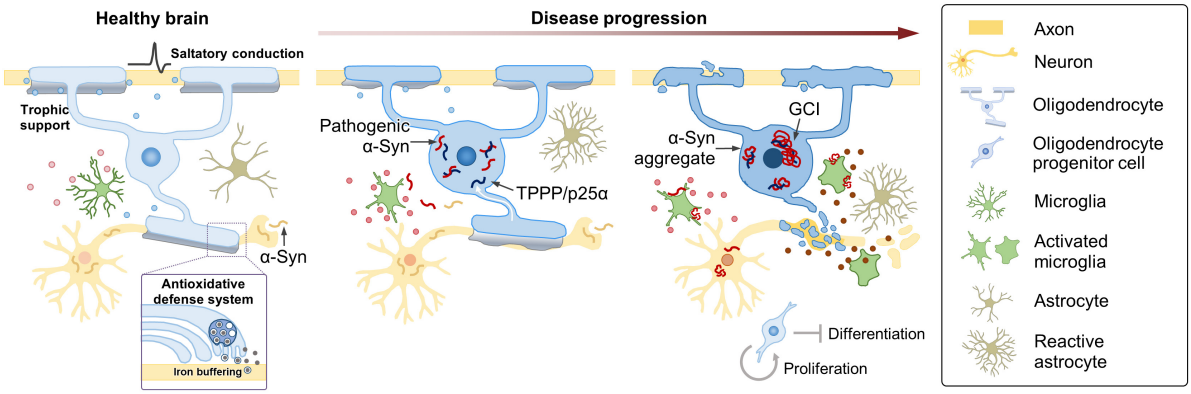

FIGURE 1
Oligodendroglial pathology and possible mechanisms contributing to MSA. Under healthy conditions, OLs enable saltatory conduction of electrical signals, provide metabolic and trophic support, and play a role in providing an antioxidant defense system to neurons. In MSA, TPPP/p25α relocates from the myelin sheath to the cell body, prior to α-Syn aggregation. Redistribution of TPPP/p25α causes cellular enlargement, and α-Syn starts to accumulate in the enlarged cytoplasm. Metabolic and trophic support of OLs to neurons is compromised, iron overload increases, and oxidative stress becomes aggravated. At later stages, α-Syn aggregates form GCIs in OLs. α-Syn is transformed into a toxic form in the intracellular environment of OL, where α-Syn seems to acquire distinct characteristics of MSA. MSA-type α-Syn might be transferred to neurons, and pathogenic α-Syn may induce neurodegeneration by directly interfering with essential neuronal functions or indirectly via aberrant activation of micro- and astrogliosis. As the disease progresses, microglia become destructive by releasing neurotoxic inflammatory mediators, such as cytokines, chemokines, and reactive oxygen and nitrogen species. The changing state of microglia, reflected in part, by their secretory profile, might play a crucial role in the progression of MSA. Enhanced proliferation of OPCs occurs, perhaps in an attempt to compensate for the myelin loss, but under the burden of α-Syn, immature oligodendroglia fail to differentiate and undergo cell death.

α-Syn. It has been suggested that pathological α-Syn in GCIs and LBs are conformationally and biologically distinct (Peng et al., 2018; Lau et al., 2020), with GCI-derived α-Syn aggregates being much more potent inducers of pathology than LB-derived aggregates (Peng et al., 2018). Peng et al. (2018) provided evidence that the different intracellular environments of OLs and neurons convert α-Syn seeds to different strains. Neuronal cytoplasmic inclusions (NCIs) are observed in MSA brains, albeit less frequently. The ultrastructure of NCIs resembles that of GCIs, rather than that of LBs from PD brains (Takeda et al., 1997), and filaments in GCIs and NCIs are morphologically indistinguishable (Murayama et al., 1992). In MSA, neurons are the likely source for the initial α-Syn (see above), but α-Syn is somehow transformed into a toxic form in the intracellular environment of OLs, where α-Syn seems to acquire distinct characteristics of MSA. To better understand MSA pathology, it will be of great importance to reveal the molecular determinants and cellular processes in the intracellular milieu of OLs that confer toxicity.

2.2 Alzheimer's disease

AD is the most common age-related NDD (Alzheimer's Association, 2019; Hou et al., 2019). AD presents cognitive and executive dysfunctions and is biologically defined by the presence of amyloid beta (Aβ) plaques and neurofibrillary tangles containing tau (Long and Holtzman, 2019; Knopman et al., 2021). Although AD is considered as a gray matter disease, postmortem AD brains clearly show white matter damages (Scheltens et al., 1995; Gouw et al., 2008; Nasrabady et al., 2018), and a number of studies have shown that the extent of myelin loss correlates with Aβ burden (Grimmer et al., 2012; Brickman et al., 2015a; Dean et al., 2017). Recently, single-cell transcriptomic analyses of individuals with AD pathology have revealed that oligodendroglia show pathology-responsive transcriptional signatures, in addition to neurons and microglia, the cell types which have been the primary focus in the AD research field (Grubman et al., 2019; Mathys et al., 2019; Chen et al., 2020). Of note, myelination-related genes were among the top differentially expressed genes perturbed in most major cell types in AD brains, suggesting that myelination has a key role in AD pathophysiology (Mathys et al., 2019). Postmortem brain samples from AD patients with the common variant of *TREM2* also showed significant changes in OLs: genes involved in differentiation were downregulated, whereas those related to lipid metabolism and oxidative stress were elevated, indicative of impaired myelination and metabolic adaptation to neuronal degeneration (Zhou et al., 2020).

Animal models of AD have greatly enhanced the understanding of the molecular and cellular mechanisms of the disease. Despite that existing models have focused largely on neurons with a particular emphasis on proteinopathy, several models exhibit defects or changes in oligodendroglia (Desai et al., 2009; Gu et al., 2018; Chacon-De-La-Rocha et al., 2020). A single-cell transcriptomic study using 5XFAD mice—a murine model of amyloidosis carrying five familial AD mutations—identified a novel OL population responding to Aβ

accumulation, defined by the expression of the complement component C4b and the serine protease inhibitor Serpina3n (Zhou et al., 2020). Other studies revealed the presence of distinct but shared OL populations, termed "disease-associated OLs," detected across many different pathological models, including mouse models of not only tauopathy and amyloidosis but also MS (Kenigsbuch et al., 2022; Pandey et al., 2022). Despite that the molecular signatures of OLs in human AD seemed to be largely distinct from those observed in mouse models (Zhou et al., 2020; Pandey et al., 2022), it is clear that OLs are vulnerable to neurodegenerative conditions and acquire a distinct cellular state in response to the changing microenvironment. A recent spatial transcriptomics study using brains from $APP^{NL\text{-}G\text{-}F}$ knock in mice (carrying Swedish KM670/671NL, Arctic E22G, and Beyreuther/Iberian I716F mutations) has demonstrated early alterations in a gene expression network enriched for myelin and OL genes (Chen et al., 2020). The gene set termed "OLIG module" mainly expressed by OLs was highly expressed under mild Aβ exposure but became downregulated in microenvironments with dense Aβ accumulation (Chen et al., 2020). Together with the postmortem analyses of human AD, data from animal models provide strong support for the notion that OLs dynamically respond to AD pathology (**Figure 2**).

In AD patients, white matter abnormalities can be detected at least a decade before clinical manifestations (Mortamais et al., 2013; Lee et al., 2016; Araque Caballero et al., 2018), and in AD mouse models, myelin disruption can be observed prior to the appearance of plaques and tangles (Desai et al., 2009). Moreover, white matter abnormalities are associated with the risk and the onset of AD (Tosto et al., 2014; Brickman et al., 2015b; Lee et al., 2016). These lines of evidence support the notion that OLs not only respond to pathology but also causally contribute to AD. Further studies are needed to examine if OL-specific gene expression can be detected in various models of AD, especially at early stages, as well as in sporadic AD and familial AD patients with other mutations to ensure that the transcriptional changes in OL lineage cells actually reflect a significant process during AD progression. More importantly, to thoroughly examine what roles oligodendroglia play in the neurodegenerative process and to investigate whether the changes in oligodendroglia are causative, it will be imperative to perform longitudinal studies in new models where initial changes take place in OPCs and/or OLs.

2.2.1 Possibility of targeting oligodendroglia for the treatment of AD

Given that myelin defect is highly associated with cognitive dysfunction, promoting myelination might provide a way to ameliorate clinical symptoms of AD. Recent studies showed that enhancing myelin renewal, by deletion of the muscarinic M1 receptor in oligodendroglia or administration of clemastine, rescued deficits in cognition and hippocampal physiology in APP/PS1 mouse—an AD model overexpressing human amyloid precursor protein (APP) and presenilin-1 (PS1) with mutations associated with early onset familial AD (Chen et al., 2021; Xie et al., 2021). To establish myelin loss as a major contributor to cognitive impairment in the context of AD, temporal dynamics of demyelination should be examined in other AD models, including those modeling tau pathology (Yoshiyama et al., 2007) and second-generation mouse models that have been generated to overcome the intrinsic drawbacks of the overexpression paradigm (Sasaguri et al., 2017).

Zhang et al. (2019) reported the presence of OPCs exhibiting a senescence-like phenotype characterized by the expression of p21/CDKN1A and p16/INK4/CDKN2A proteins in the Aβ plaque environments of brains of AD patients and the APP/PS1 mice. They also showed that the administration of senolytic drugs removed senescent OPCs from the brain, prevented plaque formation, and improved cognition in APP/PS1 mice. The exact mechanisms by which senescent OPCs contribute to the pathogenesis of AD remain to be investigated, but it is plausible to suggest that secretory profiles of the senescent OPCs play a role in triggering or enhancing local inflammation, demyelination, and/or neuronal dysfunction. In addition to serving as a reservoir for remyelination, OPCs have emerged as active participants in multiple aspects of brain function. OPCs receive synaptic information from neurons (Lin and Bergles, 2004), associate closely with the blood-brain barrier (BBB) (Seo et al., 2013), and play a role in immunomodulation by monitoring the environment and releasing various factors (Falcao et al., 2018; Kirby et al., 2019). Given the involvement of synaptic loss (Subramanian and Tremblay, 2021), BBB breakdown (Knox et al., 2022), and chronic inflammation (Stephenson et al., 2018) in the progression of AD as well as other NDDs, understanding the roles of OPCs and how they become dysregulated is likely to lay the groundwork for a new era of NDDs.

2.3 Parkinson's disease

PD is the most common neurodegenerative movement disorder (Feigin et al., 2019). The loss of dopaminergic neurons in the substantia nigra (SN) pars compacta and the deposition of α-Syn in neurons are neuropathological hallmarks of PD (Poewe et al., 2017). For PD, highly efficacious therapies to increase striatal dopamine levels are available, such as pharmacological dopamine substitution and deep brain stimulation (Poewe et al., 2017), providing an unrivaled example of an NDD that can be effectively managed. However, none of these treatments slow down disease progression, and there remains a critical unmet need for disease-modifying therapies that can delay, prevent, or reverse disease progression.

A recent study integrating genome-wide association studies with single-cell transcriptomic data from the mouse nervous

system revealed that PD is genetically associated not only with cholinergic and monoaminergic neurons, as expected, but also, unexpectedly, with OLs (Bryois et al., 2020). Interestingly, genes upregulated in PD were specifically expressed in OLs, while the downregulated genes were enriched in dopaminergic neurons. Moreover, using postmortem brain transcriptomic data, Bryois et al. (2020) confirmed that those upregulated genes in OLs were elevated across all Braak stages, even in the earliest stages of the disease. These results suggest that changes in OLs precede the emergence of pathological traits, giving new insights into the causes of PD. Consistent with these results, Agarwal et al. (2020) performed single-nuclei transcriptomics of the human SN and found that the genetic risk of PD was associated with OLs and OPCs, in addition to dopaminergic neurons. The fraction of PD genetic risk associated with OLs was distinct from that fraction associated with dopaminergic neurons (Agarwal et al., 2020), suggestive of distinct PD-associated cell etiologies. They also observed that the expression of *LRRK2* gene, which encodes leucine-rich repeat kinase 2 and which is associated with both familial and sporadic PD (Hur et al., 2019; Hur and Lee, 2021), was significantly higher in OPCs than in any other cell types in the SN (Agarwal et al., 2020). The physiological and pathological relevance of the manifestation of PD genetic risk through OLs and OPCs remains to be investigated, but it might reflect the role of oligodendroglia in controlling the local environment and regional vulnerability of the SN.

The myelination status or the degree of myelination has been suggested as a key factor determining neuronal vulnerability to Lewy pathology in PD (Braak et al., 2006; Orimo et al., 2011), along with other features, such as long highly branched axons, autonomous activity, calcium-dependent pacemaking, and high levels of oxidative stress (Braak et al., 2004; Chan et al., 2009). In postmortem studies, the accumulation of α-Syn was more evident in unmyelinated or poorly myelinated axons (Braak et al., 1999; Volpicelli-Daley et al., 2014). It is unclear if axonal hypomyelination aggravates α-Syn pathology or if the axonal accumulation of α-Syn affects membrane status or myelination, but Lewy neurites might reflect pathological changes in the structural or functional interaction between the axon and surrounding myelin. In fact, white matter abnormalities have often been reported in PD patients (Karagulle Kendi et al., 2008; Zhan et al., 2012; Melzer et al., 2013; Duncan et al., 2016). The pathogenesis is poorly understood, but white matter damage is detected in newly diagnosed PD patients and has been reported to occur before gray matter atrophy can be observed (Agosta et al., 2014; Duncan et al., 2016). A recent study taking a whole-brain connectomics approach also suggested a significantly decreased myelin content in PD patients compared with control subjects, especially along the connections emerging from the SN (Boshkovski et al., 2022). Despite the increasing evidence suggesting the possible involvement of oligodendroglia in PD, OLs have received far less attention in PD compared to MSA and AD. Further studies are needed to investigate how OL lineage cells are affected in PD and to explore if specific molecules or functional pathways in oligodendroglia can be targeted for therapeutic interventions.

3 Possible impact of defective myelin-axon coupling on neurodegeneration

Demyelination and dysfunction of oligodendroglia have been implicated in a number of NDDs, but it is difficult to ascertain whether defective oligodendroglia play a causal, or at least a primary role, in early disease stages. Oligodendroglia have long been suggested to provide trophic and metabolic support for neuronal survival. Mutant mice lacking proteolipid protein, a major myelin membrane protein, show late-onset axonal degeneration (Klugmann et al., 1997; Griffiths et al., 1998), and mice lacking 2', 3'-cyclic nucleotide 3'-phosphodiesterase, another myelin protein, exhibit abnormal axonal swelling and degeneration in the absence of major myelin alterations (Lappe-Siefke et al., 2003). These studies suggest that support from OLs is essential for long-term axonal survival (Micu et al., 2018), but also raise the question regarding the underlying mechanisms of OL-axon interactions. One way that OLs provide support to axons is via monocarboxylate transporters (MCTs), localized in myelin (MCT1) and on the axolemma (MCT2), which function to fuel lactate (Lee et al., 2012). It has been shown that disruption of MCT1 causes axonal damage and neuronal loss, and that MCT1 is reduced in patients with amyotrophic lateral sclerosis (Lee et al., 2012). The contribution of oligodendroglial MCTs to other NDDs requires further study. To determine whether oligodendroglia play a primary role in early stages of NDDs, it will be imperative to reveal the actual factors provided by OLs to nearby neurons and the mechanisms of interaction.

Postmortem studies have shown increased iron content in specific regions of MSA, PD, and AD brains (Raven et al., 2013; Carocci et al., 2018; Mochizuki et al., 2020). Although further study is needed to determine whether iron dyshomeostasis has a causal role and to investigate how much it contributes to the aggravation of neurodegeneration, there is evidence that iron dyshomeostasis is present at early stages in many NDDs (Ndayisaba et al., 2019). In the adult brain, OPCs and mature OLs are the cells with the highest iron levels (Connor and Menzies, 1996; Reinert et al., 2019). Oligodendroglia require iron as a cofactor for several enzymes that regulate the proliferation and differentiation of OPCs, as well as the production and maintenance of myelin (Todorich et al., 2009). The disturbance of iron homeostasis leads to the generation of free radicals and oxidative stress. Ferroptosis is a recently discovered type of cell death caused by the iron-dependent accumulation of lethal amounts of lipid-based reactive oxygen species (Dixon et al., 2012; Stockwell et al., 2017). Given

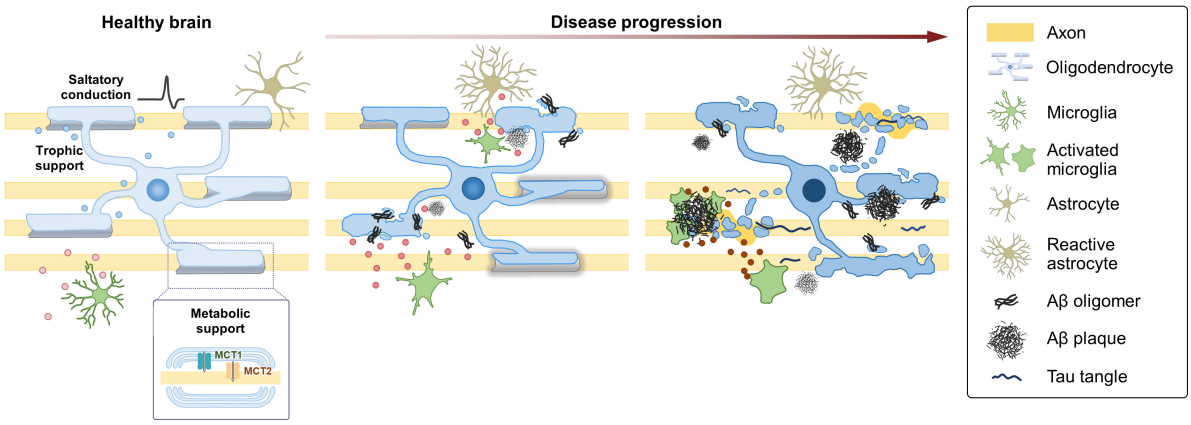

FIGURE 2
Dynamic changes of oligodendroglia during the progression of AD. Under healthy conditions, OLs enable saltatory conduction of electrical signals and provide metabolic and trophic support to neurons. In the AD brain, OLs are vulnerable to neurodegenerative conditions and acquire a distinct cellular state in response to the changing microenvironment. Under mild Aβ exposure, OLs alter gene expression and start to exhibit myelin defects. As the disease progresses, defects in OL function and myelin loss become more evident in correlation with the increased Aβ burden. Perturbation of myelin-axon coupling affects signal propagation as well as metabolic and trophic support. At later stages with higher Aβ burden, a specific subgroup of OLs express *C4b* and *Serpina3n*. Some aspects of the late-stage OLs might be shared across several NDDs. As AD progresses, microglia also become destructive by releasing neurotoxic inflammatory mediators, such as cytokines, chemokines, and reactive oxygen and nitrogen species. The changing state of microglia, reflected in part, by their secretory profile, might play a crucial role in the progression of AD.

the high intracellular iron concentration in oligodendroglia and low levels of antioxidative agents (such as glutathione and mitochondrial manganese superoxide dismutase) coupled with their high metabolic rate, it is tempting to speculate that in NDDs, oligodendroglia are extremely vulnerable to iron-induced oxidative damage and may undergo ferroptosis. Neurons are also sensitive to oxidative stress, and a recent study suggested that OLs play a role in protecting neighboring neurons from iron-mediated cytotoxicity via secretion of ferritin heavy chain (Mukherjee et al., 2020). It will be interesting to explore if ferroptosis in oligodendroglia and neurons plays a role in the pathogenesis of NDDs.

4 Uncovering the heterogeneity of oligodendroglia and the impact of aging

Recent studies have revealed that oligodendroglia comprise a heterogeneous population (Zeisel et al., 2015; Marques et al., 2016). OPCs and OLs might become morphologically and/or functionally diversified not only during development (Marques et al., 2018) but also during the course of diseases (Zhou et al., 2020). It remains to be determined if OPCs with certain genetic and molecular signatures have a higher potential to differentiate and myelinate. In the case of MS, it has been suggested that disease pathology results from the loss of a certain subclass of mature OLs rather than an overall failure of OPC differentiation, and thus, a general strategy to enhance OPC differentiation might be insufficient to enhance remyelination (Jakel et al., 2019). Therefore, elucidating heterogeneity and functional differences of the subclasses of oligodendroglia will be of great importance, and strategies to restore the ones that contribute to remyelination should be key. Analyses of AD patient brains and AD mouse models have revealed the presence of a specific population of OLs (Zhou et al., 2020; Kenigsbuch et al., 2022) exhibiting distinct gene expression profiles or phenotypes associated with pathology and/or neurodegeneration. Zhou et al. (2020) suggested that OL signatures associated with AD seemed to be different from those associated with MS (Jakel et al., 2019) or senescence (Zhang et al., 2019). By contrast, Kenigsbuch et al. (2022) suggested the presence of an OL state associated with diverse diseases, which could be found in multiple CNS pathologies, regardless of the nature of the etiology. Future studies are needed to examine whether the disease-responsive signature of OL lineage cells reported in AD models are also found in the context of other NDDs, and investigate to what extent the signatures are etiology-specific and how much they are conserved. Identification of the oligodendroglia population with the responsive vs. driving nature of the disease will also improve the understanding of the molecular and cellular pathways underlying the onset and progression of NDDs.

Advancing age is the single most prominent risk factor for NDDs. Although studies of OPC proliferation and differentiation in the developing nervous system have suggested a number of pathways that can be targeted to enhance remyelination in the mature nervous system (Fancy et al., 2011; Ishino et al., 2022), increasing evidence suggests that

young and old OPCs are not identical (Segel et al., 2019; de la Fuente et al., 2020). In fact, a substantial loss of myelinated fibers occurs with aging (Marner et al., 2003), and remyelination is thought to be one of the major processes in the brain affected by aging (Sim et al., 2002; Neumann et al., 2019). Decreased remyelination efficiency has been attributed to impaired infiltration of aged OPCs to the lesion area (Sim et al., 2002), reduced responsiveness of aged OPCs to pro-differentiation factors, and their slower inherent capacity for differentiation compared to young OPCs (Neumann et al., 2019). Transcriptomic analysis of OPCs isolated from young and old rats suggested that aged OPCs acquire a variety of hallmarks of aging. Nonetheless, OPCs persist throughout the lifespan (Young et al., 2013), and rodent studies show that aged OPCs can be rejuvenated and manipulated to undergo enhanced differentiation (Neumann et al., 2019; Wang et al., 2020; Iram et al., 2022). In addition to their contribution to remyelination, OPCs are thought to play much more diverse roles including synaptic, vascular, and immunomodulatory functions (Akay et al., 2021). Therefore, OPCs remain attractive targets with immense translational potential to overcome the effects of aging. A recent study suggested that aging was also associated with the induction of distinct subpopulations of mature OLs, one characterized by a high expression of Serpina3n and C4b and a smaller subpopulation characterized by the expression of genes related to an interferon response (Kaya et al., 2022). Much remains to be elucidated regarding how aging alters oligodendroglial lineage cells and how the changes in their cell state contribute to age-related myelin degeneration and insufficient myelin renewal. Developing methods to monitor and manipulate aged and young oligodendroglia *in vitro* and *in vivo*, technologies for *in vivo* imaging, and devising analytic tools to investigate OL physiology and function hold great potential to catalyze exciting studies deciphering functions and dysfunctions of oligodendroglia and their significance in the aging brain and NDD progression.

5 Concluding remarks

Despite the increased understanding of genetic factors and molecular mechanisms contributing to NDDs, none of the existing treatments alter the natural course of NDDs, and there has been limited success in translating the knowledge gained from preclinical studies into targeted therapies. NDD research has been neurocentric for decades, but the complexity and heterogeneity of NDDs suggest that NDDs result from the activation of more than one pathogenic pathway, perhaps involving multiple cell types as well as their interplay. Indeed, studies over the last two decades have revealed new pathways and cell types associated with NDDs, and we are beginning to appreciate that the cell types associated with the genetic risk for a particular NDD are not necessarily those cell types most directly affected by the defining pathology or those directly associated with the clinical symptoms. Here we have discussed recent findings suggesting an unexpected role of oligodendroglia, perhaps the cells that received far less attention compared to not only neurons but also other glial cells. Emerging evidence supports the view that OL lineage cells might be one of the most vulnerable cell types responding to the changing microenvironment in the brain during the course of NDDs. Moreover, OPCs and mature OLs might play a modifying role in the onset and progression of NDDs. Given that OPCs exist throughout life and retain the potential to generate new myelin, these cells may serve as reservoirs for regenerative therapy to combat NDDs. Understanding how oligodendroglia are affected in NDDs and how they can be controlled should lead to an in-depth understanding of NDDs and might help develop effective diagnostic and therapeutic approaches.

Author contributions

SH, YG, and E-MH wrote the first draft of the manuscript. E-HJ conceptualized and prepared the figures. All authors performed a literature search, contributed to revising the article, and approved the submitted version.

Funding

This work was supported by the National Research Foundation of Korea (NRF) grant funded by the Korea Government (MSIT) (NRF-2019R1A2C2010156, NRF-2021M3E5D9021369, NRF-2021R1A5A1033157 for SRC Program, Comparative Medicine Disease Research Center, NRF-2021M3F7A1083230), Research Institute for Veterinary Science at Seoul National University (SNU), and Creative-Pioneering Researchers Program through SNU (550-20210113).

Conflict of interest

The authors declare that the research was conducted in the absence of any commercial or financial relationships that could be construed as a potential conflict of interest.

Publisher's note

References

Agarwal, D., Sandor, C., Volpato, V., Caffrey, T. M., Monzón-Sandoval, J., Bowden, R., et al. (2020). A single-cell atlas of the human substantia nigra reveals cell-specific pathways associated with neurological disorders. *Nat. Commun.* 11:4183. doi: 10.1038/s41467-020-17876-0

Agosta, F., Canu, E., Stefanova, E., Sarro, L., Tomiæ, A., Špica, V., et al. (2014). Mild cognitive impairment in Parkinson's disease is associated with a distributed pattern of brain white matter damage. *Hum. Brain Mapp.* 35, 1921–1929. doi: 10.1002/hbm.22302

Ahmed, Z., Asi, Y. T., Lees, A. J., Revesz, T., and Holton, J. L. (2013). Identification and quantification of oligodendrocyte precursor cells in multiple system atrophy, progressive supranuclear palsy and Parkinson's disease. *Brain Pathol.* 23, 263–273. doi: 10.1111/j.1750-3639.2012.00637.x

Akay, L. A., Effenberger, A. H., and Tsai, L. H. (2021). Cell of all trades: oligodendrocyte precursor cells in synaptic, vascular, and immune function. *Genes Dev.* 35, 180–198. doi: 10.1101/gad.344218.120

Allen, N. J., and Lyons, D. A. (2018). Glia as architects of central nervous system formation and function. *Science* 362, 181–185. doi: 10.1126/science.aat0473

Alzheimer's Association (2019). 2019 Alzheimer's disease facts and figures. *Alzheimer's Dement.* 15, 321–387. doi: 10.1016/j.jalz.2019.01.010

Araque Caballero, M. Á, Suárez-Calvet, M., Duering, M., Franzmeier, N., Benzinger, T., Fagan, A. M., et al. (2018). White matter diffusion alterations precede symptom onset in autosomal dominant Alzheimer's disease. *Brain* 141, 3065–3080. doi: 10.1093/brain/awy229

Asi, Y. T., Simpson, J. E., Heath, P. R., Wharton, S. B., Lees, A. J., Revesz, T., et al. (2014). Alpha-synuclein mRNA expression in oligodendrocytes in MSA. *Glia* 62, 964–970. doi: 10.1002/glia.22653

Boshkovski, T., Cohen-Adad, J., Misic, B., Arnulf, I., Corvol, J.-C., Vidailhet, M., et al. (2022). The myelin-weighted connectome in Parkinson's disease. *Movement Disord.* 37, 724–733. doi: 10.1002/mds.28891

Braak, H., Bohl, J. R., Müller, C. M., Rüb, U., de Vos, R. A. I., and Del Tredici, K. (2006). Stanley Fahn Lecture 2005: the staging procedure for the inclusion body pathology associated with sporadic Parkinson's disease reconsidered. *Movement Disord.* 21, 2042–2051. doi: 10.1002/mds.21065

Braak, H., Ghebremedhin, E., Rüb, U., Bratzke, H., and Del Tredici, K. (2004). Stages in the development of Parkinson's disease-related pathology. *Cell Tissue Res.* 318, 121–134. doi: 10.1007/s00441-004-0956-9

Braak, H., Sandmann-Keil, D., Gai, W., and Braak, E. (1999). Extensive axonal Lewy neurites in Parkinson's disease: a novel pathological feature revealed by α-synuclein immunocytochemistry. *Neurosci. Lett.* 265, 67–69. doi: 10.1016/S0304-3940(99)00208-6

Brickman, A. M., Guzman, V. A., Gonzalez-Castellon, M., Razlighi, Q., Gu, Y., Narkhede, A., et al. (2015a). Cerebral autoregulation, beta amyloid, and white matter hyperintensities are interrelated. *Neurosci. Lett.* 592, 54–58. doi: 10.1016/j.neulet.2015.03.005

Brickman, A. M., Zahodne, L. B., Guzman, V. A., Narkhede, A., Meier, I. B., Griffith, E. Y., et al. (2015b). Reconsidering harbingers of dementia: progression of parietal lobe white matter hyperintensities predicts Alzheimer's disease incidence. *Neurobiol. Aging* 36, 27–32. doi: 10.1016/j.neurobiolaging.2014.07.019

Bryois, J., Skene, N. G., Hansen, T. F., Kogelman, L. J. A., Watson, H. J., Liu, Z., et al. (2020). Genetic identification of cell types underlying brain complex traits yields insights into the etiology of Parkinson's disease. *Nat. Genet.* 52, 482–493. doi: 10.1038/s41588-020-0610-9

Carocci, A., Catalano, A., Sinicropi, M. S., and Genchi, G. (2018). Oxidative stress and neurodegeneration: the involvement of iron. *BioMetals* 31, 715–735. doi: 10.1007/s10534-018-0126-2

Chacon-De-La-Rocha, I., Fryatt, G., Rivera, A. D., Verkhratsky, A., Raineteau, O., Gomez-Nicola, D., et al. (2020). Accelerated dystrophy and decay of oligodendrocyte precursor cells in the APP/PS1 model of Alzheimer's-like pathology. *Front. Cell Neurosci.* 14:575082. doi: 10.3389/fncel.2020.575082

Chan, C. S., Gertler, T. S., and Surmeier, D. J. (2009). Calcium homeostasis, selective vulnerability and Parkinson's disease. *Trends Neurosci.* 32, 249–256. doi: 10.1016/j.tins.2009.01.006

Chen, J.-F., Liu, K., Hu, B., Li, R.-R., Xin, W., Chen, H., et al. (2021). Enhancing myelin renewal reverses cognitive dysfunction in a murine model of Alzheimer's disease. *Neuron* 109, 2292–2307.e5. doi: 10.1016/j.neuron.2021.05.012.

Chen, W.-T., Lu, A., Craessaerts, K., Pavie, B., Sala Frigerio, C., Corthout, N., et al. (2020). Spatial transcriptomics and in situ sequencing to study Alzheimer's disease. *Cell* 182, 976–991.e9. doi: 10.1016/j.cell.2020.06.038.

Connor, J. R., and Menzies, S. L. (1996). Relationship of iron to oligondendrocytes and myelination. *Glia* 17, 83–93.

Correale, J., Marrodan, M., and Ysrraelit, M. C. (2019). Mechanisms of neurodegeneration and axonal dysfunction in progressive multiple sclerosis. *Biomedicines* 7:14. doi: 10.3390/biomedicines7010014

Cykowski, M. D., Coon, E. A., Powell, S. Z., Jenkins, S. M., Benarroch, E. E., Low, P. A., et al. (2015). Expanding the spectrum of neuronal pathology in multiple system atrophy. *Brain* 138, 2293–2309. doi: 10.1093/brain/awv114

de la Fuente, A. G., Queiroz, R. M. L., Ghosh, T., McMurran, C. E., Cubillos, J. F., Bergles, D. E., et al. (2020). Changes in the oligodendrocyte progenitor cell proteome with ageing. *Mol. Cell. Proteom.* 19, 1281–1302. doi: 10.1074/mcp.RA120.002102

Dean, D. C. III, Hurley, S. A., Kecskemeti, S. R., O'Grady, J. P., Canda, C., Davenport-Sis, N. J., et al. (2017). Association of amyloid pathology with myelin alteration in preclinical Alzheimer disease. *JAMA Neurol.* 74, 41–49. doi: 10.1001/jamaneurol.2016.3232

Desai, M. K., Sudol, K. L., Janelsins, M. C., Mastrangelo, M. A., Frazer, M. E., and Bowers, W. J. (2009). Triple-transgenic Alzheimer's disease mice exhibit region-specific abnormalities in brain myelination patterns prior to appearance of amyloid and tau pathology. *Glia* 57, 54–65. doi: 10.1002/glia.20734

Dixon, S. J., Lemberg, K. M., Lamprecht, M. R., Skouta, R., Zaitsev, E. M., Gleason, C. E., et al. (2012). Ferroptosis: an iron-dependent form of nonapoptotic cell death. *Cell* 149, 1060–1072. doi: 10.1016/j.cell.2012.03.042

Djelloul, M., Holmqvist, S., Boza-Serrano, A., Azevedo, C., Yeung, Maggie, S., et al. (2015). Alpha-Synuclein expression in the oligodendrocyte lineage: an in vitro and in vivo study using rodent and human models. *Stem Cell Rep.* 5, 174–184. doi: 10.1016/j.stemcr.2015.07.002

Duncan, G. W., Firbank, M. J., Yarnall, A. J., Khoo, T. K., Brooks, D. J., Barker, R. A., et al. (2016). Gray and white matter imaging: a biomarker for cognitive impairment in early Parkinson's disease? *Movement Disord.* 31, 103–110. doi: 10.1002/mds.26312

Ejlerskov, P., Rasmussen, I., Nielsen, T. T., Bergström, A.-L., Tohyama, Y., Jensen, P. H., et al. (2013). Tubulin polymerization-promoting protein (TPPP/p25α) promotes unconventional secretion of α-Synuclein through exophagy by impairing autophagosome-lysosome fusion*. *J. Biol. Chem.* 288, 17313–17335. doi: 10.1074/jbc.M112.401174

Ettle, B., Kerman, B. E., Valera, E., Gillmann, C., Schlachetzki, J. C. M., Reiprich, S., et al. (2016a). α-Synuclein-induced myelination deficit defines a novel interventional target for multiple system atrophy. *Acta Neuropathologica* 132, 59–75. doi: 10.1007/s00401-016-1572-y

Ettle, B., Schlachetzki, J. C. M., and Winkler, J. (2016b). Oligodendroglia and myelin in neurodegenerative diseases: more than just bystanders? *Mol. Neurobiol.* 53, 3046–3062. doi: 10.1007/s12035-015-9205-3

Falcao, A. M., van Bruggen, D., Marques, S., Meijer, M., Jakel, S., Agirre, E., et al. (2018). Disease-specific oligodendrocyte lineage cells arise in multiple sclerosis. *Nat. Med.* 24, 1837–1844. doi: 10.1038/s41591-018-0236-y

Fanciulli, A., and Wenning, G. K. (2015). Multiple-System atrophy. *New England J. Med.* 372, 249–263. doi: 10.1056/NEJMra1311488

Fancy, S. P. J., Chan, J. R., Baranzini, S. E., Franklin, R. J. M., and Rowitch, D. H. (2011). Myelin regeneration: a recapitulation of development? *Ann. Rev. Neurosci.* 34, 21–43. doi: 10.1146/annurev-neuro-061010-113629

Feigin, V. L., Nichols, E., Alam, T., Bannick, M. S., Beghi, E., Blake, N., et al. (2019). Global, regional, and national burden of neurological disorders, 1990–2016: a systematic analysis for the Global Burden of Disease Study 2016. *Lancet Neurol.* 18, 459–480. doi: 10.1016/S1474-4422(18)30499-X

Ferreira, N., Gram, H., Sorrentino, Z. A., Gregersen, E., Schmidt, S. I., Reimer, L., et al. (2021). Multiple system atrophy-associated oligodendroglial protein p25α stimulates formation of novel α-synuclein strain with enhanced neurodegenerative potential. *Acta Neuropathol.* 142, 87–115. doi: 10.1007/s00401-021-02316-0

Filippi, M., Bar-Or, A., Piehl, F., Preziosa, P., Solari, A., Vukusic, S., et al. (2018). Multiple sclerosis. *Nat. Rev. Dis. Primers* 4:43. doi: 10.1038/s41572-018-0041-4

Franklin, R. J. M., Frisén, J., and Lyons, D. A. (2021). Revisiting remyelination: towards a consensus on the regeneration of CNS myelin. *Sem. Cell Dev. Biol.* 116, 3–9. doi: 10.1016/j.semcdb.2020.09.009

Fu, M.-M., McAlear, T. S., Nguyen, H., Oses-Prieto, J. A., Valenzuela, A., Shi, R. D., et al. (2019). The golgi outpost protein TPPP nucleates microtubules and is critical for myelination. *Cell* 179, 132–146.e14. doi: 10.1016/j.cell.2019.08.025.

Geha, S., Pallud, J., Junier, M.-P., Devaux, B., Leonard, N., Chassoux, F., et al. (2010). NG2+/Olig2+ cells are the major cycle-related cell population of the adult

human normal brain. *Brain Pathol.* 20, 399–411. doi: 10.1111/j.1750-3639.2009.00295.x

Gibson, E. M., Purger, D., Mount, C. W., Goldstein, A. K., Lin, G. L., Wood, L. S., et al. (2014). Neuronal activity promotes oligodendrogenesis and adaptive myelination in the mammalian brain. *Science* 344:1252304. doi: 10.1126/science.1252304

Gouw, A. A., Seewann, A., Vrenken, H., van der Flier, W. M., Rozemuller, J. M., Barkhof, F., et al. (2008). Heterogeneity of white matter hyperintensities in Alzheimer's disease: post-mortem quantitative MRI and neuropathology. *Brain* 131, 3286–3298. doi: 10.1093/brain/awn265

Griffiths, I., Klugmann, M., Anderson, T., Yool, D., Thomson, C., Schwab, M. H., et al. (1998). Axonal swellings and degeneration in mice lacking the major proteolipid of myelin. *Science* 280, 1610–1613. doi: 10.1126/science.280.5369.1610

Grimmer, T., Faust, M., Auer, F., Alexopoulos, P., Förstl, H., Henriksen, G., et al. (2012). White matter hyperintensities predict amyloid increase in Alzheimer's disease. *Neurobiol. Aging* 33, 2766–2773. doi: 10.1016/j.neurobiolaging.2012.01.016

Grubman, A., Chew, G., Ouyang, J. F., Sun, G., Choo, X. Y., McLean, C., et al. (2019). A single-cell atlas of entorhinal cortex from individuals with Alzheimer's disease reveals cell-type-specific gene expression regulation. *Nat. Neurosci.* 22, 2087–2097. doi: 10.1038/s41593-019-0539-4

Gu, L., Wu, D., Tang, X., Qi, X., Li, X., Bai, F., et al. (2018). Myelin changes at the early stage of 5XFAD mice. *Brain Res. Bull.* 137, 285–293. doi: 10.1016/j.brainresbull.2017.12.013

Hampton, D. W., Rhodes, K. E., Zhao, C., Franklin, R. J. M., and Fawcett, J. W. (2004). The responses of oligodendrocyte precursor cells, astrocytes and microglia to a cortical stab injury, in the brain. *Neuroscience* 127, 813–820. doi: 10.1016/j.neuroscience.2004.05.028

Harms, A. S., Ferreira, S. A., and Romero-Ramos, M. (2021). Periphery and brain, innate and adaptive immunity in Parkinson's disease. *Acta Neuropathol.* 141, 527–545. doi: 10.1007/s00401-021-02268-5

Honglian, J., Ishikawa, K., Tsunemi, T., Ishiguro, T., Amino, T., and Mizusawa, H. (2008). Analyses of copy number and mRNA expression level of the α-synuclein gene in multiple system atrophy. *J. Med. Dental Sci.* 55, 145–153. doi: 10.11480/jmds.550117

Hou, Y., Dan, X., Babbar, M., Wei, Y., Hasselbalch, S. G., Croteau, D. L., et al. (2019). Ageing as a risk factor for neurodegenerative disease. *Nat. Rev. Neurol.* 15, 565–581. doi: 10.1038/s41582-019-0244-7

Hughes, E. G., Orthmann-Murphy, J. L., Langseth, A. J., and Bergles, D. E. (2018). Myelin remodeling through experience-dependent oligodendrogenesis in the adult somatosensory cortex. *Nat. Neurosci.* 21, 696–706. doi: 10.1038/s41593-018-0121-5

Hur, E.-M., Jang, E.-H., Jeong, G. R., and Lee, B. D. (2019). LRRK2 and membrane trafficking: nexus of Parkinson's disease. *BMB Rep.* 52, 533–539. doi: 10.5483/BMBRep.2019.52.9.186

Hur, E. M., and Lee, B. D. (2021). LRRK2 at the crossroad of aging and Parkinson's disease. *Genes (Basel)* 12:505. doi: 10.3390/genes12040505

Inoue, M., Yagishita, S., Ryo, M., Hasegawa, K., Amano, N., and Matsushita, M. (1997). The distribution and dynamic density of oligodendroglial cytoplasmic inclusions (GCIs) in multiple system atrophy: a correlation between the density of GCIs and the degree of involvement of striatonigral and olivopontocerebellar systems. *Acta Neuropathol.* 93, 585–591. doi: 10.1007/s004010050655

Iram, T., Kern, F., Kaur, A., Myneni, S., Morningstar, A. R., Shin, H., et al. (2022). Young CSF restores oligodendrogenesis and memory in aged mice via Fgf17. *Nature* 605, 509–515. doi: 10.1038/s41586-022-04722-0

Ishino, Y., Shimizu, S., Tohyama, M., and Miyata, S. (2022). Coactivator-associated arginine methyltransferase 1 controls oligodendrocyte differentiation in the corpus callosum during early brain development. *Dev. Neurobiol.* 82, 245–260. doi: 10.1002/dneu.22871

Jakel, S., Agirre, E., Mendanha Falcao, A., van Bruggen, D., Lee, K. W., Knuesel, I., et al. (2019). Altered human oligodendrocyte heterogeneity in multiple sclerosis. *Nature* 566, 543–547. doi: 10.1038/s41586-019-0903-2

Jellinger, K. A. (2018). Multiple system atrophy: an oligodendroglioneural synucleinopathy. *J. Alzheimer's Dis.* 62, 1141–1179. doi: 10.3233/JAD-170397

Jha, M. K., and Morrison, B. M. (2020). Lactate transporters mediate glia-neuron metabolic crosstalk in homeostasis and disease. *Front. Cell. Neurosci.* 14:589582. doi: 10.3389/fncel.2020.589582

Kahle, P. J., Neumann, M., Ozmen, L., Müller, V., Jacobsen, H., Spooren, W., et al. (2002). Hyperphosphorylation and insolubility of α-synuclein in transgenic mouse oligodendrocytes. *EMBO Rep.* 3, 583–588. doi: 10.1093/embo-reports/kvf109

Kaji, S., Maki, T., Ueda, J., Ishimoto, T., Inoue, Y., Yasuda, K., et al. (2020). BCAS1-positive immature oligodendrocytes are affected by the α-synuclein-induced pathology of multiple system atrophy. *Acta Neuropathol. Commun.* 8:120. doi: 10.1186/s40478-020-00997-4

Karagulle Kendi, A. T., Lehericy, S., Luciana, M., Ugurbil, K., and Tuite, P. (2008). Altered diffusion in the frontal lobe in Parkinson disease. *Am. J. Neuroradiol.* 29:501. doi: 10.3174/ajnr.A0850

Kato, D., and Wake, H. (2021). Myelin plasticity modulates neural circuitry required for learning and behavior. *Neurosci. Res.* 167, 11–16. doi: 10.1016/j.neures.2020.12.005

Kaya, T., Mattugini, N., Liu, L., Ji, H., Cantuti-Castelvetri, L., Wu, J., et al. (2022). CD8+ T cells induce interferon-responsive oligodendrocytes and microglia in white matter aging. *Nat. Neurosci.* 25, 1446–1457. doi: 10.1038/s41593-022-01183-6

Keirstead, H. S., Levine, J. M., and Blakemore, W. F. (1998). Response of the oligodendrocyte progenitor cell population (defined by NG2 labelling) to demyelination of the adult spinal cord. *Glia* 22, 161–170.

Kenigsbuch, M., Bost, P., Halevi, S., Chang, Y., Chen, S., Ma, Q., et al. (2022). A shared disease-associated oligodendrocyte signature among multiple CNS pathologies. *Nat. Neurosci.* 25, 876–886. doi: 10.1038/s41593-022-01104-7

Kirby, L., and Castelo-Branco, G. (2021). Crossing boundaries: interplay between the immune system and oligodendrocyte lineage cells. *Sem. Cell Dev. Biol.* 116, 45–52. doi: 10.1016/j.semcdb.2020.10.013

Kirby, L., Jin, J., Cardona, J. G., Smith, M. D., Martin, K. A., Wang, J., et al. (2019). Oligodendrocyte precursor cells present antigen and are cytotoxic targets in inflammatory demyelination. *Nat. Commun.* 10:3887. doi: 10.1038/s41467-019-11638-3

Kisos, H., Pukaß, K., Ben-Hur, T., Richter-Landsberg, C., and Sharon, R. (2012). Increased neuronal α-Synuclein pathology associates with its accumulation in oligodendrocytes in mice modeling α-Synucleinopathies. *PLoS One* 7:e46817. doi: 10.1371/journal.pone.0046817

Klugmann, M., Schwab, M. H., Pühlhofer, A., Schneider, A., Zimmermann, F., Griffiths, I. R., et al. (1997). Assembly of CNS myelin in the absence of proteolipid protein. *Neuron* 18, 59–70. doi: 10.1016/S0896-6273(01)80046-5

Knopman, D. S., Amieva, H., Petersen, R. C., Chételat, G., Holtzman, D. M., Hyman, B. T., et al. (2021). Alzheimer disease. *Nat. Rev. Dis. Primers* 7:33. doi: 10.1038/s41572-021-00269-y

Knox, E. G., Aburto, M. R., Clarke, G., Cryan, J. F., and O'Driscoll, C. M. (2022). The blood-brain barrier in aging and neurodegeneration. *Mol. Psychiatry* 27, 2659–2673. doi: 10.1038/s41380-022-01511-z

Konno, M., Hasegawa, T., Baba, T., Miura, E., Sugeno, N., Kikuchi, A., et al. (2012). Suppression of dynamin GTPase decreases α-synuclein uptake by neuronal and oligodendroglial cells: a potent therapeutic target for synucleinopathy. *Mol. Neurodegeneration* 7:38. doi: 10.1186/1750-1326-7-38

Kovács, G. G., László, L., Kovács, J., Jensen, P. H., Lindersson, E., Botond, G., et al. (2004). Natively unfolded tubulin polymerization promoting protein TPPP/p25 is a common marker of alpha-synucleinopathies. *Neurobiol. Dis.* 17, 155–162. doi: 10.1016/j.nbd.2004.06.006

Kragh, C. L., Fillon, G., Gysbers, A., Hansen, H. D., Neumann, M., Richter-Landsberg, C., et al. (2013). FAS-Dependent cell death in α-Synuclein transgenic oligodendrocyte models of multiple system atrophy. *PLoS One* 8:e55243. doi: 10.1371/journal.pone.0055243

Kragh, C. L., Lund, L. B., Febbraro, F., Hansen, H. D., Gai, W.-P., El-Agnaf, O., et al. (2009). α-Synuclein aggregation and Ser-129 phosphorylation-dependent cell death in oligodendroglial cells*. *J. Biol. Chem.* 284, 10211–10222. doi: 10.1074/jbc.M809671200

Lappe-Siefke, C., Goebbels, S., Gravel, M., Nicksch, E., Lee, J., Braun, P. E., et al. (2003). Disruption of Cnp1 uncouples oligodendroglial functions in axonal support and myelination. *Nat. Genet.* 33, 366–374. doi: 10.1038/ng1095

Lau, A., So, R. W. L., Lau, H. H. C., Sang, J. C., Ruiz-Riquelme, A., Fleck, S. C., et al. (2020). α-Synuclein strains target distinct brain regions and cell types. *Nat. Neurosci.* 23, 21–31. doi: 10.1038/s41593-019-0541-x

Lee, S., Viqar, F., Zimmerman, M. E., Narkhede, A., Tosto, G., Benzinger, T. L. S., et al. (2016). White matter hyperintensities are a core feature of Alzheimer's disease: evidence from the dominantly inherited Alzheimer network. *Ann. Neurol.* 79, 929–939. doi: 10.1002/ana.24647

Lee, Y., Morrison, B. M., Li, Y., Lengacher, S., Farah, M. H., Hoffman, P. N., et al. (2012). Oligodendroglia metabolically support axons and contribute to neurodegeneration. *Nature* 487, 443–448. doi: 10.1038/nature11314

Lehotzky, A., Lau, P., Tőkési, N., Muja, N., Hudson, L. D., and Ovádi, J. (2010). Tubulin polymerization-promoting protein (TPPP/p25) is critical for oligodendrocyte differentiation. *Glia* 58, 157–168. doi: 10.1002/glia.20909

Lehotzky, A., Olah, J., Fekete, J. T., Szenasi, T., Szabo, E., Gyorffy, B., et al. (2021). Co-Transmission of Alpha-Synuclein and TPPP/p25 inhibits their proteolytic degradation in human cell models. *Front. Mol. Biosci.* 8:666026. doi: 10.3389/fmolb.2021.666026

Lin, S.-C., and Bergles, D. E. (2004). Synaptic signaling between GABAergic interneurons and oligodendrocyte precursor cells in the hippocampus. *Nat. Neurosci.* 7, 24–32. doi: 10.1038/nn1162

Lindersson, E., Lundvig, D., Petersen, C., Madsen, P., Nyengaard, J. R., Højrup, P., et al. (2005). p25α stimulates α-Synuclein aggregation and is co-localized with aggregated α-Synuclein in α-Synucleinopathies*. *J. Biol. Chem.* 280, 5703–5715. doi: 10.1074/jbc.M410409200

Long, J. M., and Holtzman, D. M. (2019). Alzheimer disease: an update on pathobiology and treatment strategies. *Cell* 179, 312–339. doi: 10.1016/j.cell.2019.09.001

Magnus, T., Carmen, J., Deleon, J., Xue, H., Pardo, A. C., Lepore, A. C., et al. (2008). Adult glial precursor proliferation in mutant SOD1G93A mice. *Glia* 56, 200–208. doi: 10.1002/glia.20604

Malfertheiner, K., Stefanova, N., and Heras-Garvin, A. (2021). The concept of α-Synuclein strains and how different conformations may explain distinct neurodegenerative disorders. *Front. Neurol.* 12:737195. doi: 10.3389/fneur.2021.737195

Marner, L., Nyengaard, J. R., Tang, Y., and Pakkenberg, B. (2003). Marked loss of myelinated nerve fibers in the human brain with age. *J. Comp. Neurol.* 462, 144–152. doi: 10.1002/cne.10714

Marques, S., van Bruggen, D., Vanichkina, D. P., Floriddia, E. M., Munguba, H., Väremo, L., et al. (2018). Transcriptional convergence of oligodendrocyte lineage progenitors during development. *Dev. Cell* 46, 504–517.e7. doi: 10.1016/j.devcel.2018.07.005.

Marques, S., Zeisel, A., Codeluppi, S., van Bruggen, D., Mendanha Falcão, A., Xiao, L., et al. (2016). Oligodendrocyte heterogeneity in the mouse juvenile and adult central nervous system. *Science* 352, 1326–1329. doi: 10.1126/science.aaf6463

Mathys, H., Davila-Velderrain, J., Peng, Z., Gao, F., Mohammadi, S., Young, J. Z., et al. (2019). Single-cell transcriptomic analysis of Alzheimer's disease. *Nature* 570, 332–337. doi: 10.1038/s41586-019-1195-2

Mavroeidi, P., Arvanitaki, F., Vetsi, M., Becker, S., Vlachakis, D., Jensen, P. H., et al. (2022). Autophagy mediates the clearance of oligodendroglial SNCA/alpha-synuclein and TPPP/p25A in multiple system atrophy models. *Autophagy* 18, 2104–2133. doi: 10.1080/15548627.2021.2016256

May, V. E. L., Ettle, B., Poehler, A.-M., Nuber, S., Ubhi, K., Rockenstein, E., et al. (2014). α-Synuclein impairs oligodendrocyte progenitor maturation in multiple system atrophy. *Neurobiol. Aging* 35, 2357–2368. doi: 10.1016/j.neurobiolaging.2014.02.028

McGinley, M. P., Goldschmidt, C. H., and Rae-Grant, A. D. (2021). Diagnosis and treatment of multiple sclerosis: a review. *JAMA* 325, 765–779. doi: 10.1001/jama.2020.26858

Melzer, T. R., Watts, R., MacAskill, M. R., Pitcher, T. L., Livingston, L., Keenan, R. J., et al. (2013). White matter microstructure deteriorates across cognitive stages in Parkinson disease. *Neurology* 80:1841. doi: 10.1212/WNL.0b013e3182929f62

Micu, I., Plemel, J. R., Caprariello, A. V., Nave, K.-A., and Stys, P. K. (2018). Axo-myelinic neurotransmission: a novel mode of cell signalling in the central nervous system. *Nat. Rev. Neurosci.* 19, 49–58. doi: 10.1038/nrn.2017.128

Miller, D. W., Johnson, J. M., Solano, S. M., Hollingsworth, Z. R., Standaert, D. G., and Young, A. B. (2005). Absence of α-synuclein mRNA expression in normal and multiple system atrophy oligodendroglia. *J. Neural Transmission* 112, 1613–1624. doi: 10.1007/s00702-005-0378-1

Mochizuki, H., Choong, C.-J., and Baba, K. (2020). Parkinson's disease and iron. *J. Neural Transmission* 127, 181–187. doi: 10.1007/s00702-020-02149-3

Mortamais, M., Reynes, C., Brickman, A. M., Provenzano, F. A., Muraskin, J., Portet, F., et al. (2013). Spatial distribution of cerebral white matter lesions predicts progression to mild cognitive impairment and dementia. *PLoS One* 8:e56972. doi: 10.1371/journal.pone.0056972

Mukherjee, C., Kling, T., Russo, B., Miebach, K., Kess, E., Schifferer, M., et al. (2020). Oligodendrocytes provide antioxidant defense function for neurons by secreting ferritin heavy chain. *Cell Metab.* 32, 259–272.e10. doi: 10.1016/j.cmet.2020.05.019.

Murayama, S., Arima, K., Nakazato, Y., Satoh, J.-I., Oda, M., and Inose, T. (1992). Immunocytochemical and ultrastructural studies of neuronal and oligodendroglial cytoplasmic inclusions in multiple system atrophy. *Acta Neuropathol.* 84, 32–38. doi: 10.1007/BF00427212

Narine, M., and Colognato, H. (2022). Current insights into oligodendrocyte metabolism and its power to sculpt the myelin landscape. *Front. Cell Neurosci.* 16:892968. doi: 10.3389/fncel.2022.892968

Nasrabady, S. E., Rizvi, B., Goldman, J. E., and Brickman, A. M. (2018). White matter changes in Alzheimer's disease: a focus on myelin and oligodendrocytes. *Acta Neuropathol. Commun.* 6:22. doi: 10.1186/s40478-018-0515-3

Nave, K.-A. (2010). Myelination and the trophic support of long axons. *Nat. Rev. Neurosci.* 11, 275–283. doi: 10.1038/nrn2797

Ndayisaba, A., Kaindlstorfer, C., and Wenning, G. K. (2019). Iron in neurodegeneration – cause or consequence? *Front. Neurosci.* 13:180. doi: 10.3389/fnins.2019.00180

Neumann, B., Baror, R., Zhao, C., Segel, M., Dietmann, S., Rawji, K. S., et al. (2019). Metformin restores CNS remyelination capacity by rejuvenating aged stem cells. *Cell Stem Cell* 25, 473–485.e8. doi: 10.1016/j.stem.2019.08.015.

Nykjær, C. H., Brudek, T., Salvesen, L., and Pakkenberg, B. (2017). Changes in the cell population in brain white matter in multiple system atrophy. *Movement Disord.* 32, 1074–1082. doi: 10.1002/mds.26979

Orimo, S., Uchihara, T., Kanazawa, T., Itoh, Y., Wakabayashi, K., Kakita, A., et al. (2011). Unmyelinated axons are more vulnerable to degeneration than myelinated axons of the cardiac nerve in Parkinson's disease. *Neuropathol. Appl. Neurobiol.* 37, 791–802. doi: 10.1111/j.1365-2990.2011.01194.x

Ozawa, T., Okuizumi, K., Ikeuchi, T., Wakabayashi, K., Takahashi, H., and Tsuji, S. (2001). Analysis of the expression level of α-synuclein mRNA using postmortem brain samples from pathologically confirmed cases of multiple system atrophy. *Acta Neuropathol.* 102, 188–190. doi: 10.1007/s004010100367

Ozawa, T., Paviour, D., Quinn, N. P., Josephs, K. A., Sangha, H., Kilford, L., et al. (2004). The spectrum of pathological involvement of the striatonigral and olivopontocerebellar systems in multiple system atrophy: clinicopathological correlations. *Brain* 127, 2657–2671. doi: 10.1093/brain/awh303

Pandey, S., Shen, K., Lee, S.-H., Shen, Y.-A. A., Wang, Y., Otero-García, M., et al. (2022). Disease-associated oligodendrocyte responses across neurodegenerative diseases. *Cell Rep.* 40:111189. doi: 10.1016/j.celrep.2022.111189

Papp, M. I., Kahn, J. E., and Lantos, P. L. (1989). Glial cytoplasmic inclusions in the CNS of patients with multiple system atrophy (striatonigral degeneration, olivopontocerebellar atrophy and Shy-Drager syndrome). *J. Neurol. Sci.* 94, 79–100. doi: 10.1016/0022-510X(89)90219-0

Peng, C., Gathagan, R. J., Covell, D. J., Medellin, C., Stieber, A., Robinson, J. L., et al. (2018). Cellular milieu imparts distinct pathological α-synuclein strains in α-synucleinopathies. *Nature* 557, 558–563. doi: 10.1038/s41586-018-0104-4

Poewe, W., Seppi, K., Tanner, C. M., Halliday, G. M., Brundin, P., Volkmann, J., et al. (2017). Parkinson disease. *Nat. Rev. Dis. Primers* 3:17013. doi: 10.1038/nrdp.2017.13

Poewe, W., Stankovic, I., Halliday, G., Meissner, W. G., Wenning, G. K., Pellecchia, M. T., et al. (2022). Multiple system atrophy. *Nat. Rev. Dis. Primers* 8:56. doi: 10.1038/s41572-022-00382-6

Probst-Cousin, S., Rickert, C. H., Schmid, K. W., and Gullotta, F. (1998). Cell death mechanisms in multiple system atrophy. *J. Neuropathol. Exp. Neurol.* 57, 814–821.

Raven, E. P., Lu, P. H., Tishler, T. A., Heydari, P., and Bartzokis, G. (2013). Increased iron levels and decreased tissue integrity in hippocampus of Alzheimer's disease detected in vivo with magnetic resonance imaging. *J. Alzheimer's Dis.* 37, 127–136. doi: 10.3233/JAD-130209

Reich, D. S., Lucchinetti, C. F., and Calabresi, P. A. (2018). Multiple sclerosis. *New England J. Med.* 378, 169–180. doi: 10.1056/NEJMra1401483

Reinert, A., Morawski, M., Seeger, J., Arendt, T., and Reinert, T. (2019). Iron concentrations in neurons and glial cells with estimates on ferritin concentrations. *BMC Neurosci.* 20:25. doi: 10.1186/s12868-019-0507-7

Reyes, J. F., Rey, N. L., Bousset, L., Melki, R., Brundin, P., and Angot, E. (2014). Alpha-synuclein transfers from neurons to oligodendrocytes. *Glia* 62, 387–398. doi: 10.1002/glia.22611

Rivers, L. E., Young, K. M., Rizzi, M., Jamen, F., Psachoulia, K., Wade, A., et al. (2008). PDGFRA/NG2 glia generate myelinating oligodendrocytes and piriform projection neurons in adult mice. *Nat. Neurosci.* 11, 1392–1401. doi: 10.1038/nn.2220

Salvesen, L., Ullerup, B. H., Sunay, F. B., Brudek, T., Løkkegaard, A., Agander, T. K., et al. (2015). Changes in total cell numbers of the basal ganglia in patients with multiple system atrophy — a stereological study. *Neurobiol. Dis.* 74, 104–113. doi: 10.1016/j.nbd.2014.11.008

Sasaguri, H., Nilsson, P., Hashimoto, S., Nagata, K., Saito, T., De Strooper, B., et al. (2017). APP mouse models for Alzheimer's disease preclinical studies. *EMBO J.* 36, 2473–2487. doi: 10.15252/embj.201797397

Scheltens, P., Barkhof, F., Leys, D., Wolters, E. C., Ravid, R., and Kamphorst, W. (1995). Histopathologic correlates of white matter changes on MRI in Alzheimer's disease and normal aging. *Neurology* 45:883. doi: 10.1212/WNL.45.5.883

Schönrock, L. M., Kuhlmann, T., Adler, S., Bitsch, A., and Brück, W. (1998). Identification of glial cell proliferation in early multiple sclerosis lesions. *Neuropathol. Appl. Neurobiol.* 24, 320–330. doi: 10.1046/j.1365-2990.1998.00131.x

Segel, M., Neumann, B., Hill, M. F. E., Weber, I. P., Viscomi, C., Zhao, C., et al. (2019). Niche stiffness underlies the ageing of central nervous system progenitor cells. *Nature* 573, 130–134. doi: 10.1038/s41586-019-1484-9

Seo, J. H., Miyamoto, N., Hayakawa, K., Pham, L.-D. D., Maki, T., Ayata, C., et al. (2013). Oligodendrocyte precursors induce early blood-brain barrier opening after white matter injury. *J. Clin. Investigation* 123, 782–786. doi: 10.1172/JCI65863

Shults, C. W., Rockenstein, E., Crews, L., Adame, A., Mante, M., Larrea, G., et al. (2005). Neurological and neurodegenerative alterations in a transgenic mouse model expressing human α-synuclein under oligodendrocyte promoter: implications for multiple system atrophy. *J. Neurosci.* 25, 10689–10699. doi: 10.1523/JNEUROSCI.3527-05.2005

Sim, F. J., Zhao, C., Penderis, J., and Franklin, R. J. M. (2002). The age-related decrease in CNS remyelination efficiency is attributable to an impairment of both oligodendrocyte progenitor recruitment and differentiation. *J. Neurosci.* 22:2451. doi: 10.1523/JNEUROSCI.22-07-02451.2002

Solano, S. M., Miller, D. W., Augood, S. J., Young, A. B., and Penney, J. B. Jr. (2000). Expression of α-synuclein, parkin, and ubiquitin carboxy-terminal hydrolase L1 mRNA in human brain: genes associated with familial Parkinson's disease. *Ann. Neurol.* 47, 201–210.

Song, Y. J. C., Lundvig, D. M. S., Huang, Y., Gai, W. P., Blumbergs, P. C., Højrup, P., et al. (2007). p25α relocalizes in oligodendroglia from myelin to cytoplasmic inclusions in multiple system atrophy. *Am. J. Pathol.* 171, 1291–1303. doi: 10.2353/ajpath.2007.070201

Stephenson, J., Nutma, E., van der Valk, P., and Amor, S. (2018). Inflammation in CNS neurodegenerative diseases. *Immunology* 154, 204–219. doi: 10.1111/imm.12922

Stockwell, B. R., Friedmann Angeli, J. P., Bayir, H., Bush, A. I., Conrad, M., Dixon, S. J., et al. (2017). Ferroptosis: a regulated cell death nexus linking metabolism, redox biology, and disease. *Cell* 171, 273–285. doi: 10.1016/j.cell.2017.09.021

Subramanian, J., and Tremblay, M. -È (2021). Editorial: synaptic loss and neurodegeneration. *Front. Cell. Neurosci.* 15:681029. doi: 10.3389/fncel.2021.681029

Szunyogh, S., Oláh, J., Szénási, T., Szabó, A., and Ovádi, J. (2015). Targeting the interface of the pathological complex of α-synuclein and TPPP/p25. *Biochim. Biophys. Acta (BBA) - Mol. Basis Dis.* 1852, 2653–2661. doi: 10.1016/j.bbadis.2015.09.012

Takeda, A., Arai, N., Komori, T., Kato, S., and Oda, M. (1997). Neuronal inclusions in the dentate fascia in patients with multiple system atrophy. *Neurosci. Lett.* 227, 157–160.

Thompson, A. J., Baranzini, S. E., Geurts, J., Hemmer, B., and Ciccarelli, O. (2018). Multiple sclerosis. *Lancet* 391, 1622–1636.

Tintore, M., Vidal-Jordana, A., and Sastre-Garriga, J. (2019). Treatment of multiple sclerosis — success from bench to bedside. *Nat. Rev. Neurol.* 15, 53–58. doi: 10.1038/s41582-018-0082-z

Todorich, B., Pasquini, J. M., Garcia, C. I., Paez, P. M., and Connor, J. R. (2009). Oligodendrocytes and myelination: the role of iron. *Glia* 57, 467–478. doi: 10.1002/glia.20784

Tosto, G., Zimmerman, M. E., Carmichael, O. T., Brickman, A. M., and Alzheimer's Disease Neuroimaging Initiative. (2014). Predicting aggressive decline in mild cognitive impairment: the importance of white matter hyperintensities. *JAMA Neurol.* 71, 872–877. doi: 10.1001/jamaneurol.2014.667

Virchow, R., Chance, F., and Goodsir, J. (1860). *Cellular Pathology as Based Upon Physiological and Pathological Histology; Twenty Lectures Delivered in the Pathological Institute of Berlin During the Months of February, March, and April, 1858*. London: John Churchill.

Volpicelli-Daley, L. A., Gamble, K. L., Schultheiss, C. E., Riddle, D. M., West, A. B., and Lee, V. M. Y. (2014). Formation of α-synuclein Lewy neurite–like aggregates in axons impedes the transport of distinct endosomes. *Mol. Biol. Cell* 25, 4010–4023. doi: 10.1091/mbc.e14-02-0741

von Bartheld, C. S., Bahney, J., and Herculano-Houzel, S. (2016). The search for true numbers of neurons and glial cells in the human brain: a review of 150 years of cell counting. *J. Comp. Neurol.* 524, 3865–3895. doi: 10.1002/cne.24040

Wang, F., Ren, S.-Y., Chen, J.-F., Liu, K., Li, R.-X., Li, Z.-F., et al. (2020). Myelin degeneration and diminished myelin renewal contribute to age-related deficits in memory. *Nat. Neurosci.* 23, 481–486. doi: 10.1038/s41593-020-0588-8

Wong, Y. C., and Krainc, D. (2017). α-synuclein toxicity in neurodegeneration: mechanism and therapeutic strategies. *Nat. Med.* 23, 1–13. doi: 10.1038/nm.4269

Xie, Y.-Y., Pan, T.-T., Xu, D.-E., Huang, X., Tang, Y., Huang, W., et al. (2021). Clemastine ameliorates myelin deficits via preventing senescence of oligodendrocytes precursor cells in Alzheimer's disease model mouse. *Front. Cell Dev. Biol.* 9:733945. doi: 10.3389/fcell.2021.733945

Yazawa, I., Giasson, B. I., Sasaki, R., Zhang, B., Joyce, S., Uryu, K., et al. (2005). Mouse model of multiple system atrophy α-Synuclein expression in oligodendrocytes causes glial and neuronal degeneration. *Neuron* 45, 847–859. doi: 10.1016/j.neuron.2005.01.032

Yeung, M. S., Zdunek, S., Bergmann, O., Bernard, S., Salehpour, M., Alkass, K., et al. (2014). Dynamics of oligodendrocyte generation and myelination in the human brain. *Cell* 159, 766–774. doi: 10.1016/j.cell.2014.10.011

Yoshiyama, Y., Higuchi, M., Zhang, B., Huang, S.-M., Iwata, N., Saido, et al. (2007). Synapse loss and microglial activation precede tangles in a P301S tauopathy mouse model. *Neuron* 53, 337–351. doi: 10.1016/j.neuron.2007.01.010

Young, K. M., Psachoulia, K., Tripathi, Richa, B., Dunn, S.-J., Cossell, L., et al. (2013). Oligodendrocyte dynamics in the healthy adult CNS: evidence for myelin remodeling. *Neuron* 77, 873–885. doi: 10.1016/j.neuron.2013.01.006

Zeisel, A., Muñoz-Manchado, A. B., Codeluppi, S., Lönnerberg, P., La Manno, G., Juréus, A., et al. (2015). Cell types in the mouse cortex and hippocampus revealed by single-cell RNA-seq. *Science* 347, 1138–1142. doi: 10.1126/science.aaa1934

Zhan, W., Kang, G. A., Glass, G. A., Zhang, Y., Shirley, C., Millin, R., et al. (2012). Regional alterations of brain microstructure in Parkinson's disease using diffusion tensor imaging. *Movement Disord.* 27, 90–97. doi: 10.1002/mds.23917

Zhang, P., Kishimoto, Y., Grammatikakis, I., Gottimukkala, K., Cutler, R. G., Zhang, S., et al. (2019). Senolytic therapy alleviates Aβ-associated oligodendrocyte progenitor cell senescence and cognitive deficits in an Alzheimer's disease model. *Nat. Neurosci.* 22, 719–728. doi: 10.1038/s41593-019-0372-9

Zhou, Y., Song, W. M., Andhey, P. S., Swain, A., Levy, T., Miller, K. R., et al. (2020). Human and mouse single-nucleus transcriptomics reveal TREM2-dependent and TREM2-independent cellular responses in Alzheimer's disease. *Nat. Med.* 26, 131–142. doi: 10.1038/s41591-019-0695-9

frontiers | Frontiers in Cellular Neuroscience

TYPE Original Research
PUBLISHED 22 December 2022
DOI 10.3389/fncel.2022.1049562

OPEN ACCESS

EDITED BY
Shingo Miyata,
Kindai University, Japan

REVIEWED BY
Laura Calza,
University of Bologna, Italy
Yugo Ishino,
Kindai University Hospital, Japan

*CORRESPONDENCE
Rongrong Zhu
✉ rrzhu@tongji.edu.cn
Liming Cheng
✉ limingcheng@tongji.edu.cn
Ning Xie
✉ nxieprof18@tongji.edu.cn

SPECIALTY SECTION
This article was submitted to Non-Neuronal Cells, a section of the journal Frontiers in Cellular Neuroscience

RECEIVED 20 September 2022
ACCEPTED 08 December 2022
PUBLISHED 22 December 2022

CITATION
Zhao Q, Zhu Y, Ren Y, Yin S, Yu L, Huang R, Song S, Hu X, Zhu R, Cheng L and Xie N (2022) Neurogenesis potential of oligodendrocyte precursor cells from oligospheres and injured spinal cord.
Front. Cell. Neurosci. 16:1049562.
doi: 10.3389/fncel.2022.1049562

Neurogenesis potential of oligodendrocyte precursor cells from oligospheres and injured spinal cord

Qing Zhao[1,2], Yanjing Zhu[1], Yilong Ren[1,2], Shuai Yin[1,2], Liqun Yu[1], Ruiqi Huang[1], Simin Song[1], Xiao Hu[1,2], Rongrong Zhu[1]*, Liming Cheng[1,2]* and Ning Xie[1,2]*

[1]Key Laboratory of Spine and Spinal Cord Injury Repair and Regeneration of Ministry of Education, Orthopaedic Department of Tongji Hospital, School of Medicine, School of Life Sciences and Technology, Tongji University, Shanghai, China, [2]Division of Spine, Department of Orthopedics, Tongji Hospital, Tongji University School of Medicine, Tongji University, Shanghai, China

Severe traumatic spinal cord injury (SCI) leads to long-lasting oligodendrocyte death and extensive demyelination in the lesion area. Oligodendrocyte progenitor cells (OPCs) are the reservoir of new mature oligodendrocytes during damaged myelin regeneration, which also have latent potential for neurogenic regeneration and oligospheres formation. Whether oligospheres derived OPCs can differentiate into neurons and the neurogenesis potential of OPCs after SCI remains unclear. In this study, primary OPCs cultures were used to generate oligospheres and detect the differentiation and neurogenesis potential of oligospheres. *In vivo*, SCI models of juvenile and adult mice were constructed. Combining the single-cell RNA sequencing (scRNA-seq), bulk RNA sequencing (RNA-seq), bioinformatics analysis, immunofluorescence staining, and molecular experiment, we investigated the neurogenesis potential and mechanisms of OPCs *in vitro* and *vivo*. We found that OPCs differentiation and oligodendrocyte morphology were significantly different between brain and spinal cord. Intriguingly, we identify a previously undescribed findings that OPCs were involved in oligospheres formation which could further differentiate into neuron-like cells. We also firstly detected the intermediate states of oligodendrocytes and neurons during oligospheres differentiation. Furthermore, we found that OPCs were significantly activated after SCI. Combining scRNA-seq and bulk RNA-seq data from injured spinal cord, we confirmed the neurogenesis potential of OPCs and the activation of endoplasmic reticulum stress after SCI. Inhibition of endoplasmic reticulum stress could effectively attenuate OPCs death. Additionally, we also found

that endoplasmic reticulum may regulate the stemness and differentiation of oligospheres. These findings revealed the neurogenesis potential of OPCs from oligospheres and injured spinal cord, which may provide a new source and a potential target for spinal cord repair.

KEYWORDS

spinal cord injury, oligodendrocyte precursor cell, oligosphere, neurogenesis potential, differentiation, transformation

1 Introduction

Oligodendrocytes are critical for myelin formation through repeatedly wrapping neuronal axons (Franklin and Ffrench-Constant, 2008; Irvine and Blakemore, 2008). Severe traumatic spinal cord injury (SCI) leads to locomotor and sensory function loss largely due to long-lasting oligodendrocyte death, extensive demyelination, and Wallerian degeneration (Garcia-Ovejero et al., 2014; Ahuja et al., 2017). Even in moderate SCI and a considerable distance from the lesion area, oligodendrocyte loss and demyelination can be serious (Lytle and Wrathall, 2007). After SCI, the main source of remyelination is from oligodendrocyte progenitor cells (OPCs), also known as NG2 cells. OPCs can migrate, proliferate and gradually differentiate into mature oligodendrocytes and then wrap axons to form a new myelin sheath (Wu et al., 2012).

Previous studies described that OPCs can form oligospheres (Avellana-Adalid et al., 1996; Chen et al., 2007; Pedraza et al., 2008; Gibney and McDermott, 2009; Li et al., 2015). Oligosphere derived OPCs preserve the capacity to express differentiated antigenic and metabolic phenotypes (Avellana-Adalid et al., 1996). When transplanted into the newborn shiverer mouse brain, oligospheres were able to provide a focal reservoir of migrating and myelinating cells (Avellana-Adalid et al., 1996). Recent findings confirmed that OPCs have latent potential for neurogenic regeneration, which may represent a potential target for reprogramming strategies for spinal cord repair (Heinrich et al., 2014; Torper et al., 2015; Tai et al., 2021). However, whether oligospheres derived OPCs can differentiate into neuron-like cells and the neurogenesis potential of OPCs after SCI remains unclear (Chen et al., 2007).

In this study, primary OPCs cultures were used to generate oligospheres and to oberserve the differentiation and neurogenesis potential of oligospheres. We reported a previously undescribed oligospheres derived OPCs could differentiate into neuron-like cells. During the process of differentiation, we firstly discovered the intermediate states of oligodendrocytes and neurons. *In vivo*, by constructing juvenile and adult SCI models, combining the single-cell RNA sequencing (scRNA-seq), RNA sequencing (RNA-seq), bioinformatics analysis, immunofluorescence staining, and molecular experiment, we further investigated the neurogenesis potential of OPCs and its mechanisms after SCI.

2 Materials and methods

2.1 Primary oligodendrocyte progenitor cells culture

The experimental procedures were designed to minimize the number of animals used as well as animal suffering. All procedures were carried out in accordance with protocols approved by the Institutional Animal Care and Use Committee (IACUC) of the Tongji University School of Medicine. Animals were housed on a 12-h light/dark cycle and had food and water available *ad libitum*. Three or more independent experiments were performed.

Primary OPCs cultures were obtained from postnatal day 1–2 (P1-2) Sprague Dawley rats (Shanghai Jiesijie Laboratory Animal Co., Ltd., China) cerebral cortices and spinal cord. Briefly, cerebral cortices and spinal cord were digested by papain (5 mg/ml, Cat# LS003126, Worthington) and seeded on 0.01% poly-D-lysine (PDL, Cat# C0312, Beyotime Institute of Biotechnology, China)-coated 75-cm^2 flasks. Dissociated cells were maintained in DMEM-F12 (Cat# 11330057, Gibco) containing 10% fetal bovine serum (FBS, Cat# 16000-044, Gibco) and 1% penicillin/streptomycin (Cat# 15140122, Gibco) at 37°C for 7 days. During this time, primary OPCs cultures were used for immunofluorescence staining to detect the differences in OPCs differentiation between brain and spinal cord.

Adherent cells were dissociated by Accutase (Cat# A1110501, Gibco) after reaching 70–80% confluency for 10 min at 37°C and then reseeded in 100 mm culture dishes (Cat# 430167, Corning) for 1 h. Then, the supernatant fluid was collected to remove the astrocytes and neuron. As described in a previous study (Hattori et al., 2017; Miyamoto et al., 2020), the medium was replated onto PDL-coated plates in OPCs proliferation medium to only collect OPCs, containing neurobasal medium (Cat# 10888022, Gibco), 10 ng/ml PDGF-AA (Cat# 315-17, Peprotech), 10 ng/ml bFGF (Cat#

45033, Peprotech), 2 mM glutamine (Cat# G7513, Sigma), 1% penicillin/streptomycin, 5 ng/ml insulin (Cat# P3376-100 IU, Beyotime Institute of Biotechnology, China), 20 ug/ml NT3 (Cat# 450-03-10, Peprotech), and 2% B27 supplement (Cat# A3582801, Gibco). Finally, OPCs with >95% purity were obtained (by cell count) and reseeded in 100 mm culture dishes (Cat# 430167, Corning) and poly-D-lysine-coated 12-well culture plates with cell climbing sheets for the next experiment.

2.2 Primary OPCs culture to generate oligospheres

Primary OPCs were obtained as described above. When OPCs with >95% purity were obtained, dissociated cells were reseeded in a new 100 mm non-coated Corning dish with OPCs proliferation medium. Oligospheres started to form after 4–5 days of culture, during which time the oligospheres were blown up and dissociated for resuspension, and facilitated oligospheres formation. The culture medium was changed every 3 days depending upon the cellular density. Approximately every 3 days half of the media was changed and cells passaged without digestive enzyme digestion. After elimination of adhering cells, oligospheres were centrifuged (800 rpm for 5 min) and resuspended in OPCs proliferation medium.

When oligospheres reached the fourth generation (F4), they were seeded into glass coverslips with PDL-coated 12-well culture plates. Immunofluorescence staining was performed to detect the differentiation of oligospheres at 4 h (Day 0) and Days 1, 3, 6, 9, 14, 21, and 28 after plating. We also found that some oligospheres tended to attach to the bottom of the plate, as previously reported (Chen et al., 2007), and free-floating oligospheres only were used for passaging. The oligosphere images under white light were taken by an Olympus microscope. Three independent experiments were performed.

2.3 Oxygen-glucose deprivation model and inhibitors treatment

To mimic hypoxic-ischaemic injury, an oxygen-glucose deprivation (OGD) model (O_2 < 0.1%) was constructed by AnaeroPack (Cat# D07, Mitsubishi Gas Chemical Company, Japan) in a 2.5 L closed plastic box. After reaching 70–80% confluency at 3 days, OPCs were incubated in hypoxic conditions with glucose-free DMEM (Cat# 11966025, Gibco) for 3 h and then switched to DMEM-F12 containing 10% FBS and 1% penicillin/streptomycin. The inositol-requiring protein 1α (IRE1α) inhibitor STF083010 (Cat# 307543-71-1, MedChemExpress) (Papandreou et al., 2011; Zhao et al., 2017a) and protein kinase RNA-like ER kinase (PERK) inhibitor GSK2656157 (Cat# 1337532-29-2, MedChemExpress) (Atkins et al., 2013) with different concentrations were used to treat primary oligodendrocytes at 1 h before and after OGD stimulation, respectively. Then, OPCs were collected for quantitative real-time PCR (RT–PCR), and live/dead cells by Calcein AM/PI double staining and flow cytometry of apoptosis by Annexin V-EGFP/PI double staining (Cat# KGA103, Jiangsu KeyGen BioTech Corp., Ltd. China). Staining methods followed the reference specification. Three independent experiments were performed.

2.4 Spinal cord contusion model construction

Eight-week-old wild-type C57BL/6 J female mice (Shanghai Jiesijie Laboratory Animal Co., Ltd.) were used for contusion model construction, including sham group (n = 9) and SCI group (n = 9). Spinal cord contusion models at T10 were established using the MASCIS Impactor Model III (W.M. Keck Center for Collaborative Neuroscience, Rutgers, The State University of New Jersey, USA) (Duan et al., 2021).

Briefly, mice were weighed and deeply anesthetized with iso-flurane evaporated in a gas mixture containing 70% N_2O and 30% O_2 through a nose mask. The back skin was shaved and cleaned with 75% alcohol. A laminectomy at T10 was performed to remove the part of the vertebra overlying the spinal cord, exposing a circle of dura through an operating microscope (Zeiss, Germany) and rodent stereotaxic apparatus (RWD Life Science Co., Ltd., Shenzhen, China). The spinal column was stabilized using lateral clamps over the lateral processes at T9 and T11. Contusion was performed at T10 with a 5 g impactor and 6.25 mm height with a force of about 60kdyn, which could cause a moderate injury as previously reported (Wu et al., 2013, 2014), and then the wound was sutured. Sham mice underwent laminectomy but not contusion.

The following symbols were indicators of a successful contusion model: (1) the impact point was located in the middle of T10, (2) paralysis of both hindlimbs occurred after awakening. Unsuccessful models were excluded in the following experiment and analysis. Mice had received natural illumination to keep warm before and after the surgery. Urine was manually expressed from the bladders of the injured mice twice per day until autonomous urination recovered. Six weeks after contusion, the mice were sacrificed for immunofluorescence staining.

2.5 Spinal cord crash model construction

Eight-week-old wild-type C57BL/6 J female mice (adult mice) and 1-week-old and 2-week-old juvenile mice were used

for spinal cord crash model construction, including sham and SCI groups of 1-week-old mice (Sham_1 W, n = 3; SCI_1 W, n = 3); sham and SCI groups of 2-week-old mice (Sham_2 W, n = 3; SCI_2 W, n = 3); sham and SCI groups of 8-week-old mice (adult female mice, Sham_8 W, n = 3; SCI_8 W, n = 3). Three biological repeats were performed.

The pre-operative disinfection, anesthesia, and post-operative care were conducted as the same as contusion model. The crash model was also performed at T10 with No. 5 Dumont forceps fixed on a stereotaxic apparatus and persisted for 3 s. The paralysis of both hindlimbs occurred after awakening were indicators of a successful crash model. Unsuccessful models were excluded in the following experiment and analysis. Sham mice received laminectomy without crash. The juvenile mice were returned to the female mice cage to continue feeding after crash. Two weeks after crash, the mice were sacrificed for RNA-sequencing.

2.6 Immunofluorescence staining and analysis

Briefly, mice were under deep anesthesia and intracardially perfused with saline and then with 4% paraformaldehyde at the indicated time. After post-fixation and cryoprotection, the dissected 6 mm segment of spinal cord centered at the lesion area, or 2 mm segment of lumbar enlargement (L4-5), was coronally sectioned at 12 μm thickness and thaw-mounted onto Superfrost Plus slides (Citotest Labware Manufacturing Co., Ltd., Haimen, China). Spinal cord sections were prepared for immunofluorescence staining following procedures described previously (Ren et al., 2017). The culture cells immunofluorescence staining of methods have been described previously (Zhu et al., 2021).

The primary antibodies used were as follows: glial fibrillary acidic protein (GFAP, Cat# ab4674, Abcam, 1:500), myelin basic protein (MBP, Cat# MAB386, Millipore, 1:500), oligodendrocyte transcription Factor 2 (Oligo2, Cat# AF2418, R&D system, 1:500), neural/glial antigen 2 (NG2, Cat# AB5320, Millipore, 1:500), Nestin (Cat# ab134017, Abcam, 1:500), MAP2 (Cat# ab32454, Abcam, 1:500), Tau (Cat# MAB3420, Millipore, 1:500); the secondary antibodies were Alexa® Fluor 488 (Cat# A-32814, Invitrogen, 1:500), Alexa® Fluor 488 (Cat# A-32790, Invitrogen, 1:500), Alexa® Fluor 555 (Cat# A-32773, Invitrogen, 1:500), Alexa Fluor® 594 (Cat# ab150156, Abcam, 1:500), Alexa® Fluor 594 (Cat# ab150176, Abcam, 1:500), Alexa® Fluor 647 (Cat# A-32795, Invitrogen, 1:500). Fluorescent antibodies of the same channel including Alexa® Fluor 488 and Alexa® Fluor 594, were used to match species differences during immunofluorescence staining. The nuclei were stained with 4′,6-diamidino-2-phenylindole (DAPI, Cat# C1002, Beyotime Institute of Biotechnology), and fluorescence images were taken using confocal microscopy (LSM 700, Carl Zeiss, Jena, Germany). Image acquisition was performed with ZEN 2.3 (blue edition, Carl Zeiss), and micrographs were assembled using Adobe Illustrator CC 2018.

For immunofluorescence analysis, lesion area covered the lesion core, rostral and caudal injured spinal cords with a distance of 500 μm from lesion core, respectively. A total of three sections (eight areas of rostral and eight of caudal injured spinal cords per section) were randomly selected in per mice. Then the 160 μm × 160 μm images were exported by ZEN 2.3. For culture cells immunofluorescence staining, the images were directly exported by ZEN 2.3. Image-J software with customized macros was used to quantify the fluorescence intensity of proteins including the MBP, Olig2, and NG2 in the images mentioned above. For sham group and treatment groups, three mice per group were tested. For culture cells, three biological repeats were conducted.

2.7 RNA-sequencing and bioinformatic analysis

RNA-seq was used to examine the transcriptomes of the lesion site at 2 weeks post injury (WPI), including sham and SCI groups of 1-week-old mice (Sham_1 W, n = 3; SCI_1 W, n = 3, crash model); sham and SCI groups of 2-week-old mice (Sham_2 W, n = 3; SCI_2 W, n = 3, crash model); sham and SCI groups of 8-week-old mice (adult female mice, Sham_8 W, n = 3; SCI_8 W, n = 3, crash model). Total RNA from 18 samples with three biological replicates for each group was quantified to obtain RNA data.

Briefly, animals were euthanized after terminal anesthesia by pentobarbital overdose. Then, spinal cord tissue was dissected from the lesion site under a dissecting microscope, and 2 mm segments of the lesion site were harvested and marked. The tissues were sent to the Beijing Genomics Institute (BGI) Company (Shenzhen, China) in solid carbon dioxide for further RNA-seq. The sequencing was performed on a DNBSEQ system at BGI Company. Total RNA was isolated, and RNA sequencing libraries were generated. Bioinformatics analysis was carried out with the online platform Dr. Tom (BGI Company). Only genes with transcripts per million (TPM) > 1 were analysed. Differentially expressed genes (DEGs) were identified using the DEGseq2 method and screened with the criteria of q value $\leq$ 0.05 and log2FC $\geq$ 0.6, where FC represents the fold change. The sequence and sample data have been deposited in the NCBI database under Sequence Read Archive (SRA) with Bioproject identification number PRJNA847738 (Accession number: SRR19612226–SRR19612243).

To further detect oligodendrocyte activation in lumbar enlargement (L4-5), RNA-seq was used to examine the

transcriptomes of lumbar enlargement tissues at 6 WPI, including the sham (n = 6, female) and SCI groups (n = 6, female, contusion model). Total RNA from 12 samples with six biological replicates for each group was quantified to obtain RNA data. Spinal cord tissue was dissected from lumbar enlargements (L4-5) under a dissecting microscope, and 2 mm segments were harvested and marked. RNA-seq and bioinformatic analysis were also performed on a DNBSEQ platform and the online platform Dr. Tom (BGI Company). Only genes with TPM > 1 were analyzed. DEGs were identified using the DEGseq method and screened with the criteria of q value $\leq$ 0.05 and log2FC $\geq$ 0.6. The sequence and sample data have been deposited in the NCBI database under Sequence Read Archive (SRA) with Bioproject identification number PRJNA847704 (Accession number: SRR19611667–SRR19611678).

To further detect oligodendrocyte activation at different time after SCI, the series matrix file data of GSE45006 were downloaded from the Gene Expression Omnibus (GEO) public database, and the annotation platform was GPL1335. Data from 24 samples from the lesion area of the injured spinal cord with complete expression profiles were extracted. Bioinformatics analysis was also carried out with the online platform Dr. Tom (BGI Company). DEGs were identified using the DEGseq method and screened with the criteria of p-value $\leq$ 0.01 and log2FC $\geq$ 2. The scRNA-seq results were analyzed through online data from injured mouse spinal cords[1] (Milich et al., 2021).

2.8 Quantitative real-time PCR

The total RNA of cells was isolated with RNAiso plus (Cat# 9108, Takara). The concentration and purity of RNA samples were measured using a Nanodrop ND-2000 (Thermo Science, MA, USA) for further experiments. Five hundred nanograms of RNA was converted to complementary DNA (cDNA), which was synthesized with a PrimeScript reverse transcriptase kit (Cat# RR037A, Takara). RT–PCR was performed using a TB Green TM Premix Ex Taq Kit (Cat# RR820A, Takara) on a Light Cycler Real-Time PCR System (480II, Roche). The primer sequences (Shanghai Generay Biotech Co., Ltd., Shanghai, China) were designed through Primer-BLAST[2] and are listed in **Supplementary Table 1**. The relative amounts of mRNA were calculated using the $\Delta\Delta$Ct relative quantification method. GAPDH served as the control gene, and the mRNA levels of specific genes were normalized to GAPDH. Calculations and statistics were performed in Microsoft Excel version 16.36. Graphs were plotted in GraphPad Prism 8 version 8.4.3. Three biological repeats were performed.

2.9 Statistical analysis

All experiments were conducted with three or more duplicates. All continuous data were shown as mean ± SEM. One-way ANOVA was performed followed by Student Newman–Keuls *post-hoc* test for continuous data. P-values < 0.05 were considered statistically significant. Data analyses were conducted using the Statistical Analysis System (SAS), version 9.4 (SAS Institute, Inc., Cary, NC, USA). Plots were generated using GraphPad Prism 8 software (GraphPad Software, San Diego, CA, USA).

3 Results

3.1 OPCs differentiation were different between brain and spinal cord

In this study, OPCs with >95% purity were obtained (by cell count) and identified by Calcein AM staining and the expression of oligodendrocyte lineage cell markers NG2 and MBP (**Figures 1A, B**). Previous reports have revealed that oligodendrocytes are heterogeneous (Rowitch and Kriegstein, 2010; Bechler et al., 2015). We also observed that there were obvious differences in OPCs differentiation between brain and spinal cord (**Figures 1C, D**). On the third day of primary cell culture (mixed with OPCs, astrocytes, etc.) in the medium of DMEM-F12 containing 10% FBS and 1% penicillin/streptomycin, we found brain-derived cells were mainly OPCs with a dark cell body, tadpole-like, and only 2–3 branches (**Figure 1C**). In contrast, spinal cord-derived OPCs were easier to differentiate than brain-derived, reflected by the significant increase in branches and processes (**Figure 1D**). Immunofluorescence staining of NG2, MBP, and GFAP was further used to detect dynamic changes of OPCs in both differentiation and morphology (**Figures 1C, D**). We delineated cell morphology, and calculated the diameter and area of OPCs differentiated oligodendrocytes (**Supplementary Figure 1**). When compared with brain, we found that spinal cord-derived oligodendrocytes had larger cell areas and longer diameters after maturation (**Figures 1C–F**). Spinal cord-derived oligodendrocytes had showed longer diameter and larger cell area at the 4th day, peaked at the 6th day and were maintained until the 8th day (**Figures 1E, F**). Thus, there were significant differences in OPCs differentiation and oligodendrocytes morphology between the brain and spinal cord.

1 https://jaeleelab.shinyapps.io/sci_singlecell/

2 https://www.ncbi.nlm.nih.gov/tools/primer-blast/index.cgi

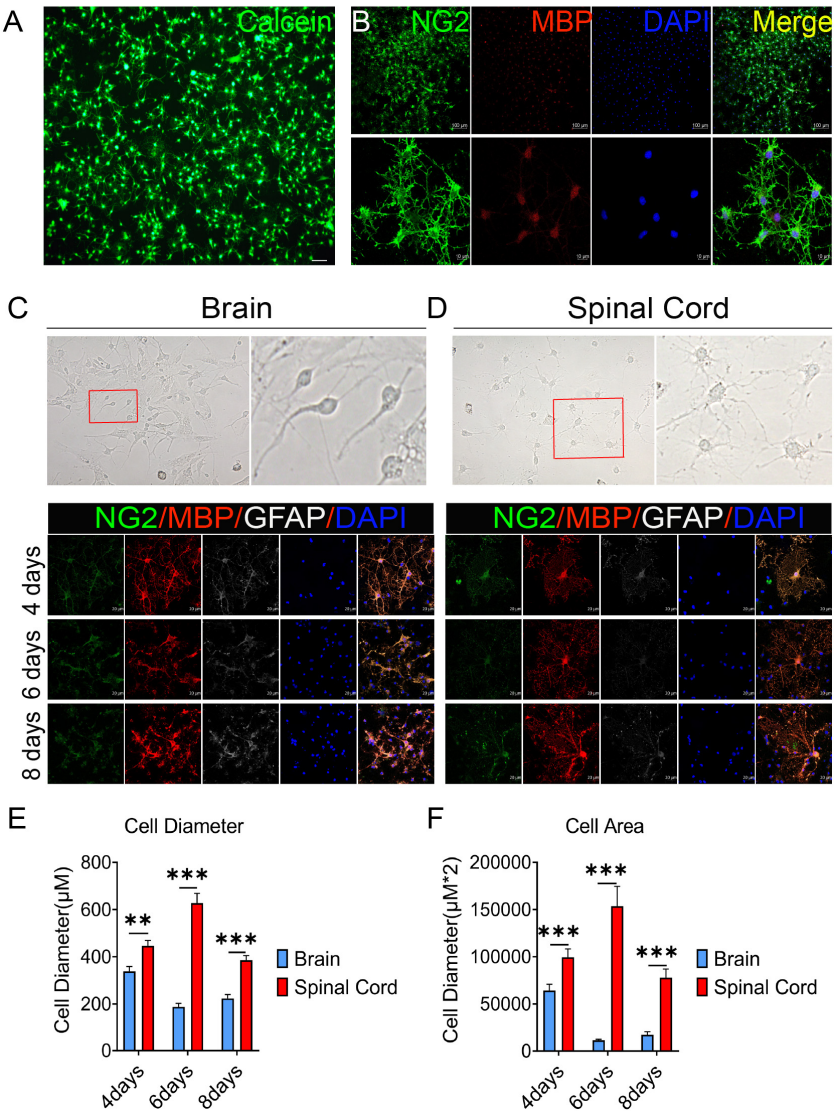

FIGURE 1
The oligodendrocyte progenitor cells (OPCs) differentiation and oligodendrocytes morphology are different between the brain and spinal cord. **(A,B)** OPCs with >95% purity were obtained (by cell count) and identified by Calcein AM staining and the expression of oligodendrocyte lineage cell markers NG2 (green) and MBP (red). **(C,D)** Spinal cord-derived OPCs were easier to differentiate and mature than brain-derived cells. Immunofluorescence staining of NG2 (green), MBP (red), and GFAP (white) was used to detect the dynamic changes in oligodendrocytes. $n = 3$ biological repeats. Scale bars are indicated in the pictures. **(E,F)** The histograms showed the statistical results of oligodendrocytes diameter and area. $n = 3$ biological repeats. Values are the mean ± SEM. Statistical significance was determined by one-way ANOVA followed by Student Newman–Keuls *post-hoc* test. $^{**}P < 0.01$, $^{***}P < 0.001$.

3.2 OPCs were involved in oligospheres formation *in vitro*

In our culture system, we found that OPCs from both brain and spinal cord could gather into oligospheres on the 8th day of OPCs proliferation (**Figure 2A** and **Supplementary Figure 2**). Compared with spinal cord, brain-derived oligospheres were more obvious in spherical and oval shapes (**Figure 2A** and **Supplementary Figure 2**). Thus, we mainly focused on the formation of brain-derived oligospheres in the next experiment and analysis. Oligospheres were plated on PDL-coated coverslips in OPCs proliferation medium to detect their differentiation (**Figure 2B** and **Supplementary Figures 3A–C**). We found that the volume of oligospheres in the first generation (F1) was small (**Supplementary Figure 3A**). Oligospheres gradually differentiated after plating (**Supplementary Figure 3A**). As previously reported (Chen et al., 2007), cells from oligospheres migrated away to form individual OPCs with bipolar and tripolar morphologies (**Supplementary Figure 3A**). According to cell morphology,

we found that a large number of OPCs and oligodendrocytes were formed and migrated out of the oligospheres at different time in the F1 generation (**Supplementary Figure 3A**). When oligospheres reached the F2 generation, the size and diameter of oligospheres increased with round and oval shapes (**Supplementary Figure 3B**). In the F3 generation, the oligospheres reached a larger size and diameter (**Supplementary Figure 3C**). In the F4 generation, the size and diameter of the oligospheres reached the most significant values (**Figure 2B**), which could also differentiate into a large number of OPCs and oligodendrocytes at different time (**Figure 2B**). We also found that a number of astrocytes were migrated out of the oligospheres at different time (**Figure 2B** and **Supplementary Figure 3**) as previous study reported (Chen et al., 2007).

3.3 Oligospheres can differentiate into oligodendrocytes and neuron-like cells

The F4 generation oligospheres were used to observe differentiation at different time through immunofluorescence staining with markers of oligodendrocytes (MBP), OPCs (NG2), and neurons (Tuj1). On the first day after plating, there were a large number of TuJ1, MBP, and NG2 positive cells in the oligospheres (**Figure 3A**). Nearly all oligospheres were Tuj1 + MBP + NG2 + triple positive oligospheres (**Figure 3A**). Meanwhile, MBP + positive oligodendrocytes and NG2 + OPCs were wrapped by Tuj1 positive neuronal cells (**Figure 3A**). As expected, we found almost all oligospheres were Nestin positive (**Supplementary Figures 4A, B**), which indicated that oligospheres have neural stemness. On the third day after plating, the oligospheres differentiated into a majority of MBP + positive oligodendrocytes, NG2 + OPCs, and a small number of Tuj1 positive neurons (**Figure 3B**).

A previous study reported that no neuronal cells indicated by the expression of Tuj1 were detected in an isolated OPCs population, although approximately 2% of cells represented other neuroglial cells or early progenitors, as evidenced by the expression of Nestin and GFAP (Chen et al., 2007). Interestingly, we found a large number of Tuj1 + MBP + NG2 + triple-positive oligodendrocytes on the sixth day after plating (**Figure 3C**), among which a large number of these cells had Tuj1-positive neurite-like branches (**Figure 3D**). We speculated that these cells may be in the intermediate state of oligodendrocytes and neurons during oligospheres differentiation, which indicated that these oligodendrocytes may *trans*-differentiate into neurons in this culture system. In addition, we detected the differentiation of oligospheres for a longer time. On the 9th, 14th, 21st, and 28th days of oligospheres differentiation, an increasing number of Tuj1 positive cells were found at different time (**Supplementary Figures 5A–D**). Through statistical fluorescence intensity at different differentiation time, we found that Tuj1 expression gradually increased, while NG2 and MBP decreased (**Figure 3E**). These results reflect that oligospheres differentiating into oligodendrocytes gradually decreased, which indicated that OPCs may *trans*-differentiate into neuron-like cells. However, these cells not grew long axon-like branches (**Figure 3D** and **Supplementary Figures 5A–D**). For most astrocytes were removed in our culture system, we speculate that one of the reasons may be the lack of secreted astrocyte factors, including BDNF and GDNF, to promote and guide the growth of neurons (Cunningham and Su, 2002; Degos et al., 2013).

Furthermore, we used more neuron markers for immunofluorescence staining, including MAP2 and Tau. The effects of different culture mediums on the results were also observed. Firstly, we found that on the 6th day of oligospheres differentiation, a large number of cells expressed MAP2 in proliferation medium (**Supplementary Figure 6A**). The cells had few branches and were in the immature state (**Supplementary Figure 6A**). In contrast, in DMEM-F12 with 5% FBS medium and on the 6th day of oligospheres differentiation, we found that a large number of cells also expressed MAP2. However, the cells were relatively mature and with abundant branches (**Supplementary Figure 6B**). Secondly, under the condition of proliferation medium culture, and on the 6th day of oligospheres differentiation, we found that some NG2 positive cells (OPCs) expressed Tau protein, and the branches were long (**Supplementary Figure 6C**). However, in DMEM-F12 with 5% FBS medium and on the 6th day of oligospheres differentiation, NG2 positive cells (OPCs) were few, and almost no NG2 positive cells (OPCs) expressed Tau protein (**Supplementary Figure 6D**). Thus, these results indicated that oligospheres can differentiate into neuron-like cells only in the proliferation medium.

3.4 OPCs are activated in the lesion area and lumbar enlargement after SCI

After spinal cord contusion injury, oligodendrocytes in the lesion area were activated at 6 weeks post injury (WPI) when compared with the sham group, reflected by the expression of the oligodendrocyte marker Oligo2, myelin marker MBP, and OPCs marker NG2 (**Figures 4A, C**). The demyelination of the lesion core was significant and not effectively repaired (**Figure 4A**). Meanwhile, the activation of OPCs (NG2+) in the lumbar enlargement was still very significant even at a distance from the injured area (**Figures 4B, D**).

Through RNA-seq, we further observed transcriptional changes in oligodendrocyte lineage cells both in the lesion area and lumbar enlargement at different ages and time (**Figures 4E–G**). Compared with juvenile mice, we confirmed that the transcripts of MBP and Oligo2 in adult mice decreased

10.3389/fncel.2022.1049562

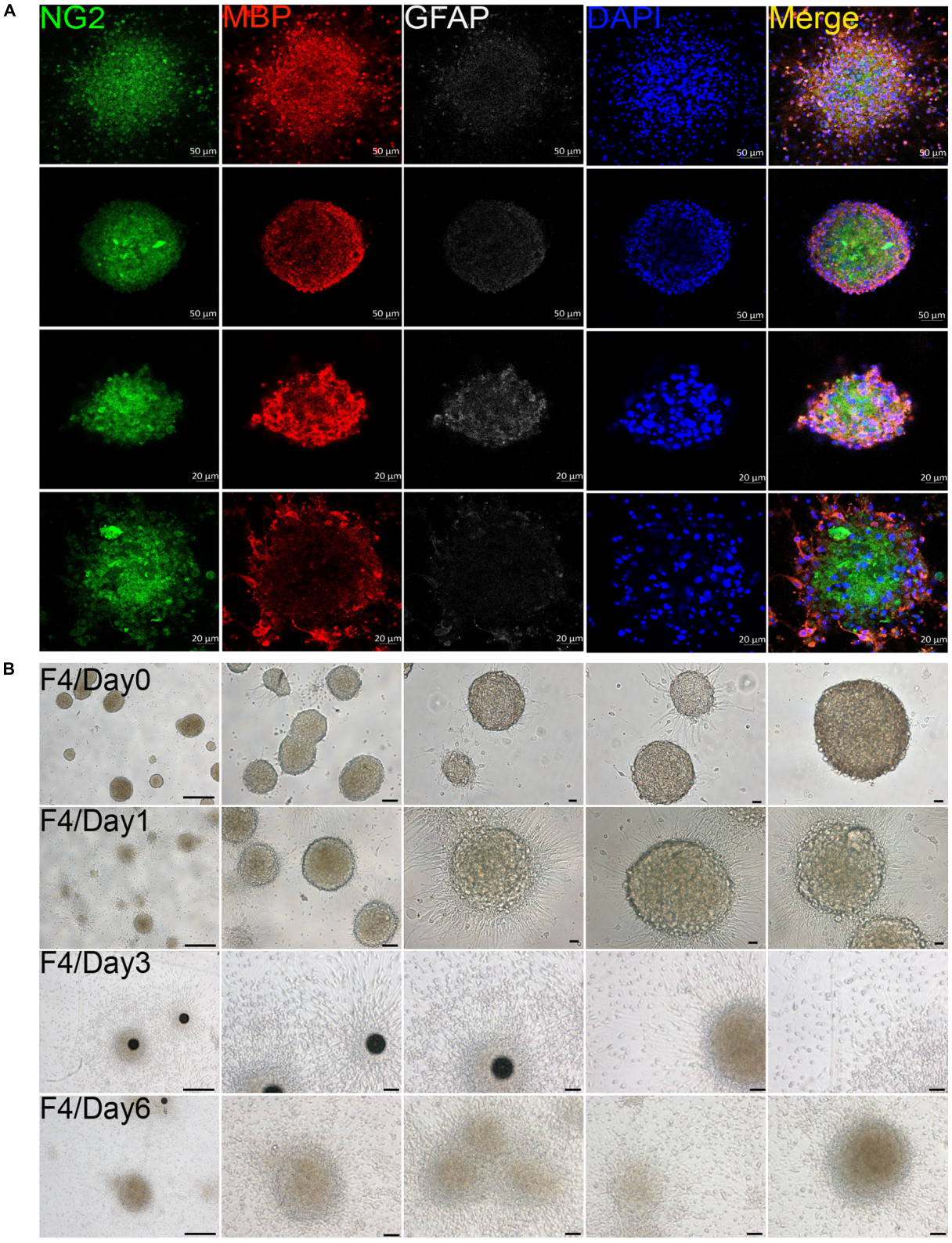

FIGURE 2
Oligodendrocyte progenitor cells (OPCs) were involved in oligospheres formation. **(A)** Oligodendrocytes from brain formed into oligospheres on the 8th day, as observed NG2 (green), MBP (red), and GFAP (white). *n* = 3 biological repeats. Scale bars are indicated in the pictures. **(B)** Oligospheres from F4 generation were plated on PDL-coated 12-well plates to detect the differentiation at different time. F4 = the fourth generation. *n* = 3 biological repeats. Scale bars are indicated in the pictures.

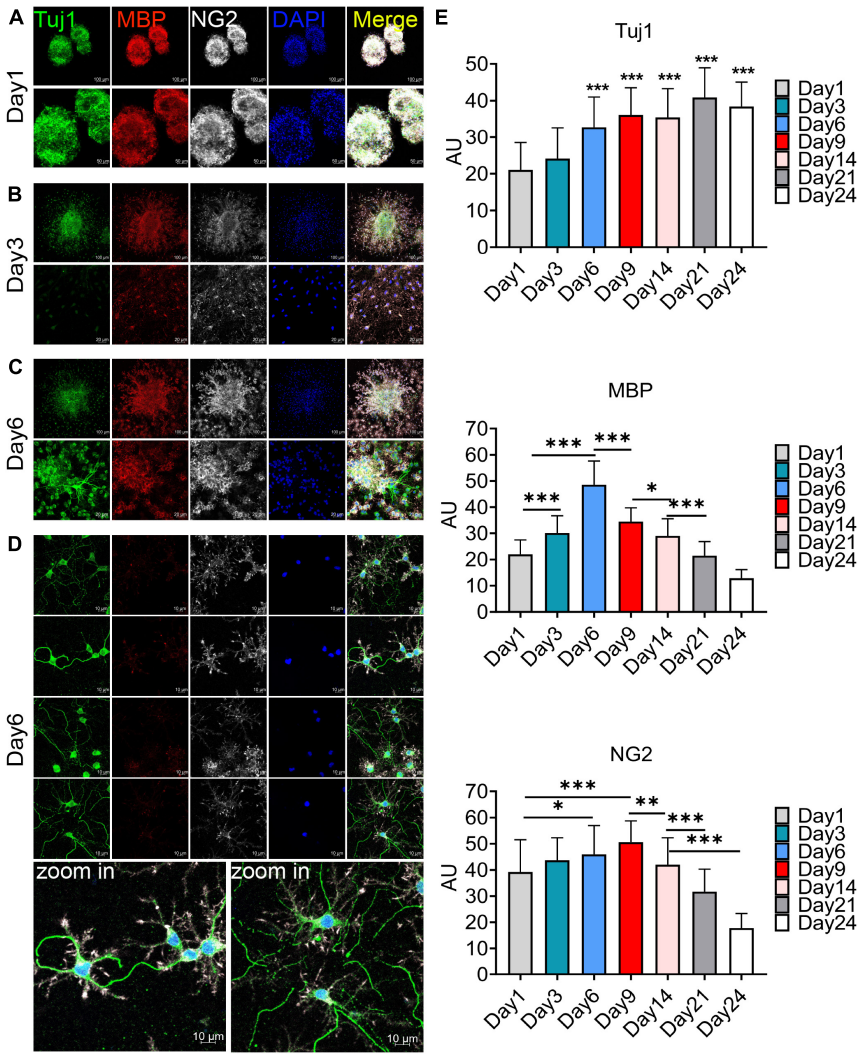

FIGURE 3
Immunofluorescence staining to detect the cellular composition of oligospheres at different differentiation period. **(A–D)** F4 generation oligospheres were used for immunofluorescence staining to detect the cellular composition of oligospheres at different time with Tuj1 (green), MBP (red), and NG2 (white). n = 3 biological repeats. Scale bars are indicated in the pictures. **(E)** The histograms showed the statistical results of fluorescence intensity. Values are the mean ± SEM. Statistical significance was determined by one-way ANOVA followed by Student Newman–Keuls *post-hoc* test. $^{*}P < 0.05$, $^{**}P < 0.01$, $^{***}P < 0.001$. n = 3 biological repeats. Scale bars had been indicated in pictures.

significantly at 2 WPI (Figure 4E), which indicated that a majority of oligodendrocyte death and extensive myelin sheath loss occurred in the lesion area. Meanwhile, NG2 (CSPG4) transcripts in adult mice were significantly up-regulated when compared with juvenile mice but did not promote remyelination of the lesion core (Figure 4E). Additionally, we also found that the transcripts of MBP and Oligo2 decreased with time after SCI, while the transcripts of NG2 were gradually up-regulated but did not promote the regeneration of the myelin sheath (Figure 4F). Interestingly, the transcripts of NG2 were also significantly up-regulated in lumbar enlargement, and the transcripts of MBP and Oligo2 were down-regulated even at a distance from the injured area at 6 WPI (Figure 4G).

3.5 Combining scRNA-seq and RNA-seq data to investigate the neurogenesis potential of OPCs after SCI

There is a dynamic process of pathophysiological changes after SCI. Its pathophysiology comprises acute and chronic stages and incorporates a cascade of pathogenic mechanisms (cell death, excitotoxicty, inflammation, neurodegeneraton, demyelination, remielination, scar formation, etc.) (Anjum et al., 2020). The regional microenvironment of injured spinal cord is quite different from that of cells cultured *in vitro*. *In vitro* experiments are also difficult to simulate complex

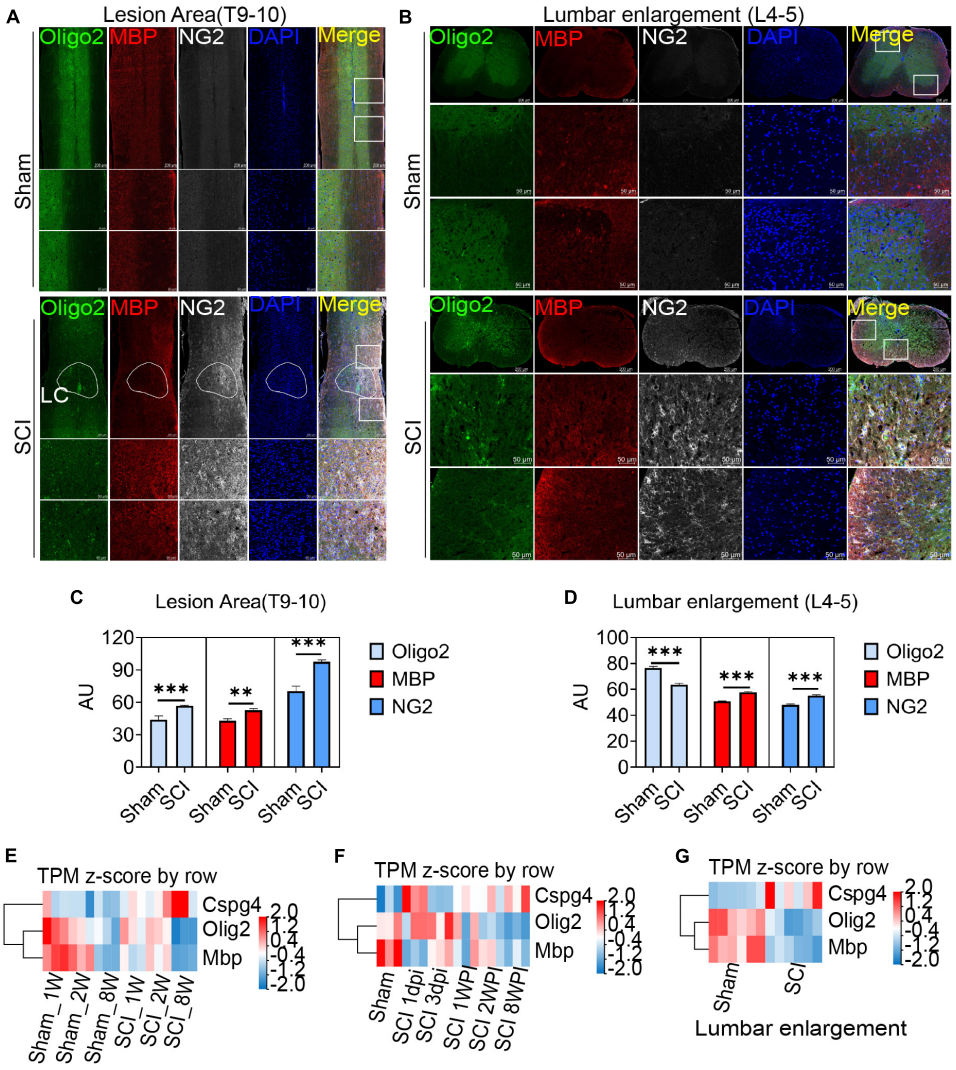

FIGURE 4
Oligodendrocyte progenitor cells (OPCs) are activated in the lesion area and lumbar enlargement after SCI. **(A,B)** Immunofluorescence staining to detect the expression of oligodendrocyte lineage cell markers in the lesion area and lumbar enlargement after SCI. Olgio2 (green), MBP (red), and NG2 (white). *n* = 3 biological repeats. Scale bars are indicated in the pictures. LC = lesion core. **(C,D)** The histogram and statistical results of Oligo2, MBP, and NG2 fluorescence intensity. *n* = 3 biological repeats. Values are the mean ± SEM. Statistical significance was determined by one-way ANOVA followed by Student Newman–Keuls *post-hoc* test. $^{**}P < 0.01$, $^{***}P < 0.001$. **(E–G)** RNA-seq results showed transcript changes in oligodendrocyte lineage cells both in the lesion area and lumbar enlargement at different ages and time. dpi, day post-injury; WPI, week post-injury; 1 W, 1-week-old; 2 W, 2-week-old; 8 W, 8-week-old; sham_1 W, 1-week-old sham group; sham_2 W, 2-week-old sham group; sham_8 W, 8-week-old sham group; SCI_1 W, 1-week-old SCI group; SCI_2 W, 2-week-old SCI group; SCI_8 W, 8-week-old SCI group.

environmental changes *in vivo*. Thus, in order to know more about the dynamic changes in different periods after SCI *in vivo*, we analysis the RNA-seq and online scRNA-seq data. By analyzing online scRNA-seq data from the injured mouse spinal cord (see text footnote 1) (Milich et al., 2021), we detected changes in the expression of Tuj1 (Tubb3) in OPCs after SCI (**Figures 5A, B**). We found that oligodendrocyte cell lines along with neurons were Tuj1-specific expressing cells under normal conditions (**Figure 5C**), as we found *in vitro* (**Figures 3A–D**). In particular, the expression of Tuj1 in OPCs increased gradually at 1 to 3 days post injury (dpi) after SCI but decreased at 7 dpi. Furthermore, we also found that most of neuron markers were expressed in OPCs [such as Map2, Mapt (Tau), Nefm (Neurofilament), Uchl1, Doublecortin (DCX), and Gap43] (**Supplementary Figures 7A–E**). Some of these markers were increased in the early stage after injury and then gradually decreased [such as TUBB3 (Tuj1), Smn1, Uchl1, Gap43] (**Figures 5A–C** and **Supplementary Figure 7F**). While, some markers were decreased in the early stage of injury, and then gradually recovered (such as DCX, Nefm, NeuroD, Tbr1, Thy1/Cd90, Mapt, Map2) (**Figure 5D** and **Supplementary Figure 7F**). Furthermore, when compared with

adult mice, most of neuron markers were well preserved in juvenile mice (**Supplementary Figure 7G**). Meanwhile, the spinal cord neurons almost did not express CSPG4 (NG2) under normal conditions or after injury (**Supplementary Figure 8**). Therefore, these Tuj1 + cells may be partly derived from NG2 positive OPCs. These results indicate that OPCs may have the potential to *trans*-differentiate into neurons but not successfully after SCI, which may be due to unknown environmental factors or a lack of factors mediating transformation.

Recent study confirmed that SOX2-mediated *in vivo* reprogramming of NG2 + glial cells could produce new excitatory and inhibitory propriospinal neurons, reduce glial scarring, and promote functional recovery after SCI (Tai et al., 2021). The microtubule-associated protein doublecortin (DCX) is normally expressed in neuroblasts and immature neurons and can serve as a reliable marker for adult neurogenesis (Tai et al., 2021). ASCL1, a master regulator expressed in neural progenitors and critical for neuronal differentiation and adult neurogenesis, was detected in 28.6% of SCI-induced DCX + cells (Tai et al., 2021). By analyzing online scRNA-seq data from the injured mouse spinal cord (Milich et al., 2021), we found that Sox2, DCX, and ASCL1 were highly or specifically expressed in OPCs under normal conditions, while these factors were significantly down-regulated after SCI (**Figure 5D**). These results further confirmed that OPCs may have the potential to *trans*-differentiate into neurons but not successful after SCI.

Furthermore, through RNA-seq, we also detected the transcriptional changes in Sox2, DCX, and ASCL1 in the lesion area at different ages and time. Compared with juvenile mice, we confirmed that the transcripts of DCX and ASCL1, along with MBP, Oligo2, and Tubb3 (Tuj1), in adult mice significantly decreased at 2 WPI (**Figure 5E**), which indicated a large number of oligodendrocytes and neuron death in the lesion area. Meanwhile, compared with juvenile mice, transcripts of SOX2 and NG2 in adult mice were significantly up-regulated but did not promote neurogenesis (**Figure 5E**). We also found that the transcripts of ASCL1 gradually decreased and NG2 (CSPG4) gradually up-regulated with time after SCI (**Figure 5F**). The transcripts of DCX, SOX2, and Tubb3 (Tuj1) underwent a process of dynamic change, first decreasing from 1 dpi to 3 dpi but gradually increasing from 1 to 2 WPI, and then decreasing again at 8 WPI (**Figure 5F**). These results suggest that the injured tissue may try to promote the regeneration of neurons after SCI but failed due to unknown factors.

3.6 ER stress inhibition could protect OPCs from death and inhibit oligospheres differentiation

Previously, we confirmed that inhibition of endoplasmic reticulum stress (ER stress) related signal pathways can effectively improve neuronal death (Zhao et al., 2017a,b). Irreversible ER stress would trigger cell death initiated by the activation of three ER stress sensors separated from immunoglobulin heavy chain binding protein (BiP/GRP78) respectively, including inositol-requiring protein 1α (IRE1α), protein kinase RNA-like ER kinase (PERK) and activating transcription factor 6 (ATF6) (Hetz, 2012). Whether inhibiting ER stress would also protect OPCs still remains unclear.

Then, we tried to detected the effect of ER stress inhibition on OPCs death *in vitro* under hypoxic conditions. The different concentrations of ER stress receptors IRE1α and PERK inhibitors were used to intervene oligodendrocytes after OGD. STF083010 is the specific inhibitor of IRE1α Rnase, whereas GSK2656157 is a specific inhibitor of the PERK kinase (Zhao et al., 2017a). Firstly, we detected the effects of different concentrations of STF083010 and GSK2656157 on oligodendrocyte mortality after OGD stimulation by Calcein AM/PI double staining (**Figures 6A, B**). We found that 35 μM STF083010 could effectively reduce the death of OPCs (**Figures 6A, C**). Meanwhile, 0.25 μM GSK2656157 could significantly inhibit the death of OPCs (**Figures 6B, D**).

Through flow cytometry of apoptosis by Annexin V-EGFP/PI double staining, we further confirmed that 35 μM STF083010 could effectively reduce the death of OPCs (**Figure 6E**), and 0.25 μM GSK2656157 could significantly inhibit the death of OPCs (**Figure 6F**). Through RNA-seq, we found the transcripts of ER stress related genes (Zhang et al., 2021) were significantly up-regulated after SCI (**Figures 7A–C**). The GO and KEGG pathway analysis also revealed that ER stress associated signaling pathways were activated (**Figures 7D, E**). We further screened the dynamic changes of ER stress key genes after SCI in scRNA-seq and RNA-seq data. We found that ER stress was activated in the early stage of SCI, and gradually decreased (**Supplementary Figures 9A–E**). Our RT-PCR results also revealed the unspliced and spliced mRNA expression of X-Box Binding Protein 1 (Xbp1), as the downstream factors of ER stress, were gradually increased after OGD stimulation, which could be significantly inhibited by STF083010 treatment (**Figure 7F**). Thus, inhibiting ER stress could reduce OPCs death under hypoxic conditions.

The ER machinery integrates various intracellular and extracellular signals. Previous study found that ER stress regulated the intestinal stem cell state through monoclonal antibody to C-Terminal binding protein 2 (CTBP2), and showed CtBP2 mediates ER stress-induced loss of stemness (Meijer et al., 2021). Therefore, we wondered whether inhibition of ER stress would have effect on oligospheres differentiation. Interesting, we found that inhibition of ER stress during oligospheres differentiation could significantly increase the expression of stem cell marker Nestin (**Figure 7G**). Furthermore, we found that mRNA expression of oligodendrocyte lineage cells marker Oligo2, and neuron markers NEUN and MAP2 were significantly increased after ER inhibition (**Figure 7H**). Thus, ER inhibition may be associated with stemness maintenance and regulating the differentiation of oligospheres.

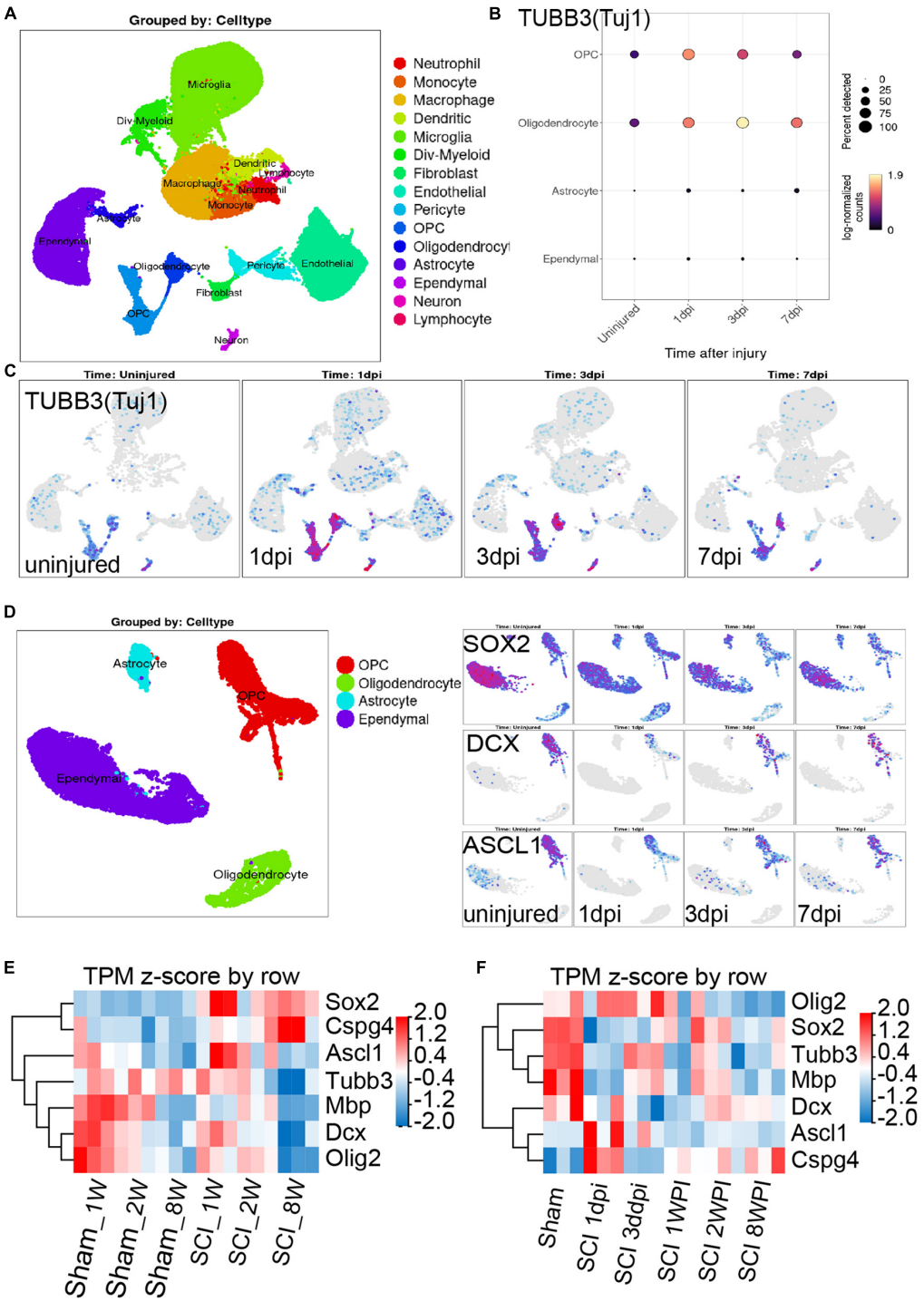

FIGURE 5
Combining the scRNA-seq and RNA-seq data to investigate the neurogenesis potential of oligodendrocyte progenitor cells (OPCs) after spinal cord injury (SCI). **(A–C)** scRNA-seq results show that oligodendrocyte lineage cell along with neurons were Tuj1-specific expressing cells under normal conditions and after SCI. dpi = day post-injury. **(D)** Sox2, DCX, and ASCL1 were highly or specifically expressed in OPCs under normal conditions, while these factors were significantly down-regulated after SCI. dpi = day post-injury. **(E,F)** RNA-seq results show the transcript changes of the above factors along with the marker of oligodendrocyte cell lines in the lesion area at different ages and time. dpi, day post-injury; WPI, week post-injury; 1 W, 1-week-old; 2 W, 2-week-old; 8 W, 8-week-old; sham_1 W, 1-week-old sham group; sham_2 W, 2-week-old sham group; sham_8 W, 8-week-old sham group; SCI_1 W, 1-week-old SCI group; SCI_2 W, 2-week-old SCI group; SCI_8 W, 8-week-old SCI group.

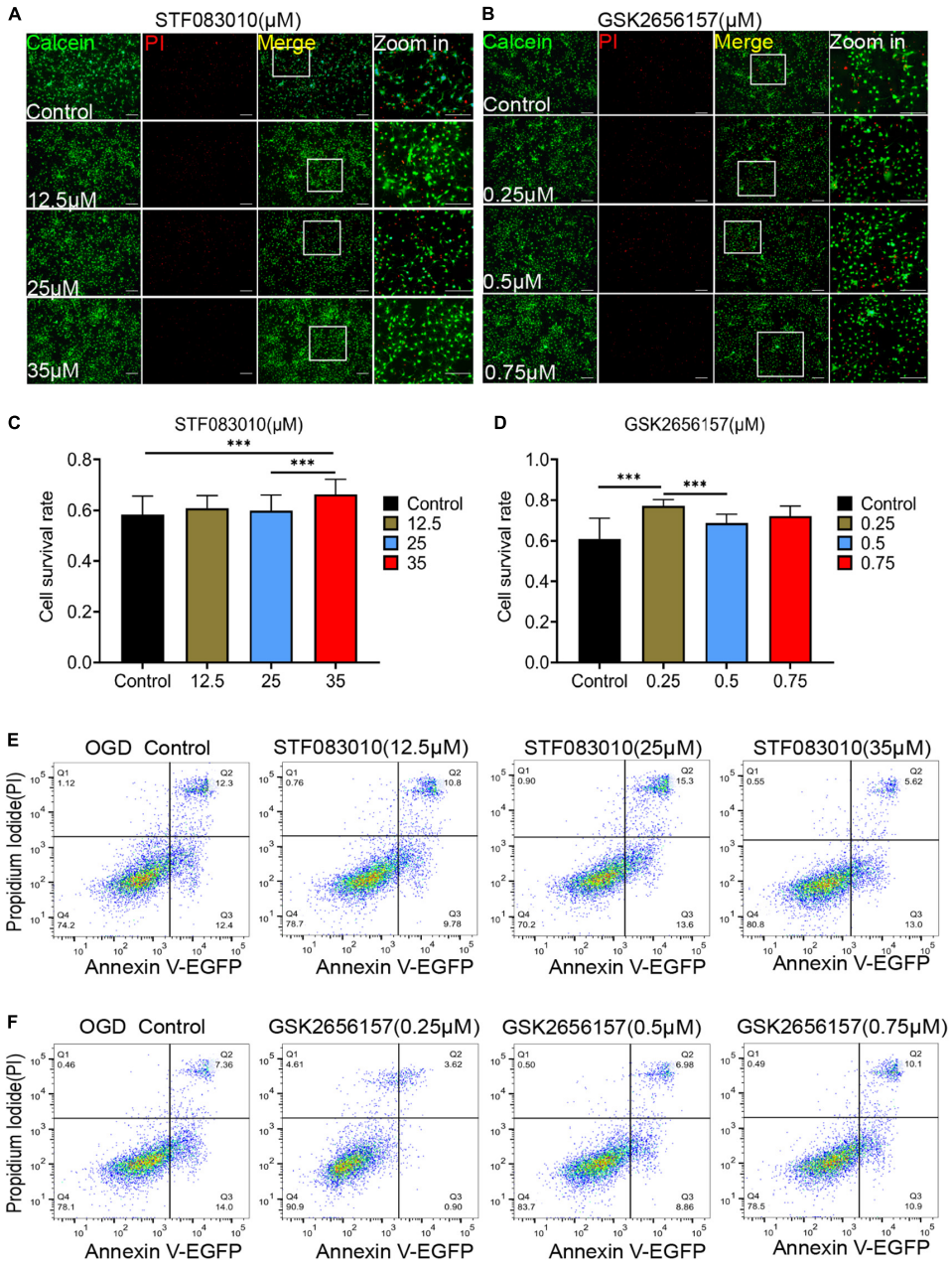

FIGURE 6
Endoplasmic reticulum stress (ER) stress inhibition protect OPCs from death after OGD stimulation. **(A,B)** The effects of different concentrations of STF083010 and GSK2656157 on OPCs mortality after OGD stimulation by Calcein AM/PI double staining. Scale bars had been indicated in pictures. $n = 3$ biological repeats. **(C,D)** The histograms revealed the statistical results of oligodendrocytes mortality after OGD stimulation. $n = 3$ biological repeats. Values are the mean ± SEM. Statistical significance was determined by one-way ANOVA followed by Student Newman–Keuls *post-hoc* test. $^{***}P < 0.001$. **(E,F)** Through flow cytometry of apoptosis by Annexin V-EGFP/PI double staining, the results revealed the roles of STF083010 and GSK2656157 in the death of OPCs. $n = 3$ biological repeats.

4 Discussion

There were several findings in this study: (1) OPCs differentiation and oligodendrocyte morphology were significantly different between brain and spinal cord; (2) OPCs were involved in oligospheres formation, which further differentiated into neuron-like cells. (3) A majority of Tuj1 + MBP + NG2 + triple-positive cells with neurite-like branches were detected during the differentiation of oligospheres; (4) OPCs were significantly activated in the lesion area and lumbar enlargement after SCI; (5) Combining scRNA-seq and RNA-seq data, the neurogenesis potential of

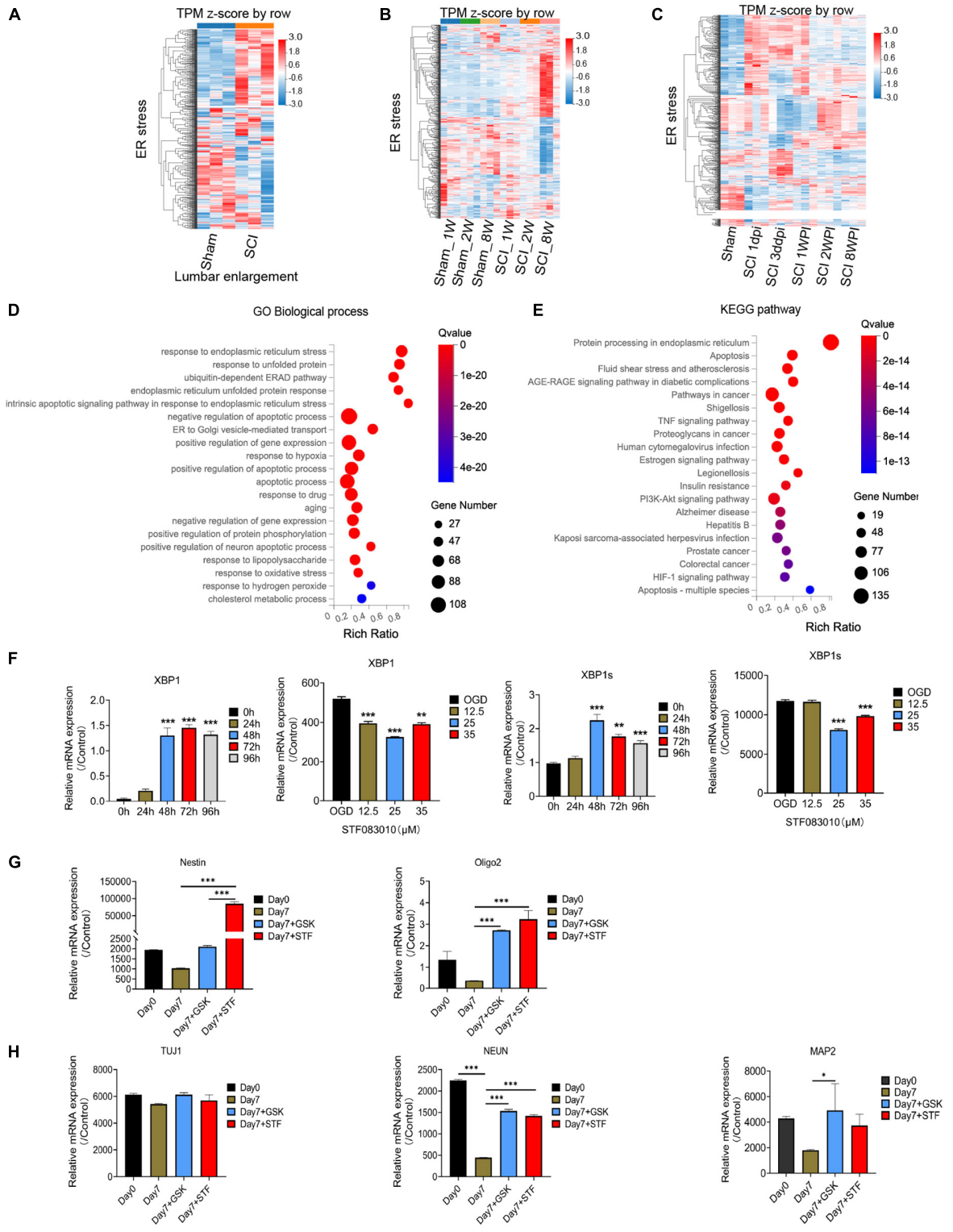

FIGURE 7
RNA-seq and bioinformatics analysis results after spinal cord injury (SCI) and RT-PCR results. **(A–C)** Heatmaps showed that the transcripts of ER stress related genes were significantly up-regulated after SCI. Dpi, day post-injury; WPI, week post-injury; Sham _1w, Sham _1 week age; Sham_2w, Sham _2 weeks age; Sham _8w, Sham_8 weeks age; SCI_1W, SCI_1 week age; SCI_2W, SCI_2 weeks age; SCI_8W, SCI_8 weeks age. **(D,E)** GO and KEGG pathway analysis also revealed that ER stress associated signaling pathways were significantly activated. **(F–H)** The RT-PCR results of Xbp1 and Xbp1s (spliced Xbp1), Nestin, Oligo2, Tuj1, NEUN, and MAP2 mRNA expression. $n = 3$ biological repeats. Values are the mean ± SEM. Statistical significance was determined by one-way ANOVA followed by Student Newman–Keuls *post-hoc* test. $^{*}P < 0.05$, $^{**}P < 0.01$, $^{***}P < 0.001$.

OPCs were detected after SCI; (6) inhibition of ER stress could effectively attenuate OPCs death; (7) ER inhibition may regulate the stemness and differentiation of oligospheres.

Oligodendrocyte progenitor cells are the source for new mature oligodendrocytes during the regeneration of damaged myelin (Zawadzka et al., 2010; Gibson et al., 2014; McKenzie et al., 2014; Hughes et al., 2018). We found that the OPCs differentiation and oligodendrocyte morphology of brain and spinal cord were significantly different. It has been established that oligodendrocytes and OPCs from different regions of the CNS have distinct origins and are functionally dissimilar, which has implications for myelination and regenerative capacity (Rowitch and Kriegstein, 2010; Bechler et al., 2015). OPCs from the cortex and spinal cord produce myelin sheaths of different lengths when cultured under similar conditions (Bechler et al., 2015), and transplanted OPCs from white matter differentiate faster than OPCs from gray matter (Viganò et al., 2013). Cholesterol is an integral component of the myelin sheath. A recent study demonstrated that OPCs in the spinal cord exhibit higher levels of cell-autonomous cholesterol biosynthesis than the equivalent stage precursors in the brain (Khandker et al., 2022). Conversely, brain oligodendrocytes have a higher capacity for extracellular cholesterol uptake (Khandker et al., 2022). In addition, OPCs in different regions show different responsiveness to growth factors (Hill et al., 2013) and vary in their capacity to differentiate when transplanted into other CNS areas (Viganò et al., 2013). Furthermore, the physiological properties of OPCs have been found to diversify increasingly over time (Spitzer et al., 2019), and mature oligodendrocytes also show transcriptional heterogeneity (Floriddia et al., 2020). Thus, oligodendrocyte heterogeneity should be taken into consideration in future OPCs transplantation to promote myelin regeneration after SCI. Previously, several studies have described that OPCs can form oligospheres (Avellana-Adalid et al., 1996; Chen et al., 2007; Pedraza et al., 2008; Gibney and McDermott, 2009; Li et al., 2015). Importantly, oligospheres-derived OPCs preserve the capacity to express differentiated antigenic and metabolic phenotypes (Avellana-Adalid et al., 1996). A previous study showed that the B104CM-containing oligospheres medium was most effective in inducing oligospheres formation from neurospheres (Chen et al., 2007). Meanwhile, the efficiency of forming oligospheres was low when using the neonatal brain compared to the embryonic brain (Chen et al., 2007). They also reported that no neuronal cells, as indicated by the expression of Tuj1, were detected in the isolated OPCs population (Chen et al., 2007). In our study, oligospheres were also effectively generated from the neonatal brain in our culture system. Interestingly, we firstly detected the intermediate states of oligodendrocytes and neurons during oligospheres differentiation, for a number of Tuj1 + MBP + NG2 + triple-positive OPCs on the sixth day after plating were observed, among which a number of these cells had Tuj1-positive neurite-like branches. Indeed, we found that MBP + positive cells were gradually decreasing in the process of oligospheres culture and differentiation. We did not add other factors to the medium to promote the differentiation of neurons. The OPCs medium is refer to the previous reports (Hattori et al., 2017; Miyamoto et al., 2020). The OPCs medium is considered to be used for OPCs proliferation, but not for OPCs differentiation. Oligospheres were formed by OPCs cells in suspension culture, and then gradually differentiated into neuron like cells after PDL coating and adherent culture. We speculated that OPCs may acquire part of neural stemness during the process of oligospheres formation, and finally differentiate into neuron like cells. Thus, we identify a previously undescribed findings that OPCs formed oligospheres could differentiate into neuron-like cells. Furthermore, we also confirmed the significant activation and neurogenesis potential of OPCs after SCI. These findings highlighted the neurogenesis potential of OPCs, which may provide a new insight for spinal cord repair.

Directly converting non-neuronal cells into induced neurons has emerged as an innovative strategy for brain and spinal cord repair. OPCs have attracted extensive attention because of their potential to self-renew, differentiate and repair the myelin sheath. Recent studies reported that overexpression of a variety of factors can induce NG2 cells (mainly OPCs) to *trans*-differentiate into neurons, such as by Sox2 and adeno-associated virus (AAV)-based reporter system (Heinrich et al., 2014; Torper et al., 2015; Tai et al., 2021). Recently, Tai et al. (2021) found that ectopic SOX2-induced neurogenesis proceeding through an expandable ASCL1 + progenitor stage was necessary and sufficient to reprogram NG2 glia (mainly OPCs) into neurons after SCI. In addition, they also demonstrated that NG2 glia were the main source of ASCL1 + cells (Tai et al., 2021). These findings indicate that OPCs have the latent potential for neurogenic regeneration, which may represent a potential target for reprogramming strategies for spinal cord repair. OPCs may be one of the main reservoirs that could further generate neurons after SCI. Thus, the rational use of transgenic or virus transfection methods and biomaterials may promote the transformation of OPCs into neurons in injured spinal cord.

Age plays a key role in nerve regeneration and age-dependent OPCs heterogeneity should be considered (Baldassarro et al., 2019, 2020). In this study, the primary cells were extracted from the brain tissue of newborn rats (P1-2), so we did not compare the OPCs between juvenile and adult. According to our experience, it may be difficult to extract primary cells from adult spinal cord and brain, because most cells are difficult to survive during the extraction. Additionally, we established SCI models in juvenile (1 week old and 2 weeks old) and adult mice, and obtained transcriptome data of injured spinal cord. We found juvenile mice had strong repair ability after SCI, and the injured area can be effectively repaired along with better functional prognosis than that of adult mice (unpublished data). Furthermore, when compared with

adult mice, our RNA-seq results also showed that the neuron related markers in juvenile mice were well preserved after SCI. Therefore, juvenile mice may have stronger nerve regeneration ability than adult mice. However, there is still a lack of research on the neurogenesis potential of OPCs in juvenile mice. More work is needed in the future.

Endoplasmic reticulum stress refers to the process that unfolded or misfolded proteins accumulate in the ER and activate the unfolded protein response (UPR) under various pathological conditions, so as to reduce unfolded protein load and restore ER homeostasis (Hetz, 2012). However, irreversible ER stress would trigger cell death initiated by the activation of three ER stress sensors separated from immunoglobulin heavy chain binding protein (BiP/GRP78) respectively, including IRE1α, PERK and activating transcription factor 6 (ATF6) (Hetz, 2012). Previously, we have confirmed that inhibition of ER stress related signal pathways can effectively improve neuronal death (Zhao et al., 2017a,b). In this study, we also confirmed that inhibiting ER stress could reduce OPCs death under hypoxic conditions. In contrast, a recent study also found that the IRE1-XBP1-mediated UPR signaling pathway contributes to restoration of ER homeostasis in oligodendrocytes and is necessary for enhanced white matter sparing and functional recovery post-SCI (Saraswat Ohri et al., 2021). Oligodendrocyte-specific deletion of Xbp1 exacerbates the ER stress response and restricts locomotor recovery after thoracic SCI (Saraswat Ohri et al., 2021). Thus, there were inconsistent association between oligodendrocyte death and ER stress, mainly for the double-sword role of ER stress in regulating programmed cell death and homeostasis to protect tissue integrity.

Several studies confirmed that ER plays an important role in regulating stem cells differentiation. Liu and colleges (Liu et al., 2012) confirmed that human embryonic stem cells (hESCs) cell line H9 express high levels of UPR markers, such as XBP1 and p-eIF2α (a downstream factor of ER Stress) that are substantially down-regulated in differentiated cells. Furthermore, researchers found that inhibition of ER stress supported self-renewal of mouse ESCs (mESCs) (Chen et al., 2014; Kratochvílová et al., 2016). Another study also found that ER stress regulates the intestinal stem cell state (Meijer et al., 2021). Additionally, adaptive ER stress signaling *via* IRE1α-XBP1 preserves self-renewal of hematopoietic and pre-leukemic stem cells (Liu et al., 2019). We also identified that ER may be associated with differentiation and stemness of oligospheres. While, more works are needed to explore the mechanisms.

There were also some limitations in this study. To our knowledge, there are no effective methods to isolate 100% pure oligodendrocytes to date, partly for current markers can also be expressed in neural stem cells. However, we did observe the intermediate states of oligodendrocytes and neurons during oligospheres differentiation, which further highlighted the neurogenesis potential of OPCs. Meanwhile, the mechanisms by which oligospheres differentiate into neuron-like cells are still unknown. Thus, further works are needed, such as lineage tracing of the generation and differentiation of oligospheres along with more in-depth characterization of neurons arise from them. Furthermore, oligospheres with biomaterials and factor modification should be transplanted into the injured spinal cord to detect their potential for neurogenesis and repair.

Data availability statement

The datasets presented in this study can be found in online repositories. The names of the repository/repositories and accession number(s) can be found in the article/**Supplementary material**.

Ethics statement

This animal study was reviewed and approved by Institutional Animal Care and Use Committee (IACUC) of the Tongji University School of Medicine.

Author contributions

QZ designed and performed experiments, analyzed the data, and drafted the manuscript. YZ, YR, SY, LY, RH, SS, and XH participated in the *in vitro* and *in vivo* experiment and data analysis. NX, LC, and RZ conceived and designed the experiments, supervised the overall project, and revised the manuscript. All authors have read and approved the article.

Funding

This work was supported by the International Cooperation Project of National Natural Science Foundation of China (Grant No. 81810001048), the National Natural Science Foundation of China (Grant Nos. 81974190, 82271419, 81901902, 81873994, 31727801, and 81701217), the National Key R&D Program of China (Grant No. 2020YFC2008703), Shanghai Rising-Star Program (Grant No. 22QA1408200), and the Fundamental Research Funds for the Central Universities (22120220555 and 22120220217).

Acknowledgments

We thank Gufa Lin, Bei Ma, Zhourui Wu, and Xu Xu of our laboratory for help and advice. We also thank Pianpian Fan (Xinhua Hospital, Shanghai Jiao Tong University School of Medicine) for article grammar check.

Conflict of interest

The authors declare that the research was conducted in the absence of any commercial or financial relationships that could be construed as a potential conflict of interest.

Publisher's note

All claims expressed in this article are solely those of the authors and do not necessarily represent those of their affiliated organizations, or those of the publisher, the editors and the reviewers. Any product that may be evaluated in this article, or claim that may be made by its manufacturer, is not guaranteed or endorsed by the publisher.

Supplementary material

The Supplementary Material for this article can be found online at: https://www.frontiersin.org/articles/10.3389/fncel.2022.1049562/full#supplementary-material

References

Ahuja, C. S., Wilson, J. R., Nori, S., Kotter, M. R. N., Druschel, C., Curt, A., et al. (2017). Traumatic spinal cord injury. *Nat. Rev. Dis. Primers* 3:17018. doi: 10.1038/nrdp.2017.18

Anjum, A., Yazid, M. D., Fauzi Daud, M., Idris, J., Ng, A. M. H., Selvi Naicker, A., et al. (2020). Spinal cord injury: Pathophysiology, multimolecular interactions, and underlying recovery mechanisms. *Int. J. Mol. Sci.* 21:7533. doi: 10.3390/ijms21207533

Atkins, C., Liu, Q., Minthorn, E., Zhang, S. Y., Figueroa, D. J., Moss, K., et al. (2013). Characterization of a novel PERK kinase inhibitor with antitumor and antiangiogenic activity. *Cancer Res.* 73, 1993–2002. doi: 10.1158/0008-5472.Can-12-3109

Avellana-Adalid, V., Nait-Oumesmar, B., Lachapelle, F., and Baron-Van Evercooren, A. (1996). Expansion of rat oligodendrocyte progenitors into proliferative "oligospheres" that retain differentiation potential. *J. Neurosci. Res.* 45, 558–570. doi: 10.1002/(SICI)1097-4547(19960901)45:5<558::AID-JNR6<3.0.CO;2-B

Baldassarro, V. A., Krężel, W., Fernández, M., Schuhbaur, B., Giardino, L., and Calzà, L. (2019). The role of nuclear receptors in the differentiation of oligodendrocyte precursor cells derived from fetal and adult neural stem cells. *Stem Cell Res.* 37:101443. doi: 10.1016/j.scr.2019.101443

Baldassarro, V. A., Marchesini, A., Giardino, L., and Calzà, L. (2020). Differential effects of glucose deprivation on the survival of fetal versus adult neural stem cells-derived oligodendrocyte precursor cells. *Glia* 68, 898–917. doi: 10.1002/glia.23750

Bechler, M. E., Byrne, L., and Ffrench-Constant, C. (2015). CNS myelin sheath lengths are an intrinsic property of oligodendrocytes. *Curr. Biol.* 25, 2411–2416. doi: 10.1016/j.cub.2015.07.056

Chen, G., Xu, X., Zhang, L., Fu, Y., Wang, M., Gu, H., et al. (2014). Blocking autocrine VEGF signaling by sunitinib, an anti-cancer drug, promotes embryonic stem cell self-renewal and somatic cell reprogramming. *Cell Res.* 24, 1121–1136. doi: 10.1038/cr.2014.112

Chen, Y., Balasubramaniyan, V., Peng, J., Hurlock, E. C., Tallquist, M., Li, J., et al. (2007). Isolation and culture of rat and mouse oligodendrocyte precursor cells. *Nat. Protoc.* 2, 1044–1051. doi: 10.1038/nprot.2007.149

Cunningham, L. A., and Su, C. (2002). Astrocyte delivery of glial cell line-derived neurotrophic factor in a mouse model of Parkinson's disease. *Exp. Neurol.* 174, 230–242. doi: 10.1006/exnr.2002.7877

Degos, V., Charpentier, T. L., Chhor, V., Brissaud, O., Lebon, S., Schwendimann, L., et al. (2013). Neuroprotective effects of dexmedetomidine against glutamate agonist-induced neuronal cell death are related to increased astrocyte brain-derived neurotrophic factor expression. *Anesthesiology* 118, 1123–1132. doi: 10.1097/ALN.0b013e318286cf36

Duan, H., Pang, Y., Zhao, C., Zhou, T., Sun, C., Hou, M., et al. (2021). A novel, minimally invasive technique to establish the animal model of spinal cord injury. *Ann. Transl. Med.* 9, 881–881. doi: 10.21037/atm-21-2063

Floriddia, E. M., Lourenço, T., Zhang, S., van Bruggen, D., Hilscher, M. M., Kukanja, P., et al. (2020). Distinct oligodendrocyte populations have spatial preference and different responses to spinal cord injury. *Nat. Commun.* 11:5860. doi: 10.1038/s41467-020-19453-x

Franklin, R., and Ffrench-Constant, C. (2008). Remyelination in the CNS: From biology to therapy. *Nat. Rev. Neurosci.* 9, 839–855.

Garcia-Ovejero, D., González, S., Paniagua-Torija, B., Lima, A., Molina-Holgado, E., De Nicola, A., et al. (2014). Progesterone reduces secondary damage, preserves white matter, and improves locomotor outcome after spinal cord contusion. *J. Neurotrauma* 31, 857–871. doi: 10.1089/neu.2013.3162

Gibney, S. M., and McDermott, K. W. (2009). Sonic hedgehog promotes the generation of myelin proteins by transplanted oligosphere-derived cells. *J. Neurosci. Res.* 87, 3067–3075. doi: 10.1002/jnr.22138

Gibson, E. M., Purger, D., Mount, C. W., Goldstein, A. K., Lin, G. L., Wood, L. S., et al. (2014). Neuronal activity promotes oligodendrogenesis and adaptive myelination in the mammalian brain. *Science* 344:1252304. doi: 10.1126/science.1252304

Hattori, T., Kaji, M., Ishii, H., Jureepon, R., Takarada-Iemata, M., Minh Ta, H., et al. (2017). CD38 positively regulates postnatal development of astrocytes cell-autonomously and oligodendrocytes non-cell-autonomously. *Glia* 65, 974–989. doi: 10.1002/glia.23139

Heinrich, C., Bergami, M., Gascon, S., Lepier, A., Vigano, F., Dimou, L., et al. (2014). Sox2-mediated conversion of NG2 glia into induced neurons in the injured adult cerebral cortex. *Stem Cell Rep.* 3, 1000–1014. doi: 10.1016/j.stemcr.2014.10.007

Hetz, C. (2012). The unfolded protein response: Controlling cell fate decisions under ER stress and beyond. *Nat. Rev. Mol. Cell Biol.* 13, 89–102. doi: 10.1038/nrm3270

Hill, R. A., Patel, K. D., Medved, J., Reiss, A. M., and Nishiyama, A. (2013). NG2 cells in white matter but not gray matter proliferate in response to PDGF. *J. Neurosci.* 33, 14558–14566. doi: 10.1523/jneurosci.2001-12.2013

Hughes, E. G., Orthmann-Murphy, J. L., Langseth, A. J., and Bergles, D. E. (2018). Myelin remodeling through experience-dependent oligodendrogenesis in the adult somatosensory cortex. *Nat. Neurosci.* 21, 696–706. doi: 10.1038/s41593-018-0121-5

Irvine, K., and Blakemore, W. (2008). Remyelination protects axons from demyelination-associated axon degeneration. *Brain* 131(Pt 6), 1464–1477. doi: 10.1093/brain/awn080

Khandker, L., Jeffries, M. A., Chang, Y. J., Mather, M. L., Evangelou, A. V., Bourne, J. N., et al. (2022). Cholesterol biosynthesis defines oligodendrocyte precursor heterogeneity between brain and spinal cord. *Cell Rep.* 38:110423. doi: 10.1016/j.celrep.2022.110423

Kratochvílová, K., Moráň, L., Pad'ourová, S., Stejskal, S., Tesařová, L., Šimara, P., et al. (2016). The role of the endoplasmic reticulum stress in stemness, pluripotency and development. *Eur. J. Cell Biol.* 95, 115–123. doi: 10.1016/j.ejcb.2016.02.002

Li, Y., Wang, P. S., Lucas, G., Li, R., and Yao, L. (2015). ARP2/3 complex is required for directional migration of neural stem cell-derived oligodendrocyte precursors in electric fields. *Stem Cell Res. Ther.* 6:41. doi: 10.1186/s13287-015-0042-0

Liu, L., Liu, C., Zhong, Y., Apostolou, A., and Fang, S. (2012). ER stress response during the differentiation of H9 cells induced by retinoic acid. *Biochem. Biophys. Res. Commun.* 417, 738–743. doi: 10.1016/j.bbrc.2011.12.026

Liu, L., Zhao, M., Jin, X., Ney, G., Yang, K. B., Peng, F., et al. (2019). Adaptive endoplasmic reticulum stress signalling via IRE1α-XBP1 preserves self-renewal of haematopoietic and pre-leukaemic stem cells. *Nat. Cell Biol.* 21, 328–337. doi: 10.1038/s41556-019-0285-6

Lytle, J. M., and Wrathall, J. R. (2007). Glial cell loss, proliferation and replacement in the contused murine spinal cord. *Eur. J. Neurosci.* 25, 1711–1724. doi: 10.1111/j.1460-9568.2007.05390.x

McKenzie, I. A., Ohayon, D., Li, H., de Faria, J. P., Emery, B., Tohyama, K., et al. (2014). Motor skill learning requires active central myelination. *Science* 346, 318–322. doi: 10.1126/science.1254960

Meijer, B. J., Smit, W. L., Koelink, P. J., Westendorp, B. F., de Boer, R. J., van der Meer, J. H. M., et al. (2021). Endoplasmic reticulum stress regulates the intestinal stem cell state through CtBP2. *Sci. Rep.* 11:9892. doi: 10.1038/s41598-021-89326-w

Milich, L. M., Choi, J. S., Ryan, C., Cerqueira, S. R., Benavides, S., Yahn, S. L., et al. (2021). Single-cell analysis of the cellular heterogeneity and interactions in the injured mouse spinal cord. *J. Exp. Med.* 218:e20210040. doi: 10.1084/jem.20210040

Miyamoto, N., Magami, S., Inaba, T., Ueno, Y., Hira, K., Kijima, C., et al. (2020). The effects of A1/A2 astrocytes on oligodendrocyte linage cells against white matter injury under prolonged cerebral hypoperfusion. *Glia* 68, 1910–1924. doi: 10.1002/glia.23814

Papandreou, I., Denko, N. C., Olson, M., Van Melckebeke, H., Lust, S., Tam, A., et al. (2011). Identification of an Ire1alpha endonuclease specific inhibitor with cytotoxic activity against human multiple myeloma. *Blood* 117, 1311–1314. doi: 10.1182/blood-2010-08-303099

Pedraza, C. E., Monk, R., Lei, J., Hao, Q., and Macklin, W. B. (2008). Production, characterization, and efficient transfection of highly pure oligodendrocyte precursor cultures from mouse embryonic neural progenitors. *Glia* 56, 1339–1352. doi: 10.1002/glia.20702

Ren, Y., Ao, Y., O'Shea, T. M., Burda, J. E., Bernstein, A. M., Brumm, A. J., et al. (2017). Ependymal cell contribution to scar formation after spinal cord injury is minimal, local and dependent on direct ependymal injury. *Sci. Rep.* 7:41122. doi: 10.1038/srep41122

Rowitch, D. H., and Kriegstein, A. R. (2010). Developmental genetics of vertebrate glial-cell specification. *Nature* 468, 214–222. doi: 10.1038/nature09611

Saraswat Ohri, S., Howard, R. M., Liu, Y., Andres, K. R., Shepard, C. T., Hetman, M., et al. (2021). Oligodendrocyte-specific deletion of Xbp1 exacerbates the endoplasmic reticulum stress response and restricts locomotor recovery after thoracic spinal cord injury. *Glia* 69, 424–435. doi: 10.1002/glia.23907

Spitzer, S. O., Sitnikov, S., Kamen, Y., Evans, K. A., Kronenberg-Versteeg, D., Dietmann, S., et al. (2019). Oligodendrocyte progenitor cells become regionally diverse and heterogeneous with age. *Neuron* 101, 459–471.e5. doi: 10.1016/j.neuron.2018.12.020

Tai, W., Wu, W., Wang, L. L., Ni, H., Chen, C., Yang, J., et al. (2021). In vivo reprogramming of NG2 glia enables adult neurogenesis and functional recovery following spinal cord injury. *Cell Stem Cell* 28, 923–937.e4. doi: 10.1016/j.stem.2021.02.009

Torper, O., Ottosson, D. R., Pereira, M., Lau, S., Cardoso, T., Grealish, S., et al. (2015). In vivo reprogramming of striatal NG2 glia into functional neurons that integrate into local host circuitry. *Cell Rep.* 12, 474–481. doi: 10.1016/j.celrep.2015.06.040

Viganò, F., Möbius, W., Götz, M., and Dimou, L. (2013). Transplantation reveals regional differences in oligodendrocyte differentiation in the adult brain. *Nat. Neurosci.* 16, 1370–1372. doi: 10.1038/nn.3503

Wu, B., Sun, L., Li, P., Tian, M., Luo, Y., and Ren, X. (2012). Transplantation of oligodendrocyte precursor cells improves myelination and promotes functional recovery after spinal cord injury. *Injury* 43, 794–801. doi: 10.1016/j.injury.2011.09.013

Wu, J., Renn, C. L., Faden, A. I., and Dorsey, S. G. (2013). TrkB.T1 contributes to neuropathic pain after spinal cord injury through regulation of cell cycle pathways. *J. Neurosci.* 33, 12447–12463. doi: 10.1523/jneurosci.0846-13.2013

Wu, J., Zhao, Z., Sabirzhanov, B., Stoica, B. A., Kumar, A., Luo, T., et al. (2014). Spinal cord injury causes brain inflammation associated with cognitive and affective changes: Role of cell cycle pathways. *J. Neurosci.* 34, 10989–11006. doi: 10.1523/jneurosci.5110-13.2014

Zawadzka, M., Rivers, L. E., Fancy, S. P., Zhao, C., Tripathi, R., Jamen, F., et al. (2010). CNS-resident glial progenitor/stem cells produce Schwann cells as well as oligodendrocytes during repair of CNS demyelination. *Cell Stem Cell* 6, 578–590. doi: 10.1016/j.stem.2010.04.002

Zhang, Q., Guan, G., Cheng, P., Cheng, W., Yang, L., and Wu, A. (2021). Characterization of an endoplasmic reticulum stress-related signature to evaluate immune features and predict prognosis in glioma. *J. Cell. Mol. Med.* 25, 3870–3884. doi: 10.1111/jcmm.16321

Zhao, Q., Che, X., Zhang, H., Fan, P., Tan, G., Liu, L., et al. (2017a). Thioredoxin-interacting protein links endoplasmic reticulum stress to inflammatory brain injury and apoptosis after subarachnoid haemorrhage. *J. Neuroinflamm.* 14:104. doi: 10.1186/s12974-017-0878-6

Zhao, Q., Che, X., Zhang, H., Tan, G., Liu, L., Jiang, D., et al. (2017b). Thioredoxin-interacting protein mediates apoptosis in early brain injury after subarachnoid haemorrhage. *Int. J. Mol. Sci.* 18:854. doi: 10.3390/ijms18040854

Zhu, Y., Huang, R., Wu, Z., Song, S., Cheng, L., and Zhu, R. (2021). Deep learning-based predictive identification of neural stem cell differentiation. *Nat. Commun.* 12:2614. doi: 10.1038/s41467-021-22758-0

frontiers | Frontiers in Cellular Neuroscience

TYPE Original Research
PUBLISHED 12 May 2023
DOI 10.3389/fncel.2023.1081190

OPEN ACCESS

EDITED BY
Hiroaki Wake,
Nagoya University, Japan

REVIEWED BY
Beatriz Garcia-Diaz,
Universidad de Málaga, Spain
Ichiro Manabe,
Chiba University, Japan

*CORRESPONDENCE
Rieko Muramatsu
✉ muramatsu@ncnp.go.jp

RECEIVED 27 October 2022
ACCEPTED 24 April 2023
PUBLISHED 12 May 2023

CITATION
Maruyama T, Tanabe S, Uyeda A, Suzuki T and Muramatsu R (2023) Free fatty acids support oligodendrocyte survival in a mouse model of amyotrophic lateral sclerosis.
Front. Cell. Neurosci. 17:1081190.
doi: 10.3389/fncel.2023.1081190

Free fatty acids support oligodendrocyte survival in a mouse model of amyotrophic lateral sclerosis

Takashi Maruyama[1,2], Shogo Tanabe[1], Akiko Uyeda[1], Tatsunori Suzuki[2,3] and Rieko Muramatsu[1]*

[1]Department of Molecular Pharmacology, National Institute of Neuroscience, National Center of Neurology and Psychiatry, Tokyo, Japan, [2]Department of Pharmacoscience, Graduate School of Pharmaceutical Sciences, Tokyo University of Science, Chiba, Japan, [3]Department of Pharmaceutical Sciences, Graduate School of Pharmaceutical Sciences, Tokyo University of Science, Chiba, Japan

Introduction: Amyotrophic lateral sclerosis (ALS) is a fatal neurodegenerative disease characterized by the white matter degeneration. Although changes in blood lipids are involved in the pathogenesis of neurological diseases, the pathological role of blood lipids in ALS remains unclear.

Methods and results: We performed lipidome analysis on the plasma of ALS model mice, mutant superoxide dismutase 1 ($SOD1^{G93A}$) mice, and found that the concentration of free fatty acids (FFAs), including oleic acid (OA) and linoleic acid (LA), decreased prior to disease onset. An *in vitro* study revealed that OA and LA directly inhibited glutamate-induced oligodendrocytes cell death via free fatty acid receptor 1 (FFAR1). A cocktail containing OA/LA suppressed oligodendrocyte cell death in the spinal cord of $SOD1^{G93A}$ mice.

Discussion: These results suggested that the reduction of FFAs in the plasma is a pathogenic biomarker for ALS in the early stages, and supplying a deficiency in FFAs is a potential therapeutic approach for ALS by preventing oligodendrocyte cell death.

KEYWORDS

free fatty acids, amyotrophic lateral sclerosis (ALS), oligodendrocyte, lipidome, SOD1

1. Introduction

Amyotrophic lateral sclerosis (ALS) is a progressive and fatal degenerative disease primarily characterized by selective loss of upper and lower motor neurons (MNs), muscle wasting, and paralysis (Brown and Al-Chalabi, 2017). Approximately 90% of ALS cases are sporadic, and the remaining 10% are inherited with mutations in genes such as superoxide dismutase 1 (SOD1). Because of the genetic diversity and heterogeneous disease progression, it takes approximately 1 year to diagnose ALS from the first symptom (Cellura et al., 2012). As early intervention is a promising therapeutic approach for neurodegenerative diseases, biomarkers that can facilitate early diagnosis and improve the prognosis of ALS are urgently needed (Sturmey and Malaspina, 2022).

Increased energy expenditure, hypermetabolism, and alterations in several metabolites, including lipids, have been reported in patients with both sporadic and familial ALS, as well as in rodent models (Dupuis et al., 2004; Godoy-Corchuelo et al., 2022). Lipids comprise diverse groups of molecules and act not only as energy sources but also as components of the cell membrane and signaling molecules that regulate a variety of cellular responses via receptors or transporters expressed on the cell surface in various organs, including the central

nervous system (CNS) (Cermenati et al., 2015). Disruptions in the lipid pathways within the CNS have been implicated in triggering neurological pathologies in ALS (Chaves-Filho et al., 2019; Tracey et al., 2021). Moreover, the importance of systemic lipid homeostasis in ALS pathology is suggested by the fact that increased dietary lipids provide neuroprotective effects and extend survival (Dupuis et al., 2004; Mattson et al., 2007), whereas restricted calorie intake aggravates neurological symptoms in ALS model mice (Pedersen and Mattson, 1999). However, global changes in systemic lipid metabolites at the early stages of ALS progression and their links to CNS pathogenesis remain unclear.

Emerging evidence has suggested that ALS is not merely a disease of MNs, and that their interactions with glial cells, including astrocytes, microglia, and oligodendrocytes (OLs), also mediate the pathology of ALS (Boillée et al., 2006; Yamanaka et al., 2008; Puentes et al., 2016). Compared to other CNS glial cells, OLs have distinct physiological functions, including forming a myelin sheath to ensure neuronal axon integrity, rapid conduction, and providing metabolic support for neurons (Lee et al., 2012; Nave and Werner, 2014). OL dysfunctions and demyelination have been reported in ALS patients (Kang et al., 2013). In a rodent ALS model (SOD1^{G93A} mice), degeneration of mature OLs and increased proliferation of oligodendrocyte precursor cells were observed prior to the appearance of neurological symptoms (Kang et al., 2013; Philips et al., 2013), suggesting that OLs mediate the early pathogenesis of ALS. We and others have reported that peripheral-derived factors, including hormones and immune cells, influence the cellular response of OLs and oligodendrocyte precursor cells in CNS disease, as vascular damage often occurs in the lesion (Kuroda et al., 2017; Hamaguchi et al., 2019; Saitoh et al., 2022). Moreover, OLs require lipids for development and function (Montani, 2021). Thus, we hypothesized that alterations in circulating lipids in ALS may affect oligodendrocyte function, thereby mediating the early pathogenesis of ALS.

In this study, we conducted a non-targeted lipidomic analysis of circulating lipids in the plasma of SOD1^{G93A} mice and found a robust decrease in subsets of FFAs, including oleic acid (OA) and linoleic acid (LA), before the onset of symptoms. In primary cultured murine oligodendrocytes, OA/LA inhibited excitotoxic oligodendrocyte death through FFAR1. Systemic LA/OA administration before disease onset ameliorated OL and MN deaths in SOD1^{G93A} mice.

2. Materials and methods

2.1. Ethics

All experimental procedures were approved by the Committee on the Ethics of Animal Experiments of the National Institutes of Neuroscience, National Center of Neurology and Psychiatry (2021013R2).

2.2. Mice

Postnatal day 1 (P1) C57BL/6J mice were obtained from Tokyo Laboratory Animals Science. SOD1-G93A transgenic mice, that is express a G93A mutant form of human SOD1 were obtained from Jackson Laboratory (#002726) and heterozygous (SOD1^{G93A}) males were bred with wild-type (WT) female C57BL/6J mice (Japan SLC). Offspring were ear punched and genotyped using PCR with following primers: *Human/Mouse Sod1* forward, CAGCAGTCACATTGCCCARGTCTCCAACATG; *Human Sod1* reverse, CCAAGATGCTTAACTCTTGTAATCAATGGC; *Mouse Sod1* reverse, GTTACATATAGGGGTTTACTTCATAATCTG. Mice not expressing the transgene were used as WT littermate controls. Mice were housed in an air-conditioned room at 22°C with a 12-h light–dark cycle, had free access to water and food, and were maintained in sterile, pathogen-free conditions. The mice were fed standard chow diets (CE-2, CLEA Japan) and water under *ad libitum* conditions.

Female SOD1^{G93A} mice were intraperitoneally administered with linoleic acid-oleic acid-albumin (10.6 mg/kg, L9655, Sigma-Aldrich) or bovine serum albumin (BSA; 1.25 g/kg, 810017, Sigma-Aldrich) twice a week between P60 and P100.

2.3. Plasma preparation and lipidomics

Cardiac blood was collected via cardiac puncture from P60, P100 SOD1^{G93A}, or WT mice under anesthesia, mixed with one-hundredth of 1.3% ethylenediaminetetraacetic acid-2K/0.9% saline, and centrifuged at 1,200 rpm for 15 min at 4°C. The supernatant was collected as plasma and stored at -80°C until using. Untargeted and unbiased lipidomic analysis were conducted at Human Metabolome Technologies Inc. (HMT, Tsuruoka, Japan).

2.4. Primary culture of oligodendrocytes

Primary cultures of oligodendrocytes were obtained from mice at P1 as previously described (Hamaguchi et al., 2019). The forebrains were dissected and minced with fine scissors in ice-cold phosphate-buffered saline (PBS). The minced tissues were dissociated with 0.25% trypsin (15090–046, Thermo Fisher Scientific, Waltham, MA, USA) in PBS at 37°C for 10 min. After neutralization with Dulbecco's modified Eagle's medium (DMEM; 12800082, Thermo Fisher Scientific) containing 10% fetal bovine serum (FBS; F7524, Sigma-Aldrich), cells were centrifuged at 1,500 rpm for 10 min, resuspended in 10% FBS-DMEM, and filtered through a 70 μm nylon cell strainer. Cells were then plated on poly-L-lysine (PLL; P2636, Sigma-Aldrich)-coated 10-cm dishes at a density of 5×10^5 cells/dish and maintained at 37°C with 5% CO_2 in 10% FBS-DMEM. 10 days after culturing, cells were washed with PBS and the remaining cells were treated with 0.05% Trypsin-PBS at 37°C for 3 min. The detached cells were filtered through a 40 μm nylon cell strainer and plated into non-coated dishes and incubated at 37°C for 30 min. Then, the non-adherent cells were collected and plated into PLL-coated 96 well glass-bottom plate (5866-960, IWAKI) at a density of 5×10^4 cells/well in culture medium, consisting of DMEM/Nutrient Mixture F-12 Ham medium (DMEM/F12; D0547, Sigma-Aldrich, St. Louis, MO, USA) supplemented with 1 mM sodium pyruvate (S8636, Sigma-Aldrich, St. Louis, MO, USA), 0.1% bovine serum albumin (BSA; 810017, Sigma-Aldrich, St. Louis, MO, USA), 50 μg/ml apo-transferrin (T5391, Sigma-Aldrich), 5 μg/ml insulin (I1882, Sigma-Aldrich), 30 nM sodium selenite

(S9133, Sigma-Aldrich), 10 nM biotin (B4639, Sigma-Aldrich), 10 nM hydrocortisone (H6909, Sigma-Aldrich), 10 ng/ml platelet-derived growth factor-AA (315-17, PeproTech), and 10 ng/ml basic fibroblast growth factor (450-33, PeproTech). For the purification of oligodendrocytes progenitor cells (OPCs), detached cells were treated with CD140a (PDGFRα) Microbead kit (130-101-547, Miltenyi Biotec, Bergisch Gladbach, Germany) and the OPCs were plated onto PLL-coated 96-well glass plate at a density of 5.0×10^4/well in culture medium. We confirmed that $90.26 \pm 0.93\%$ of cells in the culture were labeled by Olig2, an oligodendrocyte lineage cell marker, using immunocytochemical analysis (data not shown).

Three days after culturing, mouse siGENOME siRNAs (Horizon Discovery) for target genes were transfected into cultured oligodendrocytes using Lipofectamine RNAiMAX (13778075, Thermo Fisher Scientific, Waltham, MA, USA). Four hours after transfection, the cells were treated with differentiation medium and cultured for additional 3 days. Differentiation medium consisted of DMEM/F12 containing 1 mM sodium pyruvate, 0.1% BSA, 50 μg/ml apo-transferrin, 5 μg/ml insulin, 30 nM sodium selenite, 10 nM biotin, 10 nM hydrocortisone, and 20 ng/ml triiodo-L-thyronine (T2752, Sigma-Aldrich). Then the cells were treated with 30 μM Linoleic Acid-Oleic Acid-Albumin (L9655, Sigma-Aldrich) (Ahn et al., 2013; Lee et al., 2022) and 100 μM glutamate (G5889, Sigma-Aldrich, St. Louis, MO, USA) for 24 h, and dead cells were stained with 1 μg/mL Propidium Iodide (PI; 169-26281, WAKO) for 30 min.

2.5. Immunocytochemistry

Cells were fixed with 4% paraformaldehyde (PFA, Merck, Darmstadt, Germany) in PBS at room temperature for 30 min, followed by permeabilization and blocking with blocking solution (0.1% Triton X-100 and 3% BSA in PBS) for 1 h at room temperature. Then, the cells were incubated with the primary antibody, rat anti-myelin basic protein (MBP) antibody (AB7349, Abcam, Cambridge, UK) at 1:500, and rabbit anti-Cleaved caspase-3 (CC3; #9661, Cell Signaling Technology, Danvers, MA, USA) at 1:1000 dilution in the blocking solution overnight at 4°C. Primary antibody was detected by the Alexa Fluor 488-conjugated donkey antibody against rat IgG (Thermo Fisher Scientific) diluted with blocking solution at 1:500. Nuclei were stained with 4′,6-diamidino-2-phenylindole (DAPI, 1 mg/ml, Dojindo Laboratories, Kumamoto, Japan). Images were acquired using a confocal laser-scanning microscopy (FV3000, Olympus, Tokyo, Japan) with a 20×/0.75 objective lens. To estimate oligodendroglial cell death, the percentage of PI^+ MBP^+ cells in MBP^+ cells were calculated from more than 50 MBP^+ cells using ImageJ software (National institute of health).

2.6. Quantitative reverse transcription polymerase chain reaction (qRT-PCR)

Three days after siRNAs transfection, total RNA was isolated from cultured oligodendrocytes using the TRIzol reagent (10296010, Thermo Fisher Scientific, Waltham, MA, USA). For quantitative RT-PCR, cDNA was synthesized using the High-Capacity cDNA Reverse Transcriptase Kit (4368814, Applied Biosystems, Waltham, MA, USA). Real-time qRT-PCR was performed using KAPA SYBR Fast Master Mix (7959397001, KAPA Biosystems, Wilmington, MA, USA) with the following primer pairs: *Ffar1* forward, GGGCTTTCCATTGAACTTGTTAG; *Ffar1* reverse, GCCCAGATGGAGAGTGTAGACC; *Gapdh* forward, AGGTCGGTGTGAACGGATTTG; *Gapdh* reverse, TGTAGACCATGTAGTTGAGGTCA. PCR conditions included one cycle at 95°C for 30 s, followed by 39 cycles of 95°C for 5 s and 60°C for 45 s. A melting analysis was carried out following PCR to monitor amplification specificity. Relative mRNA expression was normalized against *Gapdh* mRNA levels in the same samples and calculated by the Δ/Δ-Ct method.

2.7. Immunohistochemistry

Mice were transcardially perfused with 4% PFA in PBS. Lumbar spinal cords were post-fixed with 4% PFA in PBS overnight at 4°C and then immersed in 30% sucrose in PBS at 4°C. Tissues were embedded in optimal cutting temperature compound (Tissue-Tek, Sakura Finetek), sliced into 30 μm sections and mounted on Adhesive Glass Slides (Matsunami Glass). Sections were permeabilized with 0.1% Triton X-100 in PBS and blocked with 3% normal donkey serum in PBS for 1 h at room temperature. The sections were incubated with primary antibodies overnight at 4°C and then incubated with fluorescently labeled secondary antibodies for 1 h at room temperature. The following primary antibodies were used: rabbit anti-CC3 (#9661, Cell Signaling Technology, Danvers, MA, USA, 1:1000), goat anti-Olig2 (AF2418, R&D Systems, 1:1000), mouse anti-APC (CC1; OP80, Calbiochem, 1:1000), rabbit anti-Iba1 (019-19741, Wako, 1:1000), mouse anti-glial fibrillary acidic protein (GFAP; G3893, Sigma-Aldrich, St. Louis, MO, USA, 1:1000), goat anti-choline acetyltransferase (ChAT; AB144P, Millipore, 1:1000), rabbit anti-GPCR GPR40 (FFAR1; ab236285, Abcam, Cambridge, UK, 1:500) antibodies. Alexa Fluor 488-conjugated donkey antibodies against rabbit, or mouse IgG, Alexa Fluor 568-conjugated donkey antibodies against mouse or goat IgG, and Alexa Fluor 647-conjugated donkey antibody against rabbit IgG (Thermo Fisher Scientific, Waltham, MA, USA) were used as secondary antibodies. Images were acquired using a confocal laser-scanning microscopy (FV3000, Olympus, Tokyo, Japan) with a 20×/0.75 objective lens. Oligodendroglial cell death were evaluated with percentage of $CC3^+$ $CC1^+$ $Olig2^+$ cells in $CC1^+$ $Olig2^+$cells and neuronal cell death were evaluated with the number of $ChAT^+$ cells in the anterior horn using ImageJ. To evaluate the gliosis, fluorescence intensity of GFAP and Iba1 in the anterior horn was normalized to its area using ImageJ.

2.8. Grip strength test

The grip strength test for OA/LA or BSA-treated $SOD1^{G93A}$ mice were performed twice a week between P60 and P100. The mice

10.3389/fncel.2023.1081190

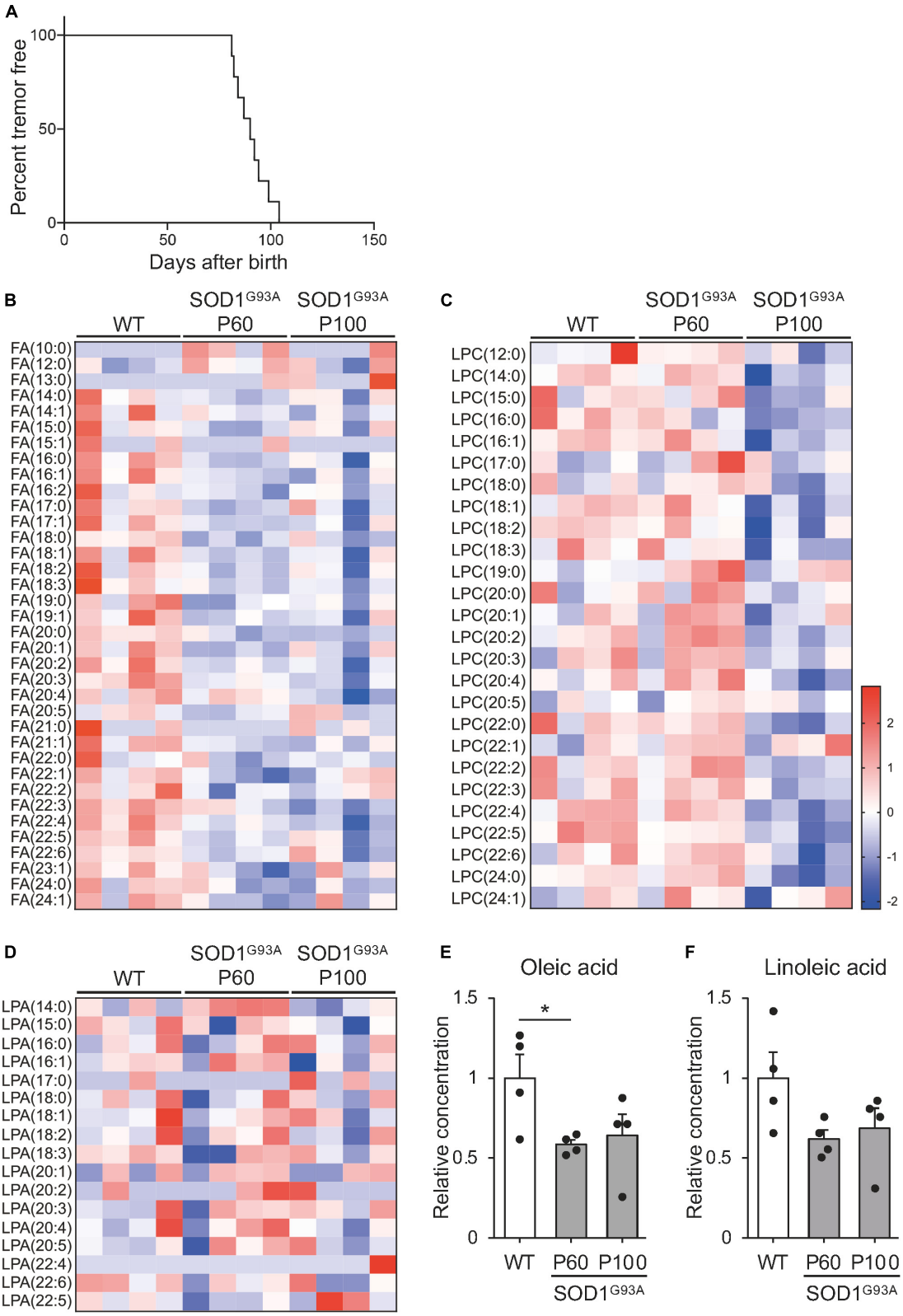

FIGURE 1

Free fatty acid (FFA) concentration is reduced in the plasma of SOD1^{G93A} mice. The plasma was obtained from WT or SOD1^{G93A} mice at P60 and P100, and subjected to mass spectrometry for lipid analysis. **(A)** Kaplan–Meier curve showing the probability of SOD1^{G93A} mice without tremor symptoms (n = 9). **(B–D)** A heat map showing the z-score of each fatty acid **(B)**, lysophosphatidylcholine **(C)**, and lysophosphatidic acid **(D)** in the plasma. The rows and columns represent lipids and samples, respectively **(E,F)**. Graph indicating the relative concentration of oleic acid (OA) **(E)**, and linoleic acid (LA) **(F)** in the plasma. The error bars represent mean ± SEM (n = 4 for each group). *P < 0.05, assessed by one-way ANOVA followed by Tukey–Kramer test for panel **(E)**.

were placed on a grid attached to grip strength meter (Bio-GS3; Bioseb). The tail was pulled until the mouse released the grid, and the maximum value (given by gram) from 10 trials was recorded.

2.9. Statical analysis

All statistical values are presented as mean values ± standard error of mean (SEM). The number of samples analyzed is given for each experiment. Significant differences were determined with Student's *t*-test, one-way analysis of variance (ANOVA) followed by Tukey–Kramer test, or two-way ANOVA followed by Sidak's multiple comparison tests. All data were analyzed using Excel 2019 (Microsoft) or EZR (Kanda, 2013).

3. Results

3.1. Reduced circulating free fatty acid in SOD1^{G93A}

There are few reports on changes in blood lipid levels before the appearance of symptoms. To investigate how circulating lipids are altered with ALS progression, we performed global lipidomic analysis of plasma from SOD1^{G93A} mice at the pre-symptomatic (P60) and symptomatic (P100) stages (Weydt et al., 2003; Kaiser et al., 2006; Rudnick et al., 2017). Consistent with previous reports, no SOD1^{G93A} mice exhibited hindlimb tremor symptoms at P60, while 88.8% of SOD1^{G93A} mice showed symptoms at P100 (**Figure 1A**). When compared to WT (P100) controls, SOD1^{G93A} mice exhibited a decrease in subsets of FFAs from the pre-symptomatic stage, which was sustained during the progression of pathology (**Figure 1B** and **Supplementary Table 1**). Conversely, we found a decrease in lysophosphatidylcholine from the symptomatic stage (**Figure 1C**) and no significant changes in lysophosphatidic acid (**Figure 1D**). Thus, we decided to focus on FFA during ALS progression. FA (16:0), FA (16:1), FA (17:0), FA (17:1), FA (18:0), FA (18:1), FA (19:0), FA (19.1), FA (20:0), FA (20:1), FA (20:2), FA (20:3), FA (21:1), FA (22:1), FA (22:3), FA (22:4), FA (22:5), and FA (22:6) were significantly reduced in SOD1^{G93A} mice at P60 (**Supplementary Table 1**). Among the downregulated FFA species, OA (FA 18:1), a monosaturated 18-carbon fatty acid that is one of the most common types of fatty acid in nature, was relatively abundant in circulation (Gonçalves-de-Albuquerque et al., 2012) and showed a significant decrease before the onset (**Figure 1E** and **Supplementary Table 1**, 58.5 ± 3.0% at P60 compared to WT, P = 0.0312). Among other 18-carbon fatty acids, LA (FA 18:2), a polyunsaturated fatty acid, also showed the second highest level in physiological conditions (**Supplementary Table 1**), and a similar decreasing trend was observed in the early stage of ALS pathogenesis (**Figure 1F**, 62.0 ± 5.6% at P60 compared to WT, P = 0.075). Notably, OA and LA have been implicated to facilitate neuroprotective effects in neurodegenerative diseases (Vesga-Jiménez et al., 2022). In addition, the mixture of OA and LA has been shown to exert synergistic effect on various cellular processes (Belal et al., 2018). These facts prompted us to investigate whether OA and LA are involved in ALS pathogenesis.

3.2. Oleic and linoleic acid prevent oligodendroglial cell death through Ffar1

Oligodendrocyte death, including apoptosis, has been reported in pre-symptomatic SOD1^{G93A} mice (Kang et al., 2013; Philips et al., 2013; Ferraiuolo et al., 2016). Excitotoxic damage has been implicated in oligodendrocyte death in CNS diseases associated with OL degeneration (Matute et al., 2007; Foran and Trotti, 2009). FFAs, including OA and LA have been suggested to inhibit apoptosis via G protein-coupled receptors (Katsuma et al., 2005). This prompted us to investigate whether FFAs support oligodendrocyte survival by inhibiting apoptosis. To test this hypothesis, we examined whether OA and LA prevented oligodendrocyte death induced by glutamate-induced excitotoxicity in murine primary cultured OLs. Treatment with glutamate increased PI$^+$ dead cells in MBP$^+$ oligodendrocytes, consistent with previous reports (Oka et al., 1993; Matute et al., 2006), while an increase in the population of PI$^+$ oligodendrocytes was diminished in the presence of the OA/LA cocktail (**Figures 2A, B**). OA/LA alone did not affect the death of OLs (**Figures 2A, B**). These results suggested that OA/LA prevent excitotoxicity-induced OL death.

Free fatty acids exert various cellular responses through receptors and transporters expressed in cells. To elucidate the molecular mechanisms by which FFAs regulate oligodendrocyte survival, we conducted siRNA-based functional screening for known cell surface receptors (FFAR1-4, GPR84, and 119) (Kimura et al., 2020), intercellular transporters (CD36 and SLC27a1-6) (Kazantzis and Stahl, 2012), intracellular transporters (FABP3, 5, 7, and 12) (Falomir-Lockhart et al., 2019), and nuclear receptors (PPARα, δ, and γ) (Varga et al., 2011) for FFAs. We used a commercially available siRNA library consisting of siRNA pools that include four distinct siRNAs targeting different regions of genes (Mukherjee et al., 2020; Allan et al., 2021; Simoneschi et al., 2021; Uyeda et al., 2021). Among the tested genes, only siRNA targeting *Ffar1* exhibited a significant reduction in the anti-cell death effect of OA/LA (**Figures 2C, D**). RT-PCR analysis confirmed the inhibition of *Ffar1* expression (**Figure 2E**), whereas *Ffar1* knockdown itself did not affect oligodendrocyte survival (**Figure 2F**). These results suggest that OA/LA prevents excitotoxic cell death in oligodendrocytes via FFAR1.

Oleic acid/linoleic acid also affect astrocytes (Murphy, 1995; Nakajima et al., 2019), which were present in the culture we used in our study. Thus, we further investigated whether OA/LA directly facilitated anti-cell death effects on oligodendrocytes through FFAR1 by purification culture of PDGFRα$^+$ OPCs using magnetic-activated cell sorting (MACS), which allows high-purity culture of Olig2$^+$ cells (90.26 ± 0.93%). We found that OA/LA suppressed glutamate-induced oligodendrocyte cell death (**Figures 3A, B**), and silencing *Ffar1* expression significantly inhibited anti-cell death effect of OA/LA in purified oligodendrocyte culture (**Figures 3C, D**), indicating that OA/LA directly supported oligodendrocyte survival via FFAR1. To investigate whether OA/LA inhibited apoptosis, we analyzed cleaved-caspase3$^+$ (CC3, an apoptosis marker) in purified oligodendrocytes culture treated with glutamate in the presence of OA/LA. The result revealed that treatment with glutamate increased CC3$^+$ MBP$^+$ oligodendrocytes, while an increase in the population of CC3$^+$

10.3389/fncel.2023.1081190

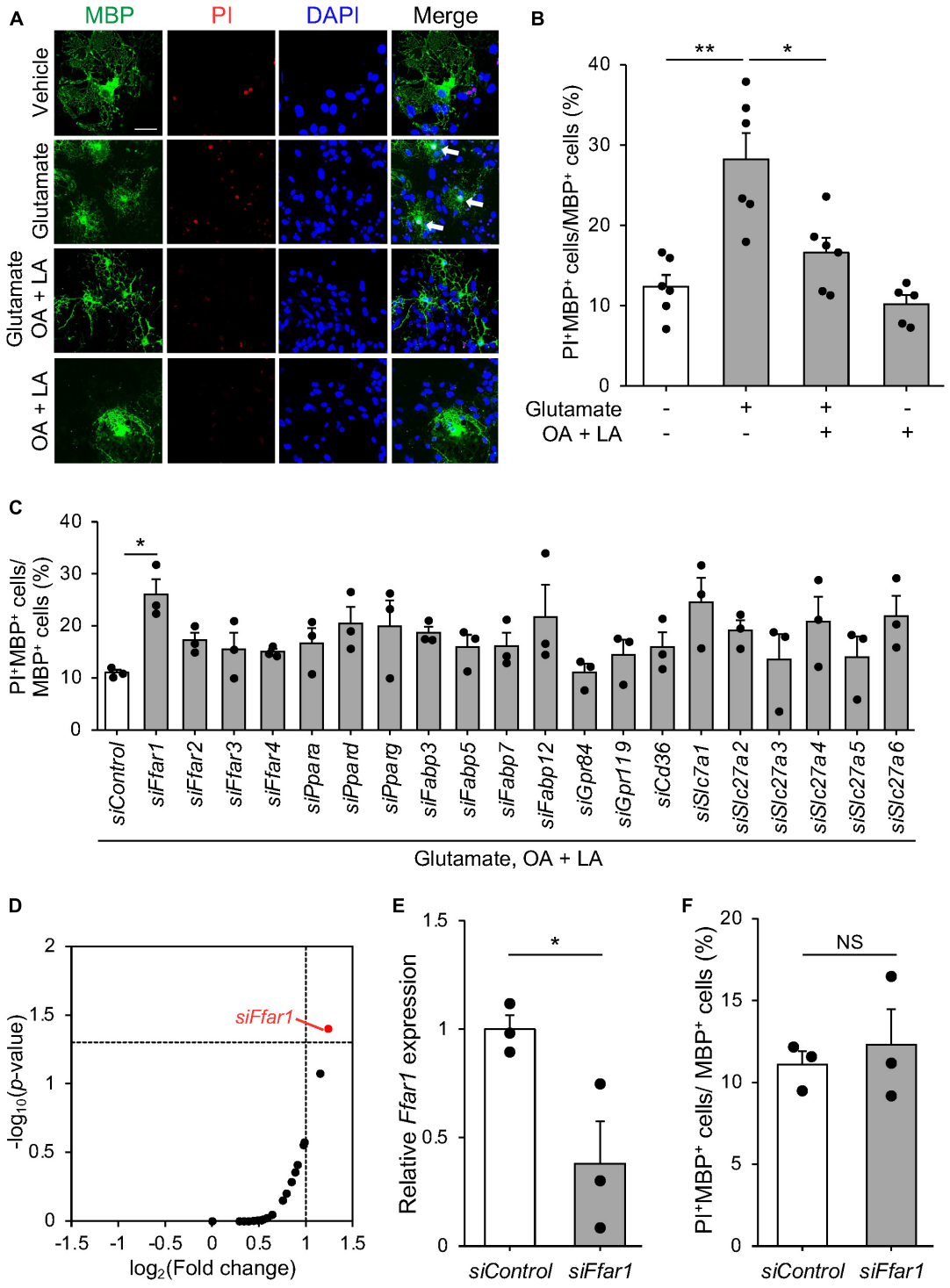

FIGURE 2
FFAR1 is a candidate molecule that regulates oligodendrocyte cell death. **(A)** Representative images show the fluorescence of PI (red) and immunocytochemistry for MBP (green) of primary oligodendrocytes treated with vehicle, glutamate, glutamate + OA + LA, OA + LA. White arrows indicate PI^+ MBP^+ cells. Scale bar: 30 μm. **(B)** Graph indicating the percentage of PI^+ MBP^+ cells in MBP^+ cells (vehicle: $n = 6$, glutamate: $n = 6$, glutamate + OA + LA: $n = 6$, OA + LA: $n = 5$). **(C)** Graph showing the percentage of PI^+ MBP^+ cells in MBP^+ cells of primary oligodendrocyte culture transfected with siRNA library followed by treatment with glutamate + OA + LA ($n = 3$ for each). **(D)** Plot indicating the $-\log_{10}$ (p-value) and $\log_2$ (fold change) of PI^+ MBP^+ cell percentage compared with control siRNA in each siRNA treatment ($n = 3$ for each group). **(E)** Relative expression of *Ffar1* mRNA in primary oligodendrocytes after control or *Ffar1* siRNA treatment ($n = 3$ for each group). **(F)** The percentage of PI^+ MBP^+ cells in MBP^+ cells after *Control* or *Ffar1* siRNA treatment ($n = 3$ for each group). Error bars represent mean ± SEM, $^{**}P < 0.01$, $^{*}P < 0.05$, assessed by one-way ANOVA followed by Tukey–Kramer test for panels **(B–D)**, and by two-sided Student's t-test for panels **(E,F)**, NS, not significant.

oligodendrocytes was diminished in the presence of the OA/LA cocktail (**Figures 3E, F**). Furthermore, inhibition of *Ffar1* expression significantly diminished the anti-apoptotic effect of OA/LA (**Figures 3G, H**), indicating that OA/LA directly supported oligodendrocyte survival via FFAR1.

3.3. OL/LA supports oligodendroglial survival in SOD1^{G93A}

We then investigated the *in vivo* role of OA/LA in oligodendrocyte survival during ALS progression. Immunohistochemical analysis revealed the expression of FFAR1 in the CC1^{+} Olig2^{+} OLs of SOD1^{G93A} mice (**Figure 4A**). SOD1^{G93A} mice were intraperitoneally administered an OA/LA cocktail from the pre-symptomatic (P60) to symptomatic (P100) stages (Avila-Martin et al., 2011). Immunohistochemical analysis showed a decrease in the number of CC3^{+} apoptotic oligodendrocytes in the anterior column of the OA/LA-treated SOD1^{G93A} spinal cord compared with that of vehicle-treated controls at the terminal point (**Figures 4B, C**), without changes in the number of CC1^{+} Olig2^{+} OLs (**Figure 4D**). These results suggest that circulating OA/LA prevents OL death during ALS pathogenesis. To investigate the functional significance of OA/LA treatment, we assessed the motor function of OA/LA-treated SOD1 mice by measuring grip strength. It was found that OA/LA treatment exerted a protective effect on loss of grip strength (**Figure 4E**), suggesting that the protective effect of OA/LA on oligodendrocyte also contributed to mitigating the ALS pathology.

3.4. OA and LA support motor neuron survival in SOD1^{G93A}

Finally, we examined whether circulating OA/LA affects other aspects of ALS pathology, such as MN loss (Rosen et al., 1993) and gliosis (Philips and Rothstein, 2014). Immunohistochemical analysis revealed a slight increase in the number of surviving ChAT^{+} MNs in the anterior column of the OA/LA-treated SOD1^{G93A} spinal cord compared to that in vehicle-treated SOD1 animals (**Figures 5A, B**). Regarding gliosis, the expression level of Iba1 (microglial marker) in the OA/LA-treated SOD1^{G93A} was comparable to that of vehicle-treated controls (**Figures 5C, D**). The expression level of GFAP (astroglial marker) was increased in the OA/LA-treated SOD1^{G93A} compared to that of vehicle-treated controls (**Figures 5E, F**), confirming the successful treatment of OA/LA *in vivo*. Taken together, these results suggest that OA/LA also have a protective effect on MNs.

4. Discussion

In this study, we applied global lipidomic analyses to identify circulating lipids that mediate ALS pathogenesis. We identified a robust decrease in circulating FFAs, including OA/LA, even in pre-symptomatic SOD1^{G93A} mice. OA/LA inhibited excitotoxic oligodendrocyte cell death via the cell surface receptor FFAR1. We also observed that the systemic administration of OA/LA ameliorated the loss of OLs and MNs in SOD1^{G93A} mice.

Alteration in lipid components has been reported in the cerebrospinal fluids and plasma in patients with ALS (Sol et al., 2021). Previous clinical studies have suggested interactions of FFAs with ALS; the levels of polyunsaturated fatty acids, including LA, was low in the FFA fraction of the blood and cerebrospinal fluids of patients with ALS (Henriques et al., 2015; Nagase et al., 2016), which is consistent with our rodent study. In ALS patients, functional decline correlates with increased resting energy expenditure, leading to a decrease in fat mass (Jésus et al., 2018), which might also decrease FFA release (Mittendorfer et al., 2009). In addition, high intake of polyunsaturated fatty acids is associated with a reduced risk of ALS (Fitzgerald et al., 2014). These reports support the notion that polyunsaturated fatty acids, including OA and LA, are protective, and reduction of polyunsaturated fatty acids in the plasma may be detrimental for ALS pathogenesis. Future studies should investigate the role of polyunsaturated fatty acids in plasma in human ALS pathology. Circulating FFAs are derived from stored triglycerides (TGs), which are the ester forms of FAs synthesized primarily in the liver and adipose tissue (Van Harmelen et al., 1999; Zechner et al., 2005). The concentration of postprandial circulating TGs was decreased in ALS mice due to increased lipid uptake in peripheral organs (Dupuis et al., 2004; Fergani et al., 2007). Furthermore, increased mobilization of lipids in ALS mice purportedly occurs to sustain metabolic requirements in peripheral glycolytic skeletal muscle, which has higher demands for fatty acid oxidization rather than as an energy source (Steyn et al., 2020). Thus, such changes in the metabolic demand for lipids might lead to a decrease in circulating FFAs prior to the onset of ALS. In contrast, we observed a tendency for circulating FFAs levels to increase as ALS progressed. This may be due to accumulated oxidative stress with disease progression, causing hydrolysis of tissue and membrane lipids to FFAs and release into the circulation (Barber et al., 2006; Nagase et al., 2016). Regarding other factors regulating circulating lipids, the gut microbiome is known to produce short-chain fatty acids (SCFAs, having fewer than six carbons) as metabolites of dietary fibers, which are released into the circulation (Dalile et al., 2019). SOD1^{G93A} mice exhibited changes in the composition and function of the gut microbiome prior to disease onset (Blacher et al., 2019). Although we could not detect SCFAs in our analysis, changes in the gut microbiome in ALS may also affect the systemic lipidome. Further investigations in peripheral organs are needed to elucidate the mechanism by which circulating FFAs levels decrease.

Our *in vitro* experiments revealed that OA/LA inhibit excitotoxic OL death. We treated OL with OA/LA at 30 μM, which is lower than plasma concentration (OA: 0.03–3.2 mM, LA: 0.2–5 mM) (Abdelmagid et al., 2015). However, FFAs, including OA and LA, were reported to be effective in cell death inhibition at a concentration of 10–50 μM *in vitro* (Ahn et al., 2013; Lee et al., 2022). Therefore, we used OA/LA at 30 μM to assess the cell death suppressive effects of OA/LA in this study. OA/LA suppressed glutamate-induced OL death via interaction with FFAR1, a G protein-coupled receptor. FFAR1 is coupled with G_q protein and activated by medium-chain fatty acids (with 6–12 carbons) and long-chain fatty acids (with more than 12 carbons), including OA and LA (Kasai et al., 2011; Ito et al., 2021). FFAR1 activation has been reported to trigger several downstream signaling cascades,

10.3389/fncel.2023.1081190

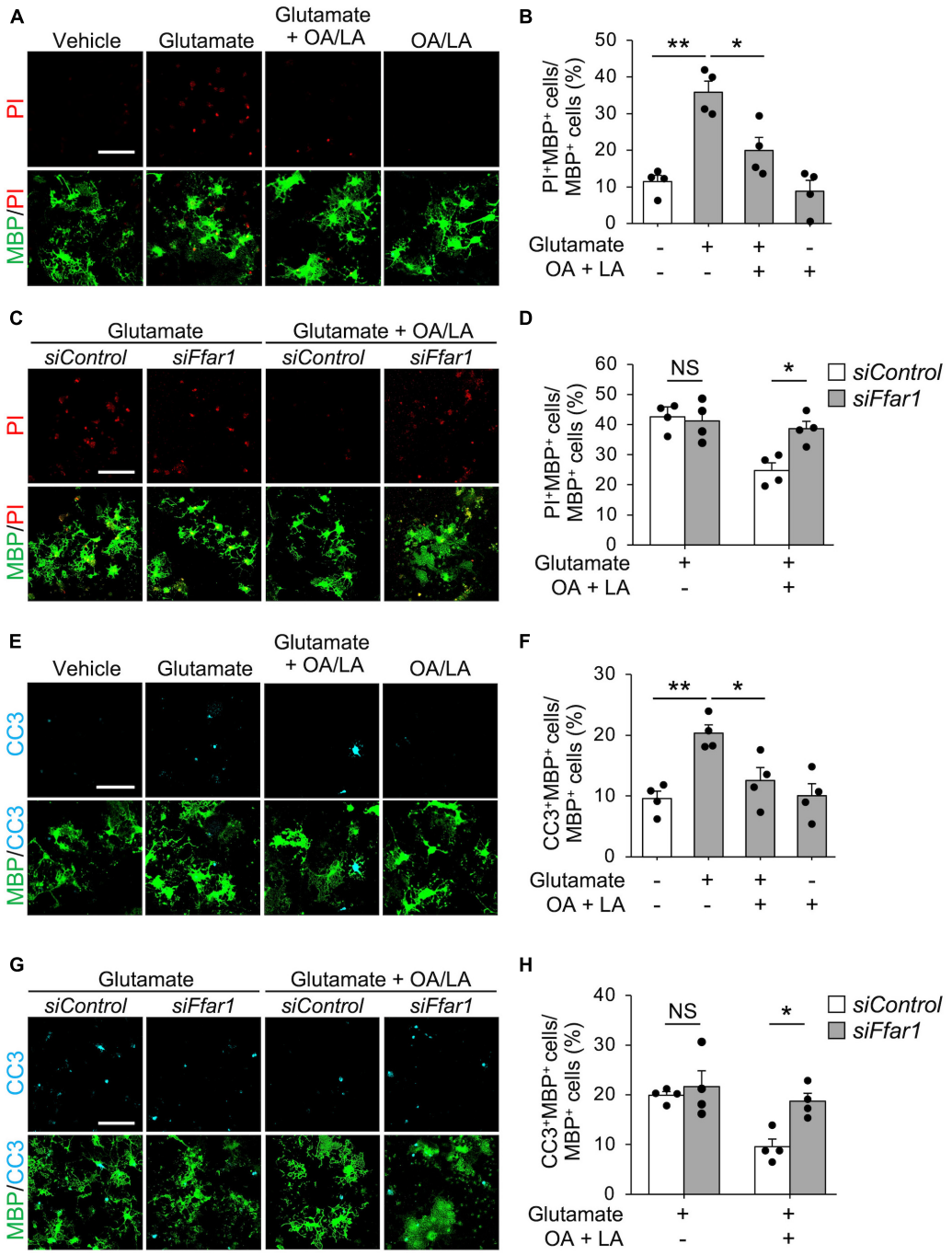

FIGURE 3
OA and LA inhibit glutamate-induced oligodendrocyte apoptosis via FFAR1. **(A)** Representative images show the fluorescence of PI (red) and immunocytochemistry for MBP (green) of purified primary oligodendrocytes treated with vehicle, glutamate, glutamate + OA/LA, and OA/LA. Scale bar: 100 μm. **(B)** Graph showing the percentage of PI^+ MBP^+ cells in MBP^+ cells assessed from panel **(A)** (Vehicle: $n = 4$, glutamate: $n = 4$, glutamate + OA/LA: $n = 4$, and OA/LA: $n = 4$). **(C)** Representative images showing the fluorescence of PI (red) and immunocytochemistry for MBP (green) in purified primary oligodendrocytes treated with *control* siRNA or *Ffar1* siRNA in the presence of glutamate with or without OA/LA. Scale bar: 100 μm. **(D)** Graph showing the percentage of PI^+ MBP^+ cells in MBP^+ cells (*Control* siRNA in glutamate: $n = 4$, *Control* siRNA in glutamate + OA/LA: $n = 4$, *Ffar1* siRNA in glutamate + OA/LA: $n = 4$, and *Ffar1* siRNA in glutamate + OA/LA: $n = 4$). **(E)** Representative images showing fluorescence of immunocytochemistry for CC3 (cyan) and MBP (green) of purified primary oligodendrocytes treated with vehicle, glutamate, glutamate + OA/LA, and OA/LA. Scale bar: 100 μm. **(F)** Graph showing the percentage of $CC3^+$ MBP^+ cells in MBP^+ cells assessed from panel **(E)** (vehicle: $n = 4$, glutamate: $n = 4$, glutamate + OA/LA: $n = 4$, and OA/LA: $n = 4$). **(G)** Representative images showing the fluorescence of immunocytochemistry for MBP (green) and CC3 (cyan) of purified primary oligodendrocytes treated with *control* siRNA or *Ffar1* siRNA in the presence of glutamate with or without OA/LA. Scale bar: 100 μm. **(H)** Graph showing the percentage of $CC3^+$ MBP^+ cells in MBP^+ cells assessed from panel **(G)** (*Control* siRNA in glutamate: $n = 4$, *Control* siRNA in glutamate + OA/LA: $n = 4$, *Ffar1* siRNA in glutamate + OA/LA: $n = 4$, and *Ffar1* siRNA in glutamate + OA/LA: $n = 4$). NS, not significant, $^*P < 0.05$, $^{**}P < 0.01$, assessed by one-way ANOVA followed by Tukey–Kramer test for panels **(B,F)**, and two-way ANOVA followed by Sidak's multiple comparison tests for panels **(D,H)**.

10.3389/fncel.2023.1081190

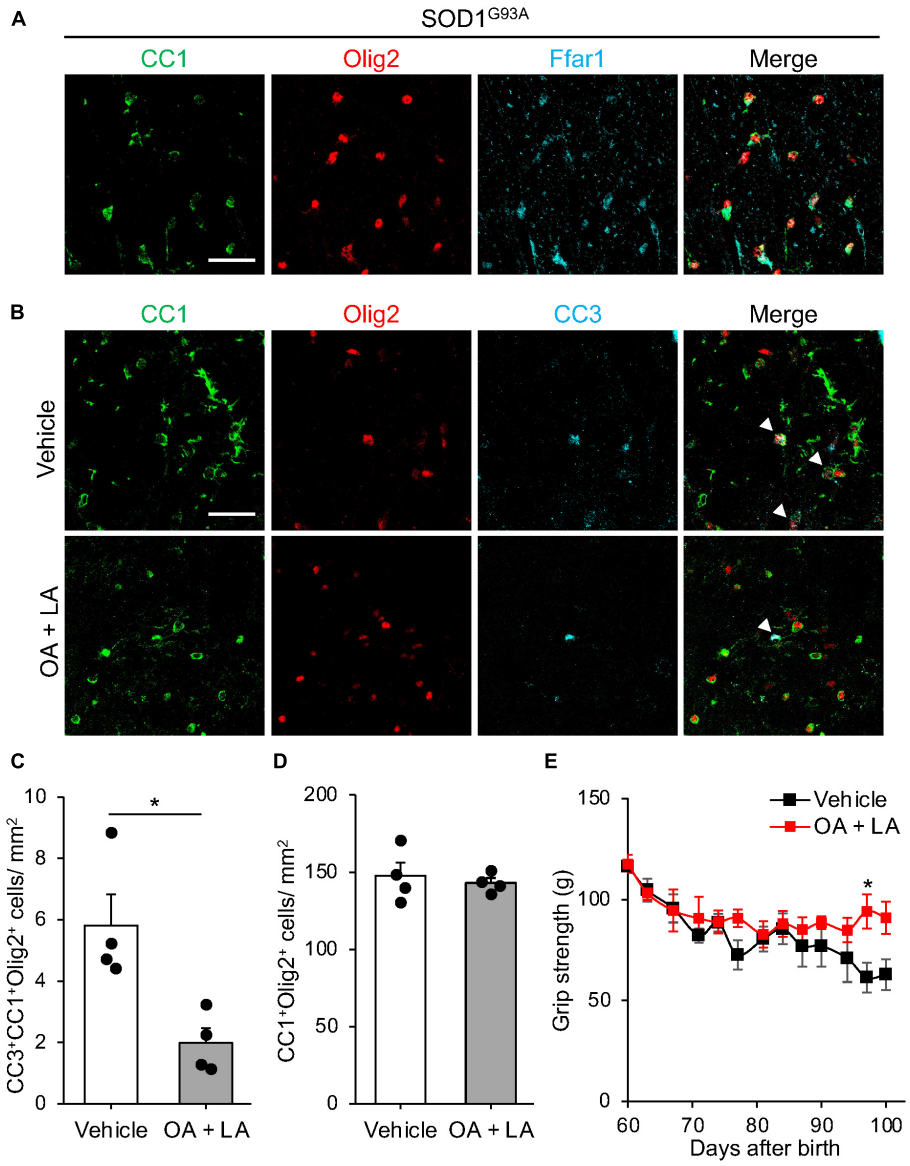

FIGURE 4
OA and LA prevent the OL loss in SOD1^{G93A} mice. **(A)** Representative images show the immunohistochemistry for CC1 (green), Olig2 (red), and Ffar1 (cyan) in the spinal cord section of SOD1^{G93A} at P100. **(B)** Representative images indicate immunohistochemistry for CC1 (green), Olig2 (red), and CC3 (cyan) in the spinal cord of Vehicle or OA + LA injected SOD1^{G93A} mice at P100. White arrows indicate CC1^{+} Olig2^{+} CC3^{+} cells. **(C)** Graph shows the number of CC1^{+} Olig2^{+} CC3^{+} cells per mm^{2} (n = 4 for each group). **(D)** Graph shows the number of CC1^{+} Olig2^{+} cells per mm^{2} (n = 4 for each group). **(E)** Graph showing the gram of grip strength (vehicle: n = 3, OA/LA: n = 4). *P < 0.05 assessed by two-sided Student's t-test for panel **(C)** and two-way ANOVA followed by Sidak's multiple comparison test for panel **(E)**. Scale bars: 25 μm for panels **(A,B)**.

including phosphatidylinositol-3 kinase (PI3K)/AKT, mitogen-activated protein kinase (MAPK)/extracellular signal-regulated kinase (ERK) signaling (Mena et al., 2016), which would protect OLs from excitotoxic apoptosis (Subramaniam and Unsicker, 2010). According to the contribution of other receptors, Gpr120 (also known as FFAR4) mediates the anti-apoptotic effect of FFAs (Katsuma et al., 2005). *Gpr120* is expressed in oligodendrocytes (Piatek et al., 2022); however, transfection of *Ffar4* siRNA did not influence the anti-apoptotic effect of OA/LA on OLs. Therefore, the anti-apoptotic role of FFAR4 might be differently regulated in cell types depending on the downstream signaling molecules they express. Further investigation is needed to elucidate the mechanism regulating the protection of OLs by OA/LA.

Our *in vivo* experiments revealed that systemic OA/LA administration ameliorated OL apoptosis without changes in the total number of mature OLs. The enhanced oligodendrogenesis and OL degeneration have been observed in pre-symptomatic SOD1^{G93A} mice (Kang et al., 2013), and the number of mature OLs is maintained during disease progression (Philips et al., 2013). These reports suggest that the oligodendrocyte turnover is enhanced in SOD1 mice, which might mask the changes in mature OLs with inhibition of apoptosis. In contrast, it has been reported that inhibition of oligodendrocyte apoptosis delayed disease progression and prolonged survival of SOD1 mutant mice (Kang et al., 2013) raising the possibility that inhibition of oligodendrocyte apoptosis is effective for ALS pathology, despite

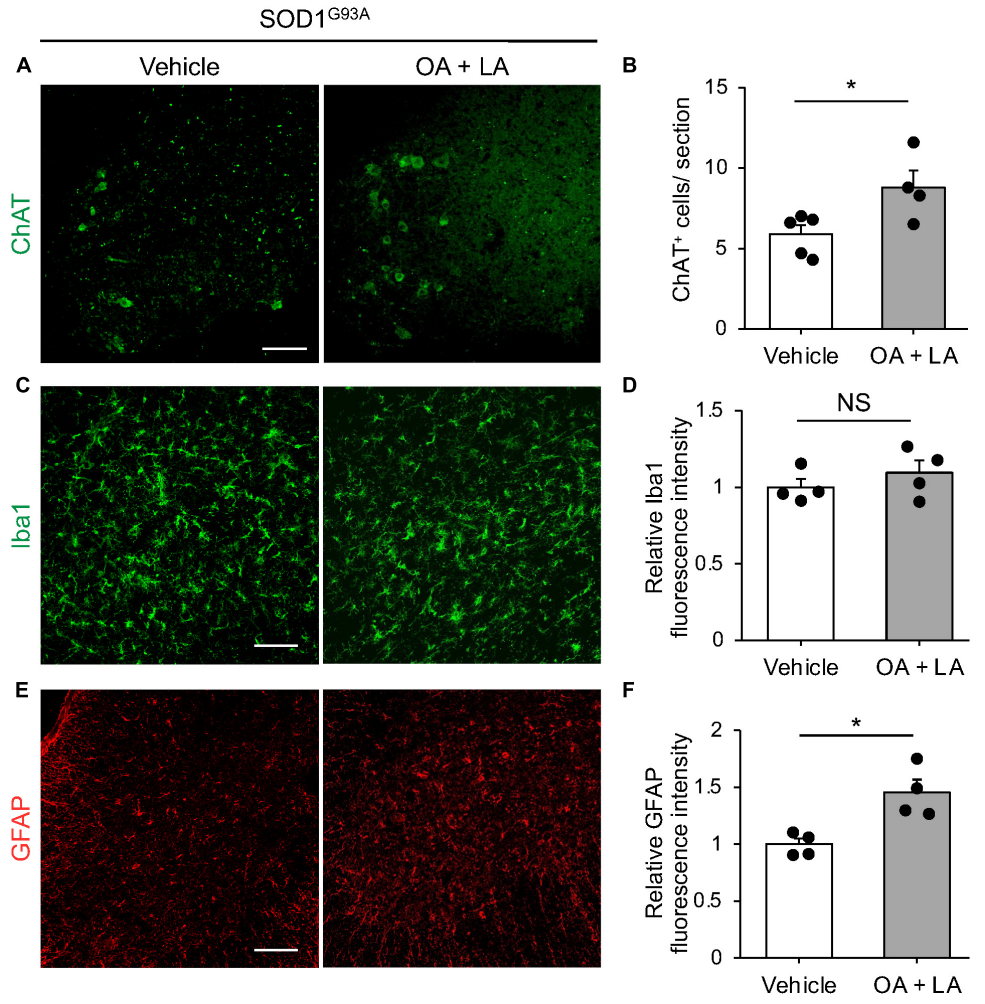

FIGURE 5
OA and LA prevent the degeneration of MNs in SOD1^{G93A} mice. **(A)** Representative images show the immunohistochemistry for ChAT in the spinal cord section. **(B)** The graph shows the number of ChAT^{+} cells per section (vehicle: n = 5, OA + LA: n = 4). **(C–F)** Representative images show the immunohistochemistry for Iba1 (green, **C**) and GFAP (red, **E**) in the spinal cord section. Graphs show the relative fluorescence intensity of Iba1 **(D)** and GFAP **(F)**, respectively (n = 4 for each group). Error bars represent mean ± SEM, *P < 0.05 assessed by two-sided Student's t-test. NS, not significant. Scale bars: 100 μm **(A,C,E)**.

the low number of apoptotic oligodendrocytes even in pathogenic condition. As oligodendrocytes support motor neuron survival, suppressing oligodendrocyte apoptosis by OA/LA would be an effective treatment for ALS pathology. Indeed, OA/LA treatment ameliorated MN loss and motor dysfunction in SOD1 mice. Although we detected FFAR1 expression in OLs of ALS mouse spinal cords, FFAR1 expression was also observed in MNs of primate spinal cords (Ma et al., 2007). Thus, OA/LA may have a protective effect on MNs. We also observed enhanced astrogliosis in OA/LA-treated SOD mice. Astrocytes are reported to express fatty acid receptors or transporters, such as FABP7 and PPARγ, which regulate astrocyte reactivity, neuronal morphology, and metabolism (Fernandez et al., 2017; Hara et al., 2020). Further investigation is needed to elucidate the prospect of astrocyte-mediated oligodendrocyte cell death suppression by OA/LA.

Recent advantages of lipidomic analysis have revealed global changes in lipids in neurological diseases, such as Parkinson's disease (Galper et al., 2022), Alzheimer's disease (Proitsi et al., 2017), and multiple sclerosis (Gonzalo et al., 2012) in addition to ALS. Further evaluation of the multiple roles of FFA in the pathogenesis of CNS diseases, including ALS, may contribute to unveiling novel molecules that can serve as both biomarkers and therapeutic targets for CNS pathologies with abnormal lipid metabolism.

Data availability statement

The raw data supporting the conclusions of this article will be made available by the authors, without undue reservation.

Ethics statement

The animal study was reviewed and approved by the Committee on the Ethics of Animal Experiments of the National Institutes of Neuroscience, National Center of Neurology and Psychiatry (2021013R2).

Author contributions

TM and ST performed the experiments. AU supported the drafting manuscript. TS advised the experiments. RM wrote the manuscript and supervised the project. All authors contributed to the article and approved the submitted version.

Funding

This work was supported by a Grant-in-Aid of Scientific Research (B) from the Japan Society for the Promotion of Sciences to RM (22H02962) and AMED under Grant Number 23wm0525016 to RM.

Acknowledgments

We thank the Human Metabolome Technologies Inc., for support the analysis.

Conflict of interest

The authors declare that the research was conducted in the absence of any commercial or financial relationships that could be construed as a potential conflict of interest.

Publisher's note

Supplementary material

The Supplementary Material for this article can be found online at: https://www.frontiersin.org/articles/10.3389/fncel.2023.1081190/full#supplementary-material

References

Abdelmagid, S. A., Clarke, S. E., Nielsen, D. E., Badawi, A., El-Sohemy, A., Mutch, D. M., et al. (2015). Comprehensive profiling of plasma fatty acid concentrations in young healthy Canadian adults. *PLoS One* 10:e0116195. doi: 10.1371/journal.pone.0116195

Ahn, J. H., Kim, M. H., Kwon, H. J., Choi, S. Y., and Kwon, H. Y. (2013). Protective effects of oleic acid against palmitic acid-induced apoptosis in pancreatic AR42J cells and its mechanisms. *Korean J. Physiol. Pharmacol.* 17, 43–50. doi: 10.4196/kjpp.2013.17.1.43

Allan, K. C., Hu, L. R., Scavuzzo, M. A., Morton, A. R., Gevorgyan, A. S., Cohn, E. F., et al. (2021). Non-canonical targets of HIF1a impair oligodendrocyte progenitor cell function. *Cell Stem Cell* 28, 257–272.e11. doi: 10.1016/j.stem.2020.09.019

Avila-Martin, G., Galan-Arriero, I., Gómez-Soriano, J., and Taylor, J. (2011). Treatment of rat spinal cord injury with the neurotrophic factor albumin-oleic acid: Translational application for paralysis, spasticity and pain. *PLoS One* 6:e26107. doi: 10.1371/journal.pone.0026107

Barber, S. C., Mead, R. J., and Shaw, P. J. (2006). Oxidative stress in ALS: A mechanism of neurodegeneration and a therapeutic target. *Biochim. Biophys. Acta* 1762, 1051–1067. doi: 10.1016/j.bbadis.2006.03.008

Belal, S. A., Sivakumar, A. S., Kang, D. R., Cho, S., Choe, H. S., and Shim, K. S. (2018). Modulatory effect of linoleic and oleic acid on cell proliferation and lipid metabolism gene expressions in primary bovine satellite cells. *Anim. Cells Syst.* 22, 324–333. doi: 10.1080/19768354.2018.1517824

Blacher, E., Bashiardes, S., Shapiro, H., Rothschild, D., Mor, U., Dori-Bachash, M., et al. (2019). Potential roles of gut microbiome and metabolites in modulating ALS in mice. *Nature* 572, 474–480. doi: 10.1038/s41586-019-1443-5

Boillée, S., Vande Velde, C., and Cleveland, D. W. (2006). ALS: A disease of motor neurons and their nonneuronal neighbors. *Neuron* 52, 39–59. doi: 10.1016/j.neuron.2006.09.018

Brown, R. H., and Al-Chalabi, A. (2017). Amyotrophic lateral sclerosis. *N. Engl. J. Med.* 377, 162–172. doi: 10.1056/NEJMra1603471

Cellura, E., Spataro, R., Taiello, A. C., and La Bella, V. (2012). Factors affecting the diagnostic delay in amyotrophic lateral sclerosis. *Clin. Neurol. Neurosurg.* 114, 550–554. doi: 10.1016/j.clineuro.2011.11.026

Cermenati, G., Mitro, N., Audano, M., Melcangi, R. C., Crestani, M., De Fabiani, E., et al. (2015). Lipids in the nervous system: From biochemistry and molecular biology to patho-physiology. *Biochim. Biophys. Acta* 1851, 51–60. doi: 10.1016/j.bbalip.2014.08.011

Chaves-Filho, A. B., Pinto, I. F. D., Dantas, L. S., Xavier, A. M., Inague, A., Faria, R. L., et al. (2019). Alterations in lipid metabolism of spinal cord linked to amyotrophic lateral sclerosis. *Sci. Rep.* 9:11642. doi: 10.1038/s41598-019-48059-7

Dalile, B., Van Oudenhove, L., Vervliet, B., and Verbeke, K. (2019). The role of short-chain fatty acids in microbiota-gut-brain communication. *Nat. Rev. Gastroenterol. Hepatol.* 16, 461–478. doi: 10.1038/s41575-019-0157-3

Dupuis, L., Oudart, H., René, F., Gonzalez de Aguilar, J.-L., and Loeffler, J.-P. (2004). Evidence for defective energy homeostasis in amyotrophic lateral sclerosis: Benefit of a high-energy diet in a transgenic mouse model. *Proc. Natl. Acad. Sci. U. S. A.* 101, 11159–11164. doi: 10.1073/pnas.0402026101

Falomir-Lockhart, L. J., Cavazzutti, G. F., Giménez, E., and Toscani, A. M. (2019). Fatty acid signaling mechanisms in neural cells: Fatty acid receptors. *Front. Cell. Neurosci.* 13:162. doi: 10.3389/fncel.2019.00162

Fergani, A., Oudart, H., Gonzalez De Aguilar, J.-L., Fricker, B., René, F., Hocquette, J.-F., et al. (2007). Increased peripheral lipid clearance in an animal model of amyotrophic lateral sclerosis. *J. Lipid Res.* 48, 1571–1580. doi: 10.1194/jlr.M700017-JLR200

Fernandez, M. O., Hsueh, K., Park, H. T., Sauceda, C., Hwang, V., Kumar, D., et al. (2017). Astrocyte-specific deletion of peroxisome-proliferator activated receptor-γ impairs glucose metabolism and estrous cycling in female mice. *J. Endocr. Soc.* 1, 1332–1350. doi: 10.1210/js.2017-00242

Ferraiuolo, L., Meyer, K., Sherwood, T. W., Vick, J., Likhite, S., Frakes, A., et al. (2016). Oligodendrocytes contribute to motor neuron death in ALS via SOD1-dependent mechanism. *Proc. Natl. Acad. Sci. U. S. A.* 113, E6496–E6505. doi: 10.1073/pnas.1607496113

Fitzgerald, K. C., O'Reilly, ÉJ., Falcone, G. J., McCullough, M. L., Park, Y., Kolonel, L. N., et al. (2014). Dietary ω-3 polyunsaturated fatty acid intake and risk for amyotrophic lateral sclerosis. *JAMA Neurol.* 71, 1102–1110. doi: 10.1001/jamaneurol.2014.1214

Foran, E., and Trotti, D. (2009). Glutamate transporters and the excitotoxic path to motor neuron degeneration in amyotrophic lateral sclerosis. *Antioxid. Redox Signal.* 11, 1587–1602. doi: 10.1089/ars.2009.2444

Galper, J., Dean, N. J., Pickford, R., Lewis, S. J. G., Halliday, G. M., Kim, W. S., et al. (2022). Lipid pathway dysfunction is prevalent in patients with Parkinson's disease. *Brain* 145, 3472–3487. doi: 10.1093/brain/awac176

Godoy-Corchuelo, J. M., Fernández-Beltrán, L. C., Ali, Z., Gil-Moreno, M. J., López-Carbonero, J. I., Guerrero-Sola, A., et al. (2022). Lipid metabolic alterations in the ALS-FTD spectrum of disorders. *Biomedicines* 10:1105. doi: 10.3390/biomedicines10051105

Gonçalves-de-Albuquerque, C. F., Burth, P., Silva, A. R., Younes-Ibrahim, M., Castro-Faria-Neto, H. C., and Castro-Faria, M. V. (2012). Leptospira and inflammation. *Mediators Inflamm.* 2012:317950. doi: 10.1155/2012/317950

Gonzalo, H., Brieva, L., Tatzber, F., Jové, M., Cacabelos, D., Cassanyé, A., et al. (2012). Lipidome analysis in multiple sclerosis reveals protein lipoxidative damage as a potential pathogenic mechanism. *J. Neurochem.* 123, 622–634. doi: 10.1111/j.1471-4159.2012.07934.x

Hamaguchi, M., Muramatsu, R., Fujimura, H., Mochizuki, H., Kataoka, H., and Yamashita, T. (2019). Circulating transforming growth factor-β1 facilitates remyelination in the adult central nervous system. *Elife* 8:e41869. doi: 10.7554/eLife.41869

Hara, T., Abdulaziz Umaru, B., Sharifi, K., Yoshikawa, T., Owada, Y., and Kagawa, Y. (2020). Fatty acid binding protein 7 is involved in the proliferation of reactive astrocytes, but not in cell migration and polarity. *Acta Histochem. Cytochem.* 53, 73–81. doi: 10.1267/ahc.20001

Henriques, A., Blasco, H., Fleury, M.-C., Corcia, P., Echaniz-Laguna, A., Robelin, L., et al. (2015). Blood cell palmitoleate-palmitate ratio is an independent prognostic factor for amyotrophic lateral sclerosis. *PLoS One* 10:e0131512. doi: 10.1371/journal.pone.0131512

Ito, M., Muramatsu, R., Kato, Y., Sharma, B., Uyeda, A., Tanabe, S., et al. (2021). Age-dependent decline in remyelination capacity is mediated by apelin–APJ signaling. *Nat. Aging* 1, 284–294. doi: 10.1038/s43587-021-00041-7

Jésus, P., Fayemendy, P., Nicol, M., Lautrette, G., Sourisseau, H., Preux, P.-M., et al. (2018). Hypermetabolism is a deleterious prognostic factor in patients with amyotrophic lateral sclerosis. *Eur. J. Neurol.* 25, 97–104. doi: 10.1111/ene.13468

Kaiser, M., Maletzki, I., Hülsmann, S., Holtmann, B., Schulz-Schaeffer, W., Kirchhoff, F., et al. (2006). Progressive loss of a glial potassium channel (KCNJ10) in the spinal cord of the SOD1 (G93A) transgenic mouse model of amyotrophic lateral sclerosis. *J. Neurochem.* 99, 900–912. doi: 10.1111/j.1471-4159.2006.04131.x

Kanda, Y. (2013). Investigation of the freely available easy-to-use software "EZR" for medical statistics. *Bone Marrow Transplant.* 48, 452–458. doi: 10.1038/bmt.2012.244

Kang, S. H., Li, Y., Fukaya, M., Lorenzini, I., Cleveland, D. W., Ostrow, L. W., et al. (2013). Degeneration and impaired regeneration of gray matter oligodendrocytes in amyotrophic lateral sclerosis. *Nat. Neurosci.* 16, 571–579. doi: 10.1038/nn.3357

Kasai, A., Kinjo, T., Ishihara, R., Sakai, I., Ishimaru, Y., Yoshioka, Y., et al. (2011). Apelin deficiency accelerates the progression of amyotrophic lateral sclerosis. *PLoS One* 6:e23968. doi: 10.1371/journal.pone.0023968

Katsuma, S., Hatae, N., Yano, T., Ruike, Y., Kimura, M., Hirasawa, A., et al. (2005). Free fatty acids inhibit serum deprivation-induced apoptosis through GPR120 in a murine enteroendocrine cell line STC-1. *J. Biol. Chem.* 280, 19507–19515. doi: 10.1074/jbc.M412385200

Kazantzis, M., and Stahl, A. (2012). Fatty acid transport proteins, implications in physiology and disease. *Biochim. Biophys. Acta* 1821, 852–857. doi: 10.1016/j.bbalip.2011.09.010

Kimura, I., Ichimura, A., Ohue-Kitano, R., and Igarashi, M. (2020). Free fatty acid receptors in health and disease. *Physiol. Rev.* 100, 171–210. doi: 10.1152/physrev.00041.2018

Kuroda, M., Muramatsu, R., Maedera, N., Koyama, Y., Hamaguchi, M., Fujimura, H., et al. (2017). Peripherally derived FGF21 promotes remyelination in the central nervous system. *J. Clin. Invest.* 127, 3496–3509. doi: 10.1172/JCI94337

Lee, D.-K., Choi, K.-H., Oh, J.-N., Kim, S.-H., Lee, M., Jeong, J., et al. (2022). Linoleic acid reduces apoptosis via NF-κB during the in vitro development of induced parthenogenic porcine embryos. *Theriogenology* 187, 173–181. doi: 10.1016/j.theriogenology.2022.05.003

Lee, Y., Morrison, B. M., Li, Y., Lengacher, S., Farah, M. H., Hoffman, P. N., et al. (2012). Oligodendroglia metabolically support axons and contribute to neurodegeneration. *Nature* 487, 443–448. doi: 10.1038/nature11314

Ma, D., Tao, B., Warashina, S., Kotani, S., Lu, L., Kaplamadzhiev, D. B., et al. (2007). Expression of free fatty acid receptor GPR40 in the central nervous system of adult monkeys. *Neurosci. Res.* 58, 394–401. doi: 10.1016/j.neures.2007.05.001

Mattson, M. P., Cutler, R. G., and Camandola, S. (2007). Energy intake and amyotrophic lateral sclerosis. *Neuromolecular Med.* 9, 17–20. doi: 10.1385/nmm:9:1:17

Matute, C., Alberdi, E., Domercq, M., Sánchez-Gómez, M.-V., Pérez-Samartín, A., Rodríguez-Antigüedad, A., et al. (2007). Excitotoxic damage to white matter. *J. Anat.* 210, 693–702. doi: 10.1111/j.1469-7580.2007.00733.x

Matute, C., Domercq, M., and Sánchez-Gómez, M.-V. (2006). Glutamate-mediated glial injury: Mechanisms and clinical importance. *Glia* 53, 212–224. doi: 10.1002/glia.20275

Mena, S. J., Manosalva, C., Carretta, M. D., Teuber, S., Olmo, I., Burgos, R. A., et al. (2016). Differential free fatty acid receptor-1 (FFAR1/GPR40) signalling is associated with gene expression or gelatinase granule release in bovine neutrophils. *Innate Immun.* 22, 479–489. doi: 10.1177/1753425916656765

Mittendorfer, B., Magkos, F., Fabbrini, E., Mohammed, B. S., and Klein, S. (2009). Relationship between body fat mass and free fatty acid kinetics in men and women. *Obesity* 17, 1872–1877. doi: 10.1038/oby.2009.224

Montani, L. (2021). Lipids in regulating oligodendrocyte structure and function. *Semin. Cell Dev. Biol.* 112, 114–122. doi: 10.1016/j.semcdb.2020.07.016

Mukherjee, C., Kling, T., Russo, B., Miebach, K., Kess, E., Schifferer, M., et al. (2020). Oligodendrocytes provide antioxidant defense function for neurons by secreting ferritin heavy chain. *Cell Metab.* 32, 259–272.e10. doi: 10.1016/j.cmet.2020.05.019

Murphy, M. G. (1995). Effects of exogenous linoleic acid on fatty acid composition, receptor-mediated cAMP formation, and transport functions in rat astrocytes in primary culture. *Neurochem. Res.* 20, 1365–1375. doi: 10.1007/BF00992513

Nagase, M., Yamamoto, Y., Miyazaki, Y., and Yoshino, H. (2016). Increased oxidative stress in patients with amyotrophic lateral sclerosis and the effect of edaravone administration. *Redox Rep.* 21, 104–112. doi: 10.1179/1351000215Y.0000000026

Nakajima, S., Gotoh, M., Fukasawa, K., Murakami-Murofushi, K., and Kunugi, H. (2019). Oleic acid is a potent inducer for lipid droplet accumulation through its esterification to glycerol by diacylglycerol acyltransferase in primary cortical astrocytes. *Brain Res.* 1725:146484. doi: 10.1016/j.brainres.2019.146484

Nave, K.-A., and Werner, H. B. (2014). Myelination of the nervous system: Mechanisms and functions. *Annu. Rev. Cell Dev. Biol.* 30, 503–533. doi: 10.1146/annurev-cellbio-100913-013101

Oka, A., Belliveau, M. J., Rosenberg, P. A., and Volpe, J. J. (1993). Vulnerability of oligodendroglia to glutamate: Pharmacology, mechanisms, and prevention. *J. Neurosci.* 13, 1441–1453. doi: 10.1523/JNEUROSCI.13-04-01441.1993

Pedersen, W. A., and Mattson, M. P. (1999). No benefit of dietary restriction on disease onset or progression in amyotrophic lateral sclerosis Cu/Zn-superoxide dismutase mutant mice. *Brain Res.* 833, 117–120. doi: 10.1016/s0006-8993(99)01471-7

Philips, T., Bento-Abreu, A., Nonneman, A., Haeck, W., Staats, K., Geelen, V., et al. (2013). Oligodendrocyte dysfunction in the pathogenesis of amyotrophic lateral sclerosis. *Brain* 136, 471–482. doi: 10.1093/brain/aws339

Philips, T., and Rothstein, J. D. (2014). Glial cells in amyotrophic lateral sclerosis. *Exp. Neurol.* 262, 111–120. doi: 10.1016/j.expneurol.2014.05.015

Piatek, P., Lewkowicz, N., Michlewska, S., Wieczorek, M., Bonikowski, R., Parchem, K., et al. (2022). Natural fish oil improves the differentiation and maturation of oligodendrocyte precursor cells to oligodendrocytes in vitro after interaction with the blood-brain barrier. *Front. Immunol.* 13:932383. doi: 10.3389/fimmu.2022.932383

Proitsi, P., Kim, M., Whiley, L., Simmons, A., Sattlecker, M., Velayudhan, L., et al. (2017). Association of blood lipids with Alzheimer's disease: A comprehensive lipidomics analysis. *Alzheimers Dement.* 13, 140–151. doi: 10.1016/j.jalz.2016.08.003

Puentes, F., Malaspina, A., van Noort, J. M., and Amor, S. (2016). Non-neuronal cells in ALS: Role of glial, immune cells and blood-CNS barriers. *Brain Pathol.* 26, 248–257. doi: 10.1111/bpa.12352

Rosen, D. R., Siddique, T., Patterson, D., Figlewicz, D. A., Sapp, P., Hentati, A., et al. (1993). Mutations in Cu/Zn superoxide dismutase gene are associated with familial amyotrophic lateral sclerosis. *Nature* 362, 59–62. doi: 10.1038/362059a0

Rudnick, N. D., Griffey, C. J., Guarnieri, P., Gerbino, V., Wang, X., Piersaint, J. A., et al. (2017). Distinct roles for motor neuron autophagy early and late in the SOD1(G93A) mouse model of ALS. *Proc. Natl. Acad. Sci. U. S. A.* 114, E8294–E8303. doi: 10.1073/pnas.1704294114

Saitoh, S. S., Tanabe, S., and Muramatsu, R. (2022). Circulating factors that influence the central nervous system remyelination. *Curr. Opin. Pharmacol.* 62, 130–136. doi: 10.1016/j.coph.2021.12.001

Simoneschi, D., Rona, G., Zhou, N., Jeong, Y.-T., Jiang, S., Milletti, G., et al. (2021). $CRL4^{AMBRA1}$ is a master regulator of D-type cyclins. *Nature* 592, 789–793. doi: 10.1038/s41586-021-03445-y

Sol, J., Jové, M., Povedano, M., Sproviero, W., Domínguez, R., Piñol-Ripoll, G., et al. (2021). Lipidomic traits of plasma and cerebrospinal fluid in amyotrophic lateral sclerosis correlate with disease progression. *Brain Commun.* 3:fcab143. doi: 10.1093/braincomms/fcab143

Steyn, F. J., Li, R., Kirk, S. E., Tefera, T. W., Xie, T. Y., Tracey, T. J., et al. (2020). Altered skeletal muscle glucose-fatty acid flux in amyotrophic lateral sclerosis. *Brain Commun.* 2:fcaa154. doi: 10.1093/braincomms/fcaa154

Sturmey, E., and Malaspina, A. (2022). Blood biomarkers in ALS: Challenges, applications and novel frontiers. *Acta Neurol. Scand.* 146, 375–388. doi: 10.1111/ane.13698

Subramaniam, S., and Unsicker, K. (2010). ERK and cell death: ERK1/2 in neuronal death. *FEBS J.* 277, 22–29. doi: 10.1111/j.1742-4658.2009.07367.x

Tracey, T. J., Kirk, S. E., Steyn, F. J., and Ngo, S. T. (2021). The role of lipids in the central nervous system and their pathological implications in amyotrophic lateral sclerosis. *Semin. Cell Dev. Biol.* 112, 69–81. doi: 10.1016/j.semcdb.2020.08.012

Uyeda, A., Quan, L., Kato, Y., Muramatsu, N., Tanabe, S., Sakai, K., et al. (2021). Dimethylarginine dimethylaminohydrolase 1 as a novel regulator of oligodendrocyte differentiation in the central nervous system remyelination. *Glia* 69, 2591–2604. doi: 10.1002/glia.24060

Van Harmelen, V., Reynisdottir, S., Cianflone, K., Degerman, E., Hoffstedt, J., Nilsell, K., et al. (1999). Mechanisms involved in the regulation of free fatty acid release from

isolated human fat cells by acylation-stimulating protein and insulin. *J. Biol. Chem.* 274, 18243–18251. doi: 10.1074/jbc.274.26.18243

Varga, T., Czimmerer, Z., and Nagy, L. (2011). PPARs are a unique set of fatty acid regulated transcription factors controlling both lipid metabolism and inflammation. *Biochim. Biophys. Acta* 1812, 1007–1022. doi: 10.1016/j.bbadis.2011.02.014

Vesga-Jiménez, D. J., Martin, C., Barreto, G. E., Aristizábal-Pachón, A. F., Pinzón, A., and González, J. (2022). Fatty acids: An insight into the pathogenesis of neurodegenerative diseases and therapeutic potential. *Int. J. Mol. Sci.* 23:2577. doi: 10.3390/ijms23052577

Weydt, P., Hong, S. Y., Kliot, M., and Möller, T. (2003). Assessing disease onset and progression in the SOD1 mouse model of ALS. *Neuroreport* 14, 1051–1054. doi: 10.1097/01.wnr.0000073685.00308.89

Yamanaka, K., Chun, S. J., Boillee, S., Fujimori-Tonou, N., Yamashita, H., Gutmann, D. H., et al. (2008). Astrocytes as determinants of disease progression in inherited amyotrophic lateral sclerosis. *Nat. Neurosci.* 11, 251–253. doi: 10.1038/nn2047

Zechner, R., Strauss, J. G., Haemmerle, G., Lass, A., and Zimmermann, R. (2005). Lipolysis: Pathway under construction. *Curr. Opin. Lipidol.* 16, 333–340. doi: 10.1097/01.mol.0000169354.20395.1c

frontiers | Frontiers in Cellular Neuroscience

TYPE Original Research
PUBLISHED 18 July 2023
DOI 10.3389/fncel.2023.1201295

OPEN ACCESS

EDITED BY
Shingo Miyata,
Kindai University, Japan

REVIEWED BY
Jeffrey Dupree,
Virginia Commonwealth University, United States
Matthew Swire,
University College London, United Kingdom

*CORRESPONDENCE
Ying Xiong
✉ ying.xiong@hubu.edu.cn
Yong Q. Zhang
✉ yqzhang@genetics.ac.cn

RECEIVED 06 April 2023
ACCEPTED 07 June 2023
PUBLISHED 18 July 2023

CITATION
Hong H, Guo C, Liu X, Yang L, Ren W, Zhao H, Li Y, Zhou Z, Lam SM, Mi J, Zuo Z, Liu C, Wang G-D, Zhuo Y, Zhang Y-P, Li Y, Shui G, Zhang YQ and Xiong Y (2023) Differential effects of social isolation on oligodendrocyte development in different brain regions: insights from a canine model.
Front. Cell. Neurosci. 17:1201295.
doi: 10.3389/fncel.2023.1201295

Differential effects of social isolation on oligodendrocyte development in different brain regions: insights from a canine model

Huilin Hong[1], Chao Guo[2,3], Xueru Liu[4,5], Liguang Yang[5,6], Wei Ren[1,5], Hui Zhao[1], Yuan Li[7], Zhongyin Zhou[3], Sin Man Lam[1], Jidong Mi[7], Zhentao Zuo[4,5], Cirong Liu[8,9], Guo-Dong Wang[3], Yan Zhuo[4,5], Ya-Ping Zhang[3], Yixue Li[6], Guanghou Shui[1,5], Yong Q. Zhang[1,5]* and Ying Xiong[1]*

[1]State Key Laboratory for Molecular and Developmental Biology, Institute of Genetics and Developmental Biology, Chinese Academy of Sciences, Beijing, China, [2]Division of Life Sciences and Medicine, School of Life Sciences, University of Science and Technology of China, Hefei, China, [3]State Key Laboratory of Genetic Resources and Evolution, Kunming Institute of Zoology, Chinese Academy of Sciences, Kunming, China, [4]State Key Laboratory of Brain and Cognitive Science, Institute of Biophysics, Chinese Academy of Sciences, Beijing, China, [5]College of Life Sciences, University of Chinese Academy of Sciences, Beijing, China, [6]Bio-Med Big Data Center, Key Laboratory of Computational Biology, CAS-MPG Partner Institute for Computational Biology, Shanghai Institute of Nutrition and Health, Shanghai Institutes for Biological Sciences, Chinese Academy of Sciences, Shanghai, China, [7]Beijing Sinogene Biotechnology Co., Ltd., Beijing, China, [8]Institute of Neuroscience, Center for Excellence in Brain Science and Intelligence Technology, Chinese Academy of Sciences, Shanghai, China, [9]Shanghai Center for Brain Science and Brain-Inspired Intelligence Technology, Shanghai, China

Social isolation (SI) exerts diverse adverse effects on brain structure and function in humans. To gain an insight into the mechanisms underlying these effects, we conducted a systematic analysis of multiple brain regions from socially isolated and group-housed dogs, whose brain and behavior are similar to humans. Our transcriptomic analysis revealed reduced expression of myelin-related genes specifically in the white matter of prefrontal cortex (PFC) after SI during the juvenile stage. Despite these gene expression changes, myelin fiber organization in PFC remained unchanged. Surprisingly, we observed more mature oligodendrocytes and thicker myelin bundles in the somatosensory parietal cortex in socially isolated dogs, which may be linked to an increased expression of ADORA2A, a gene known to promote oligodendrocyte maturation. Additionally, we found a reduced expression of blood-brain barrier (BBB) structural components Aquaporin-4, Occludin, and Claudin1 in both PFC and parietal cortices, indicating BBB disruption after SI. In agreement with BBB disruption, myelin-related sphingolipids were increased in cerebrospinal fluid in the socially isolated group. These unexpected findings show that SI induces distinct alterations in oligodendrocyte development and shared disruption in BBB integrity in different cortices, demonstrating the value of dogs as a complementary animal model to uncover molecular mechanisms underlying SI-induced brain dysfunction.

KEYWORDS

social isolation, dog, oligodendrocyte, myelin, parietal cortex, blood-brain barrier

Introduction

Social interactions are basic human needs, analogous to other basic needs such as nutrition or sleep (Baumeister and Leary, 1995; Cacioppo et al., 2011; Tomova et al., 2020), which offer safety and security, support offspring survival, reduce the need for energy expenditure, and provide a form of social reward (Eisenberger, 2012). Social interaction is important for people at all ages; a lack of or reduced social interaction, such as mandated measures during the COVID-19 pandemic, leads to socioemotional and cognitive deficits in early life (<5 years old) and an increased occurrence of psychiatric disorders such as depression and anxiety during adolescence and adult stages (Rutter et al., 2007; Cacioppo et al., 2011; Kennedy et al., 2016; Sonuga-Barke et al., 2017; Loades et al., 2020; Deoni et al., 2021; Pancani et al., 2021; Taheri Zadeh et al., 2021; Shuffrey et al., 2022). Magnetic resonance imaging and diffusion tensor imaging neuroimaging analysis revealed decreased white matter integrity in specific brain regions, including the prefrontal cortex (PFC), in children who experienced early social deprivation (Eluvathingal et al., 2006; Govindan et al., 2010; Bick et al., 2015).

The mechanisms underlying SI-induced brain structural and behavioral changes have been mostly studied in PFC using rodent models (Liu et al., 2012; Makinodan et al., 2012; Yamamuro et al., 2018; Xiong et al., 2023). For example, SI leads to reduced expression of the ErbB3 ligand neuregulin-1. The NRG1–ErbB signaling pathway, which is important for OL maturation, is linked to reduced medial PFC myelination in response to SI in juvenile mice (Makinodan et al., 2012). Since the developmental progression of various processes including myelination of different brain regions is distinct (Hong et al., 2022), different brain regions may react differently to SI. Uncovering those SI-induced molecular changes in different brain regions are critical to understand SI-induced brain dysfunction. However, it remains unclear how SI affects different brain regions at the molecular and cellular levels.

Domestic dogs (*Canis familiaris*), with a gyrencephalic brain structure similar to that of humans, have evolved complex and efficient cross-species emotional and social processing abilities during long history of coevolution with humans (Muller et al., 2015). In addition, our recent work has revealed conserved inter-regional protein expression patterns, especially myelination-related proteins, in the brain between dog and human (Hong et al., 2022). The domestic dog has been used for decades as experimental models in studies of neuroscience, cognition, evolutionary genetics, and diseases such as neurological and psychiatric disorders (Adams et al., 2000; Wang et al., 2013; Bunford et al., 2017; Liu et al., 2018; Cao et al., 2021). In particular, dogs are considered effective models for studying social behaviors and mental disorders caused by adverse early life experiences (Berns and Cook, 2016; Ogata, 2016; Bunford et al., 2017; Dietz et al., 2018).

To investigate the mechanisms underlying SI-induced brain dysfunction, we performed transcriptomic and immunochemical analyses of various brain regions from socially isolated and group-housed dogs during the juvenile stage. We found that SI decreased myelin-related gene expression specifically in PFC white matter, but myelin fiber organization remained unchanged. However, SI increased thickness of myelin bundles containing more fibers in the somatosensory parietal cortex (Par), possibly due to more mature oligodendrocytes. SI also disrupted blood-brain barrier (BBB) integrity in both PFC and Par, as evidenced by reduced expression of BBB component proteins. Consistently, myelin-related lipids were significantly increased in cerebrospinal fluid (CSF). These findings shed new light on the molecular and cellular mechanisms underlying the detrimental effects of SI on the brain.

Materials and methods

Dogs and housing conditions

Purebred healthy male Beagles were obtained from Beijing Marshall Biotechnology Co., Six male Beagle dogs (weight 2.9 ± 0.3 kg) from three different litters were maintained in a natural 12-h light-dark cycle (2 dogs in each cage). After weaning at postnatal day 51 (P51), 6 littermates were reared together in a cage until P60. Then, three males, one per litter, were housed together in one cage. The other three were housed individually in a quiet location within a building with minimum human activity for 4-weeks.

MRI data acquisition and analysis

Five beagles (3 socially isolated and 2 group-housed littermates of the socially isolated dogs; one of the 3 group-housed dogs had a chip implanted under its skin, which made it unsuitable for MRI analysis; age 96.6 ± 0.49 days, weight 4.8 ± 1.59 kg) were scanned at 3T MRI scanner (MAGNETOM Prisma, Siemens Healthcare, Erlangen, Germany) with a home-made 4-channel Tx/Rx RF coil to obtain high quality structural MRI (sMRI) and diffusion MRI (dMRI). For sMRI, T2-weighted images were acquired at the same position and spatial resolution as T1-weighted images using the SPACE sequence, which utilized different flip angles to optimize contrasts for T2 sampling. The main scan parameters: FOV = 128 × 128 mm2; TE = 3.68 ms; TR = 2,370 ms; TI = 1,030 ms; FA = 8°; acquisition data matrix size 256 × 256. DWI was acquired using an EPI sequence with multiband acceleration. The main scan parameters were: voxel 1.2 mm isotropic, FOV = 120 × 120 mm^2; TE = 86 ms; TR = 7,000 ms; FA = 90°; acquisition data matrix size 80 × 80, 64 diffusion gradients in different directions, and four b-values of 0 s/mm^2, 1,000 s/mm^2, 2,000 s/mm^2, and 3,000 s/mm^2, respectively. Each scan lasted about 30–45 min. For diffusion datasets, the original diffusion images were preprocessed using FSL, including motion and eddy-current corrected. FA, MD, RD, and AD maps were obtained using "dtifit" algorithms. The FA, AD, and RD diffusion maps of PFC and Par regions in cortical gray matter and white matter were compared between the SI and Ctrl group using a two-sample unpaired *t*-test.

Brain dissection

Brains were weighted and placed ventral side up onto a chilled glass plate on ice. Upon receipt of the dog brain, the fresh tissue was immediately embedded in a gelatin matrix using a self-made

mold (patent No. ZL 2022 2 0238374.7). The brain was positioned for coronal sectioning. In order to check for technical artifacts, 3D printing brain models were used as prefabrication. The very first rostral section was obtained from the olfactory bulb. The stereotaxic reference grid was 2 mm intervals. Sections were divided into left and right hemispheres by cutting along the midline using a long scalpel. The left brain was used for lipidomics, RNAseq, and biochemical analysis. All specimens and residual brains were stored at −80°C after frozen in liquid nitrogen. The right brain was used for staining after the sections were fixed in 4% PFA in PBS for at least 72 h. For detailed descriptions of different brain regions, we referred to the supplement of the book named The Beagle Brain in Stereotaxic Coordinates (Palazzi, 2011). To ensure consistency, all dissections were performed by Dr. Huilin Hong and Dr. Hui Zhao.

Immunohistochemistry of dog brain tissue and imaging

The animal was anesthetized with xylazine/ketamine or isoflurane and perfused with 4% PFA in PBS. The right brain hemisphere was removed and fixed in 4% PFA in PBS overnight. For cryosections, samples were transferred to 30% sucrose solution, embedded in optimal cutting temperature compound (OCT) for at least 2 days and stored at −80°C. Coronal dog brain sections (10 μm) were cut by cryostat (Leica). Sections were stored free-floating in cryoprotective solution (25% ethylene glycol, 20% glycerol, in PBS). High resolution and contrast myelin staining was achieved using the gold phosphate derivative, TrueGold Kit (BK-AC001, Oasis Biofarm Inc., Hangzhou, China), following published protocols (Schmued et al., 2008). For most staining, sections are permeabilized and blocked for 1 h with 0.2% triton-x-100, 10% Fetal Bovine Serum (FBS), and 5% Bovine Serum Albumin in PBS, and then incubated overnight at 4°C with the primary antibodies. Primary antibodies were diluted in 0.2% PBST and applied overnight at 4°C. The primary antibodies we used included rabbit anti-MBP (ab7349, 1:1,000), mouse anti-CC1 (OP80, 1:500), mouse anti-NeuN (ab104224, 1:500), rabbit anti-MYRF (OB-PRB007-02, 1:300), and guinea pig anti-Sox10 (OB-PGB001, 1:300), guinea pig anti-AQP4 (OB-PGP0016, 1:500), Goat anti-GFAP (ab53554, 1:1000), rabbit anti-laminin (L9393, 1:200), rabbit anti-occludin (71-1500, 1:500), rabbit anti-claudin1 (ab15098, 1:500). The sections were then washed with 0.2% PBST, and subsequently incubated with Alexa Fluor tagged secondary antibodies (1:1,000) for 2 h at RT.

Conventional confocal images of MBP bundles were collected at 488 nm with a Leica TCS SP8 confocal microscope using a 40× oil objective. Confocal stacks (z-step size = 1 μm) were processed with ImageJ software (National Institutes of Health). For MBP staining images, whole slide scans of tissue were collected with PerkinElmer Vectra Polaris using a 20× or 40× objective; 3D rendering and visualization were processed with Imaris 6.5 software.[1]

1 http://www.bitplane.com

Quantitative analysis of oligodendrocytes and myelin bundles

Oligodendrocyte density and morphology in dog brain were quantified as previously described (Makinodan et al., 2012; Tanti et al., 2018). Ratios of OL subgroups and morphological changes of OLs in white matter of the PFC and Par were quantified from 3 animals in each group. To quantify the number of the cellular protrusions of $CC1^+$ OLs, over 90 $CC1^+$ OLs from 3 animals of each group were characterized (the number of quantified $CC1^+$ OLs in each animal of group: Controls, 41/33/30; SI, 41/39/39). The number of OL protrusions between groups was analyzed using one-way ANOVA and the Bonferroni test. The number of $CC1^+$, $Sox10^+$ OLs was quantified in a rectangle area of 461 × 263 μm using ImageJ.

To quantify the fluorescence intensities of MBP labeled myelin bundles composed of myelin fibers, three regions of interest of 0.06 mm^2 were selected in layers 2/3 of the gray matter per sample for analysis by ImageJ. Statistical significance was calculated with two-tailed Student's *t*-test. Data are presented as means ± SEM.

RNA extraction

Tissue slices were taken from the medial PFC, Amygdala, Hippocampus, parietal lobe, occipital lobe, and flash frozen for subsequent processing. A bead mill homogenizer (Bullet Blender, Gingko Biotech) and chilled stainless-steel beads (SSB14B, Next Advance) were used to lyse the pulverized brain tissue. Total RNA was extracted using a non-phenolic procedure (RNeasy Plus Mini Kit, Qiagen), followed by DNase treatment (TURBO DNase, Ambion) as per product instructions. RNA was reverse transcribed with SuperScript™ III first-strand synthesis system for RT-PCR (Invitrogen, 18080-051) and quantitative real-time PCR (qPCR) was performed using KAPA SYBR® FAST qPCR (KAPA, KK4601) at Stratagene Mx3000P Agilent technologies.

Transcriptomic analysis

After the library was constructed, we used Qubit 2.0 for preliminary quantification, diluted the library, and then used Agilent 2100 to detect the size of the insert in the library. RNA-seq was performed by Novogene using an Illumina NovaSeq 6000 platform by PE150 sequencing strategy. After using fastp to trim reads to obtain high-quality reads, we generated at least 12 G of clean data. The paired-end reads were mapped to the Canis lupus familiaris reference genome (ROS_Cfam_1.0) using Hisat2. The sort command in Samtools was used to convert sam files to bam files. For improved gene-level analysis, StringTie was used to assemble and quantify the transcripts in each sample using the annotation gtf (ROS_Cfam_1.0.105) file for the Canis lupus familiaris reference genome. Then, the R package IsoformSwitchAnalyzeR was used to assign gene names to transcripts assembled by StringTie and estimate reads counts of gene level summaries, which can be particularly helpful in cases where StringTie could not perform assignment unambiguously. To ensure high confidence results, only the genes annotated as

"protein coding" in Biomark and supported by more than 2 samples were used for subsequent differential expression analysis. We used DESeq2 to normalize the count matrix and analyze differential expression (fold change $\geq$1.5 and adj $p \leq 0.05$).

qPCR

Extracted RNA was reverse transcribed using an iScript^{TM} cDNA Synthesis kit (BIO-RAD), followed by qPCR using KAPA SYBR(R) FAST kit (Roche, KK4601) on a Real-Time QPCR System (Agilent). The relative mRNA expression levels were analyzed according to the $\Delta\Delta$ Ct method (Livak and Schmittgen, 2001). *GAPDH* was used as the reference gene. The genes and primers used for qPCR are listed in **Supplementary Table 2**. For validation of RNA-seq results, we compared the qPCR results of representative genes including *Aqp4*, *Uqcrh*, *Ndufa12*, *Cox7a2l*, *Erbb3*, *Egfr*, *Mobp*, *Ecsit*, *Ptp4a2*, *Adora2a*, *Arnt*, *Myo5a*, *Dusp19*, *Lrrc3b*, *B3galt6*, and *Cntn2* with RNA-seq data using Pearson correlation test.

Functional enrichment analysis

Functional enrichment analysis was performed using the R package ClusterProfiler (4.4.1) (Wu et al., 2021) with default parameters (p-value cutoff = 0.05, q-value cutoff = 0.2). To ensure the accuracy of the enrichment test, only the genes involved in the differential expression analysis in the previous step were used as background. We examined all Gene Ontology terms from the latest version of "org.Cf.eg.db" and KEGG pathways from the official API.

GSEA

Target gene sets were derived from experimentally validated mouse oligodendrocyte lineage markers (Marques et al., 2016). We assessed enrichment of these markers in transcriptome data using permutation testing with 100,000 iterations. The visualization of enrichment results relied on the plotting functions that come with ClusterProfiler (4.4.1) (Wu et al., 2021), except that the specific KEGG pathway maps relied on the Pathview web tool.[2]

Lipidomics analysis

Lipids were extracted according to a modified version of the Bligh and Dyer's protocol (Lam et al., 2021). The CSF lipidome was quantified using a high-coverage targeted lipidomic approach as described previously (Lam et al., 2021). All lipidomic analyses were conducted on a system comprising an Exion-UPLC coupled with a 6500 Plus QTRAP that runs Analyst v.1.6.3 (Sciex). All quantifications were conducted using internal standard calibration. Levels of short-, medium-, and long-chain TAGs and DAGs were calculated by referencing to spiked internal standards of TAG(14:0)3-d5, TAG(16:0)3-d5, TAG(18:0)3-d5, d5-DAG17:0/17:0, and d5-DAG18:1/18:1 from Avanti Polar Lipids. Free cholesterols and cholesteryl esters were analyzed as described previously with d6-cholesterol and d6-CE18:0 cholesteryl ester (CE) (CDN isotopes) as internal standards.

2 https://pathview.uncc.edu/

Statistical analyses

Statistical significance between groups was determined by two-tailed Student's t-test, whereas multiple comparison between genotypes was determined by one-way ANOVA with a Tukey *post-hoc* test and two-way ANOVA. Asterisks above a column indicate comparisons between a specific genotype and control, whereas asterisks above a horizontal line denote comparisons between two specific genotypes. ns denotes $p > 0.05$; *indicates $p < 0.05$; **denotes $p < 0.01$; ***indicates $p < 0.001$.

Results

SI induces reduced expression of myelin-related genes in PFC white matter

To elucidate the effect of SI on brain development, we designed an experiment of SI of beagle dogs from 2 month after weaning to 3-month old. Specifically, three two-month-old beagle dogs (one from one litter) were socially isolated for 1 month, while the other three corresponding littermates were raised together in the same cage (**Supplementary Figure 1**). To examine which brain regions were affected by SI, we performed transcriptomic analysis of the prefrontal cortex (PFC) and parietal cortex, as well as the subcortical hippocampus and amygdala (**Supplementary Table 1**). The gray matter and the white matter of different cortices were analyzed separately.

We found that the white matter of the PFC showed much more differentially expressed (DE) genes than the other regions after SI. Specifically, we detected 708 and 37 DE genes in the white matter and gray matter of the PFC, respectively, compared with 7 and 20 DE genes in the white matter and gray matter of the parietal cortex (Par) (**Figure 1A**). The representative DE genes from the PFC and Par, including *myelin-associated oligodendrocyte basic protein* (*MOBP*), *aquaporin 4* (*AQP4*), and *adenosine a2a receptor* (*ADORA2A*), were independently verified by RT-PCR (**Figure 1B**; **Supplementary Tables 2**, **3**), validating the quality of the transcriptomic data. Gene Ontology (GO)/Kyoto Encyclopedia of Genes and Genomes (KEGG) analyses showed that the significantly increased genes in the PFC white matter of SI dogs are involved in ATP metabolic processes and neuron projections, while the decreased genes are involved in the extracellular matrix (ECM)-receptor interaction and cell adhesion (**Figure 1C**). No GO/KEGG pathways were identified in other regions due to a limited number of DE genes.

Although the myelin-related pathway was not enriched by GO/KEGG analysis, several myelin-related genes, including *MOBP* and *proteolipid protein 1* (*PLP1*), were significantly downregulated in the PFC white matter of SI dogs compared with control dogs (**Figure 1D**). To determine which stage of the myelination process was affected by SI in PFC, we performed gene set enrichment

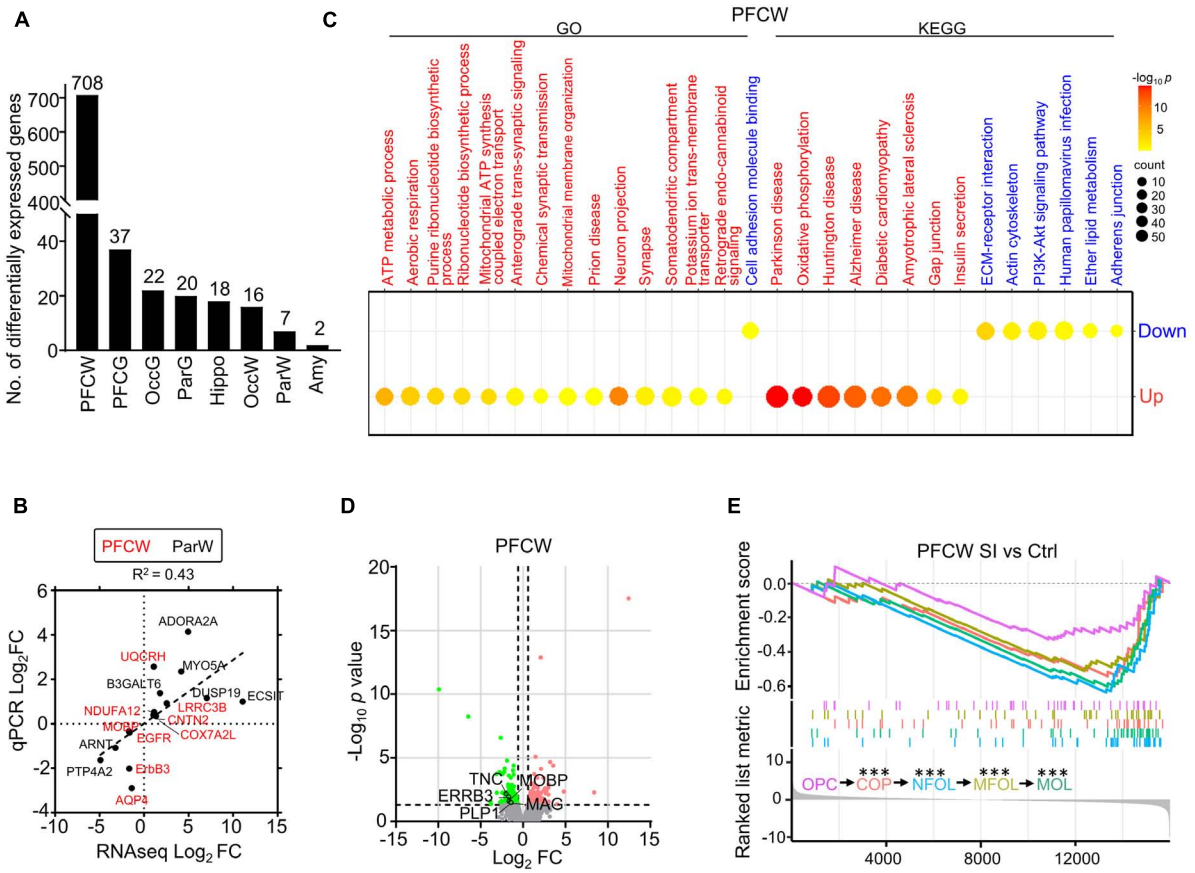

FIGURE 1
Social isolation (SI) leads to decreased levels of myelin-related gene expression and lipids in the white matter of the prefrontal cortex. **(A)** The number of differentially expressed (DE) genes in each brain region of SI dogs compared with group-housed controls. **(B)** The dot plot shows RNAseq and quantitative real-time-PCR (qRT-PCR) values of select genes with significant changes in different regions. **(C)** Bubble heatmap shows enriched GO and KEGG pathways of SI induced up- and down-regulated genes in the white matter of PFC (Fisher's exact test, fc > 1.5, adjusted $p < 0.05$). Size and color of bubbles indicate fold enrichment for that pathway and adjusted p-value, respectively. Upregulated pathways are in red, downregulated pathways are in blue. **(D)** Volcano plots of differentially expressed genes in white matter of PFC after SI. The cutoff values were set at fc > 1.5 or fc < 0.67 and $p < 0.05$. Significantly down-regulated myelin-related genes are highlighted in green. **(E)** GSEA plot shows enrichment of different stage-specific markers, most of which are significantly down-regulated in PFC of socially isolated dogs compared with control. ***$p < 0.001$.

analysis (GSEA) of RNAseq data, which assessed the distribution of predefined gene sets. We utilized 50 previously published marker genes for each of the five cell types representing different stages of the myelination process (Marques et al., 2016). All markers for oligodendrocytes (OLs) at later maturation stages including differentiation-committed oligodendrocyte precursors (COPs), newly formed oligodendrocytes (NFOLs), myelin-forming oligodendrocytes (MFOLs), and mature oligodendrocytes (MOLs) were downregulated (Figure 1E). Together, our findings demonstrated that SI leads to reduced OL maturation in the white matter of PFC.

SI induces thicker myelin bundles with more fibers in the Par but not in PFC

To examine the effects of SI-induced reduction of myelin-related gene expression on myelin, we labeled myelin fibers with an MBP antibody and the TrueGold dye, a gold phosphate derivative (Schmued, 1990). The organization of MBP-labeled myelin fibers in the gray matter of PFC and Par was different in that there was an obvious radial organization of myelin fibers from the white matter to the gray matter of the Par but not the PFC (Figures 2A–D). No obvious changes in myelin fibers in the PFC were observed after SI. However, the MBP-labeled myelin bundles by wide field microscopy were markedly thicker with parallel fibers in the Par after SI (Figures 2C–D). High magnification images showed thicker myelin bundles consisting of more parallel fibers and fewer myelin fiber crosses between longitudinal myelin bundles in the Par after SI (Figures 2G, H), but no changes in the PFC (Figures 2E, F). Specifically, the MBP intensity of myelin bundles and the number of myelin fibers in myelin bundles were significantly increased (Figure 2M). Similar to MBP staining, TrueGold staining showed thicker myelin bundles containing multiple parallel myelin fibers in the Par after SI (Figures 2I–L; Supplementary Figure 2). The thicker myelin bundles were colocalized with CC1 (a marker for mature OL) expression, suggesting a potential role of more mature OLs in regulating myelin bundle organization (Figure 2N). To identify if SI affected the distribution of mature neurons which may lead to the thicker myelin bundles, we performed immunostaining

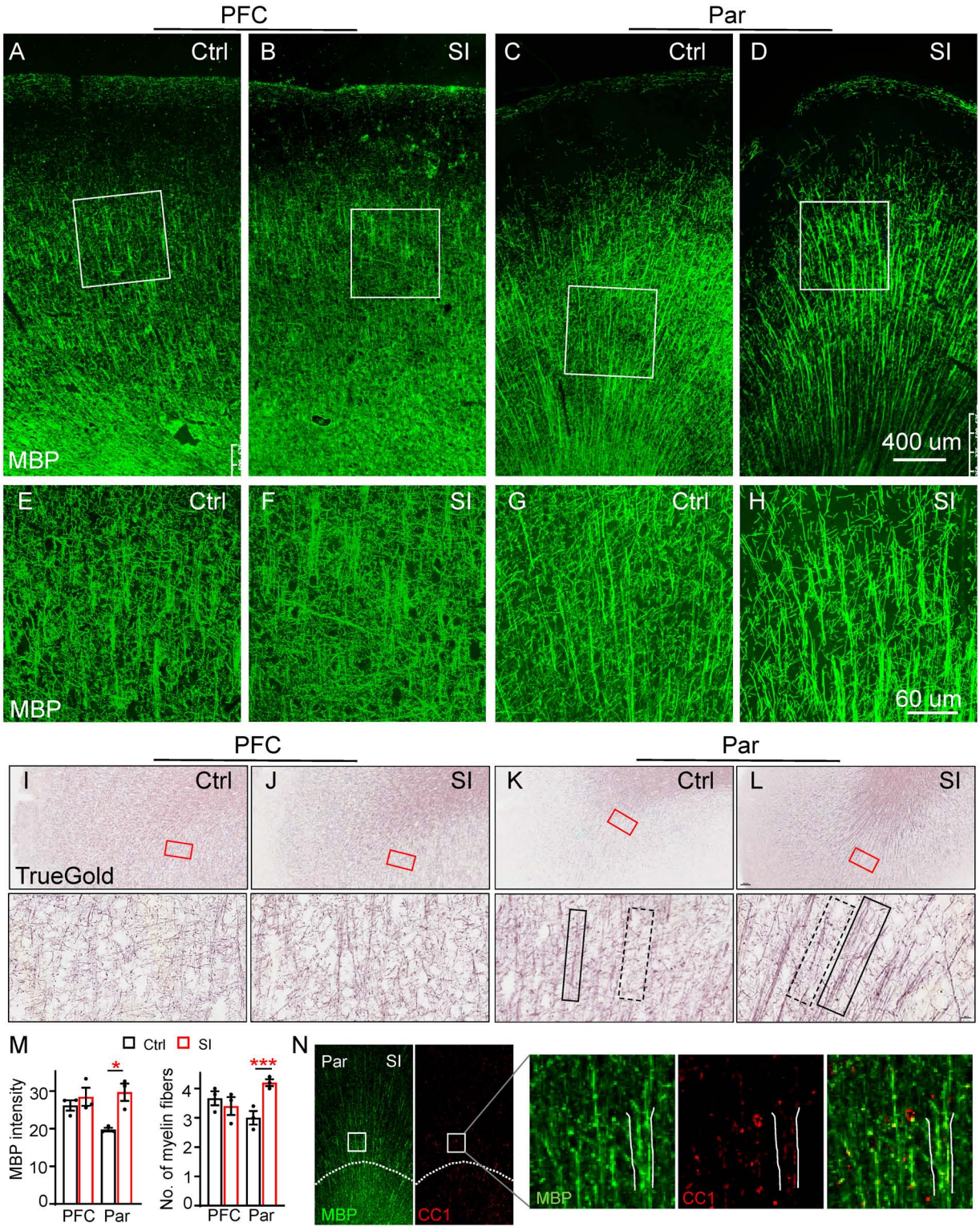

FIGURE 2
Social isolation (SI) of juvenile dogs results in the disorganization of myelinated fibers in the gray matter of the parietal cortex. **(A–D)** Confocal images of myelinated fibers labeled by MBP (green) in the PFC and Par of socially isolated and group-housed dogs. Scale bar, 400 mm. **(E–H)** Three-dimensional reconstruction images of MBP staining of Par and PFC regions boxed in the corresponding panels **(A–D)**. Scale bar, 60 μm. **(I–L)** Images of myelinated fibers labeled by TrueGold kit in PFC and Par of socially isolated and group-housed dogs. Scale bar, 10 um. No obvious changes of myelinated fibers in the gray matter of PFC but disorganized myelin fibers in Par gray matter were observed after SI. **(M)** Statistics of MBP intensity in panels **(A–D)** and the number of myelin fibers for each bundle in panels **(E–H)**. *$p < 0.05$; ***$p < 0.001$. **(N)** Co-staining images of MBP (green) and CC1 (red) in Par of socially isolated and group-housed dogs.

with antibodies against NeuN (**Supplementary Figure 3**). The results showed a linear distribution of neuronal cell bodies in Par after SI (**Supplementary Figure 3C**), which may contribute to more parallel myelinated axons. The cell adhesion protein protocadherin (PCDH) has been reported to regulate the distribution pattern of neurons in cortex (Lv et al., 2022). Specifically, down-regulated PCDH results in a similar linear distribution of neuronal cell bodies (Lv et al., 2022). Consistently, the mRNA level of PCDHB6 was decreased after SI although not to a statistically significant level probably due to a small sample size (Fold change = 0.42; $p = 0.07$; **Supplementary Figure 3D**). Thus, a reduced PCDHB6 expression may alter the distribution pattern of neurons contributing to the unique pattern of more parallel myelin fibers in the Par after SI.

To further verify SI-induced changes in myelin structure in the Par, we performed diffusion Magnetic Resonance Imaging (dMRI) of SI and control dogs. We quantified the values of fractional anisotropy (FA), mean diffusivity (MD), axial diffusivity (AD), and radial diffusivity (RD), which are commonly used parameters for describing white matter microstructure, in the PFC and Par of SI dogs and group-housed control dogs. The changes from 2 months to 3 months old between the groups were compared because the individual variance. Our results showed a trend of increased FA but decreased AD in the Par white matter of SI dogs (**Supplementary Figure 4**), indicating more organized myelin fibers, consistent with thicker myelin bundles with more parallel fibers observed by immunostaining (**Figures 2D, H, L**). No changes were observed for MD and RD in the PFC and Par after SI. The immunohistochemical and imaging results together demonstrate that juvenile SI leads to altered myelin fiber organization in the gray matter of Par but not PFC.

SI increases the number of mature OLs in Par but not in PFC white matter

While myelin-related genes were downregulated in PFC white matter, *ADORA2A*, which inhibits OPC proliferation and promotes OL maturation (Coppi et al., 2021), was upregulated (FC = 31; adj $p = 0.003$) in the Par white matter following SI (**Figure 1B**; **Supplementary Figure 5**). Consistently, immunofluorescence staining against NeuN (a marker for mature neurons), the transcription factor CC1, and MYRF [myelin regulatory factor, a marker for premyelinating OL (Huang et al., 2022)] revealed a marked increase in the density and number of $CC1^+$ cells in the Par white matter of SI dogs compared with control dogs (**Figures 3A–D**). In contrast, the number of $MYRF^+$ cells in Par white matter decreased after SI compared with that of group-housed dogs (**Figure 3C**). As a control, there were no obvious differences in the number of $CC1^+$ and $MYRF^+$ cells in the PFC white matter between SI dogs and control dogs. These results indicate that SI at the juvenile stage induced more mature $CC1^+$ OLs together with fewer immature $Myrf^+$ OLs in the white matter of the Par but not the PFC.

To quantify the proportion of immature and mature OLs, we performed double immunostaining with antibodies recognizing CC1 and the transcription factor Sox10 (**Figures 3E–G**), which is expressed throughout the whole lineage including OPCs, with gradually decreasing levels as the OLs mature (Emery et al., 2009). Antibodies specifically recognize OPCs were not available or not working in dog. We quantified the percentages of three populations of OL cells: (i) $Sox10^+CC1^-$ cells, representing OPCs/COPs/NFOLs; (ii) $Sox10^+CC1^+$ cells, representing immature MFOLs; and (iii) $Sox10^-CC1^+$ cells, representing mature MOLs with more cellular protrusions (**Figure 3F**). Immature OLs ($Sox10^+CC1^-$) showed a characteristic morphology of prominent cell bodies and few filopodia-like protrusions (**Figure 3A**). $Sox10^+$ cells were widely distributed throughout the PFC and Par white matter. OLs in the PFC white matter were relatively more immature than those in the Par white matter based on the protrusion number of $CC1^+$ OLs. No obvious changes in the three populations of OL cells were observed in the PFC after SI (**Figure 3E**). However, the number of $CC1^+$ OLs were significantly increased in the Par white matter of SI dogs compared with control dogs (**Figure 3F**; the percentage of $CC1^+$ OLs among DAPI-positive cells of 330∼420 in the Par area of 0.23 mm^2: 44.8% for control versus 55.1% for SI, $p = 0.0003$). Consistently, the number of cellular processes per $CC1^+$ OL was higher in SI dogs than the controls; the cumulative frequency of cellular processes >5 per $CC1^+$ OL was 50% in SI versus 30% in control group (**Figure 3G**). These results show that SI results in more mature OLs specifically in the Par white matter.

SI results in disrupted blood-brain barrier integrity

In addition to myelin-related changes, transcriptomic analysis also revealed a significant decrease in the expression of the gene encoding AQP4 (FC = 0.38; adj $p = 0.037$, **Figure 1B**), a water channel localized at astrocytic endfeet (a structural component of the BBB), in PFC white matter after SI. To verify whether BBB integrity was compromised by SI, we performed immunostaining and verified a significant decrease in AQP4 protein levels in the PFC and Par (**Figures 4A–H**). AQP4 was completely colocalized with GFAP around blood vessels in group-housed controls, but it was only partially colocalized with GFAP at the astrocyte endfeet in PFC after SI, suggesting AQP4 is missing at certain areas of GFAP-positive signals (**Figures 4A, B**). We also examined the expression of other structural components of the BBB, including the basement membrane protein Laminin and tight junction proteins Occludin and Claudin1 (**Figures 4A–H**; **Supplementary Figure 6**). All three proteins were expressed and colocalized with AQP4 in blood vessels in the PFC and Par of the control dogs. No obvious changes of expression level were observed for Laminin after SI. However, the expression levels of Occludin and Claudin1 were significantly decreased, similar to that of AQP4, suggesting a disruption of BBB integrity in the PFC after SI (**Figures 4C, D**; **Supplementary Figures 6C, D**). In the Par, we noticed that the co-localization of AQP4 with GFAP remained normal (**Figures 4E, F**); however, the intensity of AQP4, Occludin and Claudin1 at BBB was significantly reduced as in the PFC after SI (**Figures 4G, H**; **Supplementary Figures 6G, H**). These results suggest disrupted BBB integrity in different brain regions after SI.

Compromised BBB integrity may lead to the leakage of blood components from blood vessels to CSF. An increased level of albumin in CSF is considered a hallmark of BBB leakage

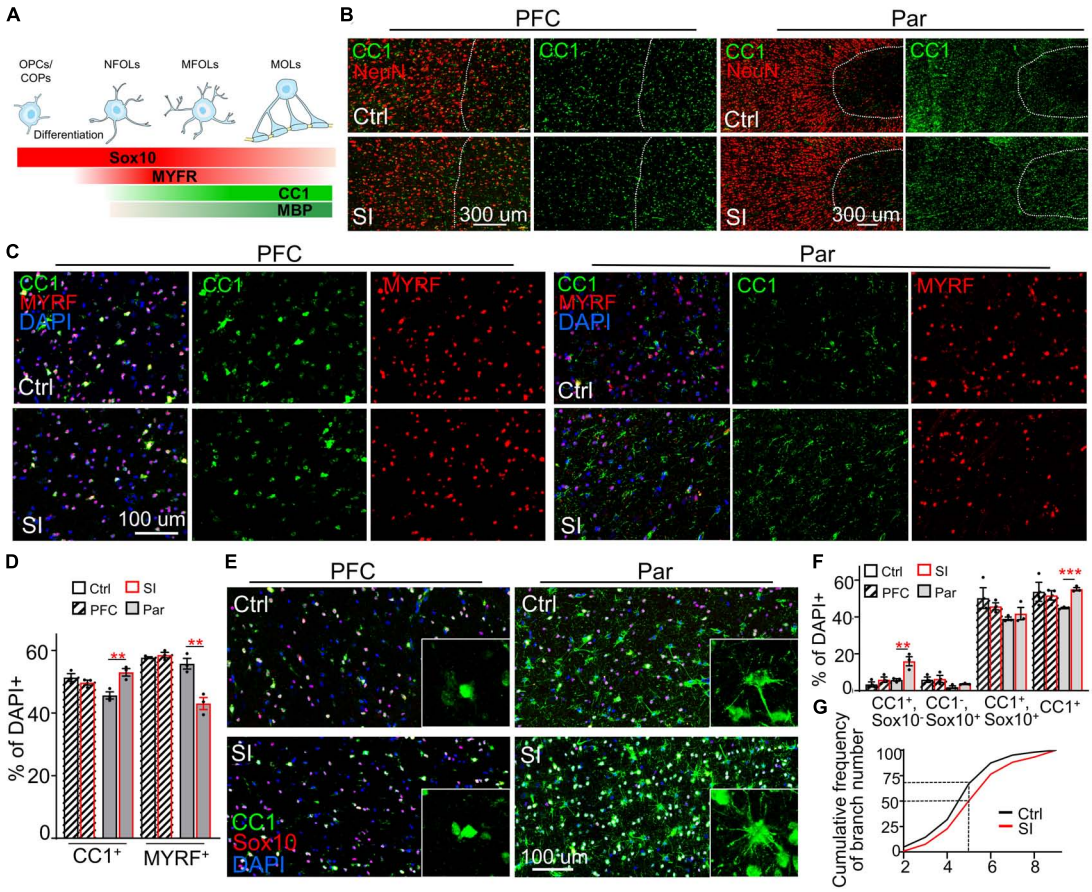

FIGURE 3
Social isolation (SI) increases the number of mature oligodendrocytes in the white matter of the parietal cortex. **(A)** Schematic representation of the stage-specific markers during OPC differentiation and oligodendrocyte maturation. Markers in bold are analyzed in the present study. **(B)** More $CC1^+$ cells in the Par white matter of SI dogs. Co-staining images of CC1 (green) and NeuN (red) in the gray matter (on the left of the interrupted white line) and white matter (on the right of the interrupted white line) of Par and PFC from socially isolated and group-housed dogs. Scale bar, 200 μm. **(C)** Co-staining confocal images of CC1, MYRF, and DAPI in the gray matter of Par and PFC from socially isolated and group-housed dogs. Scale bar, 100 μm. **(D)** Fewer $MYRF^+$ labeled immature OLs but more $CC1^+$ labeled mature OLs in the white matter of Par after SI. $^{**}p < 0.01$. **(E)** Triple staining wide-field images of CC1, Sox10, and DAPI in PFC and Par white matter of socially isolated and group-housed dog. Scale bar, 100 μm. **(F)** Statistical results of the percentages of $CC1^+Sox10^+$, $CC1^+Sox10^-$, $CC1^-Sox10^+$, and $CC1^+$cells in white matter of PFC and Par. $^{**}p < 0.01$; $^{***}p < 0.001$. **(G)** Cumulative probability plot of branch number of $CC1^+$ oligodendrocytes in Par white matter of control and SI dogs.

(Algotsson and Winblad, 2007). Consistently, we observed a higher level of albumin, although not reaching significance, in the CSF of SI dogs than in that of control dogs (**Figure 4I**), possibly due to the greatly varied albumin levels in different individuals and a small sample size. To further examine the effect of disrupted BBB integrity after SI, we performed lipidomic analysis of CSF and found significant increases in membrane polar sphingolipids, including lactosylceramide (LacCer), glucosylceramide (GluCer), galactosylceramide (GalCer), and sphingomyelin (SM), specific components of myelin, in the CSF of SI dogs compared with control dogs (**Figures 4J, K**). These results indicate that SI results in an increase in myelin-related lipids in CSF, which may be leaked from the affected brain regions through compromised BBB integrity.

Discussion

In this study, we performed a systematic analysis of multiple brain regions and CSF, from socially isolated and group-housed dogs at the juvenile stage using multiomic and immunochemical analyses. Overall, SI of dogs during juvenile stage lead to a small number of differentially expressed genes in multiple brain regions except the PFC. This could be explained by a few possibilities. First, 3–7 weeks of age of dogs is a critical period for socialization with human beings (Freedman et al., 1961; Scott, 1963). Dog pups separated from the mother at 30 to 40 days during the critical period were more likely to develop a variety of behavioral problems, including fearfulness, noise sensitivity, and excessive barking at later ages (Sargisson, 2014; Dietz et al., 2018). Thus, when dogs experienced SI starting at 2 months of age, their social development was mostly completed. Second, dogs were not completely socially isolated, as caregivers came in twice a day for feeding and cleaning.

Myelination is essential for ensuring efficient connectivity within and among different brain regions; abnormal myelination leads to cognitive dysfunction and abnormal social behaviors (Nave and Werner, 2014; Chen et al., 2020). Prolonged social isolation of adult mice decreases the level of myelin gene transcripts in PFC

10.3389/fncel.2023.1201295

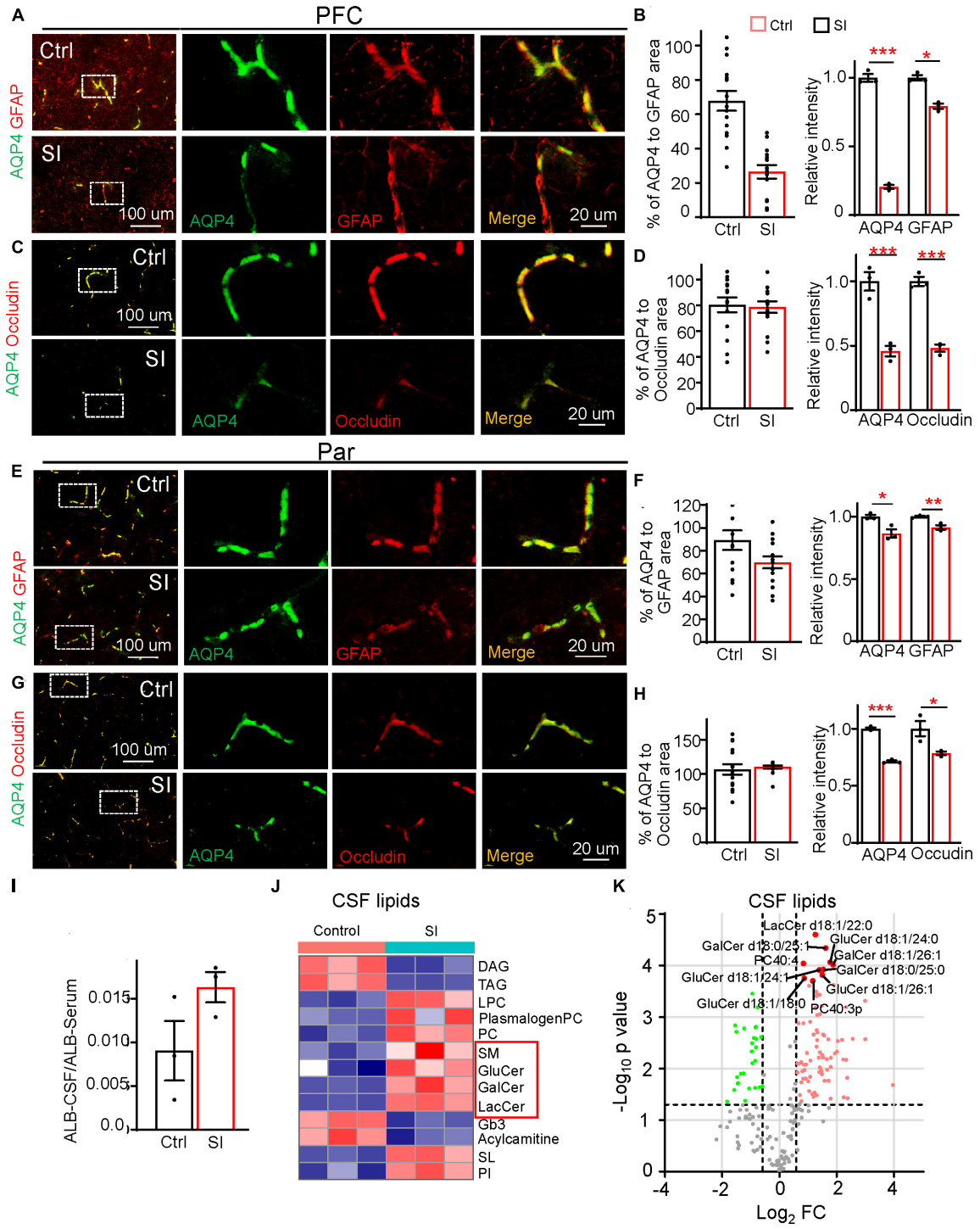

FIGURE 4

Social isolation of dogs leads to a defective blood–brain barrier and increased lipids in CSF. **(A,C,E,G)** Double staining of AQP4 (green) and GFAP or Occludin in the PFC and Par of socially isolated and group-housed dogs. Scale bar, 20 μm. **(B,D,F,H)** Quantifications of the relative area of AQP4/GFAP, AQP4/Occludin, and the mean intensity of AQP4, GFAP, and Occludin in the control and SI groups (5 GFAP-positive branches per animal). *$p < 0.05$; **$p < 0.01$; ***$p < 0.001$. **(I)** Quantification of the ratio of Albumin level [cerebrospinal fluid (CSF)/Serum] in SI and control groups. **(J)** The heatmap of different lipid class of CSF in group-housed and social isolated dogs. Red box indicates myelin-related lipids which were significantly increased after SI. **(K)** Volcano plots of differentially expressed lipids in the CSF of SI dog brains versus controls by lipidomic analysis.

(Liu et al., 2012). Here, we demonstrated a differential effect of SI on myelin-related processes of different cortices for the first time, i.e., SI during the juvenile stage of dogs induced decreased expression of myelin-related genes in the PFC but more mature OLs in the Par. There are two possible explanations: on one hand, previous studies have demonstrated an important role of neural activity in myelination. Suppressing neural activity during CNS development reduces OPC proliferation (Barres and Raff,

1993) and disrupts the myelination of the optic nerve (Demerens et al., 1996). Conversely, inducing neuronal activity via electrical stimulation or optic genetics promotes OL survival, OL maturation, and axon myelination *in vitro* (Stevens et al., 2002; Ishibashi et al., 2006; Gibson et al., 2014). The PFC is an integrative hub that receives input from all other cortical regions and functions to plan and direct motor, cognitive, affective, and social behaviors (Miller, 1999; Miller and Cohen, 2001; Forbes and Grafman, 2010; Euston et al., 2012). However, during SI, dogs were confined to a cage with much less locomotion, which may lead to decreased neural activities and thus reduced OPC differentiation and OL maturation in the PFC compared with group-housed controls. The Par area is vital for sensory perception and the integration of vision, touch, hearing, and smell (Freedman and Ibos, 2018; Xu, 2018; Medendorp and Heed, 2019). It is possible that the sensory perception would be enhanced to compensate for the broadly inhibited activities of SI dogs. Indeed, dogs showed gradually increased social expectation (heightened attentiveness and increased activities preceding the arrival of caregivers) since the second week of SI (data not shown). As a result, the enhanced sensory perception of hearing and smell in the Par may increase neuronal activity, which promotes OL maturation in the Par.

On the other hand, the effects of SI on OL development in the PFC and Par may differ as the two brain regions develop at different paces, i.e., there are differential myelination progressions in different brain regions of dogs during postnatal development (Hong et al., 2022). Double immunostaining with Sox10 and CC1 revealed that there are more mature OLs in the Par than in the PFC of 3-month-old control dogs. Previous studies have shown that OPCs in white matter form synapses with neuronal axons and establish a microenvironment via excitatory and inhibitory synaptic input from neuronal axons (Karadottir et al., 2008). As OPCs differentiate into premyelinating OLs, they lose synaptic input as well as the expression of glutamate receptors (De Biase et al., 2010). Since the PFC contains more immature OLs and probably more OPCs than the Par, there may be more synapses formed between neuronal axons and OPCs in the PFC. Thus, reduced neuronal activity due to SI may exert a more negative impact on OPC differentiation in the PFC than in the Par. Moreover, transcription and translation occur with different paces at different time points and are detected with different sensitivity, which may explain why reduced myelin gene expression in the PFC following SI didn't affect oligodendrocyte or myelin fiber number by immunostaining.

In conjunction with more mature OLs, we observed thicker myelin bundles with more parallel myelin fibers in the Par after SI. The reason for this unique myelin fiber pattern which hasn't been reported before is currently unknown. The more mature OLs and linear distribution of neurons may contribute to the thicker myelin bundles after SI. The linear distribution of neurons may be caused by reduced expression of PCDHB6 in Par; homophilic interaction of PCDHs between neighboring cells from the same progenitor cells have a repulsive effect (Schreiner and Weiner, 2010; Brasch et al., 2019). In addition, vascular endothelin has been reported to regulate the number of myelin sheaths in mouse; increasing endothelin signaling rescues SI-induced myelination defect in the PFC of mice (Swire et al., 2019). It's possible that SI may increase the expression of endothelin leading to more myelin sheaths in the Par.

Although no obvious disruption of myelin structure in PFC and Par by immunostaining, myelin-related sphingolipids were increased in CSF in the socially isolated group, indicating demyelination, defective myelin formation, or both. Electron microscopy would be needed to ascertain if myelination process in the PFC or Par was affected by SI in future. Clemastine, an antimuscarinic compound, has been shown to enhance OL progenitor differentiation and successfully reverse social avoidance behavior in socially isolated adult mice (Liu et al., 2012, 2016). Given the different effects of SI on OL development in PFC and Par, the effects of clemastine need to be assessed in different cortices. Furthermore, the effect of thicker myelin bundles on neural circuit activity in the Par after SI remains to be clarified.

In addition, we revealed disrupted BBB integrity in both PFC and Par after SI by transcriptomic, immunochemical and lipidomic analyses for the first time. How would SI disrupt BBB integrity? Inflammation and oxidative stress can lead to the overproduction of matrix metalloproteinase-9 (MMP-9) by OPCs, disrupting the integrity of the BBB (Seo et al., 2013). A recent study of SI in juvenile mice shows an increased level of neuroinflammatory cytokine IL-1β and BBB damage in amygdala (Wu et al., 2022). It is not yet clear whether the BBB disruption is due to the overproduction of MMP-9 by OPCs, neuroinflammation, or other unknown mechanisms in the cortices of SI dogs. Further research is needed to fully understand the impact of SI on the integrity of the BBB.

In summary, these findings of shared and distinct changes in multiple brain regions shed new light on the molecular and cellular mechanisms underlying the detrimental effects of SI on the brain. Our study demonstrates the value of dogs as a complementary animal model for a mechanistic study of SI-induced brain development abnormalities and disorders.

Data availability statement

The datasets presented in this study are deposited in the Genome Sequence Archive (GSA) repository, accession number CRA010898.

Ethics statement

The animal study was reviewed and approved by the Institutional Animal Care Committee of the Institute of Genetics and Developmental Biology, Chinese Academy of Sciences.

Author contributions

YQZ conceived and supervised the study. HH, WR, and HZ conducted the dissection. HH conducted the immunostaining. XL, ZZu, and YZ conducted and supervised the MRI data acquisition and analysis. SL and GS performed the lipidomics

analysis. CG, LY, ZZh, G-DW, YZ, and YiL conducted and supervised the transcriptomic data analysis. HH and YX conducted the data visualization and wrote the manuscript. JM and YuL provided and maintained the animals. YX, CL, and YQZ revised the manuscript. All authors contributed to the article and approved the submitted version.

Funding

This work was supported by grants from the National Key Research and Development Program (2019YFA0707100 to YQZ) and STI2030-Major Projects (2021ZD0203900 to YQZ and CL), the Strategic Priority Research Program B of the Chinese Academy of Sciences (XDBS1020100 to YQZ), and the National Natural Science Foundation of China (31830036 and 31921002 to YQZ and 32171088 to CL).

Acknowledgments

We thank Dr. Q. Richard Lu, Dr. Lingqiang Zhu, Dr. Qingfeng Wu, and Zhiheng Xu for discussion on the manuscript. We are grateful to Dr. Mikael Simons for advice on immunostaining of myelin, and Dr. Yong Shen and Dr. Bingyu Mao for advice on immunostaining of BBB components.

Conflict of interest

YuL and JM were employed by the Beijing Sinogene Biotechnology Co., Ltd.

The remaining authors declare that the research was conducted in the absence of any commercial or financial relationships that could be construed as a potential conflict of interest.

Publisher's note

Supplementary material

The Supplementary Material for this article can be found online at: https://www.frontiersin.org/articles/10.3389/fncel.2023.1201295/full#supplementary-material

References

Adams, B., Chan, A., Callahan, H., and Milgram, N. W. (2000). The canine as a model of human cognitive aging: Recent developments. *Prog. Neuropsychopharmacol. Biol. Psychiatry* 24, 675–692. doi: 10.1016/s0278-5846(00)00101-9

Algotsson, A., and Winblad, B. (2007). The integrity of the blood-brain barrier in Alzheimer's disease. *Acta Neurol. Scand.* 115, 403–408.

Barres, B. A., and Raff, M. C. (1993). Proliferation of oligodendrocyte precursor cells depends on electrical activity in axons. *Nature* 361, 258–260.

Baumeister, R. F., and Leary, M. R. (1995). The need to belong - desire for interpersonal attachments as a fundamental human-motivation. *Psychol. Bull.* 117, 497–529.

Berns, G. S., and Cook, P. F. (2016). Why did the dog walk into the mri? *Curr. Direct. Psychol. Sci.* 25, 363–369.

Bick, J., Zhu, T., Stamoulis, C., Fox, N. A., Zeanah, C., and Nelson, C. A. (2015). Effect of early institutionalization and foster care on long-term white matter development: A randomized clinical trial. *JAMA Pediatr.* 169, 211–219. doi: 10.1001/jamapediatrics.2014.3212

Brasch, J., Goodman, K. M., Noble, A. J., Rapp, M., Mannepalli, S., Bahna, F., et al. (2019). Visualization of clustered protocadherin neuronal self-recognition complexes. *Nature* 569, 280–283. doi: 10.1038/s41586-019-1089-3

Bunford, N., Andics, A., Kis, A., Miklosi, A., and Gacsi, M. (2017). Canis familiaris as a model for non-invasive comparative neuroscience. *Trends Neurosci.* 40, 438–452. doi: 10.1016/j.tins.2017.05.003

Cacioppo, J. T., Hawkley, L. C., Norman, G. J., and Berntson, G. G. (2011). Social isolation. *Ann. N. Y. Acad. Sci.* 1231, 17–22.

Cao, X., Liu, W., Cheng, L., Li, H., Wu, H., Liu, Y., et al. (2021). Whole genome analyses reveal significant convergence in obsessive-compulsive disorder between humans and dogs. *Sci. Bull.* 66, 187–196. doi: 10.1016/j.scib.2020.09.021

Chen, X., Wang, F., Gan, J., Zhang, Z., Liang, X., Li, T., et al. (2020). Myelin deficits caused by olig2 deficiency lead to cognitive dysfunction and increase vulnerability to social withdrawal in adult mice. *Neurosci. Bull.* 36, 419–426. doi: 10.1007/s12264-019-00449-7

Coppi, E., Cencetti, F., Cherchi, F., Venturini, M., Donati, C., Bruni, P., et al. (2021). A2 B adenosine receptors and sphingosine 1-phosphate signaling cross-talk in oligodendrogliogenesis. *Front. Neurosci.* 15:677988. doi: 10.3389/fnins.2021.677988

De Biase, L. M., Nishiyama, A., and Bergles, D. E. (2010). Excitability and synaptic communication within the oligodendrocyte lineage. *J. Neurosci.* 30, 3600–3611. doi: 10.1523/JNEUROSCI.6000-09.2010

Demerens, C., Stankoff, B., Logak, M., Anglade, P., Allinquant, B., Couraud, F., et al. (1996). Induction of myelination in the central nervous system by electrical activity. *Proc. Natl. Acad. Sci. U. S. A.* 93, 9887–9892.

Deoni, S. C., Beauchemin, J., Volpe, A., Da Sa, V., and Consortium, R. (2021). Impact of the COVID-19 pandemic on early child cognitive development: Initial findings in a longitudinal observational study of child health. *Medrxiv* [Preprint]. doi: 10.1101/2021.08.10.21261846

Dietz, L., Arnold, A. M. K., Goerlich-Jansson, V. C., and Vinke, C. M. (2018). The importance of early life experiences for the development of behavioural disorders in domestic dogs. *Behaviour* 155, 83–114.

Eisenberger, N. I. (2012). The pain of social disconnection: Examining the shared neural underpinnings of physical and social pain. *Nat. Rev. Neurosci.* 13, 421–434. doi: 10.1038/nrn3231

Eluvathingal, T. J., Chugani, H. T., Behen, M. E., Juhasz, C., Muzik, O., Maqbool, M., et al. (2006). Abnormal brain connectivity in children after early severe socioemotional deprivation: A diffusion tensor imaging study. *Pediatrics* 117, 2093–2100. doi: 10.1542/peds.2005-1727

Emery, B., Agalliu, D., Cahoy, J. D., Watkins, T. A., Dugas, J. C., Mulinyawe, S. B., et al. (2009). Myelin gene regulatory factor is a critical transcriptional regulator required for CNS myelination. *Cell* 138, 172–185.

Euston, D. R., Gruber, A. J., and Mcnaughton, B. L. (2012). The role of medial prefrontal cortex in memory and decision making. *Neuron* 76, 1057–1070.

Forbes, C. E., and Grafman, J. (2010). The role of the human prefrontal cortex in social cognition and moral judgment. *Annu. Rev. Neurosci.* 33, 299–324.

Freedman, D. G., King, J. A., and Elliot, O. (1961). Critical period in the social development of dogs. *Science* 133, 1016–1017.

Freedman, D. J., and Ibos, G. (2018). An Integrative framework for sensory, motor, and cognitive functions of the posterior parietal cortex. *Neuron* 97, 1219–1234.

Gibson, E. M., Purger, D., Mount, C. W., Goldstein, A. K., Lin, G. L., Wood, L. S., et al. (2014). Neuronal activity promotes oligodendrogenesis and adaptive myelination in the mammalian brain. *Science* 344:1252304.

Govindan, R. M., Behen, M. E., Helder, E., Makki, M. I., and Chugani, H. T. (2010). Altered water diffusivity in cortical association tracts in children with early deprivation identified with Tract-Based Spatial Statistics (TBSS). *Cereb. Cortex* 20, 561–569. doi: 10.1093/cercor/bhp122

Hong, H., Zhao, Z., Huang, X., Guo, C., Zhao, H., Wang, G. D., et al. (2022). Comparative proteome and cis-regulatory element analysis reveals specific molecular pathways conserved in dog and Human brains. *Mol. Cell Proteom.* 21:100261. doi: 10.1016/j.mcpro.2022.100261

Huang, H., He, W., Tang, T., and Qiu, M. (2022). Immunological markers for central nervous system glia. *Neurosci. Bull.* 39, 379–392.

Ishibashi, T., Dakin, K. A., Stevens, B., Lee, P. R., Kozlov, S. V., Stewart, C. L., et al. (2006). Astrocytes promote myelination in response to electrical impulses. *Neuron* 49, 823–832.

Karadottir, R., Hamilton, N. B., Bakiri, Y., and Attwell, D. (2008). Spiking and nonspiking classes of oligodendrocyte precursor glia in CNS white matter. *Nat. Neurosci.* 11, 450–456. doi: 10.1038/nn2060

Kennedy, M., Kreppner, J., Knights, N., Kumsta, R., Maughan, B., Golm, D., et al. (2016). Early severe institutional deprivation is associated with a persistent variant of adult attention-deficit/hyperactivity disorder: Clinical presentation, developmental continuities and life circumstances in the English and Romanian Adoptees study. *J. Child Psychol. Psychiatry* 57, 1113–1125. doi: 10.1111/jcpp.12576

Lam, S. M., Zhang, C., Wang, Z., Ni, Z., Zhang, S., Yang, S., et al. (2021). A multi-omics investigation of the composition and function of extracellular vesicles along the temporal trajectory of COVID-19. *Nat. Metab.* 3, 909–922. doi: 10.1038/s42255-021-00425-4

Liu, C., Yang, D., Li, J., Li, D., Yang, M., Sun, W., et al. (2018). Dynamic diffusion tensor imaging of spinal cord contusion: A canine model. *J. Neurosci. Res.* 96, 1093–1103.

Liu, J., Dietz, K., Deloyht, J. M., Pedre, X., Kelkar, D., Kaur, J., et al. (2012). Impaired adult myelination in the prefrontal cortex of socially isolated mice. *Nat. Neurosci.* 15, 1621–1623.

Liu, J., Dupree, J. L., Gacias, M., Frawley, R., Sikder, T., Naik, P., et al. (2016). Clemastine enhances myelination in the prefrontal cortex and rescues behavioral changes in socially isolated mice. *J. Neurosci.* 36, 957–962. doi: 10.1523/JNEUROSCI.3608-15.2016

Livak, K. J., and Schmittgen, T. D. (2001). Analysis of relative gene expression data using real-time quantitative Pcr and the 2(-Delta Delta C(T)) Method. *Methods* 25, 402–408.

Loades, M. E., Chatburn, E., Higson-Sweeney, N., Reynolds, S., Shafran, R., Brigden, A., et al. (2020). Rapid systematic review: The impact of social isolation and loneliness on the mental health of children and adolescents in the context of COVID-19. *J. Am. Acad. Child Adolesc. Psychiatry* 59, 1218–1239.e3.

Lv, X., Li, S., Li, J., Yu, X. Y., Ge, X., Li, B., et al. (2022). Patterned cpcdh expression regulates the fine organization of the neocortex. *Nature* 612, 503–511. doi: 10.1038/s41586-022-05495-2

Makinodan, M., Rosen, K. M., Ito, S., and Corfas, G. (2012). A critical period for social experience-dependent oligodendrocyte maturation and myelination. *Science* 337, 1357–1360. doi: 10.1126/science.1220845

Marques, S., Zeisel, A., Codeluppi, S., Van Bruggen, D., Mendanha Falcao, A., Xiao, L., et al. (2016). Oligodendrocyte heterogeneity in the mouse juvenile and adult central nervous system. *Science* 352, 1326–1329.

Medendorp, W. P., and Heed, T. (2019). State estimation in posterior parietal cortex: Distinct poles of environmental and bodily states. *Prog. Neurobiol.* 183:101691. doi: 10.1016/j.pneurobio.2019.101691

Miller, E. K. (1999). The prefrontal cortex: Complex neural properties for complex behavior. *Neuron* 22, 15–17.

Miller, E. K., and Cohen, J. D. (2001). An integrative theory of prefrontal cortex function. *Annu. Rev. Neurosci.* 24, 167–202.

Muller, C. A., Schmitt, K., Barber, A. L., and Huber, L. (2015). Dogs can discriminate emotional expressions of human faces. *Curr. Biol.* 25, 601–605.

Nave, K. A., and Werner, H. B. (2014). Myelination of the nervous system: Mechanisms and functions. *Annu. Rev. Cell Dev. Biol.* 30, 503–533.

Ogata, N. (2016). Separation anxiety in dogs: What progress has been made in our understanding of the most common behavioral problems in dogs? *J. Vet. Behav.* 16, 28–35.

Palazzi, X. (2011). *The beagle brain in stereotaxic coordinates*. New York, NY: Springer.

Pancani, L., Marinucci, M., Aureli, N., and Riva, P. (2021). Forced social isolation and mental health: A study on 1,006 italians under COVID-19 lockdown. *Front. Psychol.* 12:663799. doi: 10.3389/fpsyg.2021.663799

Rutter, M., Colvert, E., Kreppner, J., Beckett, C., Castle, J., Groothues, C., et al. (2007). Early adolescent outcomes for institutionally-deprived and non-deprived adoptees. I: Disinhibited attachment. *J. Child Psychol. Psychiatry* 48, 17–30.

Sargisson, R. J. (2014). Canine separation anxiety: Strategies for treatment and management. *Vet. Med.* 5, 143–151. doi: 10.2147/VMRR.S60424

Schmued, L. C. (1990). A Rapid, Sensitive Histochemical Stain for Myelin in Frozen Brain Sections. *J. Histochem. Cytochem.* 38, 717–720. doi: 10.1177/38.5.1692056

Schmued, L., Bowyer, J., Cozart, M., Heard, D., Binienda, Z., and Paule, M. (2008). Introducing Black-Gold Ii, a highly soluble gold phosphate complex with several unique advantages for the histochemical localization of myelin. *Brain Res.* 1229, 210–217. doi: 10.1016/j.brainres.2008.06.129

Schreiner, D., and Weiner, J. A. (2010). Combinatorial homophilic interaction between gamma-protocadherin multimers greatly expands the molecular diversity of cell adhesion. *Proc. Natl. Acad. Sci. U. S. A.* 107, 14893–14898. doi: 10.1073/pnas.1004526107

Scott, J. P. (1963). The process of primary socialization in canine and human infants. *Monogr. Soc. Res. Child Dev.* 28, 1–47.

Seo, J. H., Miyamoto, N., Hayakawa, K., Pham, L. D., Maki, T., Ayata, C., et al. (2013). Oligodendrocyte precursors induce early blood-brain barrier opening after white matter injury. *J. Clin. Invest.* 123, 782–786. doi: 10.1172/JCI65863

Shuffrey, L. C., Firestein, M. R., Kyle, M. H., Fields, A., Alcantara, C., Amso, D., et al. (2022). Association of birth during the COVID-19 pandemic with neurodevelopmental status at 6 months in infants with and without in utero exposure to maternal Sars-CoV-2 infection. *JAMA Pediatr.* 176:e215563.

Sonuga-Barke, E. J. S., Kennedy, M., Kumsta, R., Knights, N., Golm, D., Rutter, M., et al. (2017). Child-to-adult neurodevelopmental and mental health trajectories after early life deprivation: The young adult follow-up of the longitudinal English and Romanian Adoptees study. *Lancet* 389, 1539–1548. doi: 10.1016/S0140-6736(17)30045-4

Stevens, B., Porta, S., Haak, L. L., Gallo, V., and Fields, R. D. (2002). Adenosine: A neuron-glial transmitter promoting myelination in the CNS in response to action potentials. *Neuron* 36, 855–868. doi: 10.1016/s0896-6273(02)01067-x

Swire, M., Kotelevtsev, Y., Webb, D. J., Lyons, D. A., and Ffrench-Constant, C. (2019). Endothelin signalling mediates experience-dependent myelination in the CNS. *Elife* 8:e49493. doi: 10.7554/eLife.49493

Taheri Zadeh, Z., Rahmani, S., Alidadi, F., Joushi, S., and Esmaeilpour, K. (2021). Depresssion, anxiety and other cognitive consequences of social isolation: Drug and non-drug treatments. *Int. J. Clin. Pract.* 75:e14949. doi: 10.1111/ijcp.14949

Tanti, A., Kim, J. J., Wakid, M., Davoli, M. A., Turecki, G., and Mechawar, N. (2018). Child abuse associates with an imbalance of oligodendrocyte-lineage cells in ventromedial prefrontal white matter. *Mol. Psychiatry* 23, 2018–2028. doi: 10.1038/mp.2017.231

Tomova, L., Wang, K. L., Thompson, T., Matthews, G. A., Takahashi, A., Tye, K. M., et al. (2020). Acute social isolation evokes midbrain craving responses similar to hunger. *Nat. Neurosci.* 23, 1597–1605.

Wang, G. D., Zhai, W., Yang, H. C., Fan, R. X., Cao, X., Zhong, L., et al. (2013). The genomics of selection in dogs and the parallel evolution between dogs and humans. *Nat. Commun.* 4:1860.

Wu, T., Hu, E., Xu, S., Chen, M., Guo, P., Dai, Z., et al. (2021). clusterProfiler 4.0: A universal enrichment tool for interpreting omics data. *Innovation* 2:100141. doi: 10.1016/j.xinn.2021.100141

Wu, X., Ding, Z., Fan, T., Wang, K., Li, S., Zhao, J., et al. (2022). Childhood social isolation causes anxiety-like behaviors via the damage of blood-brain barrier in amygdala in female mice. *Front. Cell Dev. Biol.* 10:943067. doi: 10.3389/fcell.2022.943067

Xiong, Y., Hong, H., Liu, C., and Zhang, Y. Q. (2023). Social isolation and the brain: Effects and mechanisms. *Mol. Psychiatry* 28, 191–201.

Xu, Y. (2018). The posterior parietal cortex in adaptive visual processing. *Trends Neurosci.* 41, 806–822.

Yamamuro, K., Yoshino, H., Ogawa, Y., Makinodan, M., Toritsuka, M., Yamashita, M., et al. (2018). Social isolation during the critical period reduces synaptic and intrinsic excitability of a subtype of pyramidal cell in mouse prefrontal cortex. *Cereb. Cortex* 28, 998–1010.

frontiers | Frontiers in Cellular Neuroscience

TYPE Original Research
PUBLISHED 31 October 2023
DOI 10.3389/fncel.2023.1154196

OPEN ACCESS

EDITED BY
Jason R. Plemel,
University of Alberta, Canada

REVIEWED BY
Brad Zuchero,
Stanford University, United States
Shin Hyeok Kang,
Temple University, United States

*CORRESPONDENCE
Hiroaki Wake
✉ hirowake@med.nagoya-u.ac.jp

RECEIVED 30 January 2023
ACCEPTED 11 October 2023
PUBLISHED 31 October 2023

CITATION
Yoshida K, Kato D, Sugio S, Takeda I and Wake H (2023) Activity-dependent oligodendrocyte calcium dynamics and their changes in Alzheimer's disease.
Front. Cell. Neurosci. 17:1154196.
doi: 10.3389/fncel.2023.1154196

Activity-dependent oligodendrocyte calcium dynamics and their changes in Alzheimer's disease

Kenji Yoshida[1], Daisuke Kato[1,2], Shouta Sugio[1,2], Ikuko Takeda[1,2] and Hiroaki Wake[1,2,3]*

[1]Department of Anatomy and Molecular Cell Biology, Nagoya University Graduate School of Medicine, Nagoya, Japan, [2]Division of Multicellular Circuit Dynamics, National Institute for Physiological Sciences, National Institute of Natural Sciences, Okazaki, Japan, [3]Core Research for Evolutional Science and Technology, Japan Science and Technology Agency, Saitama, Japan

Oligodendrocytes (OCs) form myelin around axons, which is dependent on neuronal activity. This activity-dependent myelination plays a crucial role in training and learning. Previous studies have suggested that neuronal activity regulates proliferation and differentiation of oligodendrocyte precursor cells (OPCs) and myelination. In addition, deficient activity-dependent myelination results in impaired motor learning. However, the functional response of OC responsible for neuronal activity and their pathological changes is not fully elucidated. In this research, we aimed to understand the activity-dependent OC responses and their different properties by observing OCs using *in vivo* two-photon microscopy. We clarified that the Ca^{2+} activity in OCs is neuronal activity dependent and differentially regulated by neurotransmitters such as glutamate or adenosine triphosphate (ATP). Furthermore, in 5-month-old mice models of Alzheimer's disease, a period before the appearance of behavioral abnormalities, the elevated Ca^{2+} responses in OCs are ATP dependent, suggesting that OCs receive ATP from damaged tissue. We anticipate that our research will help in determining the correct therapeutic strategy for neurodegenerative diseases beyond the synapse.

KEYWORDS

Alzheimer's disease, ATP, glutamate, oligodendrocyte, two photon microscopy

1. Introduction

Oligodendrocytes (OCs) form myelin around axons to regulate conduction velocity (Fields, 2008; Emery, 2010; Nave, 2010). Accumulated studies have shown the activity-dependent myelin plasticity associated with training and learning in humans and rodents (Scholz et al., 2009; Gibson et al., 2014; McKenzie et al., 2014; Xiao et al., 2016; Kato et al., 2020). Activation of neuronal activity promotes proliferation and differentiation of oligodendrocyte precursor cells (OPCs) and myelination (Wake et al., 2011; Hines et al., 2015; Mensch et al., 2015; Wake et al., 2015). Inhibition of OPC differentiation due to specific gene deletion (MyRF) in adults results in impaired motor learning process. The promotion of activity-dependent myelination increases the conduction velocity that changes the spike arrival time and contributes to temporal regulation of neuronal activity and spike timing dependent plasticity (Markram et al., 1997; Bi and Poo, 1998; Feldman, 2012). Over expression of the proteolipid protein 1 (PLP) gene results

in impaired regulation of myelin basic protein (MBP) expression, which is associated with the motor learning process. Impaired activity-dependent myelination causes abnormal neuronal populational activity (increased spontaneous activity and reduced task associated activity), which ultimately results in deficient motor learning process (Kato et al., 2020).

To appropriately regulate the conduction velocity, OCs should receive information associated with neuronal impulse. Previous studies showed that OCs express receptors for neurotransmitters such as glutamate and adenosine triphosphate (ATP) and affect their metabolism (Groc et al., 2002; Agresti et al., 2005; Karadottir et al., 2005; Salter and Fern, 2005; Fields and Burnstock, 2006; Micu et al., 2006; Zonouzi et al., 2011; Fannon et al., 2015; Feng et al., 2015; Gautier et al., 2015; Spitzer et al., 2019). OPCs form a synapse-like structure with neurons, where glutamatergic signaling induces depolarization and development of Ca^{2+} transients via α-amino-3-hydroxy-5-methyl-4-isoxazolepropionic acid receptors (AMPAR) and P/Q and L type voltage-gated Ca^{2+} channels (Kukley et al., 2007; Berret et al., 2017; Barron and Kim, 2019) to promote OPC differentiation and myelination (Paez et al., 2009; Cheli et al., 2015, 2016; Barron and Kim, 2019). Optogenetically induced OC depolarization in the subiculum of the hippocampus facilitates conduction velocity in these axons, which affects the bursts of pyramidal neurons and long term potentiation (Yamazaki et al., 2019), suggesting the role of OC depolarization in glutamatergic neuronal circuitry activity. In contrast, ATP is released from presynaptic terminals via synaptic vesicles and this release is a co-release with glutamate and acetylcholine (Li and Harlow, 2014). ATP is also released from axonal segments that are situated away from the synaptic terminal (Wieraszko et al., 1989), i.e., the neuronal soma via extra synaptic vesicles. The receptors for ATP metabolism such as adenosine diphosphate, adenosine monophosphate, and adenosine expressed in OCs finally bind with P2 and P1 receptors, which show synergistic or opposing effects such as migration, proliferation, and differentiation (Stevens et al., 2002). ATP is even released in extracellular spaces of the damaged brain, suggesting that ATP contribute to the development of neurodegenerative diseases (Zelentsova et al., 2022). Myelinated axons in white matter are associated with cognitive function, and their impairment is known as Alzheimer's disease (AD) (Amlien and Fjell, 2014). In this research, we proposed to study the differing effects of neurotransmitters on Ca^{2+} activity in OCs. Our results demonstrated that Ca^{2+} activities in OCs were differentially regulated by neuronal transmitters such as ATP or glutamate. In 5-month-old mice models of AD, larger Ca^{2+} activities in OCs were ATP dependent. These data suggest that OCs in mice models of AD mainly receive purinergic signals from the release of ATP caused by damaged tissue. This research will provide insights into the physiological and pathological responses of OCs that contribute to the pathogenesis of neurodegenerative disorders.

2. Materials and methods

2.1. Mice

All experimental protocols used in animals were approved by the Animal Care and Use Committees of Nagoya University Graduate School of Medicine and Kobe University Graduate School of Medicine. For two-photon imaging, we used male mice to avoid potential variability due to estrus cycles. All animals used in this study were allowed free access to food and water and housed under a 12 h light/dark cycle. We used C57BL/6 (WT) mice and a bi-genic mouse (C57BL/6 genetic background) that harbored PLP-tTA (RBRC05446, RIKEN BRC, Wako, Japan) and tetO-GCaMP6 transgenes (RBRC09552, RIKEN BRC, Wako, Japan), which resulted in the expression of a fluorescence Ca^{2+} indicator, GCaMP6, in OCs/OPCs (PLP-GCaMP6 mouse) (Inamura et al., 2012; Ohkura et al., 2012; Tanaka et al., 2012). The genotype of the PLP-GCaMP6 mouse was determined using PCR with the following primer sequences: PLP-tTA, 5'-TTTCC CATGG TCTCC CTTGA GCTT-3′, 5'-CGGAG TTGAT CACCT TGGAC TTGT-3′, 5'-CTAGG CCACA GAATT GAAAG ATCT-3′, and 5′-GTAGG TGGAA ATTCT AGCAT CATCC-3′; tetO-GCaMP6, 5'-ATTTC TGAAT GGCCC AGGTC TGAG-3′, 5'-CTGCT CTGGT GTCTG TGTTA CCTG-3′, and 5′- AAGGC AGGAT GATGA CCAGG ATGT-3′. We also used tri-genic mice (C57BL/6 genetic background) harboring $App^{NL\text{-}G\text{-}F/NL\text{-}G\text{-}F}$, PLP-tTA, and tetO-GCaMP6 transgenes. $App^{NL\text{-}G\text{-}F/NL\text{-}G\text{-}F}$ knock-in mice express Swedish (KM670/671NL), Beyreuther/Iberian (I716F), and Arctic (E693G) mutations in the App gene because of the presence of an endogenous promoter of C57BL/6J background (Saito et al., 2014). Each experiment was performed using mice of the appropriate age for the experiment (WT mice, 6–24 weeks old; PLP-GCaMP6 mice, 6–24 weeks old; $App^{NL\text{-}G\text{-}F/NL\text{-}G\text{-}F}$, 16–24 weeks old; and mice crossed with $App^{NL\text{-}G\text{-}F/NL\text{-}G\text{-}F}$ and PLP-GCaMP6 mice, 16–24 weeks old).

2.2. Surgery and adeno associated virus injection

Under anesthesia with ketamine (74 mg/kg, i.p.) and xylazine (10 mg/kg, i.p.), the skin was disinfected with 70% (w/v) ethanol, the skull was exposed and cleaned, and a custom-made metallic plate was firmly attached to the skull with a dental cement (C-CEM ONE; GC, Tokyo, Japan). The surface of the intact skull was coated with an acrylic-based dental resin (Super bond; Sun Medical, Shiga, Japan) to avoid drying of the surface. The metallic plate facilitated securing the mice to a manipulating frame for performing craniotomy, AAV injection, and two-photon imaging. One or two days after plate attachment, craniotomy (circular shape; 2.5 mm in diameter) and/or AAV injection were performed under isoflurane (1.0%) anesthesia. The position of the cranial window was determined by stereotaxic manipulation, according to the mouse brain atlas (centered 0.8 mm anterior and 1.2 mm lateral to the bregma). The surface of the brain was covered with 2% (w/v) agarose L (Nippon Gene, Tokyo, Japan) in saline and a glass window composed of two coverslips (2.0 mm [square] and 4.5 mm [round] in diameter; Matsunami, Osaka, Japan) joined using ultraviolet light-polymerized adhesive (NOR-61, Norland Product, Cranbury, NJ). The edge of the cranial window was sealed with an ultraviolet light-polymerized adhesive and dental cement.

2.3. Chemogenetic manipulation

For chemogenetic activation of neuronal activity, a 750 nL recombinant AAV encoding the hM3D DREADD (designer receptor exclusively activated by designer drugs) vector solution was injected into the left motor cortex (M1) or the ventral-anterior/ventral-lateral thalamic nuclei (VA/VL) in the left hemisphere using a glass capillary

(tip diameter, 10 μm). The axons of the VA/VL neurons extended to the ipsilateral side of M1. To visualize the Ca^{2+} response of axons, AAV1-human synapsin1 (hSyn)-axon GCaMP6s-P2A-mRuby3 (Addgene; 1 μL, 1.8×10^{13} viral genomes/mL) was used. The positions of M1 and VA/VL were determined by stereotaxic manipulation according to the mouse brain atlas, and a small hole was made in the skull to introduce the glass capillary into the M1 (centered 0.8 mm anterior and 1.2 mm lateral to the bregma, at a depth of 0.5 mm from the cortical surface) or VA/VL (centered 1.0 mm posterior and 1.0 mm lateral to the bregma, at a depth of 3.2 mm from the cortical surface). An AAV vector encoding the hSyn promoter driven Gq-DREAAD (a genetically modified human muscarin receptor) and AAV8-hSyn-hM3D-mCherry (Addgene; 1.5×10^{12} viral genomes/mL diluted in sterile saline in a 1:1 ratio) was used. After AAV injection, the small hole and the intact skull were covered with 2% (w/v) agarose gel (Nippon Gene, Tokyo, Japan) and the dental cement to avoid drying. For the combined performance of chemogenetic activation and two-photon microscopy, craniotomy above the M1 cortices was performed after AAV injection. The mice were housed individually and allowed to recover for at least 3 weeks. All experiments were started approximately 3–5 weeks after the surgical operation (AAV injection and craniotomy). Clozapine *N*-oxide (CNO, Sigma-Aldrich) was used to activate DREADD and dissolved in a 0.5 mg/mL saline stock solution. As shown in Figure 1, Supplementary Figures 2, 3, Ca^{2+} imaging of OCs was performed during a quiet resting state without CNO, and the same region was imaged again 1 to 5 h after CNO intraperitoneal injection (5 mg/kg).

2.4. Drug application on brain surface *in vivo*

For the *in vivo* saline or drug application on the brain surface after Pre-imaging, the cover glass was removed and saline, tetrodotoxin (5 μM TTX, Tocris Bioscience, Minneapolis, MN), 6-cyano-7-nitroquinoxaline-2,3-dione disodium (100 μM CNQX, Tocris Bioscience, Minneapolis, MN), Suramin hexasodium salt (100 μM Suramin, Tocris Bioscience, Minneapolis, MN), and pyridoxalphosphate-6-azophenyl-2′,4′-disulfonic acid tetrasodium salt (300 μM PPADS, Tocris Bioscience, Minneapolis, MN) were applied on the mice brain surface and incubated for 30 min under isoflurane (1.0%) anesthesia. After saline or drug application, the brain surface was covered with a custom-made cover window comprising two cover slips. The edge of the window was sealed with the ultraviolet light-polymerized adhesive and the dental cement.

2.5. Two-photon imaging

Two-photon images were acquired from the left M1/M2 cortices using a laser scanning system (C2 plus and A1, Nikon, Japan) equipped with two types of water-immersion objective lens (25×, numerical aperture [N.A.] = 1.10 and 16×, N.A. = 0.80; Nikon, Japan). The two-photon imaging based on C2 plus excitation light beams used aTi:sapphire laser (Coherent, Santa Clara, CA) and imaging based on A1 excitation light beams used aTi:sapphire laser (Spectra-Physics, Santa Clara, CA) operating at a 920–950 nm wavelength. The imaging fields were 203 × 203 μm (objective lens 25×, digital zoom 2.5) and 198 × 198 μm (objective lens 16×, digital zoom 4.0) at a 100–250 μm depth below the brain surface. The scan speed was 500 or 1,000 ms/frame. Continuous 500- or 1,000-frame serial images were acquired for each imaging field with no interval time.

2.6. Imaging analysis

Images were analyzed using ImageJ (National Institute of Health) and MATLAB software packages (Math Works, Natick, MA). Videos and 3D images were corrected for focal plane displacement using ImageJ plugin TurboReg and StackReg. The observed cell body area and the number of primary processes of GCaMP' + ve (PLP' + ve) cells were as follows and did not differ between groups (cell body area [μm^2]: PLP-GCaMP6 mice, 86.60 ± 1.94 [8–12 weeks old], 90.68 ± 4.65 [4 months old], 88.17 ± 3.11 [5 months old], mice crossed with $App^{NL\text{-}G\text{-}F/NL\text{-}G\text{-}F}$ and PLP-GCaMP6 mice, 88.58 ± 3.70 [4 months old], 86.91 ± 1.60 [5 months old]; number of primary processes: PLP-GCaMP6 mice, 7.80 ± 0.17 [8–12 weeks old], 7.83 ± 0.27 [4 months old], 8.04 ± 0.28 [5 months old], mice crossed with $App^{NL\text{-}G\text{-}F/NL\text{-}G\text{-}F}$ and PLP-GCaMP6 mice, 8.00 ± 0.38 [4 months old], 7.81 ± 0.16 [5 months old], Kruskal–Wallis test followed by Dunn's test, Supplementary Figure 1A). To estimate the M1 OC Ca^{2+} activity, the regions of interest in M1 were determined using non-negative matrix factorization. For the detection and analysis of Ca^{2+} transients, baseline fluorescence was defined as the 35th percentile of the total fluorescence intensity histogram, which was obtained during all imaging periods (F_0). Ca^{2+} transients were calculated using the equation $\Delta F/F_0$ ($\Delta F = F\text{-}F_0$), where ΔF is the instantaneous fluorescence signal and ΔF exceeded 4 standard deviations (SDs) of the baseline fluorescence (F_0). We used an F_0 set at the 35th percentile of the total fluorescence distribution while re-analyzing the results. The frequency of occurrence of Ca^{2+} transients was calculated as the ratio of the total number of transients over all the imaging periods. The intensity of each Ca^{2+} transient ($\Delta F/F_0$) was subsequently computed using area under the curve (AUC), which was calculated by integrating area between traces representing Ca^{2+} transients and a horizontal line expressing baseline fluorescence. Amplitude was calculated as the maximum $\Delta F/F_0$ of each Ca^{2+} transient. Latency was calculated as the duration between the occurrence of the first Ca^{2+} transient that exceeded and was less than 4 SDs of baseline fluorescence.

2.7. Electrophysiology

Sixteen-channel silicone probes with recording sites measuring 177 μm^2 (NeuroNexus Technologies), spaced 25 μm apart at depths of 3.2 mm below the cortical surface, were utilized to record neuronal activity in VA/VL neurons in 9-week-old mice under 0.5% isoflurane anesthesia. *In vivo* recordings were conducted using the Omniplex system (Plexon, Dallas, TX) at baseline, during chemogenetic activation before, and after administration of CNQX (100 μM), Suramin (100 μM) and PPADS (300 μM). Spike signals were filtered within the bandpass of 300 Hz to 8 kHz. Spikes were detected through threshold-level crossing, typically set at 50 μV (Kato et al., 2020, 2023). Single unit sorting was performed using principal component analysis in an offline sorter (Plexon).

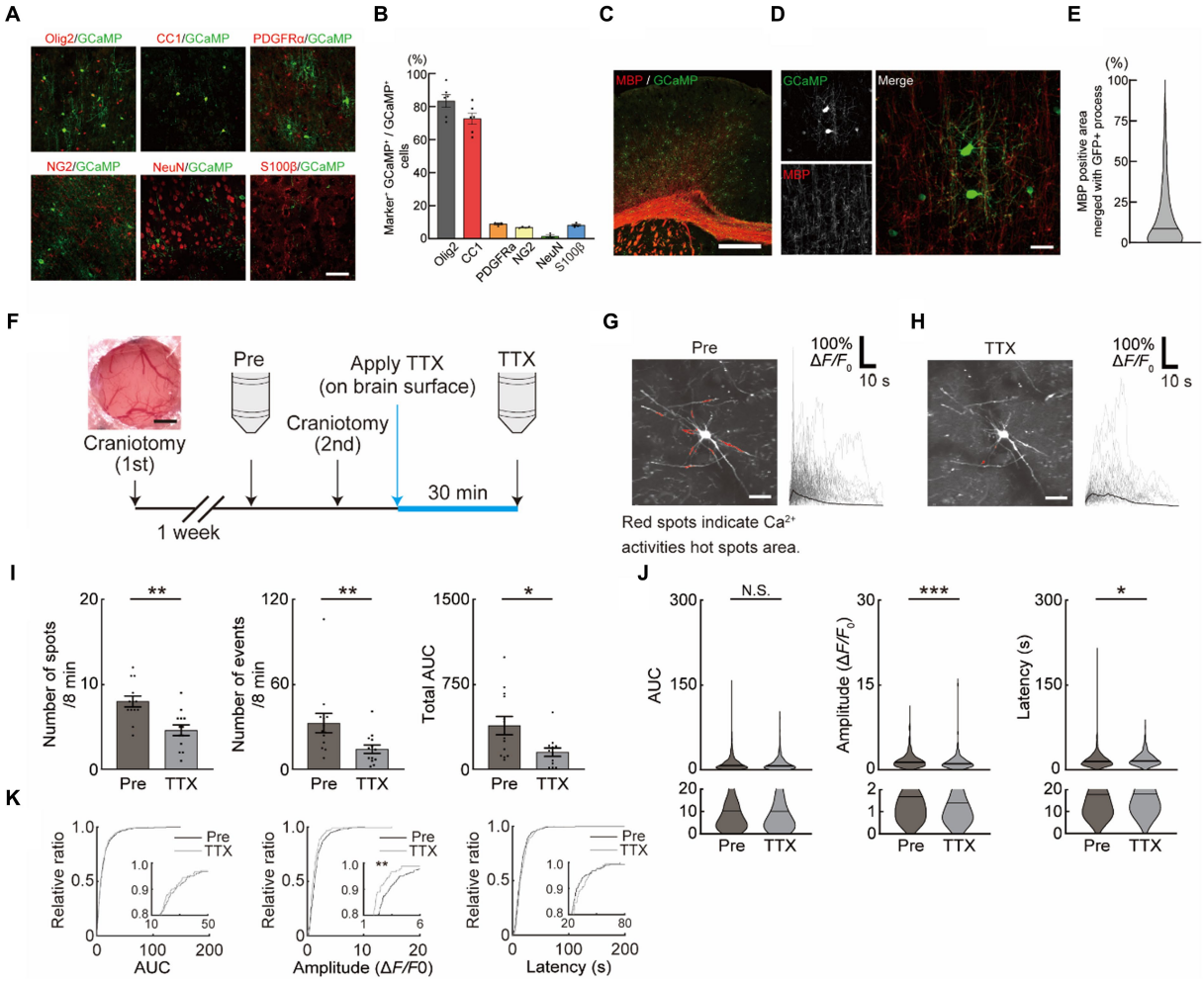

FIGURE 1
Neuronal activity-dependent Ca^{2+} activities in oligodendrocytes (OCs). **(A,B)** Representative images **(A)** and quantification **(B)** of GCaMP expression in the motor cortex of PLP-GCaMP mice and co-localization with markers for OC + oligodendrocyte precursor cell (OPC) (Olig2), OC (CC1), OPC (PDGFRα, NG2), neuron (NeuN), astrocyte (S100β) (Olig2 [83.41 ± 3.899%], CC1 [72.65 ± 3.464%], PDGFRα+ [9.979 ± 0.9322%], NG2 [6.736 ± 0.2401%], NeuN [1.481 ± 0.7246%], and S100β [8.156 ± 0.5504%]). Scale bar, 30 µm. **(C,D)** Representative images of MBP immunostaining in the motor cortex of PLP-GCaMP6 mice. Scale bars: in **(C)**, 100 µm; in **(D)**, 30 µm. **(E)** Quantitative analysis of the co-localization areas of MBP and GCaMP′ + ve processes based on immunostaining data. The proportion of MBP′ + ve processes in the processes of GCaMP′ + ve cells was about 15%. **(F)** Experimental protocol of Ca^{2+} imaging in OCs. The first craniotomy was performed one week before Pre-imaging (Pre) using two-photon microscopy. After Pre-imaging, a second craniotomy was performed and TTX was applied for 30 min, followed by a second imaging (TTX) of the same cells. **(G,H)** Representative image of GCaMP′ + ve cells of the motor cortex in PLP-GCaMP6 mice before and after TTX application. Red spots indicate the Ca^{2+} activated areas (spot). Scale bar = 30 µm. Representative Ca^{2+} traces from spots of typical GCaMP′ + ve cells are shown. **(I)** Changes in Ca^{2+} spots, Ca^{2+} events and total area under the curve (AUC) of GCaMP′ + ve cells between before and after TTX application. The number of Ca^{2+} spots and Ca^{2+} events and total AUC were significantly decreased after TTX application. Pre: $n = 6$ mice, 13 imaging fields (cells); TTX: $n = 6$ mice, 13 imaging fields (cells). $^{*}p < 0.05$, $^{**}p < 0.01$, Mann–Whitney U test. Data are presented as mean ± standard error of mean. For detailed data, check the source data file. **(J)** Changes in AUC, Amplitude, and Latency of GCaMP′ + ve cells between before and after TTX application. AUC was not significantly changed, Amplitude was significantly decreased, and Latency was significantly increased after TTX application. Pre: $n = 6$ mice, 426 events; TTX: $n = 6$ mice, 189 events. N.S., not significant, $^{*}p < 0.05$, $^{***}p < 0.001$, Mann–Whitney U test. Violin plots show median (black line) and distribution of the data. For detailed data, check the source data file. **(K)** Proportions of AUC and Latency were not significantly changed between before and after TTX application. The proportion of lower Amplitude was significantly increased after TTX application. N.S., not significant, $^{**}p < 0.01$, Kolmogorov–Smirnov test. For detailed data, check the source data file.

2.8. Immunohistochemistry

The mice were deeply anesthetized with isoflurane and transcardially perfused with 4% paraformaldehyde in phosphate buffer (pH 7.4). Their brains were post-fixed in the same fixative overnight at 4°C, which were then extracted from the skull and equilibrated in 30% sucrose solution in phosphate buffer saline (PBS). The brains were cut in 30 µm-thick sections using a microtome (Leica Microsystems, Wetzlar, Germany). After blocking and permeabilization for 1 h in 5% bovine serum albumin and 0.5% Triton X-100 in PBS, the slices were incubated at 4°C overnight with a primary antibody diluted in PBS. After washing with PBS, the slices were subsequently incubated with a secondary antibody in PBS at room temperature for 3 h and mounted on glass slides in Fluoromount-G (Southern Biotech, Birmingham, AL). Imaging was conducted using an FV3000 confocal microscope (Olympus) with 10×

(Olympus; N.A. = 0.3) and 60× oil-immersion objectives (N.A. = 0.9). The primary antibodies used in this study were as follows: anti-Olig2 (rabbit; Millipore, AB9610; 1:1000), anti-adenomatous polyposis coli (clone CC1) (mouse; Calbiochem, OP80; 1:500), anti-PDGFRα (goat; R&D systems, AF1062; 1:200), anti-NG2 (rabbit; Millipore, AB5320; 1:500), anti-NeuN (mouse; Millipore, MAB377; 1:500), anti-S100β (rabbit; Abcam, ab52642; 1:1000), anti-MBP (mouse; BioLegend, clone SMI 99; 1:100), and anti-GFP (chicken; Novus biologicals, NB100-1614; 1:2000). Amyloid β (Aβ) deposition was visualized by intraperitoneal administration of Methoxy-X04 (Tocris Bioscience, 4,920; 2 mg/kg). To visualize dying or dead cells in the brain, Fluoro-Jade C staining (Biosensis, TR-100-FJT) was performed using brain tissue from 5-month-old $App^{NL\text{-}G\text{-}F/NL\text{-}G\text{-}F}$ and age-matched control mice, according to the manufacturer's recommended protocol.

2.9. Y-maze test

The mice were housed individually before transferring to the behavioral laboratory, where they were kept during the behavioral analysis. The laboratory had a 12 h light/dark cycle (lights on at 06:00 am) and was air-conditioned and maintained at a temperature of approximately 22–23°C and a humidity of approximately 50–55%. All experiments were conducted in the light phase (06:00–18:00) and started at the same time. The Y-maze apparatus was composed of white plastic and comprised three compartments (6 cm in width, 40 cm in length, and 12 cm in height) radiating out from the center platform (6 × 6 × 6 cm triangle). In this test, each mouse was placed in the center of the maze facing toward one of the arms and was then allowed to explore the maze freely for 8 min. An arm entry was defined as the entry of four legs in an arm, and the investigator counted the sequence of entries on a television monitor from behind a partition. An alternation was defined as entries in all three arms on consecutive choices (the maximum number of alternations was the total number of entries minus 2). The percent alternation was calculated as (actual alternations divided by maximum alternations) × 100, which was the spontaneous alternation behavior of the mouse, and was considered a measure of memory performance.

2.10. Data analysis and statistics

Data were analyzed using GraphPad Prism 9 statistical software (GraphPad Software Inc., La Jolla, CA). All data are presented as mean ± standard error of mean. Unpaired *t*-test, Mann–Whitney *U*-, Kolmogorov–Smirnov test and Kruskal–Wallis test and Friedman test followed by Dunn's test were used to test for statistical significance.

3. Results

3.1. Neuronal activity inhibition reduced the functional response of OCs

Neuronal activity-dependent myelination has been demonstrated in humans and rodents. Its impairment has been shown to result in asynchronized activity in late stages of motor learning tasks reducing the motor learning efficacy (Kato et al., 2020), suggesting that the OC response is associated with neuronal activity. We first assessed the functional response of OCs, which may contribute to the activity-dependent process. The mice specifically expressing the Ca^{2+} indicator (GCaMP6) under the PLP promotor (PLP-GCaMP mice) were used to observe the functional response of OCs in M1 *in vivo*. Immunohistochemical staining was performed to identify the differentiation level of GCaMP' + ve (PLP' + ve) cells in PLP-GCaMP mice. Approximately 85% of the GCaMP' + ve cells were OCs/OPCs and about 75% of them were CC1 positive, which indicated that most of the GCaMP' + ve cells were mature OCs (Figures 1A,B). In addition, the proportion of MBP' + ve processes in the GCaMP' + ve cells was about 15% (Figures 1C–E), suggesting that the GCaMP' + ve cells were mature but pre-myelinating OCs. Furthermore, we only chose OC that have more than 5 processes (Supplementary Figure 1A). We performed Pre-imaging in mice that had undergone craniotomy (1st) several weeks prior to drug administration. We then performed a craniotomy (2nd), applied TTX to the brain surface to inhibit neuronal activity, and obtained the second image after 30 min (Figure 1F). Next, we observed the Ca^{2+} response of OCs *in vivo* in M1 using a two-photon microscope (Figures 1G,H and Supplementary movie 1). We analyzed the Ca^{2+} response of OCs using a MATLAB-based script (Maruyama et al., 2014). We counted the number of Ca^{2+} spots in the imaging frame (Ca^{2+} spots), number of Ca^{2+} events in the imaging frame (Ca^{2+} events), total AUC of all Ca^{2+} responses in the imaging frame (total AUC), individual AUC of all Ca^{2+} responses (AUC), individual amplitude of all Ca^{2+} responses (Amplitude), and latency of all Ca^{2+} responses (Latency) in the imaging frame. Before the application of drugs, to exclude the effects of craniotomy, we first applied saline (for 30 min) with craniotomy after Pre-imaging (initial imaging) (Supplementary Figure 1B). Saline application with craniotomy did not affect Ca^{2+} spots and Ca^{2+} events, total AUC, AUC, Amplitude, and Latency in OCs (Supplementary Figures 1C,D). Ca^{2+} spots (Pre: 8.000 ± 0.6405, TTX: 4.615 ± 0.6257, $p = 0.0009$), Ca^{2+} events (Pre: 32.77 ± 6.800, TTX: 15.00 ± 2.990, $p = 0.0086$), total AUC (Pre: 387.2 ± 80.60, TTX: 152.4 ± 36.77, $p = 0.0256$), and Amplitude (Pre: 1.650 ± 0.06944, TTX: 1.293 ± 0.1003, $p = 0.0004$) in OC Ca^{2+} responses were significantly reduced with TTX application on the brain surface (Figures 1I,J). Furthermore, applying the same analysis as described above at the individual mouse level showed that Amplitude did not change, but Ca^{2+} spots, Ca^{2+} events and total AUC significantly reduced with TTX application (Supplementary Figures 1E,F), suggesting that these factors were neuronal activity-dependent. Accumulation curves showed that number of lower amplitude Ca^{2+} activities was increased after TTX application (Figure 1K).

3.2. Neuronal activity promotes functional response of OCs

We next promoted neuronal activity using the chemogenetic method. The AAV coding hM3Dq designer receptor, a modified human M3 muscarinic receptor under the hSyn promotor, was injected in VA/VL of PLP-GCaMP6 mice. To verify whether axonal activity increased with chemogenetic activation, we visualized the axonal Ca^{2+} responses (visualized by AAV [AAV1-hSyn-axon-GCaMP6s-P2A-mRuby3] injection into VA/VL) that projected from VA/VL neurons to M1 (Supplementary Figures 2A–E). The AUC and

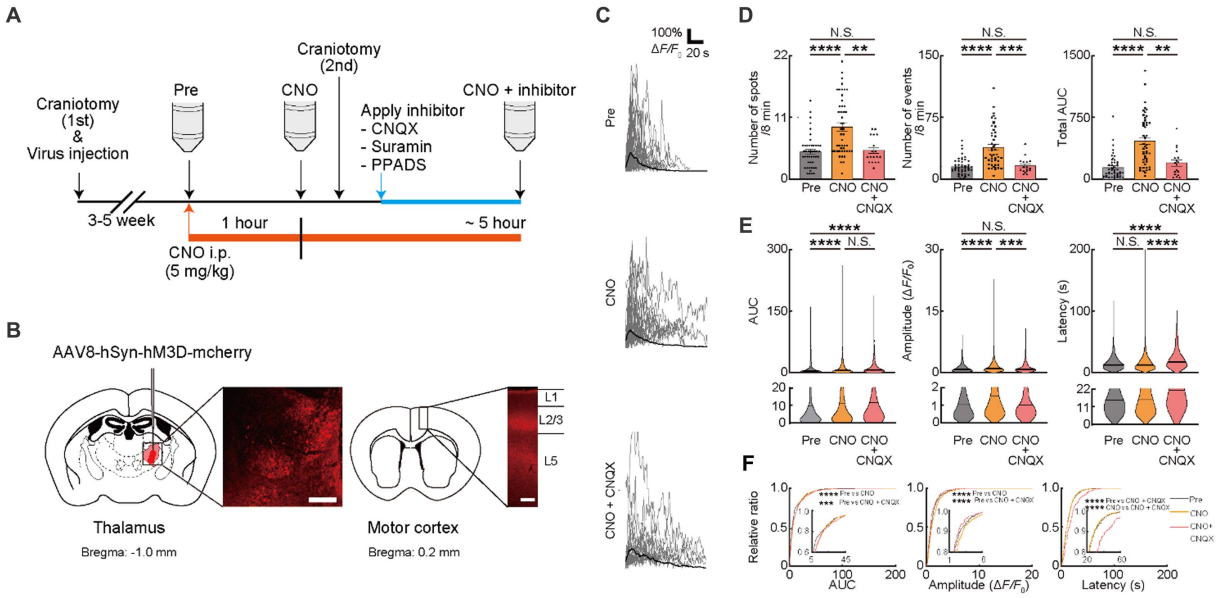

FIGURE 2
Ca^{2+} activities in oligodendrocytes (OCs) are regulated by glutamate. **(A)** Experimental protocol of the chemogenetic activation of the thalamocortical circuit and two-photon Ca^{2+} imaging with the application of neurotransmitter receptor antagonists, 6-cyano-7-nitroquinoxaline-2,3-dione disodium (CNQX), Suramin hexasodium salt (Suramin), and pyridoxalphosphate-6-azophenyl-2′,4′-disulfonic acid tetrasodium salt (PPADS). An adeno associated virus (AAV) vector coding Gq-DREAAD (hM3D) was injected into the motor thalamus and craniotomy (first) was performed. Then, 3–5 weeks after surgical operation (AAV injection and craniotomy [first]), two-photon Ca^{2+} imaging of OC was performed. A synthetic ligand clozapine *N*-oxide (CNO) was administered for hM3D activation (5 mg/kg, i.p.) after Pre-imaging (Pre). One hour after CNO application, two-photon Ca^{2+} imaging was performed again (CNO). After second imaging (CNO), neurotransmitter receptor antagonists were applied on the brain surface by craniotomy (second), and then, third imaging was performed (CNO + inhibitor). Two-photon Ca^{2+} imaging of OCs was obtained from the same cells in all imaging sessions. **(B)** Representative images showing the hM3D-mCherry expression in the motor thalamus and thalamocortical axons of motor cortices 5 weeks after the AAV injection. **(C)** Representative Ca^{2+} traces from spots of typical GCaMP' + ve cells at Pre-imaging, and after CNO and CNO + CNQX application. **(D)** Ca^{2+} spots, Ca^{2+} events and total area under the curve (AUC) were significantly increased after CNO application. CNQX application significantly decreased these parameters. Pre: $n = 23$ mice, 48 imaging fields (cells); CNO: 23 mice, 48 imaging fields (cells); CNO + CNQX: $n = 7$ mice, 18 imaging fields (cells), N.S., not significant, $^{**}p < 0.01$, $^{***}p < 0.001$, $^{****}p < 0.0001$, Kruskal–Wallis test followed by Dunn's test. Data are presented as mean ± standard error of mean. For detailed data, check the source data file. **(E)** No statistically significant differences were detected in Latency between pre-imaging and after CNO application. AUC and Amplitude was significantly increased after CNO application. CNQX, application significantly decreased Amplitude. AUC was not significantly different between CNO and CNO + CNQX applications. Amplitude and Latency was significantly increased between CNO and CNO + CNQX applications. Pre: $n = 23$ mice, 736 events; CNO: $n = 23$ mice, 2047 events; CNO + CNQX: $n = 7$ mice, 286 events. N.S., not significant, $^{***}p < 0.001$, $^{****}p < 0.0001$, Kruskal–Wallis test followed by Dunn's test. Violin plots show median (black line) and distribution of the data. For detailed data, check the source data file. **(F)** Proportions of larger AUC and higher Amplitude were significantly higher after CNO application than before. The proportion of lower Amplitude was significantly higher after CNO + CNQX application than after CNO application. The proportion of longer Latency was increased after CNO + CNQX application than after CNO application. Pre: $n = 23$ mice, 736 events; CNO: $n = 23$ mice, 2047 events; CNO + CNQX: $n = 7$ mice, 286 events. $^{***}p < 0.001$, $^{****}p < 0.0001$, Kolmogorov–Smirnov test. For detailed data, check the source data file.

total AUC of axonal Ca^{2+} responses significantly increased with CNO injection and that persisted for 5 h (Supplementary Figures 2A–E). We then examined these effects on OCs in M1 (Supplementary Figure 2F). Ca^{2+} responses of OCs in M1 were visualized in PLP-GCaMP mice to quantify the changes associated with the chemogenetic activation of VA/VL axons. Ca^{2+} spots, Ca^{2+} events, total AUC, and Amplitude of Ca^{2+} responses of OCs in M1 significantly increased 1 h after CNO administration and persisted for at least 5 h (Supplementary Figures 2F–J), suggesting only a small effect of different time courses of Ca^{2+} imaging. We further assessed whether Ca^{2+} responses of OCs in M1 were affected only by VA/VL axonal activity or even with neuronal activity in M1. We injected AAV coding hM3Dq under hSyn promoter in M1 to promote activation of cortical neurons and tested whether that activated OCs in L1 of M1 (Supplementary Figure 2K). Ca^{2+} spots, Ca^{2+} events, total AUC, AUC, Amplitude, and Latency of Ca^{2+} responses of OCs in L1 of M1 did not show any detectable changes, suggesting the minimum impact of neurons of M1 but significant impact of VA/VL axonal activity on OCs in L1 of M1 (Supplementary Figures 2L–O). These results indicated that the increased Ca^{2+} response in OC requires enhanced activity of VA/VL axons projecting to M1 (Figures 2A,B). We then measured the Ca^{2+} response in OCs with chemogenetic activation of axons projecting from VA/VL neurons. Ca^{2+} spots (Pre: 4.885 ± 0.4102, CNO: 9.333 ± 0.7324, $p < 0.0001$), Ca^{2+} events (Pre: 15.22 ± 1.449, CNO: 38.72 ± 3.534, $p < 0.0001$), total AUC (Pre: 142.4 ± 20.83, CNO: 465.1 ± 44.16, $p < 0.0001$), AUC (Pre: 9.249 ± 0.5549, CNO: 11.48 ± 0.3921, $p < 0.0001$) and Amplitude (Pre: 1.141 ± 0.04281, CNO: 1.422 ± 0.03225, $p < 0.0001$) were increased after CNO administration, consistent with TTX application, suggesting that these factors were affected by neuronal transmitters such as glutamate and ATP. OCs express receptors for ATP and glutamate such as AMPAR, P2X-R, and P2Y-R (Groc et al., 2002; Agresti et al., 2005; Fields and Burnstock, 2006; Zonouzi et al., 2011; Fannon et al., 2015; Feng et al., 2015; Gautier et al., 2015; Spitzer et al., 2019). We, therefore, attempted to

identify specific transmitters affecting these factors of OC Ca^{2+} responses by treating with specific inhibitors. Using *in vivo* electrophysiology, we first tested whether neuronal activity in VA/VL was altered by CNQX, Suramin, PPADS application on the brain surface during chemogenetic activation. We observed no significant changes in the activity of VA/VL neurons activated by chemogenetic method before and after administration of these inhibitors (Supplementary Figures 2P–R). We next attempted to evaluate the contribution of glutamatergic transmission in the activity-dependent OC responses. To inhibit AMPAR expressed on the cell surface of OCs, the antagonist for AMPAR (CNQX) was used after CNO injection (Figure 2A). CNQX applied after the second craniotomy showed minimum effects on Ca^{2+} responses of OCs (Supplementary Figures 1A–C). CNQX treatment significantly reduced Ca^{2+} spots (CNO: 9.333 ± 0.7324, CNO + CNQX; 5.111 ± 0.5417, $p = 0.0032$), Ca^{2+} events (CNO: 38.72 ± 3.534, CNO + CNQX: 16.24 ± 2.316, $p = 0.0002$), total AUC (CNO: 465.1 ± 44.16, CNO + CNQX: 197.9 ± 38.29, $p = 0.0027$), Amplitude (CNO: 1.141 ± 0.04281, CNO + CNQX: 1.124 ± 0.06736, $p = 0.0004$) and Latency (CNO: 15.46 ± 0.2839, CNO + CNQX: 21.31 ± 0.9205, $p < 0.0001$) of OCs, indicating that AMPAR mediating Ca^{2+} activity contribute to of OC responses (consistent with Figure 1) (Figures 2C–F). The accumulation curve showed that the number of higher Amplitude Ca^{2+} activities was increased after CNO administration. On the other hand, the number of lower Amplitude Ca^{2+} activities was increased after CNQX application (Figure 2F).

We further examined whether these factors changed with the inhibition of ATP signaling. To inhibit P2 receptors, the antagonist for P2 receptors (Suramin) and P2X and Y receptors (PPADS) were used after CNO injection (Figure 2A). Inhibition of P2 receptors with Suramin reduced Ca^{2+} spots (CNO: 9.333 ± 0.7324, CNO + Suramin; 4.633 ± 0.3887, $p < 0.00223$), Ca^{2+} events (CNO: 38.72 ± 3.534, CNO + Suramin: 16.03 ± 2.476, $p = 0.0004$), total AUC (CNO: 465.1 ± 44.16, CNO + Suramin: 141.2 ± 30.56, $p = 0.0001$), AUC (CNO: 11.48 ± 0.3921, CNO + Suramin: 7.373 ± 0.7401, $p < 0.0001$), Amplitude (CNO: 1.422 ± 0.03225, CNO + Suramin: 1.021 ± 0.07104, $p < 0.0001$) and Latency (CNO: 15.46 ± 0.2839, CNO + Suramin: 12.70 ± 0.5211, $p < 0.0001$) of OCs (Figures 3A–D). Consistent with data from Suramin application, inhibition of P2X and Y receptors using PPADS reduced Ca^{2+} spots (CNO: 9.333 ± 0.7324, CNO + PPADS; 3.533 ± 0.4641, $p < 0.0001$), Ca^{2+} events (CNO: 38.72 ± 3.534, CNO + PPADS: 11.23 ± 1.218, $p < 0.0001$), total AUC (CNO: 465.1 ± 44.16, CNO + PPADS: 72.35 ± 14.37, $p < 0.0001$), AUC (CNO: 11.48 ± 0.3921, CNO + PPADS: 5.320 ± 0.5848, $p < 0.0001$), Amplitude (CNO: 1.422 ± 0.03225, CNO + PPADS: 0.8632 ± 0.05715, $p < 0.0001$) and Latency (CNO: 15.46 ± 0.2839, CNO + PPADS: 12.67 ± 0.7579, $p < 0.0001$) of OCs (Figures 3E–H). The accumulation curve showed that the number of lower Amplitude Ca^{2+} activities was increased after Suramin and PPADS application (Figures 3D,H). As previously described, the chemogenetic activation of VA/VL neurons promoted activity in VA/VL axons and OCs in L1 of M1 for 5 h. To verify that the effect of antagonists was not due to differences in the time course after chemogenetic activation, we performed Pre-imaging followed by CNO administration. Subsequently, we applied saline or PPADS following craniotomy, and finally performed imaging 1 h after CNO administration with saline or PPADS (imaging 1 h after CNO + saline and 1 h after CNO + PPADS, respectively). The results showed that Ca^{2+} responses in OCs persisted in the saline group, whereas in the PPADS group, Ca^{2+} responses in OCs significantly reduced, indicating an effect of neurotransmitter antagonists (Supplementary Figures 3A,B). In addition, glutamate and ATP differentially affected the latency of Ca^{2+} transients in OCs (Figures 2E,F, 3C,D,G,H). Suramin and PPADS application significantly shortened the latency of Ca^{2+} transients in OCs, suggesting that ATP induced longer latency of Ca^{2+} transients. In contrast, CNQX lengthened the latency of Ca^{2+} transients in OCs, indicating that glutamate induced faster latency of Ca^{2+} transients in OCs. Thus, the latency of Ca^{2+} responses in OCs is regulated by different types of neurotransmitters previously known to elicit Ca^{2+} responses in OCs (Gallo et al., 1996; Bergles et al., 2000; Chittajallu et al., 2004; Lin and Bergles, 2004; Lin et al., 2005; Kukley et al., 2007; Káradóttir et al., 2008; Kougioumtzidou et al., 2017). Furthermore, our analysis of Ca^{2+} responses in OCs at the individual mouse level was similar to that at the imaging fields (cells) level (Supplementary Figures 3C–H).

3.3. OC responses in mice model of AD

The release of ATP from the dying and dead cells of the damaged brain (Honda et al., 2001; Davalos et al., 2005; Haynes et al., 2006; Matute et al., 2007; Duan et al., 2009) increases extracellular ATP concentrations and contributes to AD pathology (Burnstock, 2008; Cieslak and Wojtczak, 2018; Francistiova et al., 2020). Therefore, we attempted to detect the difference in OC responses in mice models of AD. We used $App^{NL\text{-}G\text{-}F/NL\text{-}G\text{-}F}$ mice, as reported previously and provided by Dr. Saido, as the mice models of AD (Saito et al., 2014). We first assessed the behavioral abnormalities and found no detectable changes in 4- or 5-month-old $App^{NL\text{-}G\text{-}F/NL\text{-}G\text{-}F}$ mice. However, 6-month-old $App^{NL\text{-}G\text{-}F/NL\text{-}G\text{-}F}$ mice had impaired alteration ratio (Supplementary Figure 4A), though the number of entries was not impaired, which is consistent with the result of a previous study (Saito et al., 2014). Since white matter lesions appear in head magnetic resonance imaging of patients with AD before the onset of cognitive decline (Lee et al., 2016), we next focused on the period before the onset of behavioral abnormalities at 4 or 5 months of age, by observing OC Ca^{2+} responses in $App^{NL\text{-}G\text{-}F/NL\text{-}G\text{-}F}$ mice (Figures 4A,B). Ca^{2+} spots, Ca^{2+} events, total AUC, AUC, Amplitude, and Latency were not increased in 4-month-old $App^{NL\text{-}G\text{-}F/NL\text{-}G\text{-}F}$mice, suggesting that OCs in 4-month-old $App^{NL\text{-}G\text{-}F/NL\text{-}G\text{-}F}$ mice did not show abnormal Ca^{2+} activities (Figures 4C–F). In contrast, Ca^{2+} spots, Ca^{2+} events, total AUC, AUC, Amplitude, and Latency increased significantly in 5-month-old $App^{NL\text{-}G\text{-}F/NL\text{-}G\text{-}F}$ mice than in control mice (Supplementary movies 2, 3), both at the imaging field (cells) (Figures 4G–J; see also source data file) and individual mouse levels (Supplementary Figures 4B,C), suggesting abnormal Ca^{2+} activities are present in 5-month-old $App^{NL\text{-}G\text{-}F/NL\text{-}G\text{-}F}$ mice. Furthermore, we confirmed by immunohistochemical staining that the differentiation levels of GCaMP'+ve cells do not differ between 5-month-old $App^{NL\text{-}G\text{-}F/NL\text{-}G\text{-}F}$ mice and age-matched control mice (Supplementary Figure 4D). These increased abnormal Ca^{2+} activities in OCs were not inhibited by TTX treatment (Figure 5A), suggesting that neuronal activity did not contribute to increased abnormal Ca^{2+} activities in OCs of 5-month-old $App^{NL\text{-}G\text{-}F/NL\text{-}G\text{-}F}$ mice (Figures 5B–E). Therefore, we hypothesized that dying or dead cells in 5-month-old $App^{NL\text{-}G\text{-}F/NL\text{-}G\text{-}F}$ mice released ATP, enhancing the functional OC

10.3389/fncel.2023.1154196

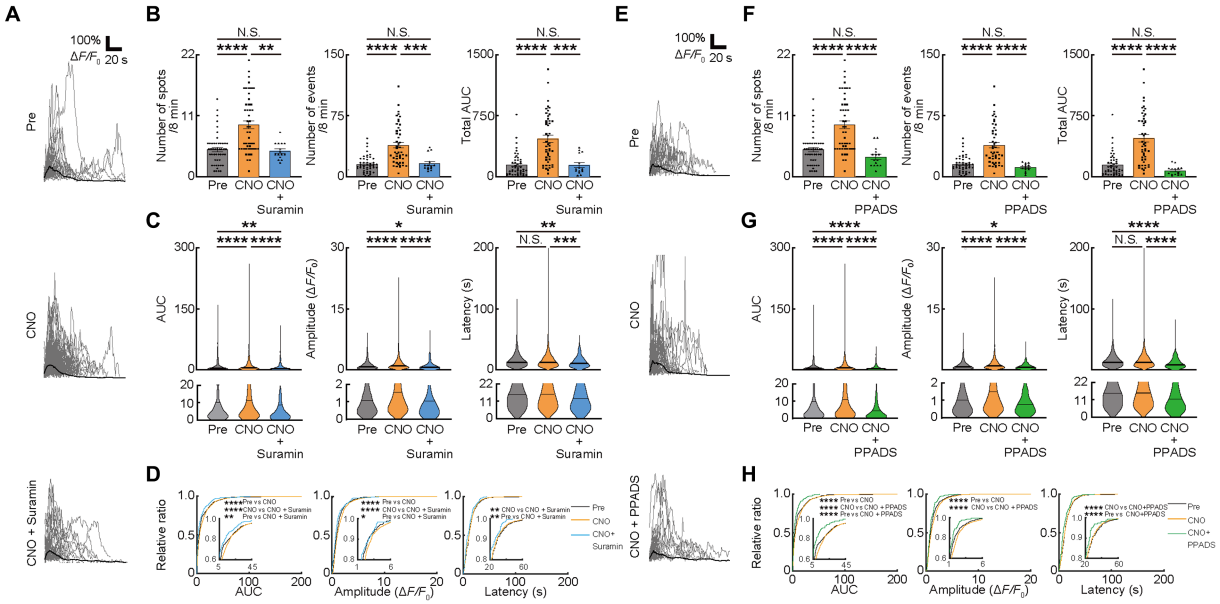

FIGURE 3
Ca^{2+} activities in oligodendrocytes (OCs) are regulated by ATP. **(A,E)** Representative Ca^{2+} traces from spots of typical GCaMP' + ve cells at Pre-imaging, and after CNO, CNO + Suramin, and CNO + PPADS applications. **(B,F)** Ca^{2+} spots, Ca^{2+} events and total area under the curve (AUC) were significantly increased after CNO application. Suramin, and PPADS applications significantly decreased these parameters. Pre: $n = 23$ mice, 48 imaging fields (cells); CNO: 23 mice, 48 imaging fields (cells); CNO + Suramin: 9 mice, 15 imaging fields (cells): CNO + PPADS: $n = 7$ mice, 15 imaging fields (cells), N.S., not significant, $^{**}p < 0.01$, $^{***}p < 0.001$, $^{****}p < 0.0001$, Kruskal–Wallis test followed by Dunn's test. Data are presented as mean ± standard error of mean. For detailed data, check the source data file. **(C,G)** No statistically significant differences were detected in Latency between pre-imaging and after CNO application. AUC and Amplitude was significantly increased after CNO application. Suramin, and PPADS applications significantly decreased Amplitude. Suramin and PPADS significantly decreased AUC, Amplitude and Latency. Pre: $n = 23$ mice, 736 events; CNO: $n = 23$ mice, 2047 events; CNO + Suramin: $n = 9$ mice, 289 events; CNO + PPADS: $n = 7$ mice, 289 events. N.S., not significant, $^{*}p < 0.05$, $^{**}p < 0.01$, $^{***}p < 0.001$, $^{****}p < 0.0001$, Kruskal–Wallis test followed by Dunn's test. Violin plots show median (black line) and distribution of the data. For detailed data, check the source data file. **(D,H)** Proportions of larger AUC and higher Amplitude were significantly higher after CNO application than before. The proportion of lower Amplitude was significantly higher after CNO + Suramin, and CNO + PPADS applications than after CNO application. The number of shorter Latency Ca^{2+} activities was increased after CNO + Suramin and Suramin + PPADS applications than after CNO application. Pre: $n = 23$ mice, 736 events; CNO: $n = 23$ mice, 2047 events; CNO + Suramin: $n = 9$ mice, 289 events; CNO + PPADS: $n = 7$ mice, 289 events. $^{*}p < 0.05$, $^{**}p < 0.01$, $^{****}p < 0.0001$, Kolmogorov–Smirnov test. For detailed data, check the source data file.

responses. To test this hypothesis, we first stained 5-month-old $App^{NL\text{-}G\text{-}F/NL\text{-}G\text{-}F}$ mice with Fluoro-Jade C to investigate whether they had more dying or dead cells compared to age-matched control mice. As expected, the number of dying or dead cells was significantly increased in 5-month-old $App^{NL\text{-}G\text{-}F/NL\text{-}G\text{-}F}$ mice compared to that in age-matched control mice (Supplementary Figure 4E). To further explore whether the abnormal Ca^{2+} activities in OCs were due to the increased ATP in 5-month-old $App^{NL\text{-}G\text{-}F/NL\text{-}G\text{-}F}$ mice, Suramin and PPADS were administered to 5-month-old $App^{NL\text{-}G\text{-}F/NL\text{-}G\text{-}F}$ mice (Figure 5A). Suramin and PPADS application significantly reduced Ca^{2+} spots (Pre: 8.206 ± 1.613, Suramin + PPADS: 2.618 ± 0.2829, $p = 0.0044$), Ca^{2+} events (Pre: 33.56 ± 5.976, Suramin + PPADS: 7.559 ± 0.8920, $p < 0.0001$), total AUC (Pre: 443.3 ± 77.70, Suramin + PPADS: 46.20 ± 9.347, $p < 0.0001$), AUC (Pre: 13.86 ± 0.8542, Suramin + PPADS: 7.286 ± 0.8543, $p < 0.0001$), Amplitude (Pre: 1.751 ± 0.06353, Suramin + PPADS: 1.041 ± 0.08171, $p < 0.0001$). Suramin and PPADS application also reduced Latency (Pre: 15.71 ± 0.4135, Suramin + PPADS: 12.59 ± 0.7377, $p < 0.0001$) both at imaging fields (cells) (Figures 5F–H) and individual mouse levels (Supplementary Figures 4F,G). Accumulation curves also showed a significant change in the distribution of AUC, Amplitude and Latency after Suramin + PPADS application (Figure 5I). In contrast, CNQX application did not show detectable changes in OC Ca^{2+} responses in 5-month-old $App^{NL\text{-}G\text{-}F/NL\text{-}G\text{-}F}$ mice (Figures 5J–M). Furthermore, properties of Ca^{2+} responses (AUC, Amplitude, and Latency) did not correlate with the distance between Ca^{2+} spots and Aβ deposition, but they were definitely more effectively suppressed by ATP inhibitors in OCs of 5-month-old $App^{NL\text{-}G\text{-}F/NL\text{-}G\text{-}F}$ mice than in OCs of age-matched control mice (Supplementary Figures 4H,I). These data suggest that OCs in 5-month-old $App^{NL\text{-}G\text{-}F/NL\text{-}G\text{-}F}$ mice mainly receive ATP released from dying or dead cells.

4. Discussion

In this research, we observed OC Ca^{2+} responses. Activity-dependent glutamate and ATP release from neurons or astrocytes trigger OC responses with different properties of Ca^{2+} responses. In mice models of AD, these activity-dependent responses were lost but higher frequency of ATP release induced Ca^{2+} responses due to neurodegeneration.

Myelination is essential for efficient information processing in the brain. OPCs originate in the ventral ventricular layer of the zona limitans intrathalamica in the mesencephalon. From here, OPCs proliferate and migrate to be widely distributed in the brain. After they settle in the brain, OPCs differentiate and myelinate the axons

10.3389/fncel.2023.1154196

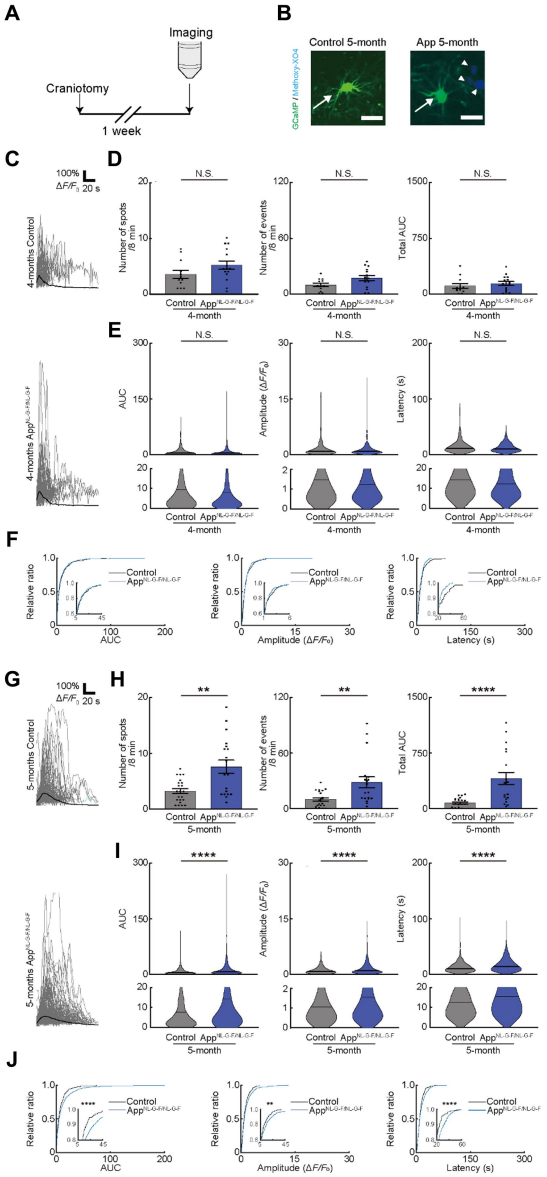

FIGURE 4
Ca^{2+} activity of oligodendrocytes (OCs) is altered in 5-month-old $App^{NL\text{-}G\text{-}F/NL\text{-}G\text{-}F}$ mice. **(A)** Experimental protocol of two-photon Ca^{2+} imaging of OCs in $App^{NL\text{-}G\text{-}F/NL\text{-}G\text{-}F}$ mice. For this purpose, transgenic mice (PLP-GCaMP6) were crossed with $App^{NL\text{-}G\text{-}F/NL\text{-}G\text{-}F}$ mice and craniotomy was performed one week before imaging. **(B)** Representative image of GCaMP' + ve cells in the motor cortex of 5-month-old age-matched control and $App^{NL\text{-}G\text{-}F/NL\text{-}G\text{-}F}$ mice. Arrow indicates a GFP^{+} cell. Arrowhead indicates amyloid β deposition visualized by intraperitoneal administration of Methoxy-X04. Scale bar, 30 μm. **(C)** Representative Ca^{2+} traces from typical GCaMP' + ve cell processes from 4-month-old age-matched control and AppNL-G-F/NL-G-F mice. **(D)** No statistically significant differences were detected in Ca^{2+} spots, Ca^{2+} events and total area under the curve (AUC) between Control and $App^{NL\text{-}G\text{-}F/NL\text{-}G\text{-}F}$ mice at 4 months of age. Control: $n = 6$ mice, 12 imaging fields (cells); $App^{NL\text{-}G\text{-}F/NL\text{-}G\text{-}F}$: $n = 6$ mice, 15 imaging fields (cells). N.S., not significant by Mann–Whitney *U*-test. Data are presented as mean ± standard error of mean. For detailed data, check the source data file. **(E)** No statistically significant differences were detected in the AUC, Amplitude, and Latency between Control and $App^{NL\text{-}G\text{-}F/NL\text{-}G\text{-}F}$ mice at 4 months of age. Control; $n = 6$ mice, 233 events; $App^{NL\text{-}G\text{-}F/NL\text{-}G\text{-}F}$; $n = 6$ mice, 418 events. N.S., not significant, Mann–Whitney *U*-test. Violin plots show median (black line) and distribution of the data. For detailed data, check the source data file. **(F)** Proportions of larger AUC, Amplitude, and Latency were not significantly different between Control and $App^{NL\text{-}G\text{-}F/NL\text{-}G\text{-}F}$ mice at 4 months of age. Control; $n = 6$ mice, 233 events; $App^{NL\text{-}G\text{-}F/NL\text{-}G\text{-}F}$; $n = 6$ mice, 418 events. N.S., not significant, Kolmogorov–Smirnov test. For detailed data, check the source data file. **(G)** Representative Ca^{2+} traces from typical GCaMP' + ve cell processes from 5-month-old age-matched control and $App^{NL\text{-}G\text{-}F/NL\text{-}G\text{-}F}$ mice. **(H)** Ca^{2+} spots, Ca^{2+} events and total AUC were significantly higher in $App^{NL\text{-}G\text{-}F/NL\text{-}G\text{-}F}$ mice than in Control mice at 5 months of age. Control: $n = 8$ mice, 22 imaging fields (cells); $App^{NL\text{-}G\text{-}F/NL\text{-}G\text{-}F}$: $n = 8$ mice, 18 imaging fields (cells). $^{**}p < 0.01$, $^{****}p < 0.0001$, Mann–Whitney *U*-test. Error bar shows mean ± standard error of mean. For detailed data, check the source data file. **(I)** AUC, Amplitude, and Latency were significantly higher in $App^{NL\text{-}G\text{-}F/NL\text{-}G\text{-}F}$ mice than in Control mice at 5 months of age. Control: $n = 8$ mice, 364 events; $App^{NL\text{-}G\text{-}F/NL\text{-}G\text{-}F}$: $n = 8$ mice, 877 events. $^{****}p < 0.0001$, Mann–Whitney *U*-test. Violin plots show median (black line) and distribution of the data. For detailed data, check the source data file. **(J)** Proportions of larger AUC and higher Amplitude and Latency were significantly higher in $App^{NL\text{-}G\text{-}F/NL\text{-}G\text{-}F}$ mice than in Control mice at 5 months of age. Control: $n = 8$ mice, 364 events; $App^{NL\text{-}G\text{-}F/NL\text{-}G\text{-}F}$: $n = 8$ mice, 877 events. $^{**}p < 0.01$, $^{****}p < 0.0001$, Kolmogorov–Smirnov test. For detailed data, check the source data file.

10.3389/fncel.2023.1154196

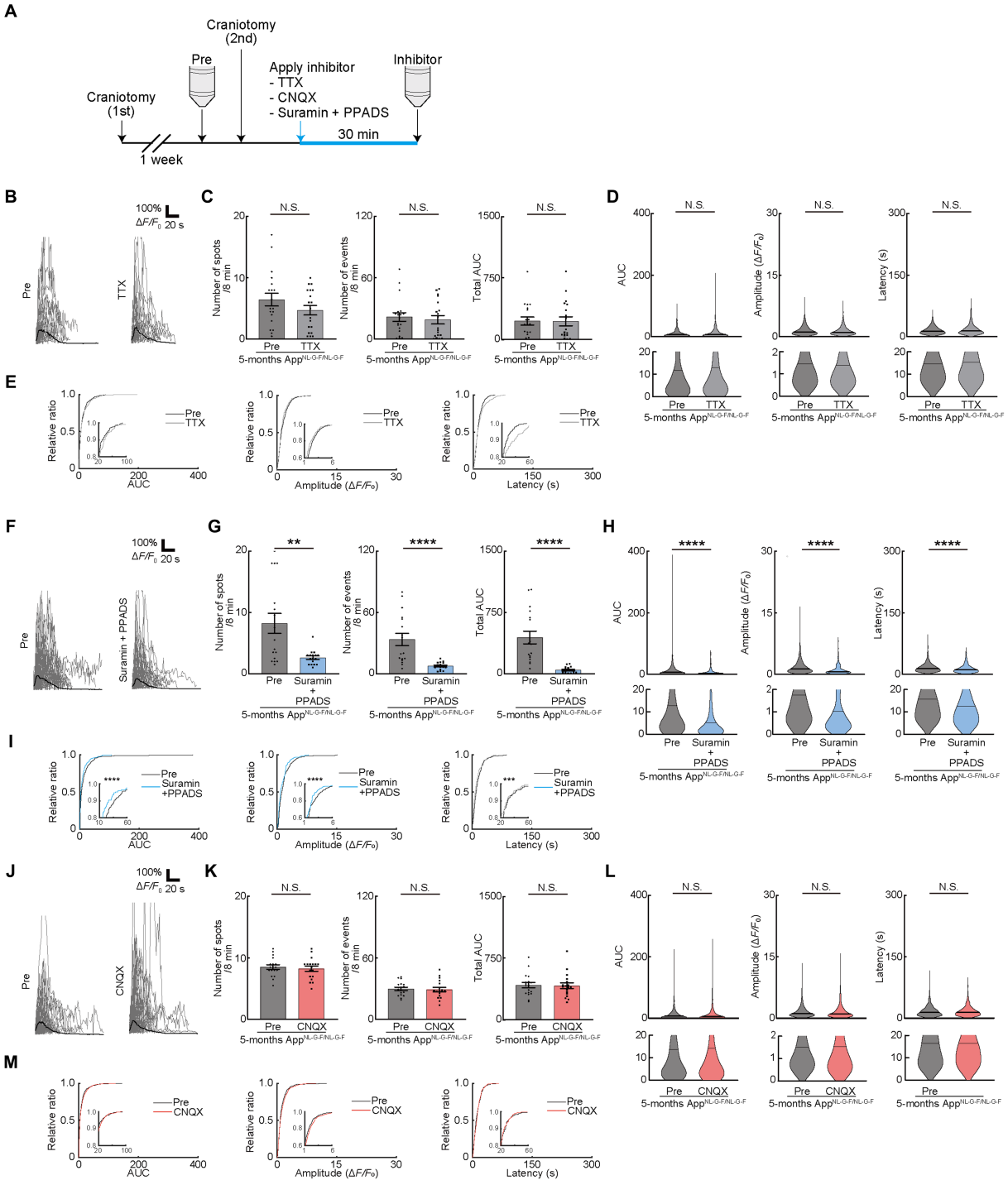

FIGURE 5

Pharmacological manipulation of oligodendrocyte (OC) Ca^{2+} activities in $App^{NL-G-F/NL-G-F}$ mice at 5 months. **(A)** Experimental protocol of two-photon Ca^{2+} imaging of OCs in $App^{NL-G-F/NL-G-F}$ mice at 5 months of age. One week after craniotomy (first), two-photon Ca^{2+} imaging was performed (Pre). After Pre- imaging, TTX or neurotransmitter receptor antagonists (CNQX or Suramin and PPPADS) were applied on the brain surface by craniotomy (second), and then, second imaging was performed (Inhibitor). Two-photon Ca^{2+} imaging of OCs was obtained from the same cells in all imaging sessions. **(B)** Representative Ca^{2+} traces from typical GCaMP' + ve cell processes after TTX application. **(C)** No statistically significant differences were detected in Ca^{2+} spots, Ca^{2+} events and total area under the curve (AUC) between before and after TTX application. Pre: $n = 9$ mice, 19 imaging fields (cells); TTX: $n = 9$ mice, 19 imaging fields (cells). N.S., not significant, Mann–Whitney *U*-test. Data are presented as the mean ± standard error of mean. For detailed data, check the source data file. **(D)** No statistically significant differences were detected in AUC, Amplitude, and Latency between before and after TTX application. Pre: $n = 9$ mice, 611 events; TTX: $n = 9$ mice, 517 events. N.S., not significant, Mann–Whitney *U*-test. Violin plots show median (black line) and distribution of the data. For detailed data, check the source data file. **(E)** Proportions of AUC, Amplitude, and Latency were not significantly different between before and after TTX application. Pre: $n = 9$ mice, 611 events; TTX: $n = 9$ mice, 517 events. N.S., not significant, Kolmogorov–Smirnov test. **(F)** Representative Ca^{2+} traces from typical GCaMP' + ve cell processes after Suramin + PPADS application. **(G)** Ca^{2+} spots, Ca^{2+} events and total AUC were significantly decreased after Suramin + PPADS application. Pre: $n = 10$ mice, 17 imaging fields (cells); Suramin + PPADS:

(Continued)

FIGURE 5 (Continued)
$n = 10$ mice, 17 imaging fields (cells). $^{**}p < 0.01$, $^{****}p < 0.0001$, Mann–Whitney *U*-test. Data are presented as the mean ± standard error of mean. For detailed data, check the source data file. **(H)** AUC, Amplitude, and Latency were significantly decreased after Suramin + PPADS application. Pre: $n = 10$ mice, 777 events; Suramin + PPADS: $n = 10$ mice, 208 events. $^{****}p < 0.0001$, Mann–Whitney *U*-test. Violin plots show median (black line) and distribution of the data. For detailed data, check the source data file. **(I)** Proportions of smaller AUC, lower Amplitude, and shorter Latency were significantly increased after Suramin + PPADS application. Pre: $n = 10$ mice, 777 events; Suramin + PPADS: $n = 10$ mice, 208 events. $^{***}p < 0.001$, $^{****}p < 0.0001$, Kolmogorov–Smirnov test. For detailed data, check the source data file. **(J)** Representative Ca^{2+} traces from typical GCaMP' + ve cell processes after CNQX application. **(K)** No statistically significant differences were detected in Ca^{2+} spots, Ca^{2+} events, and total area under the curve (AUC) between before and after CNQX application. Pre: $n = 10$ mice, 18 imaging fields (cells); CNQX: $n = 10$ mice, 18 imaging fields (cells). N.S., not significant, Mann–Whitney *U*-test. Data are presented as the mean ± standard error of mean. For detailed data, check the source data file. **(L)** No statistically significant differences were detected in AUC, Amplitude, and Latency between before and after CNQX application. Pre: $n = 10$ mice, 822 events; CNQX: $n = 10$ mice, 780 events. N.S., not significant, Mann–Whitney *U*-test. Violin plots show median (black line) and distribution of the data. For detailed data, check the source data file. **(M)** Proportions of AUC, Amplitude, and Latency were not significantly different between before and after CNQX application. Pre: $n = 10$ mice, 822 events; CNQX: $n = 10$ mice, 780 events. N.S., not significant, Kolmogorov–Smirnov test. For detailed data, check the source data file.

to regulate the conduction velocity. Previous studies showed that proliferation and differentiation of OPCs and myelination depend on neuronal activity (Menn et al., 2006; Xing et al., 2014). TTX injection into the eyes reduced OPC proliferation, and inhibition of neurotransmitter release by the botulinus or tetanus toxin resulted in deficient activity-dependent myelination due to impaired local translation of myelin basic protein (Barres and Raff, 1993). OCs express various receptors for neurotransmitters such as AMPA, NMDA (N-methyl-D-aspartic acid), gamma-aminobutyric acid B, and purinergic P1 and P2 receptors. Growing evidence suggested that neurotransmitters regulate migration and proliferation of OPCs, differentiation into OCs, and myelination in mature OCs (Nishiyama et al., 2021). Adenosine, the metabolite of ATP, has been shown to inhibit proliferation of OPCs, in contrast to ATP, which itself is a contradictory result. In addition, OPCs form a synapse-like structure with axons and receive glutamate on AMPAR, which promotes OPC proliferation and inhibits their differentiation into OCs (Agresti et al., 2005; Kato et al., 2018). AMPA, NMDA, and P1 and P2 signaling mediates Ca^{2+} transients in OCs/OPCs that regulate downstream signaling. The developmental changes in these receptor expressions have been known (Matute et al., 2007; Spitzer et al., 2019).

Here, we showed that glutamate-mediated Ca^{2+} transients in OC exhibited a short decay, but ATP-mediated Ca^{2+} transients in OC exhibited a long decay. These differences may induce various gene expressions to regulate their fate differently. Deficient activity-dependent myelin regulation in adult mice impaired temporal regulation of spike arrival, leading to increased spontaneous neuronal activity and reduced movement-induced neuronal activity in the primary motor cortex, which in turn impaired the motor learning process (Kato et al., 2020). Although a previous study demonstrated that Ca^{2+} transients in myelin sheaths of L5 or L6 PLP-positive cells in mice are not dependent on neuronal activity but are dependent on mitochondria (Battefeld et al., 2019), our study showed that L1 GCaMP' + ve (PLP' + ve) cells were predominantly CC1 positive but a few were MBP positive, suggesting that pre-myelinating OCs showed neuronal activity dependent responses.

ATP is known to be released abundantly from degenerative brain tissue. Released ATP activates P2X7 signaling, which promotes inflammatory response in neurodegenerative diseases, such as AD, amyotrophic lateral sclerosis, multiple sclerosis, and spinal cord injury that cause apoptosis or dysmorphic changes in OCs, and ultimately induces de-myelination to promote disease progression. Specifically, in studies in patients with AD and mice models of AD, spatial transcriptome analysis revealed that genetic changes in OCs around Aβ deposition occur early in the disease (Chen et al., 2020). Furthermore, OCs/OPCs have been found to show accelerated aging in mice models of AD and removal of these cells have been found to improve their cognitive function (Zhang et al., 2019). We used mice models of AD and found that the abundant ATP released from degenerative brain tissue increased abnormal Ca^{2+} responses in OCs, which may cause dysmorphic changes in OCs. In addition, the increased abnormal Ca^{2+} responses in OCs may trigger myelin defects, abnormal myelination, or abnormal turnover in OPC differentiation. A recent study suggested that structural defects in myelin promote Aβ deposition and is an upstream risk factor for AD (Depp et al., 2023), which may be associated with abnormal Ca^{2+} responses in OC observed at 5 months of age prior to the onset of behavioral abnormalities. Further studies are needed to clarify the effects of abnormal Ca^{2+} responses in OCs on disease progression.

Data availability statement

The original contributions presented in the study are included in the article/Supplementary material, further inquiries can be directed to the corresponding author.

Ethics statement

All experimental protocols used in animals were approved by the Animal Care and Use Committees of Nagoya University Graduate School of Medicine and Kobe University Graduate School of Medicine. The study was conducted in accordance with the local legislation and institutional requirements.

Author contributions

KY, DK, and HW designed research and wrote the paper. KY, DK, and SS performed research. KY, DK, SS, IT, and HW analyzed data. All authors contributed to the article and approved the submitted version.

Funding

This study was financially supported by Grants-in-Aid for Scientific Research on Innovative Areas (19H04753, 19H05219, and 25110732 to HW); Grants-in-Aid for Transformative Research Areas (A) (20H05699 to HW, 21H05587 to DK); Fostering Joint International Research (B) (20KK0170 to HW); Grant-in-Aid for Scientific Research (B) (18H02598 and 21H02662 to HW); Japan Agency for Medical Research and Development (JP22ak0101150 to DK and JP23gm1410011 h0002 to HW); and JST CREST (JPMJCR1755 and JPMJCR22P6 to HW).

Acknowledgments

We thank Takaomi C. Saido (RIKEN) for sharing App$^{NL-G-F/NL-G-F}$ mice. We thank Bryan Roth (University of North Carolina) for providing AAV8-hSyn-hM3D (Gq)-mCherry and thank Lin Tian for providing AAV1-hSynapsin1-axon-GCaMP6s-P2A-mRuby3.

Conflict of interest

The authors declare that the research was conducted in the absence of any commercial or financial relationships that could be construed as a potential conflict of interest.

Publisher's note

All claims expressed in this article are solely those of the authors and do not necessarily represent those of their affiliated organizations, or those of the publisher, the editors and the reviewers. Any product that may be evaluated in this article, or claim that may be made by its manufacturer, is not guaranteed or endorsed by the publisher.

Supplementary material

The Supplementary material for this article can be found online at: https://www.frontiersin.org/articles/10.3389/fncel.2023.1154196/full#supplementary-material

References

Agresti, C., Meomartini, M. E., Amadio, S., Ambrosini, E., Serafini, B., Franchini, L., et al. (2005). Metabotropic P2 receptor activation regulates oligodendrocyte progenitor migration and development. *Glia* 50, 132–144. doi: 10.1002/glia.20160

Amlien, I. K., and Fjell, A. M. (2014). Diffusion tensor imaging of white matter degeneration in Alzheimer's disease and mild cognitive impairment. *Neuroscience* 276, 206–215. doi: 10.1016/j.neuroscience.2014.02.017

Barres, B. A., and Raff, M. C. (1993). Proliferation of oligodendrocyte precursor cells depends on electrical activity in axons. *Nature* 361, 258–260. doi: 10.1038/361258a0

Barron, T., and Kim, J. H. (2019). Neuronal input triggers ca (2+) influx through AMPA receptors and voltage-gated ca (2+) channels in oligodendrocytes. *Glia* 67, 1922–1932. doi: 10.1002/glia.23670

Battefeld, A., Popovic, M. A., de Vries, S. I., and Kole, M. H. P. (2019). High-frequency microdomain ca (2+) transients and waves during early myelin internode remodeling. *Cell Rep.* 26, 182–191.e5. doi: 10.1016/j.celrep.2018.12.039

Bergles, D. E., Roberts, J. D., Somogyi, P., and Jahr, C. E. (2000). Glutamatergic synapses on oligodendrocyte precursor cells in the hippocampus. *Nature* 405, 187–191. doi: 10.1038/35012083

Berret, E., Barron, T., Xu, J., Debner, E., Kim, E. J., and Kim, J. H. (2017). Oligodendroglial excitability mediated by glutamatergic inputs and Nav 1.2 activation. *Nat. Commun.* 8:557. doi: 10.1038/s41467-017-00688-0

Bi, G. Q., and Poo, M. M. (1998). Synaptic modifications in cultured hippocampal neurons: dependence on spike timing, synaptic strength, and postsynaptic cell type. *J. Neurosci.* 18, 10464–10472. doi: 10.1523/JNEUROSCI.18-24-10464.1998

Burnstock, G. (2008). Purinergic signalling and disorders of the central nervous system. *Nat. Rev. Drug Discov.* 7, 575–590. doi: 10.1038/nrd2605

Cheli, V. T., Santiago Gonzalez, D. A., Namgyal Lama, T., Spreuer, V., Handley, V., Murphy, G. G., et al. (2016). Conditional deletion of the L-type Calcium Channel Cav 1.2 in oligodendrocyte progenitor cells affects postnatal myelination in mice. *J. Neurosci.* 36, 10853–10869. doi: 10.1523/JNEUROSCI.1770-16.2016

Cheli, V. T., Santiago González, D. A., Spreuer, V., and Paez, P. M. (2015). Voltage-gated ca++ entry promotes oligodendrocyte progenitor cell maturation and myelination in vitro. *Exp. Neurol.* 265, 69–83. doi: 10.1016/j.expneurol.2014.12.012

Chen, W. T., Lu, A., Craessaerts, K., Pavie, B., Sala Frigerio, C., Corthout, N., et al. (2020). Spatial transcriptomics and in situ sequencing to study Alzheimer's disease. *Cells* 182:e919, 976–991.e19. doi: 10.1016/j.cell.2020.06.038

Chittajallu, R., Aguirre, A., and Gallo, V. (2004). NG2-positive cells in the mouse white and grey matter display distinct physiological properties. *J. Physiol.* 561, 109–122. doi: 10.1113/jphysiol.2004.074252

Cieslak, M., and Wojtczak, A. (2018). Role of purinergic receptors in the Alzheimer's disease. *Purinergic Signal* 14, 331–344. doi: 10.1007/s11302-018-9629-0

Davalos, D., Grutzendler, J., Yang, G., Kim, J. V., Zuo, Y., Jung, S., et al. (2005). ATP mediates rapid microglial response to local brain injury *in vivo*. *Nat. Neurosci.* 8, 752–758. doi: 10.1038/nn1472

Depp, C., Sun, T., Sasmita, A. O., Spieth, L., Berghoff, S. A., Nazarenko, T., et al. (2023). Myelin dysfunction drives amyloid-β deposition in models of Alzheimer's disease. *Nature* 618, 349–357. doi: 10.1038/s41586-023-06120-6

Duan, Y., Sahley, C. L., and Muller, K. J. (2009). ATP and NO dually control migration of microglia to nerve lesions. *Dev. Neurobiol.* 69, 60–72. doi: 10.1002/dneu.20689

Emery, B. (2010). Regulation of oligodendrocyte differentiation and myelination. *Science* 330, 779–782. doi: 10.1126/science.1190927

Fannon, J., Tarmier, W., and Fulton, D. (2015). Neuronal activity and AMPA-type glutamate receptor activation regulates the morphological development of oligodendrocyte precursor cells. *Glia* 63, 1021–1035. doi: 10.1002/glia.22799

Feldman, D. E. (2012). The spike-timing dependence of plasticity. *Neuron* 75, 556–571. doi: 10.1016/j.neuron.2012.08.001

Feng, J. F., Gao, X. F., Pu, Y. Y., Burnstock, G., Xiang, Z., and He, C. (2015). P2X7 receptors and Fyn kinase mediate ATP-induced oligodendrocyte progenitor cell migration. *Purinergic Signal* 11, 361–369. doi: 10.1007/s11302-015-9458-3

Fields, R. D. (2008). White matter in learning, cognition and psychiatric disorders. *Trends Neurosci.* 31, 361–370. doi: 10.1016/j.tins.2008.04.001

Fields, R. D., and Burnstock, G. (2006). Purinergic signalling in neuron-glia interactions. *Nat. Rev. Neurosci.* 7, 423–436. doi: 10.1038/nrn1928

Francistiova, L., Bianchi, C., Di Lauro, C., Sebastian-Serrano, A., de Diego-Garcia, L., Kobolak, J., et al. (2020). The role of P2X7 receptor in Alzheimer's disease. *Front. Mol. Neurosci.* 13:94. doi: 10.3389/fnmol.2020.00094

Gallo, V., Zhou, J. M., McBain, C. J., Wright, P., Knutson, P. L., and Armstrong, R. C. (1996). Oligodendrocyte progenitor cell proliferation and lineage progression are regulated by glutamate receptor-mediated K+ channel block. *J. Neurosci.* 16, 2659–2670. doi: 10.1523/JNEUROSCI.16-08-02659.1996

Gautier, H. O., Evans, K. A., Volbracht, K., James, R., Sitnikov, S., Lundgaard, I., et al. (2015). Neuronal activity regulates remyelination via glutamate signalling to oligodendrocyte progenitors. *Nat. Commun.* 6:8518. doi: 10.1038/ncomms9518

Gibson, E. M., Purger, D., Mount, C. W., Goldstein, A. K., Lin, G. L., Wood, L. S., et al. (2014). Neuronal activity promotes oligodendrogenesis and adaptive myelination in the mammalian brain. *Science* 344:1252304. doi: 10.1126/science.1252304

Groc, L., Gustafsson, B., and Hanse, E. (2002). Spontaneous unitary synaptic activity in CA1 pyramidal neurons during early postnatal development: constant contribution of AMPA and NMDA receptors. *J. Neurosci.* 22, 5552–5562. doi: 10.1523/JNEUROSCI.22-13-05552.2002

Haynes, S. E., Hollopeter, G., Yang, G., Kurpius, D., Dailey, M. E., Gan, W. B., et al. (2006). The P2Y12 receptor regulates microglial activation by extracellular nucleotides. *Nat. Neurosci.* 9, 1512–1519. doi: 10.1038/nn1805

Hines, J. H., Ravanelli, A. M., Schwindt, R., Scott, E. K., and Appel, B. (2015). Neuronal activity biases axon selection for myelination *in vivo*. *Nat. Neurosci.* 18, 683–689. doi: 10.1038/nn.3992

Honda, S., Sasaki, Y., Ohsawa, K., Imai, Y., Nakamura, Y., Inoue, K., et al. (2001). Extracellular ATP or ADP induce chemotaxis of cultured microglia through Gi/o-coupled P2Y receptors. *J. Neurosci.* 21, 1975–1982. doi: 10.1523/JNEUROSCI.21-06-01975.2001

Inamura, N., Sugio, S., Macklin, W. B., Tomita, K., Tanaka, K. F., and Ikenaka, K. (2012). Gene induction in mature oligodendrocytes with a PLP-tTA mouse line. *Genesis* 50, 424–428. doi: 10.1002/dvg.20808

Karadottir, R., Cavelier, P., Bergersen, L. H., and Attwell, D. (2005). NMDA receptors are expressed in oligodendrocytes and activated in ischaemia. *Nature* 438, 1162–1166. doi: 10.1038/nature04302

Káradóttir, R., Hamilton, N. B., Bakiri, Y., and Attwell, D. (2008). Spiking and nonspiking classes of oligodendrocyte precursor glia in CNS white matter. *Nat. Neurosci.* 11, 450–456. doi: 10.1038/nn2060

Kato, D., Aoyama, Y., Nishida, K., Takahashi, Y., Sakamoto, T., Takeda, I., et al. (2023). Regulation of lipid synthesis in myelin modulates neural activity and is required for motor learning. *Glia* 71, 2591–2608. doi: 10.1002/glia.24441

Kato, D., Eto, K., Nabekura, J., and Wake, H. (2018). Activity-dependent functions of non-electrical glial cells. *J. Biochem.* 163, 457–464. doi: 10.1093/jb/mvy023

Kato, D., Wake, H., Lee, P. R., Tachibana, Y., Ono, R., Sugio, S., et al. (2020). Motor learning requires myelination to reduce asynchrony and spontaneity in neural activity. *Glia* 68, 193–210. doi: 10.1002/glia.23713

Kougioumtzidou, E., Shimizu, T., Hamilton, N. B., Tohyama, K., Sprengel, R., Monyer, H., et al. (2017). Signalling through AMPA receptors on oligodendrocyte precursors promotes myelination by enhancing oligodendrocyte survival. *elife* 6:e28080. doi: 10.7554/eLife.28080

Kukley, M., Capetillo-Zarate, E., and Dietrich, D. (2007). Vesicular glutamate release from axons in white matter. *Nat. Neurosci.* 10, 311–320. doi: 10.1038/nn1850

Lee, S., Viqar, F., Zimmerman, M. E., Narkhede, A., Tosto, G., Benzinger, T. L., et al. (2016). White matter hyperintensities are a core feature of Alzheimer's disease: evidence from the dominantly inherited Alzheimer network. *Ann. Neurol.* 79, 929–939. doi: 10.1002/ana.24647

Li, H., and Harlow, M. L. (2014). Individual synaptic vesicles from the electroplaque of *Torpedo californica*, a classic cholinergic synapse, also contain transporters for glutamate and ATP. *Physiol. Rep.* 2:e00206. doi: 10.1002/phy2.206

Lin, S. C., and Bergles, D. E. (2004). Synaptic signaling between GABAergic interneurons and oligodendrocyte precursor cells in the hippocampus. *Nat. Neurosci.* 7, 24–32. doi: 10.1038/nn1162

Lin, S. C., Huck, J. H., Roberts, J. D., Macklin, W. B., Somogyi, P., and Bergles, D. E. (2005). Climbing fiber innervation of NG2-expressing glia in the mammalian cerebellum. *Neuron* 46, 773–785. doi: 10.1016/j.neuron.2005.04.025

Markram, H., Lubke, J., Frotscher, M., and Sakmann, B. (1997). Regulation of synaptic efficacy by coincidence of postsynaptic APs and EPSPs. *Science* 275, 213–215. doi: 10.1126/science.275.5297.213

Maruyama, R., Maeda, K., Moroda, H., Kato, I., Inoue, M., Miyakawa, H., et al. (2014). Detecting cells using non-negative matrix factorization on calcium imaging data. *Neural Netw.* 55, 11–19. doi: 10.1016/j.neunet.2014.03.007

Matute, C., Torre, I., Perez-Cerda, F., Perez-Samartin, A., Alberdi, E., Etxebarria, E., et al. (2007). P2X(7) receptor blockade prevents ATP excitotoxicity in oligodendrocytes and ameliorates experimental autoimmune encephalomyelitis. *J. Neurosci.* 27, 9525–9533. doi: 10.1523/JNEUROSCI.0579-07.2007

McKenzie, I. A., Ohayon, D., Li, H., de Faria, J. P., Emery, B., Tohyama, K., et al. (2014). Motor skill learning requires active central myelination. *Science* 346, 318–322. doi: 10.1126/science.1254960

Menn, B., Garcia-Verdugo, J. M., Yaschine, C., Gonzalez-Perez, O., Rowitch, D., and Alvarez-Buylla, A. (2006). Origin of oligodendrocytes in the subventricular zone of the adult brain. *J. Neurosci.* 26, 7907–7918. doi: 10.1523/JNEUROSCI.1299-06.2006

Mensch, S., Baraban, M., Almeida, R., Czopka, T., Ausborn, J., El Manira, A., et al. (2015). Synaptic vesicle release regulates myelin sheath number of individual oligodendrocytes in vivo. *Nat. Neurosci.* 18, 628–630. doi: 10.1038/nn.3991

Micu, I., Jiang, Q., Coderre, E., Ridsdale, A., Zhang, L., Woulfe, J., et al. (2006). NMDA receptors mediate calcium accumulation in myelin during chemical ischaemia. *Nature* 439, 988–992. doi: 10.1038/nature04474

Nave, K. A. (2010). Myelination and support of axonal integrity by glia. *Nature* 468, 244–252. doi: 10.1038/nature09614

Nishiyama, A., Shimizu, T., Sherafat, A., and Richardson, W. D. (2021). Life-long oligodendrocyte development and plasticity. *Semin. Cell Dev. Biol.* 116, 25–37. doi: 10.1016/j.semcdb.2021.02.004

Ohkura, M., Sasaki, T., Sadakari, J., Gengyo-Ando, K., Kagawa-Nagamura, Y., Kobayashi, C., et al. (2012). Genetically encoded green fluorescent Ca2+ indicators with improved detectability for neuronal Ca2+ signals. *PLoS One* 7:e51286. doi: 10.1371/journal.pone.0051286

Paez, P. M., Fulton, D., Colwell, C. S., and Campagnoni, A. T. (2009). Voltage-operated ca (2+) and Na(+) channels in the oligodendrocyte lineage. *J. Neurosci. Res.* 87, 3259–3266. doi: 10.1002/jnr.21938

Saito, T., Matsuba, Y., Mihira, N., Takano, J., Nilsson, P., Itohara, S., et al. (2014). Single app knock-in mouse models of Alzheimer's disease. *Nat. Neurosci.* 17, 661–663. doi: 10.1038/nn.3697

Salter, M. G., and Fern, R. (2005). NMDA receptors are expressed in developing oligodendrocyte processes and mediate injury. *Nature* 438, 1167–1171. doi: 10.1038/nature04301

Scholz, J., Klein, M. C., Behrens, T. E., and Johansen-Berg, H. (2009). Training induces changes in white-matter architecture. *Nat. Neurosci.* 12, 1370–1371. doi: 10.1038/nn.2412

Spitzer, S. O., Sitnikov, S., Kamen, Y., Evans, K. A., Kronenberg-Versteeg, D., Dietmann, S., et al. (2019). Oligodendrocyte progenitor cells become regionally diverse and heterogeneous with age. *Neuron* 101:e455, 459–471.e5. doi: 10.1016/j.neuron.2018.12.020

Stevens, B., Porta, S., Haak, L. L., Gallo, V., and Fields, R. D. (2002). Adenosine: a neuron-glial transmitter promoting myelination in the CNS in response to action potentials. *Neuron* 36, 855–868. doi: 10.1016/S0896-6273(02)01067-X

Tanaka, K. F., Matsui, K., Sasaki, T., Sano, H., Sugio, S., Fan, K., et al. (2012). Expanding the repertoire of optogenetically targeted cells with an enhanced gene expression system. *Cell Rep.* 2, 397–406. doi: 10.1016/j.celrep.2012.06.011

Wake, H., Lee, P. R., and Fields, R. D. (2011). Control of local protein synthesis and initial events in myelination by action potentials. *Science* 333, 1647–1651. doi: 10.1126/science.1206998

Wake, H., Ortiz, F. C., Woo, D. H., Lee, P. R., Angulo, M. C., and Fields, R. D. (2015). Nonsynaptic junctions on myelinating glia promote preferential myelination of electrically active axons. *Nat. Commun.* 6:7844. doi: 10.1038/ncomms8844

Wieraszko, A., Goldsmith, G., and Seyfried, T. N. (1989). Stimulation-dependent release of adenosine triphosphate from hippocampal slices. *Brain Res.* 485, 244–250. doi: 10.1016/0006-8993(89)90567-2

Xiao, L., Ohayon, D., McKenzie, I. A., Sinclair-Wilson, A., Wright, J. L., Fudge, A. D., et al. (2016). Rapid production of new oligodendrocytes is required in the earliest stages of motor-skill learning. *Nat. Neurosci.* 19, 1210–1217. doi: 10.1038/nn.4351

Xing, Y. L., Roth, P. T., Stratton, J. A., Chuang, B. H., Danne, J., Ellis, S. L., et al. (2014). Adult neural precursor cells from the subventricular zone contribute significantly to oligodendrocyte regeneration and remyelination. *J. Neurosci.* 34, 14128–14146. doi: 10.1523/JNEUROSCI.3491-13.2014

Yamazaki, Y., Abe, Y., Shibata, S., Shindo, T., Fujii, S., Ikenaka, K., et al. (2019). Region- and cell type-specific facilitation of synaptic function at destination synapses induced by oligodendrocyte depolarization. *J. Neurosci.* 39, 4036–4050. doi: 10.1523/JNEUROSCI.1619-18.2019

Zelentsova, A. S., Deykin, A. V., Soldatov, V. O., Ulezko, A. A., Borisova, A. Y., Belyaeva, V. S., et al. (2022). P2X7 receptor and purinergic signaling. *Orchestr. Mitochond. Dysfunct. Neurodegener. Dis. eNeuro* 9:ENEURO.0092-22.2022. doi: 10.1523/ENEURO.0092-22.2022

Zhang, P., Kishimoto, Y., Grammatikakis, I., Gottimukkala, K., Cutler, R. G., Zhang, S., et al. (2019). Senolytic therapy alleviates Abeta-associated oligodendrocyte progenitor cell senescence and cognitive deficits in an Alzheimer's disease model. *Nat. Neurosci.* 22, 719–728. doi: 10.1038/s41593-019-0372-9

Zonouzi, M., Renzi, M., Farrant, M., and Cull-Candy, S. G. (2011). Bidirectional plasticity of calcium-permeable AMPA receptors in oligodendrocyte lineage cells. *Nat. Neurosci.* 14, 1430–1438. doi: 10.1038/nn.2942

Frontiers in
Cellular Neuroscience

Leading research in cellular mechanisms underlying brain function and development

Part of the world's most cited neuroscience journal series that advances our understanding of the cellular mechanisms underlying cell function in the nervous system across all species.

Discover the latest Research Topics

See more →

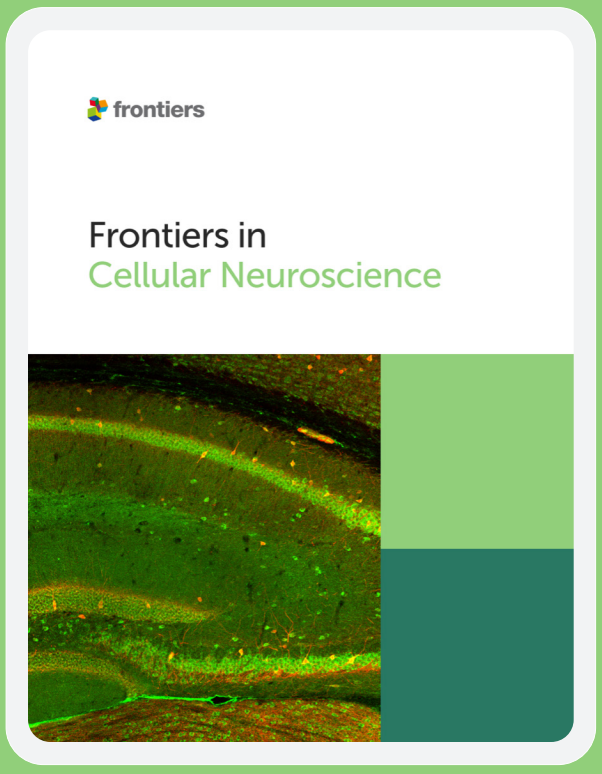

Frontiers

Avenue du Tribunal-Fédéral 34
1005 Lausanne, Switzerland
frontiersin.org

Contact us

+41 (0)21 510 17 00
frontiersin.org/about/contact